

ABSTRACT

MIDANI, MOHAMAD SAMIR. The Influence of Weave and Structural Parameters on the Performance of Composites from 3D Orthogonal Woven Preforms. (Under the direction of Dr. Abdel-fattah Seyam and Dr. Mark Pankow).

Over the past few decades there have been an increasing interest in woven preforms as a reinforcement for composites. Woven preforms not only offer ease of handling and structure uniformity, but also offer directional properties and high fiber volume fraction. The internal structure of a woven preform is dictated by the yarn spacing, interlacing pattern, yarn cross-section, yarn size, and other structural parameters that greatly influence the mechanical properties of the preform and hence the composite.

The invention of 3D Orthogonal Weaving (3DOW) technology, introduced new and enhanced features to the conventional 2D woven preforms. 3D woven preforms can be woven to near net shape, eliminate the need for stacking, have a through-thickness yarn component that significantly enhances the out-of-plane properties, and delamination resistance, in addition to having straight warp and filling yarns with no crimp, plus other features that are important to the composite industry.

Modeling the tensile behavior of 3DOW composites, is very useful to the industry, it helps in characterizing the composite material, with minimal need for coupon testing. A significant number of models have been developed to predict the tensile behavior of the 3DOW composites, however, most of these models were focused on composites made from plain woven preforms with jammed structure. In this study a generalized analytical model was developed to predict the entire load-extension curve of the 3DOW preforms and composites including the non-linear region, using the finite deformation approach. The model was

generalized to predict the properties of any 3DOW structure, made with spun or filament yarn, jammed and non-jammed, which have any weave architecture, including hybrid composites. The model was verified experimentally for a broad range of experimental composites, including hybrid ones. The results indicated that there was a general good agreement between the experimental and theoretical curves. Moreover, a numerical parametric study was performed to reveal the architecture potential of 3DOW preforms.

A range of 3D woven E-glass preforms were woven using a patented 3D orthogonal weaving technology, and then converted into composites, using vacuum assisted resin transfer molding technology. The composite samples, had varying structural parameters, such as, number of Y-yarn layers, X-yarn pick density, Z-yarn interlacing weave pattern, and Z: Y-yarn/ layer ratio. The purpose was to study the effect of changing those structural parameters on the mechanical properties of the 3DOW composites.

The response of the 3DOW composites subjected to different modes of impact was investigated. The study indicated that, the number of Y-yarn layers, had the most significant effect on the total Tup, Izod, and Charpy impact energies. The X-yarn pick density, had slight effect on the three modes of impact, while the Z-yarn weave design only had a slight significant effect on the Tup and Charpy impact energy. Additionally, when testing the overall correlation between the three impact energies, there was a strong correlation between the results of all three impact modes. However, after normalization there was a weak correlation between the Tup and Charpy impact results, very weak correlation between Charpy and Izod results, and no correlation between Izod and Tup results.

Further, the effect of changing the Z: Y-yarn/ layer ratio on the in- and out-of-plane properties of the 3DOW composites was investigated. The study indicated that changing the amount of

Z-yarn in the structure didn't have any significant effect on the tensile, Izod, and Charpy properties (in-plane), yet, it had a significant effect on the Tup impact properties (out-of-plane). Moreover, it had a strong significant effect on the failure mechanisms of all four types of tests, and as the amount of Z-yarn was reduced, delamination became more significant.

© Copyright 2016 Mohamad Midani

All Rights Reserved

The Influence of Weave and Structural Parameters on the Performance of Composites from
3D Orthogonal Woven Preforms

by
Mohamad Samir Midani

A dissertation submitted to the Graduate Faculty of
North Carolina State University
in partial fulfillment of the
requirements for the degree of
Doctor of Philosophy

Fiber and Polymer Science

Raleigh, North Carolina

2016

APPROVED BY:

Dr. Abdel-fattah Seyam

Co-chair of Advisory Committee

Dr. Mark Pankow

Co-chair of Advisory Committee

Dr. William Oxenham

Committee member

Dr. Kavita Mathur

Committee member

Dedication

This work is dedicated to my people and my nation, a nation that has been suffering for a long time from oppression, ignorance, and misguidance. I hope that the experience which I've gained throughout my career and my Ph.D. study would help me change their unfortunate reality, and make a tangible difference in their lives.

This work is also dedicated to the soul of my beloved grandmother, who always inspired me with her generosity, humbleness, and beautiful speech. My dad, who taught me the real purpose of life, and the importance of the family, and the value of maintaining balance in this life. My mum, my joy and my childhood, no words can describe her patience, persistence and dedication. My 2 brothers and 2 sisters (my gang), who were always by my side, and with whom I never felt alone even when I'm away from home.

To my beloved wife Wessam Elmalky, who went with me through all the ups and downs in this life, she is not just my wife, she is my soul mate, my best friend, and my counselor. To my daughter Jury, and my son Zaineldeen, for bearing the burden of traveling and leaving their comfort life, and showing resilience and ability to adapt with changing situations.

To all my friends and family.

Biography

Mohamad Samir Midani was born in Cairo –Egypt in 1983. He descends from a famous Syrian family, who runs a textile business in Egypt since 1960. He grew up around the textile mills, where he started building his passion for textile materials, machines, and products.

He earned his Bachelor of Science degree in Mechanical Engineering, with a major in Design and Production, and was awarded a 3rd class honor, from Ain Shams University in Cairo – Egypt in 2006. After graduation Mohamad joined his family business, he worked in different positions, and different function groups, such as technical sales, process improvement, and management systems.

In 2010 Mohamad moved to Raleigh, NC to start his textiles study, and earned his Master degree in Textiles Technology and Management, from the College of Textiles, NC State University in 2012. After graduation, Mohamad worked as a product development engineer in the textile industry in Egypt for a year and a half.

In 2014 Mohamad started his Ph.D. program in Fiber and Polymer Science, at the College of Textiles, NC State University. He also worked as a teaching and research assistant, and in 2015 he received a certificate of recognition for excellence in teaching. After graduation Mohamad is planning to go back to Egypt to start his career in academia as a teaching assistant, in addition to starting up a company that develops innovative products from green composites.

Acknowledgements

I would like to express my sincere gratitude to everyone who helped me throughout my Ph.D. study. I was fortunate to have a great advisory committee, who provided me with continuous guidance and support. I'm grateful to my advisor Dr. Seyam for his sponsorship, guidance, trust and motivation, surely he treated me like a son, and I'm proud of being his son in academia. I'm thankful to my committee's co-chair Dr. Pankow for his valuable inputs and feedback, I would also like to extend my sincere thanks to Dr. Oxenham, Dr. Mathur, and Dr. Bourham.

I'm grateful to PPG industries for their generous donation of the E-glass rovings, and Ashland Inc. for donating the Vinylester resin. I greatly appreciated, the help of Mehmet Ince in weaving the 3D preforms, and Karim Aly in the resin infusion. Great thanks to NC State University, College of Textiles, and the Graduate School, for providing great learning, skills building, and research resources.

Thanks are due to my dad Samir Elmidany, and my aunt Iman Elmidany for their generous and continuous financial support.

I would like to thank all my colleagues for their help and motivation, Rahul Vallabh, Anuradha Gupta, Hadir Eldeeb, and special thanks to the best colleague ever Elizabeth-Lane (Betsy) Claunch.

Table of Contents

List of Tables	ix
List of Figures.....	x
1. INTRODUCTION.....	1
1.1. Reinforcement Forms (Preforms).....	3
1.1.1. Woven fabrics	4
2. LITERATURE REVIEW	11
2.1. Analytical Modeling of the Mechanical Behavior of 3DOW Composites.....	11
2.1.1. Modeling the woven preform structure.....	11
2.1.2. Modeling the load-extension behavior of woven preforms.....	15
2.1.3. Modeling mechanical behavior of 3DOW composites.....	18
2.2. Effect of the Z-Yarn on the In- and Out-of-Plane Performance of 3DOW Composites	29
2.3. Response of 3DOW Composites under Different Modes of Impact and their Relationship	44
2.3.1. Flexed beam tests.....	45
2.3.2. Flexed plate impact testing	45
3. OBJECTIVES	48
4. GENERALIZED MODEL FOR THE LOAD-EXTENSION BEHAVIOR OF 3DOW COMPOSITES.....	51
4.1. Generalized Load-Extension Model of 3DOW Preforms.....	51
4.1.1. Nomenclature	53
4.1.2 Geometrical model of general weaves.....	55
4.1.3. Computation of load extension properties of general weaves in biaxial loading	59

4.2. Generalized Load-Extension Model of 3DOW Composites	64
4.2.1. Hamburger theory of blended yarns	65
4.2.2. Volume fraction of yarns and matrix components	66
4.3. Numerical Example.....	67
4.3.1. Load-extension properties of unit structure A and B of Z-yarn	68
4.3.2. Load-extension properties of X- and Y-yarns.....	72
4.3.3. Load-extension properties of the preform.....	73
4.3.4. Load-extension properties of the composite.....	73
4.4. Experimental Verification of the Model.....	76
4.4.1. Composite tensile test	76
4.5. Numerical parametric study	112
4.5.1. Effect on composite peak load	114
4.5.2. Effect on Z stretch ratios.....	118
4.6. Conclusion.....	120
5. EXPERIMENTAL	122
5.1. Materials	122
5.1.1. Fibers	122
5.1.2. Resin and curing agents	123
5.2. Experimental Design.....	126
5.2.1. Design of experiment A	126
5.2.2. Design of experiment B	127
5.3. Preforms Formation.....	127
5.3.1. Weaving non-interlaced preforms	130
5.4. Resin Infusion	131
5.5. Testing and Evaluation	133

5.5.1. Tensile test	135
5.5.2. Tup impact test	135
5.5.3. Charpy impact test	136
5.5.4. Izod impact test	136
5.5.5. Measuring the fiber volume fraction	136
5.6. Statistical Analysis.....	136
5.7. Sampling.....	137
6. RESULTS AND DISCUSSION	139
6.1. Experiment A.....	139
6.1.1. Main effects of structural parameters on impact resistance	141
6.1.2 Correlation between different modes of impact	171
6.1.3. Conclusion on Experiment A.....	206
6.2. Experiment B	208
6.2.1 Effect of Z: Y-yarn/ layer ratio on mechanical properties	208
6.2.2. Failure analysis	229
6.2.3. Conclusion on Experiment B	238
7. OVERALL CONCLUSION AND SUGGESTION FOR FUTURE STUDIES	241
REFERENCES.....	246
APPENDICES.....	253
APPENDIX A: Statistical analysis of Tup impact energy for Experiment A	254
APPENDIX B: Statistical analysis of Izod impact energy in Y-axis direction for Experiment A.....	270
APPENDIX C: Statistical analysis of Izod impact energy in X- axis direction for Experiment A.....	286
APPENDIX D: Statistical analysis of Charpy impact energy in Y- axis direction for Experiment A.....	302

APPENDIX E: Statistical analysis of Charpy impact energy in X- axis direction for Experiment A.....	318
APPENDIX F: Statistical correlation between impact energies of Tup, Izod, and Charpy impact tests of all samples for Experiment A	334
APPENDIX G: Statistical correlation between impact energies of Tup, Izod, and Charpy impact tests of plain samples for Experiment A.....	338
APPENDIX H: Statistical correlation between impact energies of Tup, Izod, and Charpy impact tests of twill samples for Experiment A	342
APPENDIX I: Statistical correlation between impact energies of Tup, Izod, and Charpy impact tests of basket samples for Experiment A	346
APPENDIX J: Statistical correlation between impact energies of Tup, Izod, and Charpy impact tests of balanced samples for Experiment A	350
APPENDIX K: Statistical analysis of tensile results from Experiment B	354
APPENDIX L: Statistical analysis of Tup impact results from Experiment B	368
APPENDIX M: Statistical analysis of Izod impact results from Experiment B	373
APPENDIX N: Statistical analysis of Charpy impact results from Experiment B...	383
APPENDIX O: Tup Impact Load-Deflection Curves for all Specimens in Experiment B	393
APPENDIX P: Tup Impact Delamination Area Image Analysis for Experiment B	395

List of Tables

Table 1	Structure of sample preform.....	67
Table 2	3DOW composites specifications	77
Table 3	Weaves considered for the parametric study	113
Table 4	Fixed parameters used in the parametric study	114
Table 5	Warp, weft, and binder yarns specifications	122
Table 6	Typical liquid resin properties of Derakane [®] 8084.....	123
Table 7	Typical properties of post cured Derakane [®] 8084 resin clear casting	124
Table 8	Typical properties of initiator (NOROX [®] MEKP-925H)	124
Table 9	Typical gel times for Derakane [®] 8084 Resin.....	125
Table 10	Design of experiment A	127
Table 11	Design of experiment B	127
Table 12	List of mechanical tests on final composite structures.....	133
Table 13	Experiment A samples ID and their variable parameters.....	140
Table 14	Tup impact results [59]	141
Table 15	Izod impact results in Y-axis direction	146
Table 16	Izod impact results in X-axis direction	147
Table 17	Type of breaks in Izod impact specimens according to ASTM D256	148
Table 18	Charpy impact results in Y-axis direction.....	154
Table 19	Charpy impact results in X-axis direction.....	155
Table 20	Experiment B samples ID and their variable parameter	208
Table 21	Tup impact results	209
Table 22	Tensile test results in Y-axis direction	213
Table 23	Tensile test results in X-axis direction	213
Table 24	Izod impact results in Y-axis direction	219
Table 25	Izod impact results in X-axis direction	219
Table 26	Charpy impact results in Y-axis direction.....	224
Table 27	Charpy impact results in X-axis direction.....	224

List of Figures

Figure 1 Composites classification based on the dispersed phase [1]	2
Figure 2 Composites classification based on the matrix phase [1]	2
Figure 3 (Left) Cross section image (right) and surface image (left) of a woven fabric from spun yarns [8]	5
Figure 4 Tensile stress-strain curve of a woven fabric [9].....	6
Figure 5 Classification of 3D woven fabrics [13].....	7
Figure 6 Illustration of conventional 2D weaving principle, (a) 2D fabric, (b) 3D angle interlock fabric [16]	8
Figure 7 3D Through-thickness angle interlock weave [16].....	8
Figure 8 3D orthogonal woven fabric [16]	9
Figure 9 Peirce's circular cross section geometry of plain weave fabrics [18]	12
Figure 10 Peirce's approximate treatment of flattened yarn geometry of plain weave fabrics [18].....	13
Figure 11 Kemp's racetrack section geometry of plain weave fabric [18].....	13
Figure 12 Hearle's lenticular geometry, (a) plain weave fabric, (b) yarn lenticular C.S. [18]	14
Figure 13 Seyam and Elsheikh's geometry of woven fabric, warp C.S. (left), and filling C.S. (right) [23]	15
Figure 14 Straight lines approach used to represent the woven fabric used by Sun et al. [28]	16
Figure 15 Repeat of one yarn structure in the warp direction [28]	17
Figure 16 Schematic diagram of one construction repeat of a woven fabric [28]	17
Figure 17 Repeat along the warp axis, showing unit structures A and B [28].....	18
Figure 18 Nagai et al. unit cell (a) 3DOW constituents, (b) Infinitesimal volume element in the 3D anisotropic space. [30]	21
Figure 19 Cox and Dadkhah 3DOW composite geometry [33].....	22
Figure 20 Kou & Pon unit cell for 3DOW composite (a) Straight yarns, (b) undulated yarns [34].....	23
Figure 21 Schematic of Tan et al. (a) X-model, (b) Y-model, and (c) Z-model [36]	24
Figure 22 Naik et al. 3DOW composite unit cell for analysis (a) discretization, (b) idealized geometry [39]	25

Figure 23 Wu et al. 3DOW composite unit cell discretization [40]	26
Figure 24 Chen et al. simplified unit cell for 3DOW composite [43]	27
Figure 25 Pankow et al. representative unit cell of 3DOW composite [45]	28
Figure 26 Schematic diagram of Leong 3DOW structure [46].....	30
Figure 27 Warp cross sections of the 3DOW performs, (a) normal structure, and (b) modified structure [46]	30
Figure 28 Schematic diagram showing crimping of the warp yarn due to high tension of the binder yarn [46]	31
Figure 29 Rao et al. schematic representation of the 3DOW architecture, (a) plan view, (b) front cross sectional view, and the (c) detail of the modified unit cell [47].....	32
Figure 30 Schematic of the structures investigated by Mouritz et al., (a) 3DOW structure, (b) 3D angular interlock structure, (c) quasi-isotropic stitched structure, and (d) pinned structure [48].....	34
Figure 31 Schematic of different 3D woven structures, (a) layer-to-layer, (b) angle-interlock, and (c) orthogonal [49].....	35
Figure 32 Crimp analysis of 3D woven structures [49].....	36
Figure 33 Bilisik et al. 3D woven structures using different insertion mechanisms, (a) pin insertion, (b) shuttle insertion, and (c) single rapier insertion [50]	37
Figure 34 3D nonwoven carbon fiber needle punched web [51].....	39
Figure 35 Stacked laminate of multi-layer plain woven preforms, Z-stitched in the through thickness direction [51]	39
Figure 36 Dhiman representative volume element of 3DOW, (a) structure 1, and (b) structure 2 [52].....	41
Figure 37 Hexagonal packing of individual fibers within the carbon tows [51]	41
Figure 38 Dai et al. 3DOW structures with varying Z-yarn architecture, (a) W-1 plain 1x1, (b) W-2.1 3x3 weave, (c) W-2.2 3x3 weave, and (d) W-2.3 3x3 weave [53].....	43
Figure 39 Schematic diagram of (a) Charpy, (b) Izod impact equipment [55].....	45
Figure 40 Schematic diagram of flexed plate impact testing [55]	46
Figure 41 Force-time diagram (left) and energy- time diagram (right) [54]	46
Figure 42 Ince’s generalized 3D woven preform geometry of non-jammed structure for (a) rectangular yarn cross section, and (b) circular yarns cross section [59, 60]	52

Figure 43 Kawabata’s unit structure at weave intersection in the deformed state [24]	53
Figure 44 Schematic diagram of one construction repeat of 3DOW preform	57
Figure 45 Repeat of one yarn structure in the Y-direction for (a) rectangular yarn cross section, and (b) circular yarn cross section.....	58
Figure 46 Z-yarn unit structure A subjected to biaxial loading	60
Figure 47 Effect of stress strain characteristics on blend strength [62]	65
Figure 48 Tensile properties of the yarns used	68
Figure 49 Graph for solving F_c	69
Figure 50 Average resistance to compression of Z-and X-yarns	69
Figure 51 The parameter F_c for uniform biaxial extension.....	70
Figure 52 Relation between F_z and λ_z^A	70
Figure 53 Relation between F_z and λ_z^B	71
Figure 54 Relation between F_z and λ_z	72
Figure 55 Relation between F_x (F_y) and λ_x (λ_y).....	72
Figure 56 Preform resultant tensile properties in y-axis direction for one structural repeat .	73
Figure 57 Tensile properties of Vinylester matrix at different fiber volume fractions for one structural repeat	74
Figure 58 Composite tensile properties in Y-axis direction for one structural repeat	75
Figure 59 Composite tensile properties in X-axis direction for one structural repeat	75
Figure 60 Yarn vs. fiber tensile properties for, (a) Spectra, (b) Vectran, (c) Zylon, (d) E-glass $\rho_1=275$ tex, (e) E-glass $\rho_1=735$ tex, and (f) E-glass $\rho_1=2400$ tex [63]	78
Figure 61 Experimental vs. model tensile load-strain for 3DOW plain E-glass composite with 2.44 picks/ cm in X- and Y-axis directions, (a) 4 layers, (b) 3 layers, and (c) 2 layers.....	80
Figure 62 Experimental vs. model tensile load-strain for 3DOW 2x2 Twill E-glass composite with 2.44 picks/ cm in X- and Y-axis directions, (a) 4 layers, (b) 3 layers, and (c) 2 layers.	83
Figure 63 Experimental vs. model tensile load-strain for 3DOW 2x2 Basket E-glass composite with 2.44 picks/ cm in X- and Y-axis directions, (a) 4 layers, (b) 3 layers, and (c) 2 layers.	86

Figure 64 Experimental vs. model tensile load-strain for 3DOW plain E-glass composite with 2.74 picks/ cm in X- and Y-axis directions, (a) 4 layers, (b) 3 layers, and (c) 2 layers.....	89
Figure 65 Experimental vs. model tensile load-strain for 3DOW 2x2 Twill E-glass composite with 2.74 picks/ cm in X- and Y-axis directions, (a) 4 layers, (b) 3 layers, and (c) 2 layers.	92
Figure 66 Experimental vs. model tensile load-strain for 3DOW 2x2 Basket E-glass composite with 2.74 picks/ cm in X- and Y-axis directions, (a) 4 layers, (b) 3 layers, and (c) 2 layers.	95
Figure 67 Experimental vs. model tensile load-strain for 3DOW plain E-glass composite with 2.925 picks/ cm in X- and Y-axis directions, (a) 4 layers, (b) 3 layers, and (c) 2 layers.....	98
Figure 68 Experimental vs. model tensile load-strain for 3DOW 2x2 Twill E-glass composite with 2.925 picks/ cm in X- and Y-axis directions, (a) 4 layers, (b) 3 layers, and (c) 2 layers.	101
Figure 69 Experimental vs. model tensile load-strain for 3DOW 2x2 Basket E-glass composite with 2.925 picks/ cm in X- and Y-axis directions, (a) 4 layers, (b) 3 layers, and (c) 2 layers.	104
Figure 70 Experimental vs. model tensile load-strain for 3DOW plain hybrid composites in X- and Y-axis directions, (a) Spectra, (b) Vectran, and (c) Zylon.	107
Figure 71 Tensile specimen showing retroreflective tape used for laser extensometer strain measurements	111
Figure 72 The effect of the Z-yarn weave factor and linear density on the peak load of the composite in the Y-axis direction.....	115
Figure 73 The effect of the Z-yarn weave factor and linear density on the peak load of the composite in the X-axis direction.....	116
Figure 74 The effect of number of Y-yarn layers, and X-yarn pick density on the peak load of the composite in the Y-axis direction.....	117
Figure 75 The effect of number of Y-yarn layers, and X-yarn pick density on the peak load of the composite in the X-axis direction.....	117
Figure 76 The effect of Z-yarn weave factor on Z stretch ratios	118

Figure 77 The effect of Y-yarn number of layers on Z stretch ratios	119
Figure 78 The effect of X-yarn pick density on Z stretch ratios	120
Figure 79 3D weaving loom donated by 3TEX Inc	128
Figure 80 Denting plan for a 3 layers preform at various Z- to Y-yarns/ Y-layer ratios (a) 1:1, (b) 2:3, (c) 1:3, (d) 0:1	129
Figure 81 Woven preforms at various Z- to Y-yarns/ Y-layer ratios (a) 1:1, (b) 2:3, (c) 1:3, (d) 0:1	130
Figure 82 Non-interlaced 3DOW preform, (a) with supporting Z-yarns, and (b) Supporting Z-yarns removed.....	131
Figure 83 Consolidation using VARTM technique, (a) VacMobiles® vacuum pump, (b) vacuum bagging assembly.....	132
Figure 84 Specimens from the produced composites for design of experiment B	133
Figure 85 MTS Servo hydraulic 370 load frame for tensile testing.....	134
Figure 86 Instron impact testing equipment, (a) drop tower impact CEAST 9350, and (b) pendulum impactor II	134
Figure 87 Specimens sampling plan	137
Figure 88 High precision waterjet cut composite panels	138
Figure 89 Typical punctured Tup impact specimen, (a) Front view, (b) back view, and (c) side view	142
Figure 90 Types of breaks in Izod impact specimens.....	148
Figure 91 Types of breaks in Charpy impact specimens	156
Figure 92 Main effect of number of layers on impact energy, (a) Y-direction, and (b) X-direction.....	163
Figure 93 Main effect of X-yarn density on impact energy, (a) Y-direction, and (b) X-direction.....	163
Figure 94 Main effect of weave pattern on impact energy, (a) Y-direction, and (b) X-direction.....	164
Figure 95 Main effect of (a) specimen direction, and (b) impact mode, on impact energy. 164	
Figure 96 Main effect of number of layers on impact energy normalized by composite thickness, (a) Y-direction, and (b) X-direction.....	165

Figure 97 Main effect of X-yarn density on impact energy normalized by composite thickness, (a) Y-direction, and (b) X-direction.....	165
Figure 98 Main effect of weave pattern on impact energy normalized by composite thickness, (a) Y-direction, and (b) X-direction.....	166
Figure 99 Main effect of (a) specimen direction, and (b) impact mode, on impact energy normalized by composite thickness.....	166
Figure 100 Main effect of number of layers on impact energy normalized by composite areal density, (a) Y-direction, and (b) X-direction.....	167
Figure 101 Main effect of X-yarn density on impact energy normalized by composite areal density, (a) Y-direction, and (b) X-direction.....	167
Figure 102 Main effect of weave pattern on impact energy normalized by composite areal density, (a) Y-direction, and (b) X-direction.....	168
Figure 103 Main effect of (a) specimen direction, and (b) impact mode, on impact energy normalized by composite areal density	168
Figure 104 Main effect of number of layers on impact energy normalized by preform areal density, (a) Y-direction, and (b) X-direction.....	169
Figure 105 Main effect of X-yarn density on impact energy normalized by preform areal density, (a) Y-direction, and (b) X-direction.....	169
Figure 106 Main effect of weave pattern on impact energy normalized by preform areal density, (a) Y-direction, and (b) X-direction.....	170
Figure 107 Main effect of (a) specimen direction, and (b) impact mode, on impact energy normalized by preform areal density	170
Figure 108 Impact energies of plain weave samples in, (a) Y-axis direction, and (b) X-axis direction.....	175
Figure 109 Impact energies normalized by composite thickness of plain weave samples in, (a) Y-axis direction, and (b) X-axis direction.....	177
Figure 110 Impact energies normalized by composite areal density of plain weave samples in, (a) Y-axis direction, and (b) X-axis direction	179
Figure 111 Impact energies normalized by preform areal density of plain weave samples in, (a) Y-axis direction, and (b) X-axis direction.....	181

Figure 112 Impact energies of twill weave samples in, (a) Y-axis direction, and (b) X-axis direction	183
Figure 113 Impact energies normalized by composite thickness of twill weave samples in, (a) Y-axis direction, and (b) X-axis direction.....	185
Figure 114 Impact energies normalized by composite areal density of twill weave samples in, (a) Y-axis direction, and (b) X-axis direction	187
Figure 115 Impact energies normalized by preform areal density of twill weave samples in, (a) Y-axis direction, and (b) X-axis direction.....	189
Figure 116 Impact energies of basket weave samples in, (a) Y-axis direction, and (b) X-axis direction	191
Figure 117 Impact energies normalized by composite areal density of basket weave samples in, (a) Y-axis direction, and (b) X-axis direction	193
Figure 118 Impact energies normalized by composite areal density of basket weave samples in, (a) Y-axis direction, and (b) X-axis direction	195
Figure 119 Impact energies normalized by preform areal density of basket weave samples in, (a) Y-axis direction, and (b) X-axis direction.....	197
Figure 120 Impact energies of balanced samples in, (a) Y-axis direction, and (b) X-axis direction	199
Figure 121 Impact energies normalized by composite thickness of balanced samples in, (a) Y-axis direction, and (b) X-axis direction	201
Figure 122 Impact energies normalized by composite areal density of balanced samples in, (a) Y-axis direction, and (b) X-axis direction.....	203
Figure 123 Impact energies normalized by preform areal density of balanced samples in, (a) Y-axis direction, and (b) X-axis direction	205
Figure 124 Tup impact, (a) peak loads, and (b) typical load - deflection curves	211
Figure 125 Tup impact energy in X- and Y- directions, (a) non-normalized, (b) normalized by composite thickness, (c) by composite areal density, and (d) by preform areal density	212
Figure 126 Tensile properties in X- and Y-directions, (a) peak load, (b) failure strain, (c) Modulus, and (d) typical load-strain curve.....	216
Figure 127 Typical tensile load – strain curves, (a) Y-direction, and (b) X-direction.....	217

Figure 128 Normalized tensile load in X- and Y-directions, (a) by composite thickness, (b) by composite areal density, (c) by preform areal density, and (d) total fiber Tex	218
Figure 129 Izod impact energy in X- and Y-directions, (a) non-normalized, (b) normalized by composite thickness, (c) by composite areal density, (d) by preform areal density, and (e) by total fiber Tex	221
Figure 130 Charpy impact energy in X- and Y-directions, (a) non-normalized, (b) normalized by composite thickness, (c) by composite areal density, (d) by preform areal density, and (e) by total fiber Tex.....	226
Figure 131 Failure analysis of typical Tup impact specimens, showing 3 different views .	231
Figure 132 Effect of Z: Y-yarn/ layer ration on delamination area	232
Figure 133 Failure analysis of typical tensile specimens in, (a) Y-direction, and (b) X-direction	234
Figure 134 Failure analysis of typical Izod impact specimens in, (a) Y-direction, and (b) X-direction	236
Figure 135 Failure analysis of typical Charpy impact specimens in, (a) Y-direction, and (b) X-direction.....	238

1. INTRODUCTION

Conventional engineering materials are usually classified into, metals, ceramics, and polymers. However, each of these single phase materials, has their advantages and disadvantages, which dictate their end use and applications. For instance, metals are heavy but they are favored for their high strength and toughness, also ceramics are brittle, but they are favored for strength and thermal resistance, as for conventional polymers, they have low strength, but they are favored for ductility and light weight. Nowadays, modern technologies and industries requirements are pushing towards more innovation in materials offerings, since those single phase materials are no longer meeting their performance criteria. For instance, in the aerospace industry there is an ongoing demand for lighter, stronger, and stiffer materials, with higher abrasion, corrosion, and impact resistance. Such requirements can't be satisfied by using a single phase material, for example, if metal is used to increase strength, this has to be accompanied by an increase in weight and decrease in ductility, due to the nature and limitations of metals [1].

Thus, there was a need to selectively combine features and attributes from specific materials and engineer them into a new class of materials called composite materials. Composite materials, contains two or more constituent materials that have different chemical and physical properties, and they remain distinct within the final composite. This combination of materials results in a material with properties superior to that of their constituents due to the synergetic effect taking place. A good example to illustrate this synergetic effect, is a glass fiber reinforced plastic, where short strands of glass fibers are embedded in a polymer matrix, thus, while glass fibers provide strength and stiffness, the polymer matrix provide increased ductility and weight reduced density of the final composite structure. Although composite materials are multi-phase materials, yet they still respond to external effects such as physical, mechanical, and environmental effects as a single unified material [2, 3].

The most commonly used composites, are two-phase composites that are comprised of two constituents. The first phase is in a continuous form, known as the matrix or binder phase, and the second phase is known as the dispersant phase, and it's surrounded by the matrix and could be continuous or discrete. Figure 1 and Figure 2 classify composite material based on the dispersed phase and matrix phase, respectively [1].

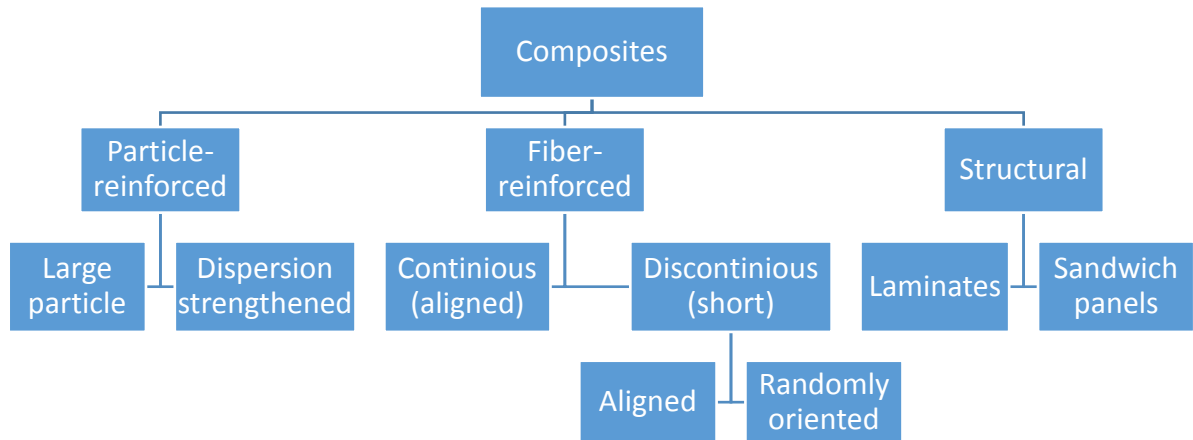


Figure 1 Composites classification based on the dispersed phase [1]

Composite materials can also be classified based on the matrix phase as illustrated in Figure 2.

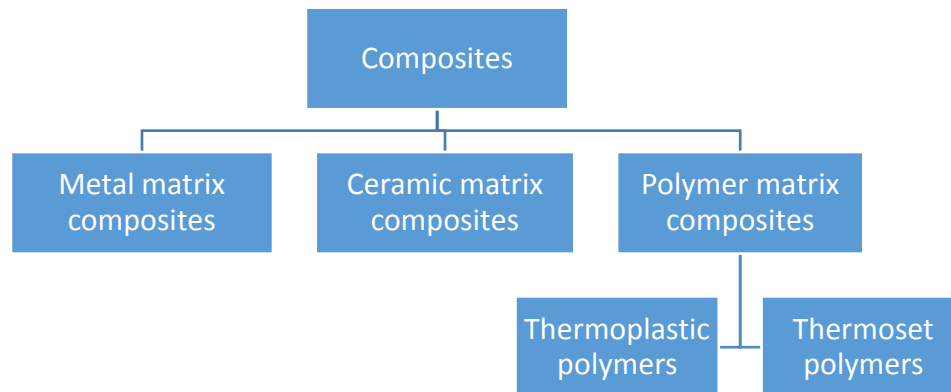


Figure 2 Composites classification based on the matrix phase [1]

The most commonly used matrix phase in composites, is the polymer matrix, they could either be thermoplastic, or thermoset polymer matrix. The type of interaction between the polymer molecules is what dictates whether it's a thermoset or a thermoplastic, for instance, if the polymer has strong intermolecular covalent bonds in the backbone of the polymer then it's a thermoset, whereas, if it has a weak secondary bonding then it's a thermoplastic. One of the advantages of thermoset polymers, is that it's generally liquid at room temperature, and it could infiltrate or impregnate the reinforcement in the liquid form. Thermosets solidifies or cure through cross linking, which is a chemical reaction that results in crosslinks between the

polymer molecules, unlike thermoplastic polymers which melt by heating and solidify by cooling. The crosslinking resulting from curing thermosets, have a unique interconnected 3D network structures, which have very high molecular weight. The high molecular weight crosslink networks, increase the melting temperature of the polymer beyond its degradation point. This leads to a major distinction between the thermosets and the thermoplastics, which is thermosets char by increasing temperature instead of melting, while thermoplastics melt as temperature increases [3].

The science of composite material is broad and diverse, which can be clearly seen from the above classifications. However, the scope of work of this research is limited to fiber reinforced polymer composites, using continuous or staple aligned fibers as the dispersed phase, and thermoset polymer as the matrix phase.

One of the main design considerations when designing fiber reinforced polymer composites, is the strength to weight ratio, and the stiffness to weight ratio, which is referred to as specific strength and specific stiffness. The specific properties of the composite are calculated by normalizing (dividing) the composite properties by its density, and since the fibers and the matrix used in fiber reinforced polymer composites have low density and high strength, thus the resulting composite would have high specific strength and stiffness [1, 3].

1.1. Reinforcement Forms (Preforms)

The form of fiber reinforcement used in composites, which is also known as preform in the composite field, comes in different forms, such as fibers, yarns, mats, woven fabrics and knitted fabrics. The reinforcement form or the preform along with the manufacturing techniques, dictates the final properties of the composite material. It's also worth mentioning that the type of preform used also dictates the processing technique. This means that knowledge of preform structure is a prerequisite for understanding and predicting the mechanical behavior of the produced composites.

There are many types of fiber reinforcement available in the composite market today. It could be in any form of fibrous assembly, so fiber itself can be used as reinforcement, or it could be converted into sheet format such as strands mats and fabrics. The technologies used to produce

fiber reinforcements are mostly textile technologies, such as nonwoven, weaving, braiding, and knitting technologies [4].

The eighties and the nineties have witnessed a great interest in composite research and development. Langley Research Center, which was part of NASA Advanced Composites Technology program, was leading the way in researching and investigating textile structures for composite reinforcement. The main focus of NASA's research program was to produce structural parts for passenger's aircrafts, such as wings and fuselage, using textile reinforcement due to their favored damage tolerant internal structure that is much better than tape laminates [5, 6].

Textiles reinforcements from yarns such as woven and knitted fabrics have numerous advantages, one of which is the ease of handling and transportation with limited distortion to the preform structure, this unique feature is due to the inter fiber friction resulting from the yarns interlacement which produce more cohesive preforms. With the recent developments in textile technologies, preforms can be produced in near-net-shape form, which means that the preform has a very similar shape to that of the final composite product, eliminating waste, machining, and the need for parts assembly that usually involves weaker joints formation using bolts or adhesive [7].

1.1.1. Woven fabrics

In order to understand the mechanical behavior of the composites with textile reinforcement, it's important to have a sound knowledge of the structure and mechanics of the textile reinforcement phase first.

Woven fabrics are considered the feedstock for different industries such as clothing, composites and technical textiles. The study of fabric mechanics under stress is of utmost importance, as it dictates how this fabric will perform in subsequent end uses. However, the study of the woven fabric mechanics is not as easy as studying the mechanics of isotropic homogeneous structures, due to the anisotropic nature of the woven fabric that result in a more sophisticated behavior [8].

Textile materials are totally different from engineering materials, because they are inhomogeneous and they lack continuity in addition to the high anisotropy. Moreover, textile

material could be easily deformed and they experience high strain percentage even at low stresses, they are nonlinear and plastic at such low level of stresses [8].

2D woven fabrics

Woven fabrics have an extremely complicated geometrical structure; Figure 3 shows a cross sectional and a surface image of a woven fabric from spun yarns. It's obvious that individual yarns inside the fabric are crimped. Furthermore, if the fabric is composed of spun yarns, the geometrical complication increases, due to the irregular nature of the spun yarns, as shown in Figure 3 [8].



Figure 3 (Left) Cross section image (right) and surface image (left) of a woven fabric from spun yarns [8]

The woven fabric is composed of a set of warp yarns and a set of weft yarns orthogonally interlacing. This interlacing holds the structure together by friction between the yarns and fibers. The interlacing design (or woven fabric design) contributes significantly to the amount of inter fiber/yarn friction and to the fabric properties. The distance between two adjacent yarns and the spaces within fibers in the yarns result in the porosity of the fabric. This porosity is what makes a porous fabric different from a continuum engineering structure.

Woven fabric is known for its large deformability which means that it experiences high percentage of strain at low stress levels. Figure 4 shows a tensile stress-strain curve of a woven fabric, where the applied tensile force per unit width is plotted against the tensile strain, which is one common way to express the loading on a woven fabric. The figure shows that the fabric experience large strains even at low stresses and this is mainly due to the straightening of the

crimped yarn within the fabric, which result in a very low initial tensile modulus when compared to engineering materials [9].

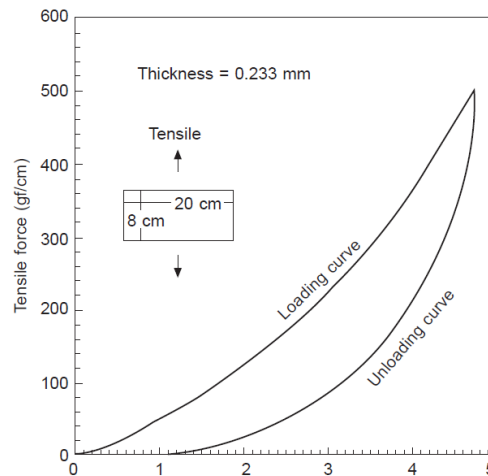


Figure 4 Tensile stress-strain curve of a woven fabric [9]

Woven fabrics are also prone to bending deformations under transverse loading; assuming that slippage between fibers is not constrained. When comparing the yarn bending stiffness with that of a solid rod of same cross section, it's obvious that the yarn would have greater flexibility since it is composed of numerous fine constituent fibers. Moreover, 2D woven fabrics usually have very small thickness which results in a further lower bending stiffness [10].

In conventional engineering materials low stresses results in low strains and it shows a linear behavior. However, in the case of woven fabrics the stress strain curve is nonlinear especially at low stresses, and it becomes more linear beyond a critical stress level, which varies for different modes of deformations. This critical stress level can be very high for the tensile deformation mode, and can be very low in case of bending or shear deformation modes [10].

In general, this very unique stress strain behavior of the woven fabrics is resulting from its porous, crimped and loosely connected structure. In tensile deformation mode when fabrics are subjected to low stresses, the crimped yarns start to straighten and this is why it has a low initial modulus. Afterwards, when loading continues to a higher stress level, the straightening of the crimped yarn is almost complete, the inter-fiber friction increases, the fibers become more oriented and the fabric structure becomes more consolidated. At this critical stress level,

the fabric starts to exhibit a more linear stress strain behavior which is similar to solid engineering materials [10].

3D woven preforms

Three-dimensional (3D) woven preforms are fabrics that could be formed to near net shape with considerable thickness. There is no need for layering to create a 3D part, because a single fabric provides the full 3D reinforcement. The 3D weaving process is a variant of the 2D weaving process and it's an extension of the very old technique of creating double and triple woven cloth. 3D weaving allows the production of fairly thick fabrics [11].

In 3D orthogonal woven fabrics, yarns placed in thickness direction are called z-yarns, warp weaver, or binder yarns. More than one layer of fabric is woven at the same time, and z-yarns interlace warp and weft yarns of different layers during the process. At the end of the weaving process, an integrated 3D woven structure, which has a considerable thickness, is produced [12].

There are several types of 3D woven fabrics that are commercially available; they could be classified according to their weaving technique as shown in Figure 5 [13]. The first type is the 3D woven angular interlock fabrics, which are fabrics produced on a traditional 2D weaving loom, using proper weave design and techniques, it could either have the weaver or z-yarn going through all the thickness of the fabric or from layer to layer as illustrated in Figures 6 and 7 [14, 15].

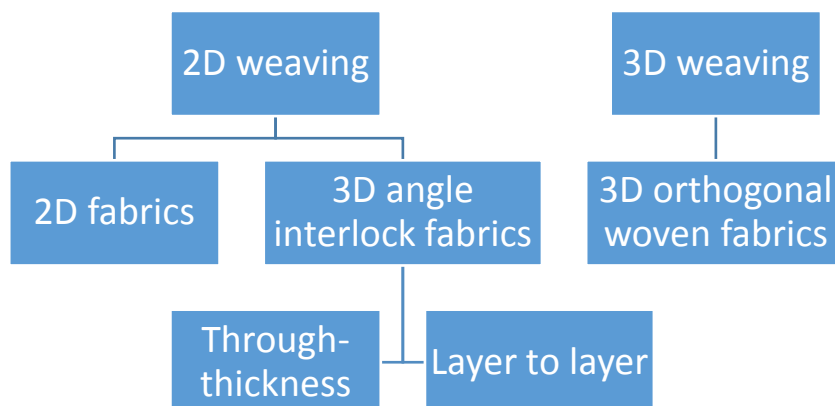


Figure 5 Classification of 3D woven fabrics [13]

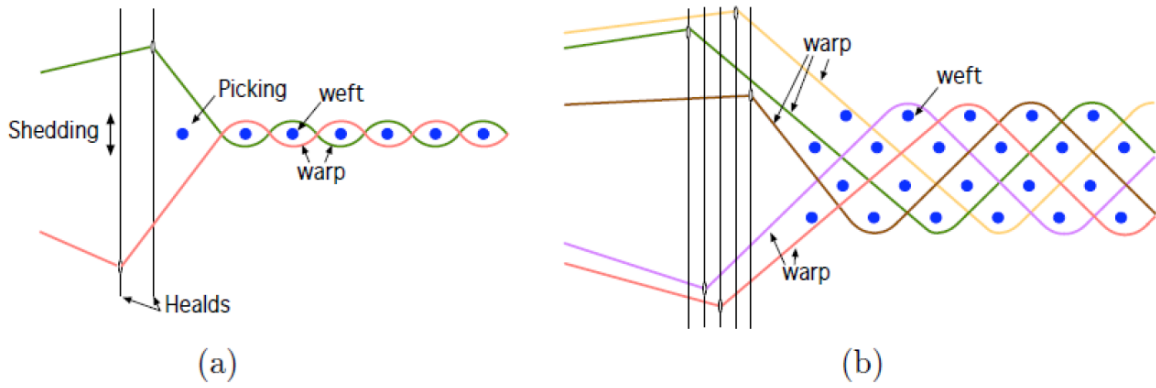


Figure 6 Illustration of conventional 2D weaving principle, (a) 2D fabric, (b) 3D angle interlock fabric [16]

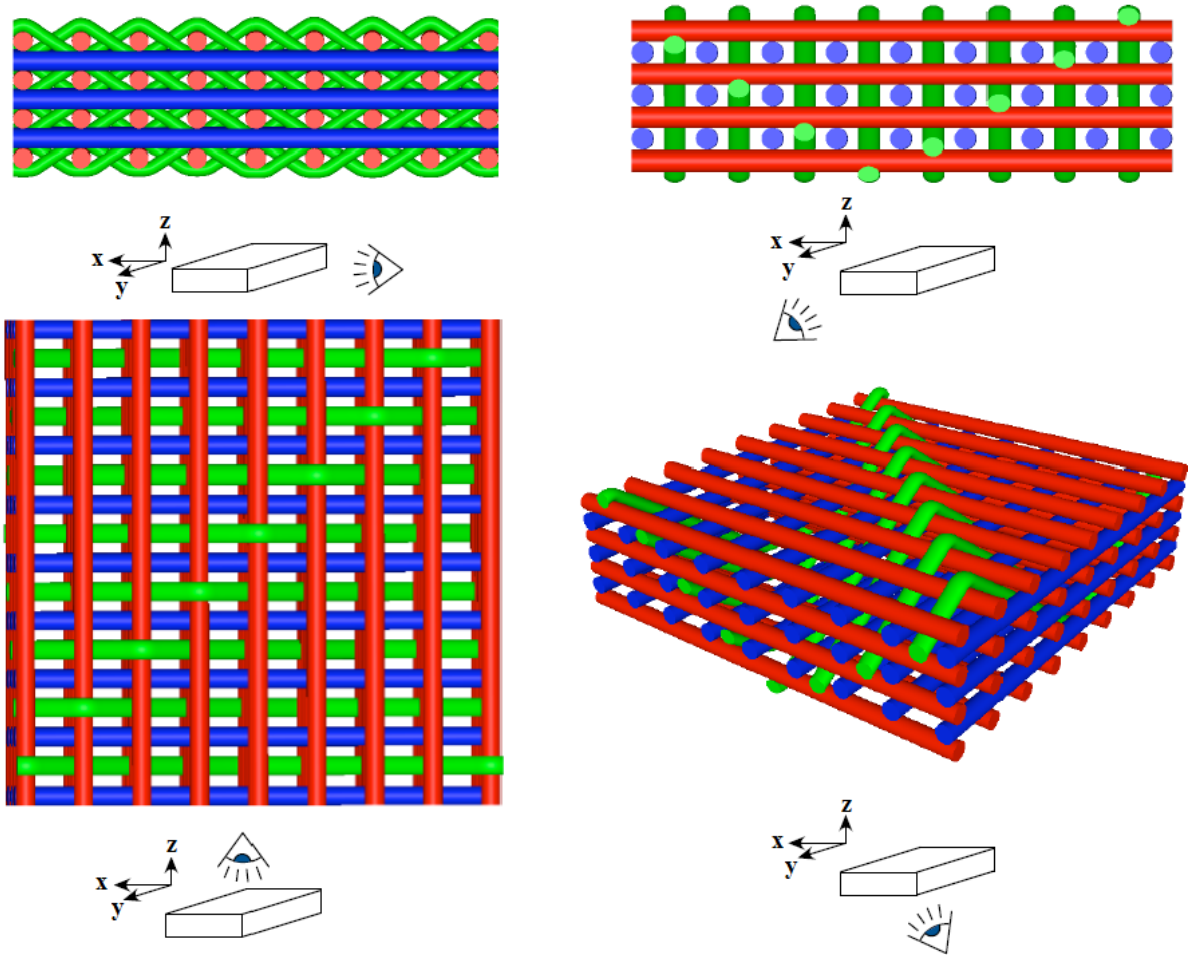


Figure 7 3D Through-thickness angle interlock weave [16]

The second type is 3D orthogonal woven fabrics, which are produced on a special 3D weaving loom. The process to form such fabric was patented by Mohamed and Zhang [17]. The architecture of the 3D orthogonal woven fabric consists of three different sets of yarns; warp yarns (y-yarn), weft yarns (x-yarn), and (z-yarn). Z-yarn is placed in the through-thickness direction of the preform. In 3D orthogonal woven fabric there is no interlacing between warp and weft yarns and they are straight and perpendicular to each other. On the other hand, z-yarns combine the warp and the weft layers by interlacing (moving up and down) along the y-direction over the weft yarn. The interlacing is performed from surface to surface, through the entire thickness of the preform as illustrated in Figure 8 [14, 15].

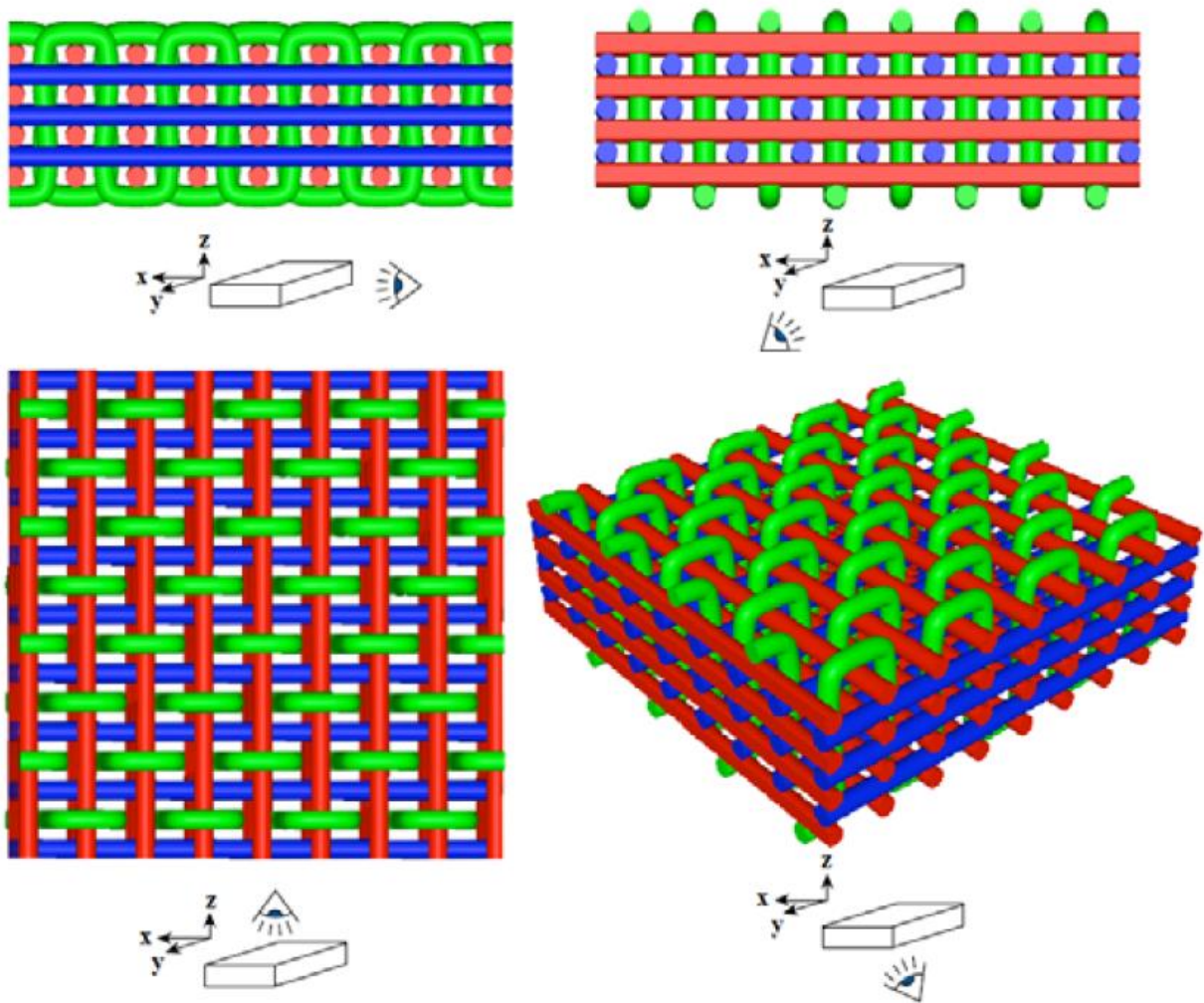


Figure 8 3D orthogonal woven fabric [16]

3D woven fabrics are very useful in applications where the composite structure is subjected to out-of-plane or impact loading, due to the extra strength provided by the (z-yarn) in the through thickness dimension. Thus it can better resist delamination, which is the separation of layers because of out-of-plane forces [12]. 3D woven fabrics have a high formability, which means it could easily take the shape of the mold in case of complex composite designs. Also, they have extremely low or no x- and y-yarn crimp; therefore, mechanical properties of fibers are almost fully utilized in warp and weft directions, and it could benefit from the maximum load carrying capacity of high performance fibers in these directions [17]. Moreover, the shape of 3D woven fabrics could be tapered in all three directions during the weaving process, producing near net shape fabrics, such as I-beams and stiffeners, which mean that these preforms could be placed directly in the mold without any additional labor work. There is no need for layering to create a part, because the single fabric has a considerable required thickness that provides the full three-dimensional reinforcement [11].

2. LITERATURE REVIEW

The scope of this research is limited to fiber reinforced composites, with 3D Orthogonal Woven (3DOW) fabrics as the reinforcement, and thermoset resin as the matrix. It involves analytical modeling of the mechanical behavior of the 3DOW composites, effect of Z-yarn on the in-plane and out-of-plane properties, and the relation between the different impact loading modes on the properties of the final composite. This chapter is a critical review of current and prior relevant research in these areas.

2.1. Analytical Modeling of the Mechanical Behavior of 3DOW Composites

2.1.1. Modeling the woven preform structure

The structure of woven fabrics has a very strong influence on their mechanical properties and behavior, for example, when a 2D woven fabric is stretched in the warp direction; it results in a contraction in the weft direction and an increase in the weft yarn crimp and decrease in warp crimp (crimp interchange). Therefore, it's important to study the fabric geometry to understand the relationship between the different geometrical parameters such as crimp, weave angle, thread spacing, etc. Furthermore, this understanding will help in the prediction of the mechanical properties by combining fabric geometry with yarn properties [18].

Fabrics are not regular structure that could be described in geometrical mathematical forms; however, it's possible to simplify the general characteristics of the woven fabrics into simple geometrical forms and physical parameters.

There have been different approaches for representing the geometrical configuration of the yarns in the woven fabrics. The most common approach idealized the general characters of the fabrics into simple geometrical forms and it assumed arbitrary geometrical models for the weave crimp and yarn cross-section shapes, and dealt with the micro mechanics of the woven fabrics on the basis of a unit cell approach and hence obtaining a mathematical expression for the geometrical configuration. To determine the yarn configuration in the fabric it's important to define the main two parameters representing this yarn, the first one is the crimp waves and the second one is the yarn cross sectional shape and fiber packing factor. There are five popular models used to define the yarn cross sectional (C.S.) shape [18]. These are Peirce's Circular

C.S. model, Peirce's elliptical C.S. model, Kemp's race track C.S. model, Hearle et al's Lenticular C.S. model, and Seyam and Elsheikh's geometric model for jammed structures.

In 1937, Peirce published a model about plain weave fabrics. His model was based on the assumptions that the yarns are uniform cylinders, inextensible, and completely flexible. The unit cell of plain weave (or half weave repeat) of Figure 9 depicts the Peirce geometry. The geometry of the unit cell was built by superimposing linear and circular yarn segments to produce the geometry that fit the assumptions. It was then possible to derive relationships between the geometrical parameters such as; yarn diameter, yarn length, thread spacing, weave crimp, weave angle and fabric thickness. Peirce's model has been very useful in the ordering and interpretations of the observations. Peirce's assumptions were especially valid in very open structures [19], and his geometry was very useful in predicting the maximum construction of woven fabrics [20]. However, his assumptions of circular cross section, uniformity of structure in longitudinal direction and incompressibility were not always valid [18].

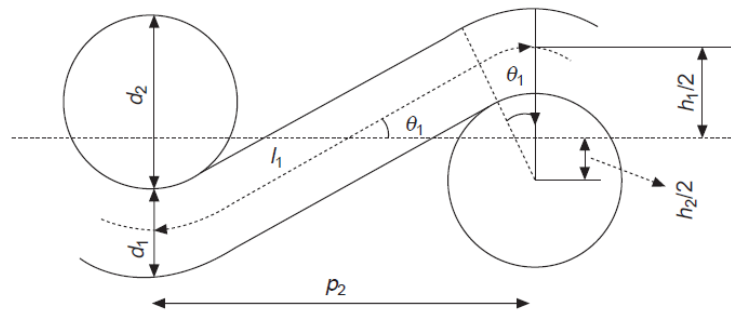


Figure 9 Peirce's circular cross section geometry of plain weave fabrics [18]

In woven fabrics, the inter-thread pressure cause threads to flatten. Peirce recognized this and proposed another model that considers the yarn cross section as elliptical, and to avoid the complexity of the elliptical geometry he just considered replacing the yarn diameter in the case of circular cross section with the minor diameter of the elliptic section, as illustrated in Figure 10. Still, the elliptical cross section model was not valid to define the jammed structures [18].

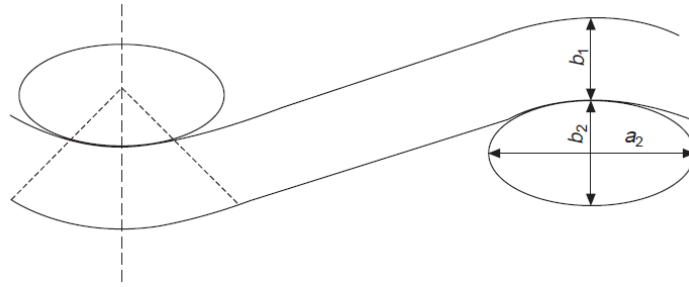


Figure 10 Peirce's approximate treatment of flattened yarn geometry of plain weave fabrics [18]

In 1958 Kemp proposed the race track cross sectional shape, which consisted of a rectangle enclosed by two semi-circles, and it had the advantage of using the simple relation of Peirce's circular thread geometry as illustrated in Figure 11. In 1978 Hearle et al. proposed a more accurate and general mathematical model that considered the thread cross section to be lenticular as illustrated in Figure 12 [18, 21, 22]. While the assumption that yarn cross section is non-circular (elliptical, racetrack, or lenticular) is closer to practical yarn shape in open and medium tight fabrics, this requires information about the dimensions of the cross section geometry such as minor and major diameters in elliptical cross section as an example. Unfortunately, the cross section dimensions of non-circular yarns are not constant and varies with the degree of tightness of the fabric. Research is required to establish relationships of yarn cross section dimensions and degree of fabric tightness [28].

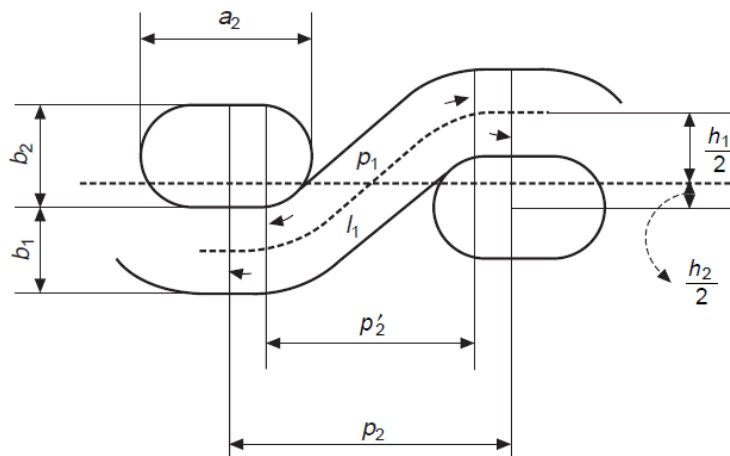


Figure 11 Kemp's racetrack section geometry of plain weave fabric [18]

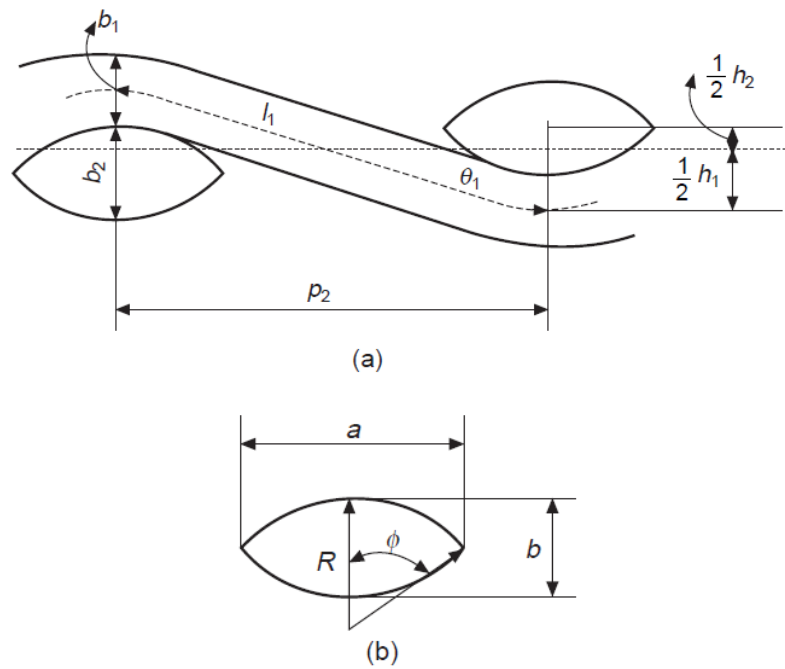


Figure 12 Hearle's lenticular geometry, (a) plain weave fabric, (b) yarn lenticular C.S. [18]

Later, Seyam and El-Shiekh's proposed a new geometry for jammed structures, as illustrated in Figure 13, which is proposed for use as a reference fabric to quantify fabric degree of tightness. They found that the proposed new geometry can be used to represent a vast majority of the weave designs being used to produce woven fabrics, such as plain weaves, twill weaves up to 13 harnesses, satin weaves up to 10 harnesses and basket weaves up to 8 ends [23].

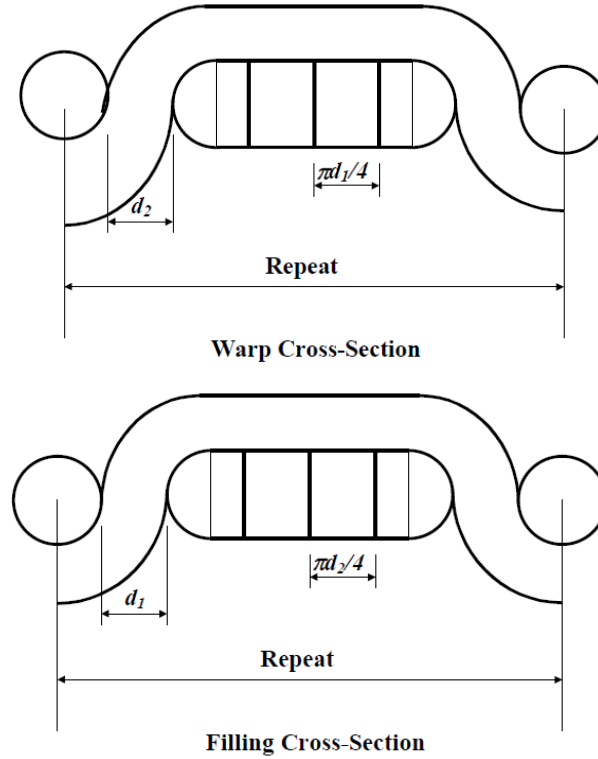


Figure 13 Seyam and Elsheikh’s geometry of woven fabric, warp C.S. (left), and filling C.S. (right) [23]

The structural parameters of the woven fabric could be derived from these geometric theories, and by combining the structural parameters with the yarns properties, the mechanical behavior of the woven fabric could be predicted. Thus, understanding the effect of fabric geometry on its mechanical properties is a prerequisite for developing fabrics with the right combination of engineering characteristics.

2.1.2. Modeling the load-extension behavior of woven preforms

There are two common approaches used to analytically model the load-extension behavior of woven fabrics, one is the energy approach, and the second is the force approach. However, this section will only cover the work of Kawabata et al. and Sun et al. which is based on the force approach, which is more relevant to this research work, and it’s considered the foundation for the proposed model.

In 1973 Kawabata et al. developed a model to predict the load-extension behavior of 2D plain and 2x2 twill woven fabric, using finite-deformation theory, where the yarns are represented as straight line segments [24-26]. The parameters considered in this model, are the lateral yarn compression, and the measured nonlinear yarn tensile properties. However, this model didn't consider the effect of yarn bending stiffness, which was introduced later as an improvement to the model [27]. This model could accurately predict the properties of plain woven fabric, if the correct yarn properties are used. Later, Kawabata et al. applied a method of analysis, to predict the uniaxial and biaxial tensile behavior of plain woven fabrics subjected to large deformations [24-26].

The unique advantage of this model is that it's nonlinear and it could predict the entire load-extension curve of the plain woven fabric, from small strains region to the finite deformation region near the breaking strain. This model is partially based on an empirical approach, which rely on measured yarn properties to predict the load-extension properties of woven fabric which is nonlinear in nature, and that's why this approach is more realistic than other approaches.

In 1995 Sun et al. [28] proposed a generalized model, based on Kawabata's work. The model is also simple and can predict the entire load-extension curve of any woven fabric. Sun et al. adopted the simple straight line geometry used by Kawabata as shown in Figure 14, and despite that it doesn't simulate the actual geometry, but it still predicts results that are in good agreement with experimental values.

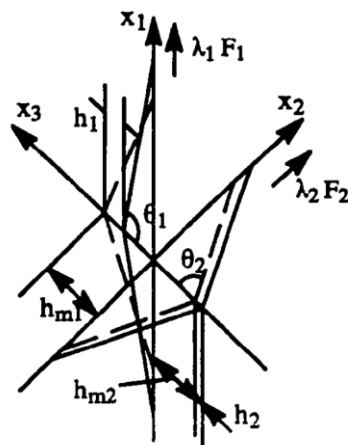


Figure 14 Straight lines approach used to represent the woven fabric used by Sun et al. [28]

Kawabata's work was limited to plain weave and 2x2 Twill weave, thus one of the important modifications that Sun et al. did to this model, was generalizing it to be applicable to any weave construction and degree of tightness. The model included a factor that represents the weave and considers the yarn interlacing. The model also considered hybrid woven fabric comprising, more than one kind of warp or filling yarn, as well as variable thread spacing as shown in Figure 15 and 16. They also considered 2 modes of loading, uniaxial and bi-axial loading.

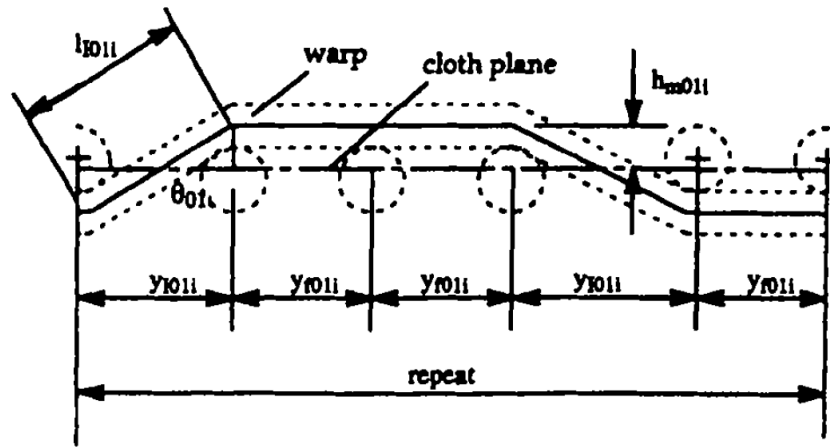


Figure 15 Repeat of one yarn structure in the warp direction [28]

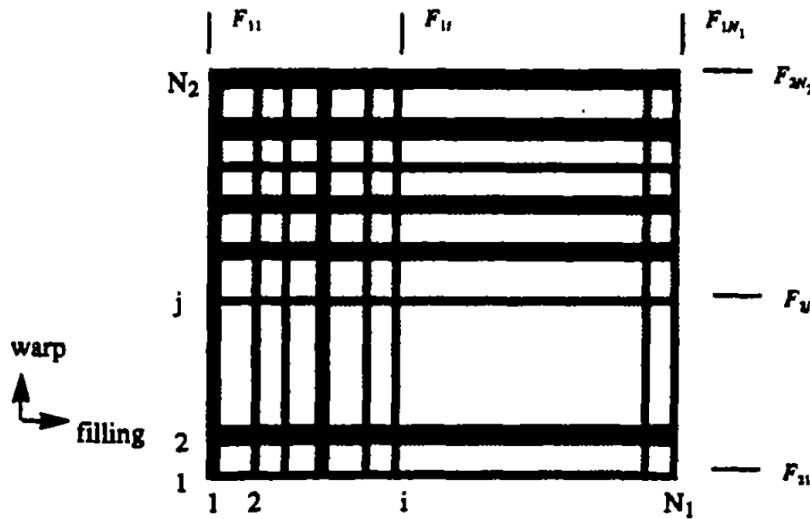


Figure 16 Schematic diagram of one construction repeat of a woven fabric [28]

Under tensile loading, the model considers two kinds of unit structures. Unit structure A which is the inclined portion, and unit structure B, which is the straight portion (float), while taking into account the interlacing pattern as shown in Figure 17. By computing the load-extension curve for unit structure A, given the local fabric stretch ratio λ_{1i}^A , the fabric tensile force per thread F_{1i} is obtained. Afterwards, the load-extension curve of unit structure B is determined, and hence the load-extension curve of the fabric can be computed.

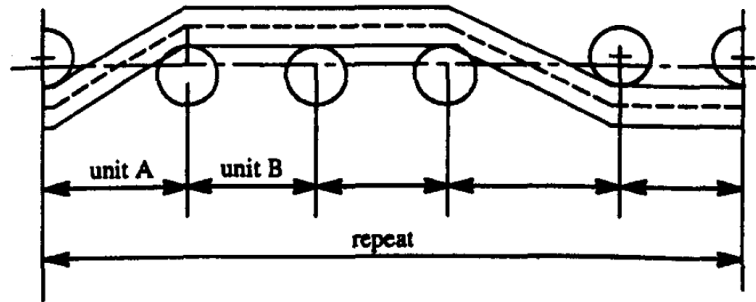


Figure 17 Repeat along the warp axis, showing unit structures A and B [28]

Sun et al. model was verified experimentally, and the predicted results were in great agreement to the experimental values. Despite that this model was very successful in generalizing Kawabata's model to be used in predicting the load-extension properties of literally any kind of woven fabric, yet this model is limited to 2D woven structures, and cannot be used to predict the mechanical behavior of 3D woven preforms, unless it's properly modified. Modifying this model involves, defining the geometry and structural parameters of the 3D woven preform, as well as applying new assumptions that match the nature of such preforms. Once modified, this model can be used in conjunction with the rule-of-mixture to predict the tensile behavior of the composite material reinforced with such preforms. This will be covered in more details in the model proposed in this research.

2.1.3. Modeling mechanical behavior of 3DOW composites

Over the past years there have been a significant amount of models that were developed to analyze the mechanical behavior of 3D orthogonal woven (3DOW) composites. Each model had its own limitations in characterizing the mechanical behavior of such unique material. This

section covers the different analytical models that were developed to predict the elastic and strength properties of the 3D woven composites under tensile loading.

Analytical models are mostly based on classical laminate theory and/or predictive models for 2D woven composites. They are very useful for simple geometries and can be used for quick prediction of mechanical behavior, which means that a full parametric study of different design iterations can be done in a relatively short time, to illustrate the effect of the fabric architecture and the constituent yarns' properties on the behavior of the final composite material. This feature is unique to analytical model, and is an advantage over Finite Element Analysis (FEA) models, despite that FEA models are powerful in defining complex shapes and deformations, yet it's computationally intensive and requires a very long time to run the analysis. This means that FEA will not be practical when doing a parametric study.

The classical laminate theory is a widely used approach to predict the elastic properties of inhomogeneous, anisotropic, materials such as 2D and 3D woven composites. The Classical Laminate Theory (CLT) along with other theories such as the rule-of-mixtures, represent the foundation for many of the modeling approaches that will be discussed later in this chapter. In the CLT approach the elastic properties of the composite are based on the relationship between the stresses and the strains, and the material is assumed to be linear elastic, which means that the reaction due to loading is a linear function of the loading, Equation 1 [29].

$$\sigma_{ij} = c_{ijkl} \epsilon_{kl} \quad (1)$$

Where σ_{ij} and ϵ_{kl} are the tensors of stress and strain respectively, and C_{ijkl} is the stiffness coefficients.

Similarly, Equation 2

$$\epsilon = s_{ijkl} \sigma_{kl} \quad (2)$$

Where S_{ijkl} are the compliance coefficients. Since the tensors of the stress and strain are symmetric, therefore 21 of the 81 stiffnesses and compliances are independent. This number of independent constants can be further reduced if there are other symmetries in the material, such as in the case of orthotropic unidirectional lamina the number of independent constant is

reduced to 9. The reduced stress–strain relationship for an orthotropic system is represented in Equation 3 [29].

$$\begin{pmatrix} \sigma_{11} \\ \sigma_{22} \\ \sigma_{33} \\ \tau_{23} \\ \tau_{31} \\ \tau_{12} \end{pmatrix} = \begin{pmatrix} c_{11} & c_{12} & c_{13} & 0 & 0 & 0 \\ c_{21} & c_{22} & c_{23} & 0 & 0 & 0 \\ c_{31} & c_{32} & c_{33} & 0 & 0 & 0 \\ 0 & 0 & 0 & c_{44} & 0 & 0 \\ 0 & 0 & 0 & 0 & c_{55} & 0 \\ 0 & 0 & 0 & 0 & 0 & c_{66} \end{pmatrix} \begin{pmatrix} \epsilon_{11} \\ \epsilon_{22} \\ \epsilon_{33} \\ \gamma_{23} \\ \gamma_{31} \\ \gamma_{12} \end{pmatrix} \quad (3)$$

Where γ is the shear strain, τ is the shear stress, σ is the tensile stress and ϵ is the tensile strain. Similarly, the compliance matrix can be given as Equation 4.

$$\begin{pmatrix} \epsilon_{11} \\ \epsilon_{22} \\ \epsilon_{33} \\ \gamma_{23} \\ \gamma_{31} \\ \gamma_{12} \end{pmatrix} = \begin{pmatrix} s_{11} & s_{12} & s_{13} & 0 & 0 & 0 \\ s_{21} & s_{22} & s_{23} & 0 & 0 & 0 \\ s_{31} & s_{32} & s_{33} & 0 & 0 & 0 \\ 0 & 0 & 0 & s_{44} & 0 & 0 \\ 0 & 0 & 0 & 0 & s_{55} & 0 \\ 0 & 0 & 0 & 0 & 0 & s_{66} \end{pmatrix} \begin{pmatrix} \sigma_{11} \\ \sigma_{22} \\ \sigma_{33} \\ \tau_{23} \\ \tau_{31} \\ \tau_{12} \end{pmatrix} \quad (4)$$

The compliance matrix can be written in terms of engineering constants E_{ii} , ν_{ij} and G_{ij} , where E is the modulus of elasticity, G is the shear modulus and ν is the Poisson's ratio for transverse strain, as shown in Equation 5 [29].

$$\begin{pmatrix} 1/E_{11} & -\nu_{21}/E_{22} & -\nu_{31}/E_{33} & 0 & 0 & 0 \\ -\nu_{12}/E_{11} & 1/E_{22} & -\nu_{32}/E_{33} & 0 & 0 & 0 \\ -\nu_{13}/E_{11} & -\nu_{23}/E_{22} & 1/E_{33} & 0 & 0 & 0 \\ 0 & 0 & 0 & 1/G_{32} & 0 & 0 \\ 0 & 0 & 0 & 0 & 1/G_{31} & 0 \\ 0 & 0 & 0 & 0 & 0 & 1/G_{12} \end{pmatrix} \quad (5)$$

In 1994 Nagai et al. [30] developed an analytical model to predict the elastic properties of 3DOW composites based on the rule-of-mixtures. Their model used a unit cell of 3D anisotropic space, in which the material properties differ according to the orientation direction. This unit cell is then composed of infinitesimal volume elements, which represent each point inside this 3D anisotropic space as illustrated in Figure 18. Each infinitesimal volume element could either represent a fiber, matrix, or void, which are then averaged over the whole unit cell,

to be able to determine the elastic properties in the three orthogonal directions using the rule-of-mixtures, given the elastic properties of the constituents. Nagai et al. compared the predicted results of their model to the experimental results, and found that there was a good agreement between the results. However, their model was specific to the given weave architecture and cannot be generalized to include different weave constructions.

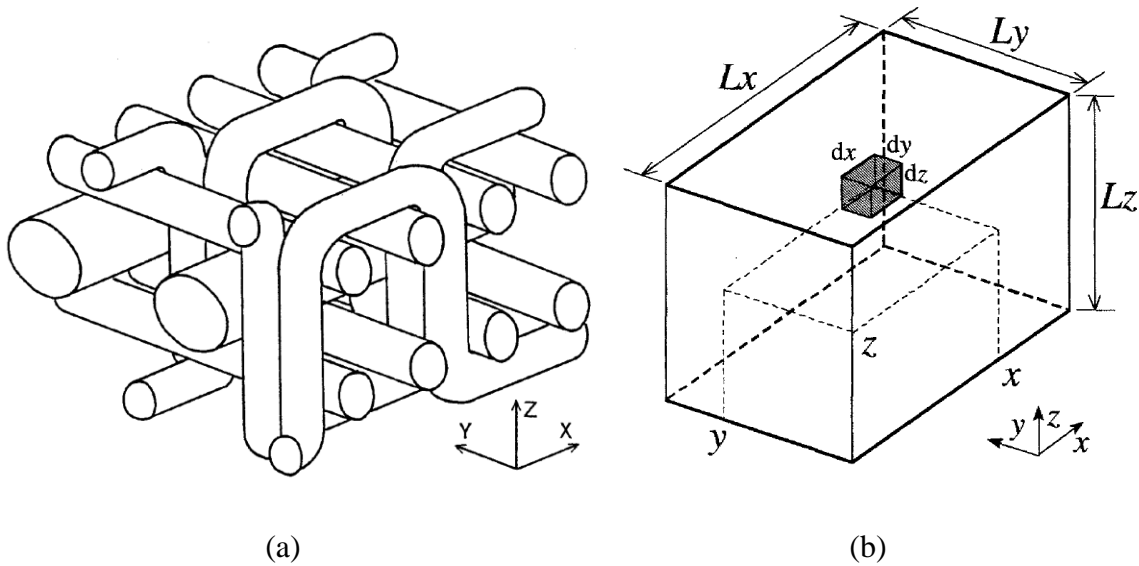


Figure 18 Nagai et al. unit cell (a) 3DOW constituents, (b) Infinitesimal volume element in the 3D anisotropic space. [30]

In the late 70's Kregers et al. used the so called Orientation Averaging (OA) method to determine the elastic properties of 2D and 3D composites based on a representative body approach. The model divides this representative body into smaller volume elements based on their tow orientation, to be able to treat these volume elements as a transversely isotropic unidirectional lamina. Afterwards, the elastic properties of the composite can be calculated by volume averaging the behavior of the representative body, while assuming either iso-stress or iso-strain condition. The predicted results of this method were greater than the experimental results, since it didn't account for tows undulation associated with using woven preforms [31, 32].

In 1995 Cox and Dadkhah [33] modified the Kregers orientation averaging (OA) model to be used for 3D textile composites, with 3DOW composites as an application as shown in Figure

19. The authors introduced the undulation of the warp and filler tows, while considering a stiffness knock down factor η of the Z- or binder tows to account for the degradation resulting from the tow waviness. However, the authors found that the undulation of the warp and filling tows are insignificant when compared to that of the binder tows, thus they decided to neglect it, and considered the warp and filling tows to be straight. The model incorporates the knock down factor as follow, when a composite is loaded in the fiber direction the elastic constants E_1 and ν_{12} will change to ηE_1 and $\eta \nu_{12}$. Afterwards, the elastic constants are volume averaged using the OA method assuming either iso-strain or iso-stress condition. The predicted results from this modified model were significantly improved over Kregers OA method, however neglecting the z-tows may not be justified for structures with out-of-plane performance. In the latter case the z-tows are significant in number and/or linear density.

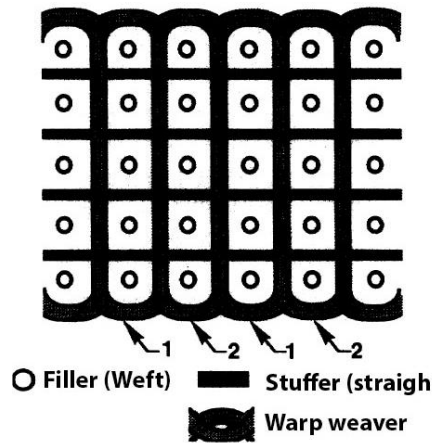


Figure 19 Cox and Dadkhah 3DOW composite geometry [33]

In 1997 Kou and Pon [34] developed an analytical model based on the classical laminate theory to obtain the elastic constants of 3DOW composites. In their model they assumed the tows within the unit cells to be undulated oriented solids as illustrated in Figure 20, taking into account one-dimensional stress concentration and strains thereof $\epsilon_x(x)$, $\epsilon_y(y)$, $\epsilon_z(z)$. They further assumed that there is no coupling between shear and normal stresses, and used an averaging approach to include the Poisson's ratio effect. From the geometry and the stiffness constants of the constituent tows, they calculated the normal strain functions $\bar{\epsilon}_{ij}$ from the global applied stresses at the force equilibrium state. Afterwards, the global strain could be calculated

in any specific direction, by simply averaging the normal strain functions over the unit cell dimensions. Hence, the stiffness and compliance matrices of the composite can be obtained from the global applied stress and strain vectors, and consequently the global elastic constants of the composite. The predicted Young's moduli were lower than the experimental results, and as the undulation factor $\frac{\lambda_i}{L_i}$ increased the predicted Young's moduli decreased and the difference between the predicted and the experimental values became bigger. Also, averaging the strains over the unit cell is not very accurate, especially when using tows of different fibers or linear densities.

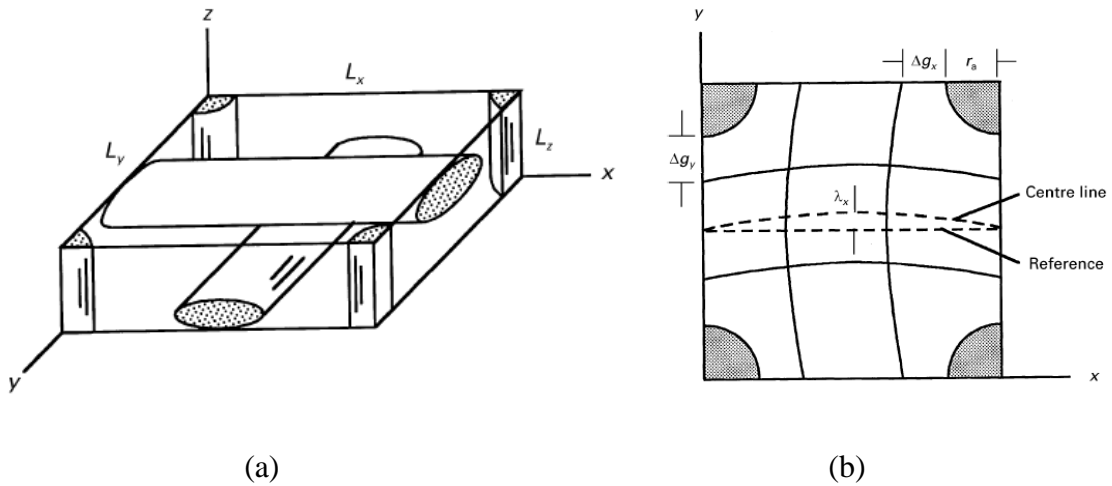


Figure 20 Kou & Pon unit cell for 3DOW composite (a) Straight yarns, (b) undulated yarns [34]

In 1997 Tan et al. [35, 36] proposed a range of analytical models to define the elastic behavior of 3DOW composites in the 3 orthogonal directions x , y , and z , with the names; the X-model, the Y-model, and the Z-model. These models divided the Representative Volume Element (RVE) into micro blocks, where N^A and N^B are assemblies of micro blocks A and B, respectively, in the x , y , and z directions using a mixed iso-stress and iso-strain conditions as illustrated in Figure 21. The constituents inside the RVE which are represented by micro blocks, could either be resin, warp tows, filling tows, or binder tows blocks. Those micro blocks are assembled to calculate the elastic properties thereafter according to the XYZ-model, YXZ-model, ZXY-model, or ZYX-model, which are combinations of the X-, Y-, and Z-

models. For instance, in the YXZ model the micro blocks are assembled in the y-, x-, and z- directions, respectively, according to the Y-, X-, and Z- models. The predicted results are in good agreement with the experimental work, however, the authors didn't mention any preferential conditions for using one model among the others.

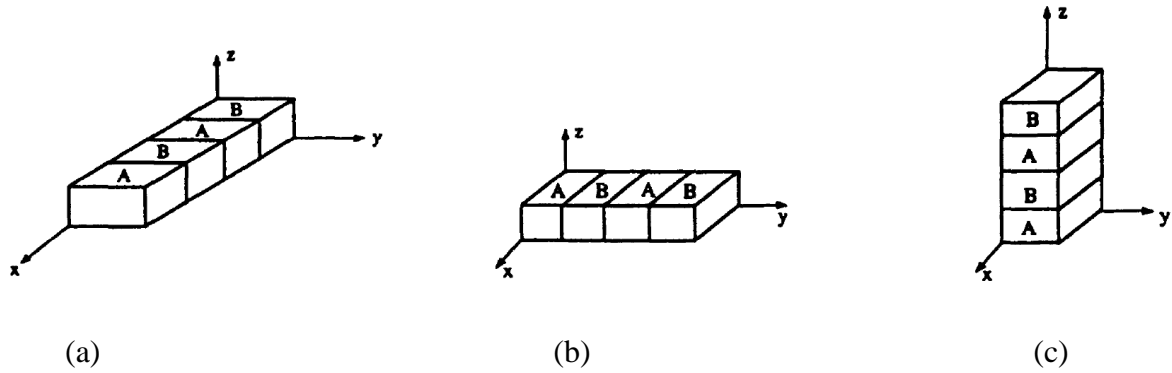


Figure 21 Schematic of Tan et al. (a) X-model, (b) Y-model, and (c) Z-model [36]

In 1999 Yushanov et al. [37] developed an analytical model for predicting the elastic behavior of 3DOW composites, referred to as the generalized modified matrix method, which is based on the modified matrix method developed by Abolnsh [38] in 1996. The proposed model accounts for the anisotropic properties of the composite and the constituent fibers, while considering the composite as a macro-homogeneous medium. From the unidirectional macro-mechanics' point of view, the tows in the i-direction were considered to be embedded in an isotropic matrix, while tows in the j-direction are transversely isotropic in the j-k plane, since they are considered to be embedded in a transversely isotropic matrix. Whereas the tows in the 3-direction has two orthogonal planes of isotropy, i-k and j-k, and are considered to be embedded in an orthotropic matrix. From the aforementioned assumptions, the elements of the compliance matrix are calculated, and further used to predict the elastic response of the 3DOW composite. This method was accurate in predicting the in-plane elastic properties, however the out-of-plane elastic properties were slightly lower than the experimental results.

In 2001 Naik et al. [39] developed a model to predict the elastic and strength properties of 3DOW composites using analytical volume averaging approach, which is similar to the OA approach discussed earlier. The authors discretized the repeating unit cell into sections

perpendicular to the loading direction, and elements in the transverse direction. The elements resulting from the first level discretization could either represent the resin, or the fiber tows in any of the 3 orthogonal directions, furthermore, those elements are discretized again into sub-sections and sub-elements as illustrated in Figure 22 (a). The authors used the iso-strain assumption at the element and sub-element levels, and obtained the unit cell elastic properties from the elastic behavior of the sub-elements by using the elasticity theory. The predicted results of this model was compared to the experimental results of Cox and Dadkhah [33], and it wasn't in good agreement, this is because this model used an idealized geometry as shown in Figure 22 (b).

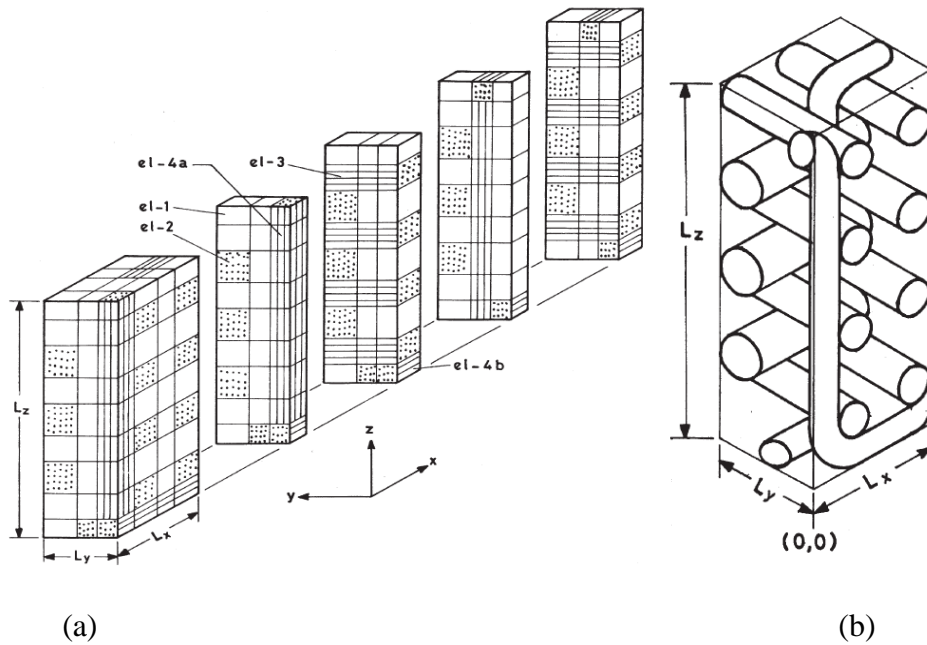


Figure 22 Naik et al. 3DOW composite unit cell for analysis (a) discretization, (b) idealized geometry [39]

In 2002 Wu et al. [40] proposed an analytical model to predict the stiffness of the 3DOW composites, through the discretization of the composite unit cell into orthotropic slices (layers) and then strips (elements) as illustrated in Figure 23. A discretized strip or element, acts like a unidirectional lamina, and is made up of fiber tows and matrix. By assuming either iso-stress or iso-strain condition, the elastic properties of each slice or layer can be calculated from the properties of the elements assembly. Consequently, the elastic properties of the composite unit

cell are obtained from the elastic properties of the slices assembly thereafter. The predicted results were higher than the experimental ones, which could be due in part to the assumption that all tows have rectangular cross sections. In 2010 Buchanan et al. [41] used the same methodology used by Wu et al. to model the elastic response of the 3DOW composites, based on a more realistic geometry of the unit cell, rather than the idealized geometry [42], which yielded a much accurate results, and more agreement with the experimental results.

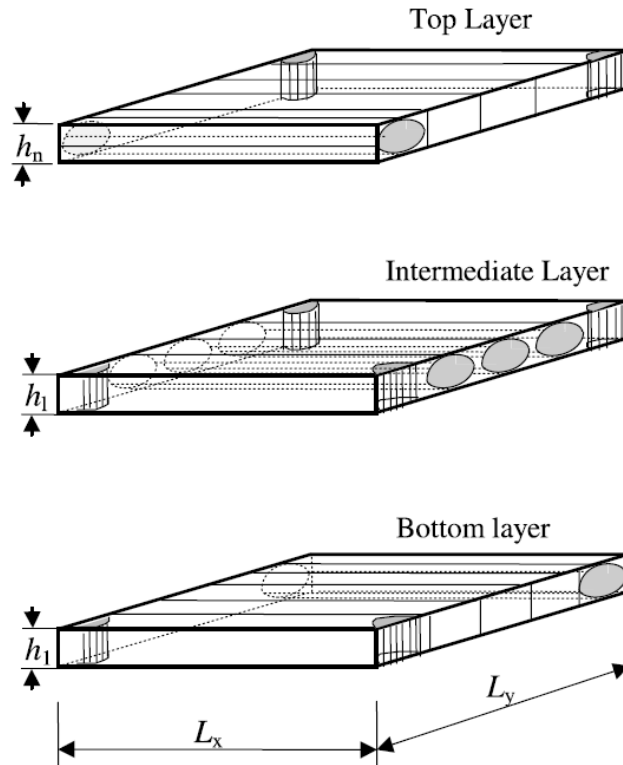


Figure 23 Wu et al. 3DOW composite unit cell discretization [40]

In 2002 Chen et al. [43] developed a model to predict the thermo-elastic response of 3DOW composites at the unit cell level, using an analytical homogenization scheme. This model builds on the work of Tan et al. [36] discussed earlier, the model takes into account the coupling between the thermal and the mechanical behavior in the principal directions. The model divides the unit cell into segments, according to its constituent warp tows, filling tows, binder tows, or matrix as shown in Figure 24. Afterwards, the elastic and thermo-elastic properties could be predicted by assembling the unit cells, according to the X-, Y- or Z-model. The predicted

results from this model were in good agreement with FEA predictions and with experimental data.

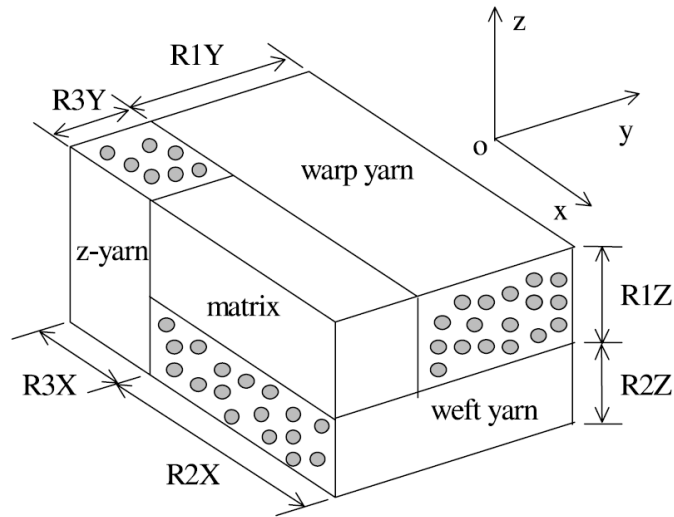


Figure 24 Chen et al. simplified unit cell for 3DOW composite [43]

In 2006 Huang and Abdi [44] presented a general analytical model to predict the stiffness and the strength of 3D textile composites, and used 3DOW composite as an example. The proposed model makes use of a modified laminate theory and OA approach to calculate the elastic properties of the composite. They considered the 3D composite to be a laminate that is made up of a number of plies, and each ply would either represent warp tows layer or a Filling tows layer, with each layer having a portion of the binder tows passing through it. By using the OA approach, the elastic properties of each ply is calculated from the constituent tows stiffness. Afterwards, the global elastic properties of the composite laminate are calculated from the different layers' properties using the modified laminate theory. The authors verified the model experimentally, and the predicted results were in good agreement with the experimental results.

In 2009 Pankow et al. [45] developed a new lamination theory to predict the effective linear elastic extensional and bending stiffnesses of 3D woven composites at the representative unit cell level, with the 3DOW composite as an application as illustrated in Figure 25, assuming iso-strain condition. The proposed model accounts for the undulation of the warp tows, filling tows, and binder tows, as well as other manufacturing induced effects. The model uses the orientation averaging approach to calculate the elastic response of the unit cell based on the

stiffness of the constituents, assuming that each tow is a transversely isotropic linear elastic solid. The model was verified experimentally, showing high correlation between the predicted results and the experimental results. However, this model relies heavily on the accurate determination of the volume fraction of the constituents that require micro-computed tomography (micro-CT) scans, and a finite element model to convert the slices into a 3D model. The micro-CT scanning requirement hinders the potential of this model from being generalized for any weave construction.

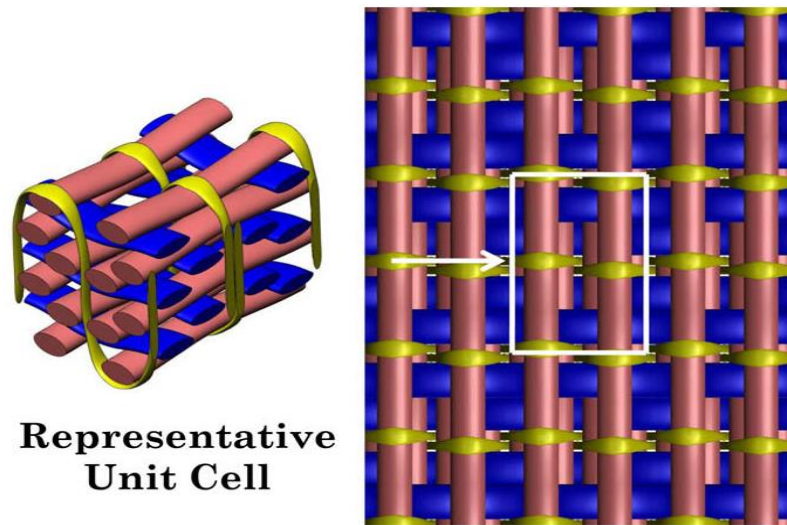


Figure 25 Pankow et al. representative unit cell of 3DOW composite [45]

From the previous review, it was concluded that most of the research work that has been done in modeling the mechanical behavior of 3DOW composites were focused on the linear elastic region, where the 3D composite behaves very similar to 2D laminates. Whilst there hasn't been much work in predicting the behavior in the plastic region where stresses are redistributed and damage accumulation occurs, and the 3DOW composite behaves different from 2D laminates due to the presence of the Z-yarn component. Also, most of the work has been limited to jammed plain woven structures, which hindered the generalization potential of any model to be applied to any woven architecture, whether it's simple weaves or complex weaves to reveal the architecture potential of 3DOW preforms and better understand the effect of the woven architecture on the behavior of the final composite. Moreover, all models were limited to composites with one kind of reinforcing material (i.e. one type of fibers), and failed to meet

the need for modeling hybrid composites with a combination of different fiber types, linear density, spacing, etc.

Thus one of the objectives of this research was to develop a simple analytical generalized model that could predict the entire load-extension curve, including plastic region, and can be applied to any kind of 3DOW reinforcement, with various weave constructions, and material hybridization to reveal the real potential of such kind of reinforcements.

2.2. Effect of the Z-Yarn on the In- and Out-of-Plane Performance of 3DOW Composites

The path of the Z- or binder yarn in the 3DOW composites is usually inclined to the cloth plane in non-jammed structures, or perpendicular to the cloth plane in jammed structures. The orientation of the Z-yarn contributes to the out-of-plane properties; however, this contribution is at the expense of the in-plane properties. Thus, there is a need for optimizing the amount of Z-yarns used, so that the structure would have good out-of-plane strength without compromising the in-plane strength.

The effect of the Z-yarns can be controlled, by either changing the Z-yarn linear density, interlacing pattern, or the amount of Z-yarn in the structure which can also be expressed as the ratio of the Z-yarns to Y-yarns.

In 2000 Leong et al. [46] investigated the effect of Z-yarn path on the tensile properties and failure of 3DOW carbon fiber composite. They used two different structures of 6 warp layers and 5 weft or filling layers, which were woven on a modified hand loom. The Z-yarns path was parallel to the X-yarns path as illustrated in Figure 26. The X- and Y-yarns linear densities were 12 K, whereas the linear density of the Z-yarns was 1 K. The produced preform was then consolidated using Resin Transfer Molding (RTM) method. The 2 woven structures had the same weaving parameters, except for the Z-yarn tension, where the normal structure having slightly higher tension illustrated in Figure 27 (a) showing the binder yarn path with a sinusoidal wave pattern, whereas the modified structure with low Z-yarns tension illustrated in Figure 27 (b) showing the Z-yarns path with more of a square shaped wave pattern. The high tension of the Z-yarns in the normal structure resulted in slight crimping of the warp yarn at the cross over points as illustrated in Figure 28. Leong et al. have tested coupons from the two structures in both the warp and the weft directions, and the results revealed that the normal

structure with the high binder yarn tension, are producing composite with lower fiber volume fraction, and lower tensile properties. The reduced properties of the normal structure were due to the collimation of the top warp tows due to the high tension of the binder yarn, which produced stress concentration regions as well as resin rich regions. The work of Leong et al. has only tackled the effect of the binder yarn path and tension on the in-plane properties, however, they didn't check the effect on the out-of-plane properties. Moreover, the results might not be very accurate, since they used a manual hand loom, without any control over the yarns tension or weft yarns spacing. Additionally, this work is limited to plain weave.

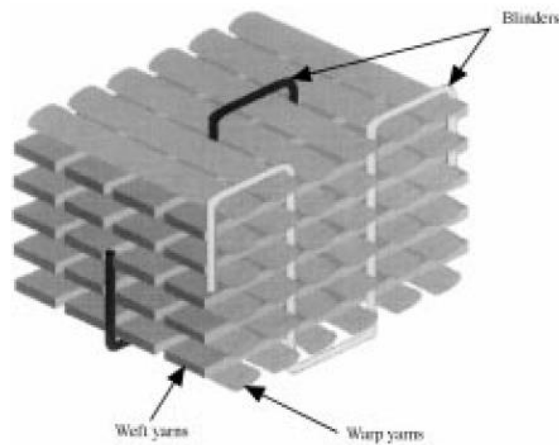


Figure 26 Schematic diagram of Leong 3DOW structure [46]

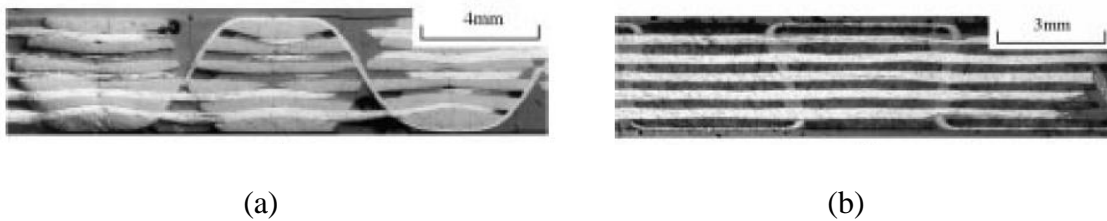


Figure 27 Warp cross sections of the 3DOW performs, (a) normal structure, and (b) modified structure [46]

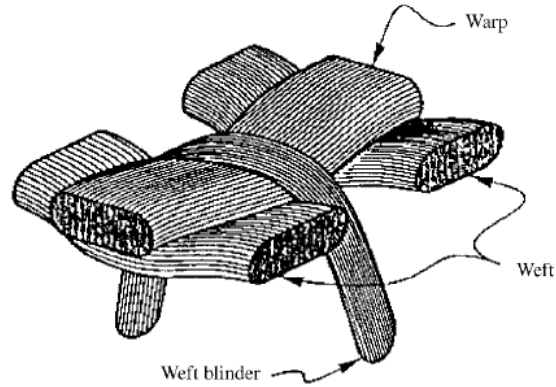


Figure 28 Schematic diagram showing crimping of the warp yarn due to high tension of the binder yarn [46]

In 2009 Rao et al. [47] developed a finite element analysis model to investigate the effect of the Z-yarns on the stiffness and strength of the 3DOW composites, and they used the data available in the literature to verify their model. The structure that was used was a plain woven jammed structure, with the out-of-plane Z-yarns component perpendicular to the cloth plane as shown in Figure 29. The main objective of their study was to include the Z-yarns crowns in their model and to compare it with existing models that didn't account for the crowns. The tow materials were modeled as transversely isotropic, and the matrix was considered as isotropic material, and they used the Tsai-Hill criterion to compute and simulate the composite failure. Rao et al. found that models considering Z-yarns without the crowns (uncrowned) had a knockdown in the longitudinal and transverse stiffnesses, of 16%, and 10%, respectively, and that the properties were similar to 2D cross-ply laminates of stacked in $[0/90]$. Whereas, considering the Z-yarns crowns (crowned) in their model, resulted in a knockdown in the longitudinal and transverse stiffnesses to 30%, and 24%, respectively. The work of Rao et al. was limited to plain woven preforms with jammed structures, and cannot be generalized to include other Z-yarn patterns.

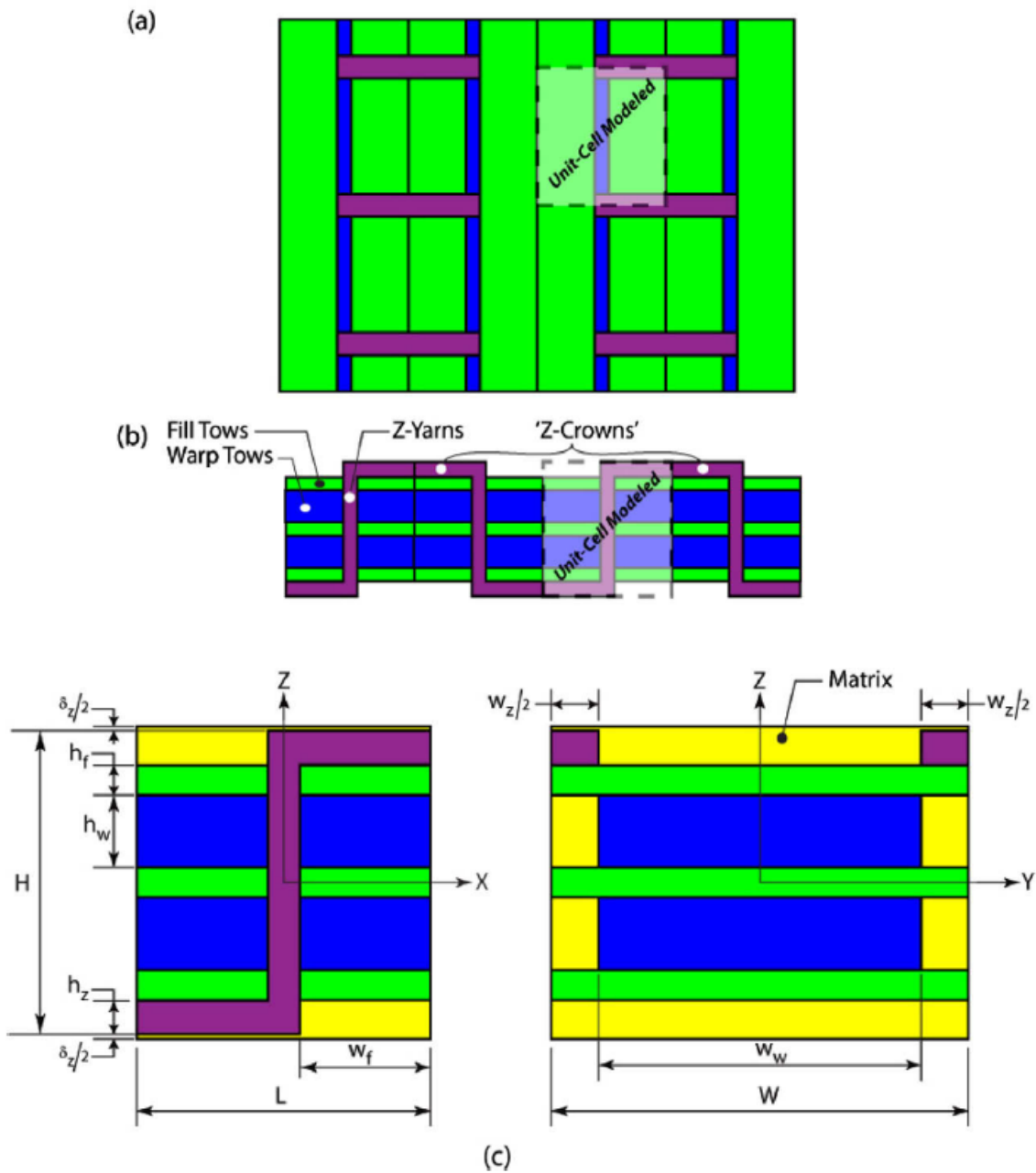


Figure 29 Rao et al. schematic representation of the 3DOW architecture, (a) plan view, (b) front cross sectional view, and the (c) detail of the modified unit cell [47]

In 2010 Mouritz et al. [48] conducted a mechanistic comparison between 3D plain woven, stitched, and pinned structures in terms of the in-plane properties based on a wide range of collated data from published papers, the four structures investigated in their work are illustrated

in Figure 30. Mouritz et al. found that the in-plane static properties of the composites can be increased with respect to the 2D stacked laminate, by using out-of-plane reinforcement such as Z-binder in 3D weaving or stitching, but that was never the case for pinning. Surprisingly, they found that this increase in the in-plane properties is not or weakly dependent on the linear density of the binder component, and they claimed that this increase in properties can be attributed to the compaction or jamming that happens to the in-plane yarn components due to the binder tension, which results in an increased in-plane fiber volume fraction and hence, mechanical properties. On the other hand, they found that there can be a reduction in the in-plane properties within the range of 20% of the 3D woven and stitched composites, which wasn't correlated to the Z-yarn diameter or size. However, in the case of pinned structure the reduction in the in-plane properties is strongly correlated to the pin content and pin size. They related this reduction in strength to the geometric defects, such as fiber crimp and waviness, which result in local softening in the material surrounding the Z-yarn, they also attributed this reduction in properties to micro-structural defects, such as clusters of broken and damaged fibers. Their finding implies that increasing the volume fraction of the out-of-plane binder component in the 3DOW and stitched composites, doesn't necessarily lead to a reduction in the in-plane properties as previously perceived, whereas in the pinned structure increasing the volume fraction of the pin component would progressively decrease the in-plane properties. Mouritz et al. have covered a large body of literature over the past 20 years, however they were not able to do a full quantitative analysis of the defects in 3D woven and stitched composites and correlate those defects with the failure mechanisms of each structure, therefore theoretical prediction of the failure strength of these structures cannot be predicted until this information is available.

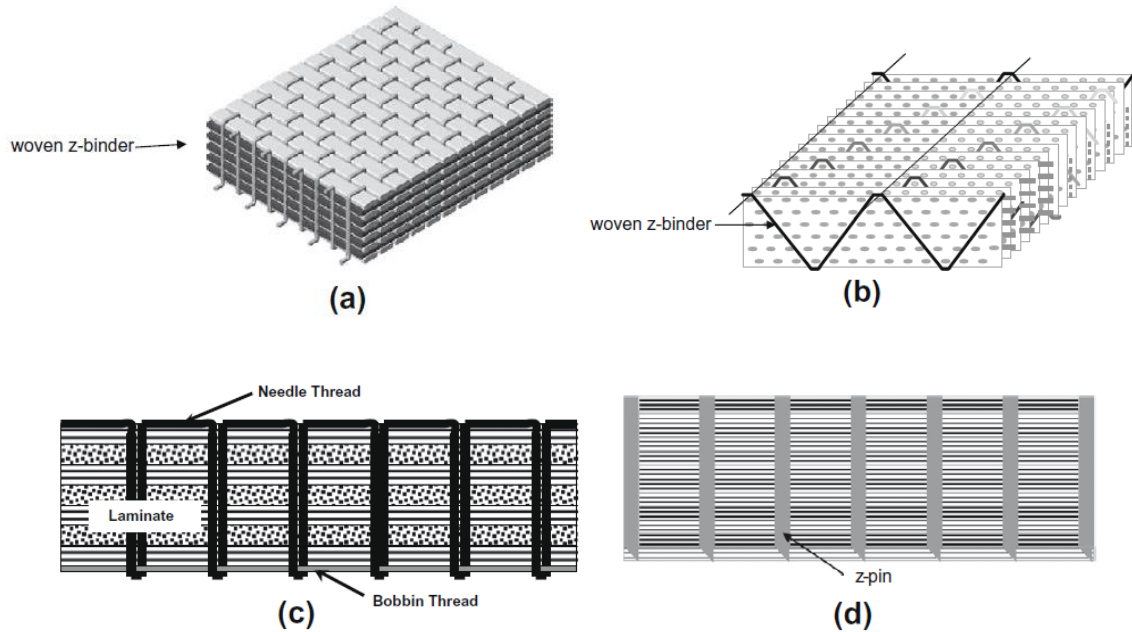


Figure 30 Schematic of the structures investigated by Mouritz et al., (a) 3DOW structure, (b) 3D angular interlock structure, (c) quasi-isotropic stitched structure, and (d) pinned structure [48]

In 2012 Peerzada et al. [49] studied the effect of the binder yarn architecture on the tensile strength of different 3D woven carbon fiber composites in the warp and weft directions. Their study included 3D angular interlock, layer-to-layer interlock, and 3DOW composites as illustrated in Figure 31, the 3 structures were made from the same yarns with almost the same parameters, such as the number of layers, the thread spacing, areal density, etc. to be able to spot the effect of the binder architecture on the in-plane properties of the final composites. They analyzed the crimp and waviness of the 3 yarns components and found that the binder crimp had a significant difference between these 3 structures, with the layer-to-layer interlock having the highest binder yarn crimp as illustrated in Figure 32. They also found that when the specimen is subjected to tensile loading in the warp direction, the warp yarns carry most of the loads, this straightening tendency of the warp yarns will result in stress concentrations at the cross over points of the binder yarns, which might initiate localized damage, even when the level of loading is lower than the ultimate tensile strength of the composite, and this is why fracture always occurs at the cross over points when the structure is loaded in the warp

direction. In addition, the stress-strain behavior of the angle interlock was similar to that of the orthogonal woven in the warp and weft directions, and on the other hand, the layer-to-layer woven structure had higher load carrying capacity in the warp direction, and lowest strain to failure. They realized that crimp plays an important role in the tensile properties of the 3D woven composites, and that if the crimp can be shifted from the load bearing yarns such as the warp yarn, to the binder yarn, then the strength of the structure can be increased, which is the case in the layer-to-layer structure. The work of Peerzada et al. has shed the light on an important structural factor, which is the crimp, however they didn't elaborate on the effect of the crimp within each structure, such as, the effect of different interlacing patterns within 3DOW composites, moreover, they didn't study the effect of the binder yarn architecture on the out-of-plane properties, which is very important in optimizing the overall composite properties.

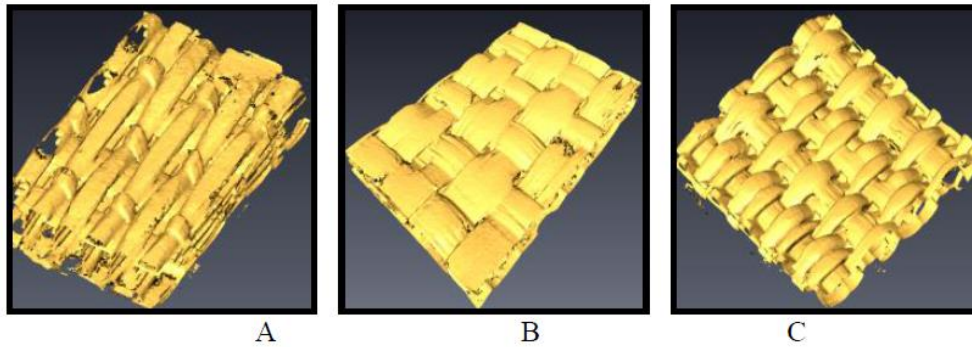


Figure 31 Schematic of different 3D woven structures, (a) layer-to-layer, (b) angle-interlock, and (c) orthogonal [49]

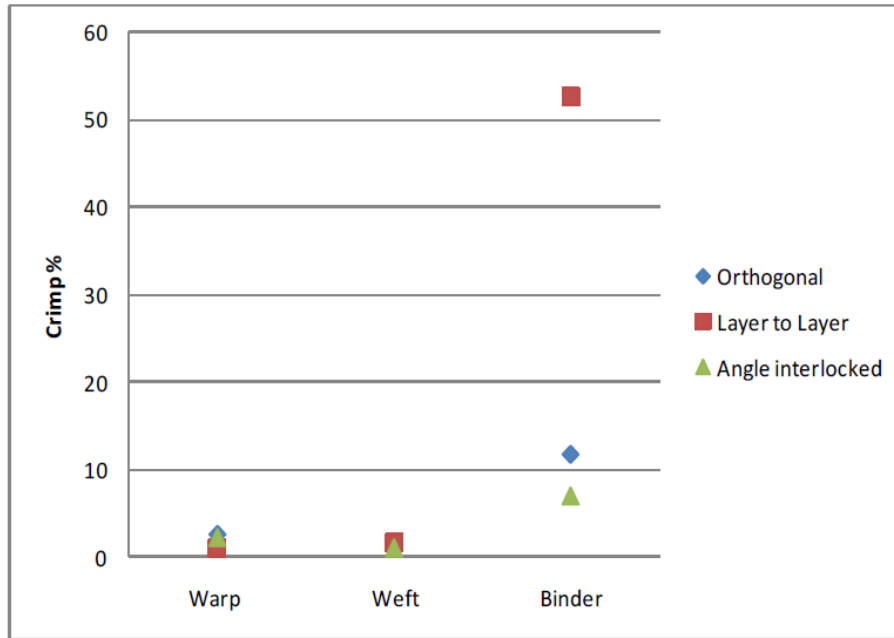


Figure 32 Crimp analysis of 3D woven structures [49]

In 2013 Bilisik et al. [50] studied the effect of weave pattern and number of layers of 3D woven fully interlaced and semi-interlaced structures made of polypropylene tubes of 5 mm diameter and 1mm wall thickness as illustrated in Figure 33. They developed plain, twill and satin representative woven preform structures, and they investigated the yarn-to-yarn spaces, yarns angles, yarns lengths and crimps. They found that the yarn-to-yarn spaces were high for the fully interlaced and semi-interlaced structures, due to the directional interlacements. They also found that the warp, and filling yarns angles or waviness were controlled by the weave architecture, whereas the z-yarn angle is controlled by the take-up rate. What was really special about this research was their study of the Z-yarn crimp of different 3D woven structures, and they found that the crimp in the fully interlaced and semi-interlaced structures were slightly dependent on the weave pattern and number of layers. This research was mostly a geometrical study of preform structures based on different architectural parameters, the authors used polypropylene tubes to illustrate their structures, which they couldn't transform into composite, and thus couldn't do a thorough analysis of the mechanical properties of each structure, which is considered a major limitation of this study.

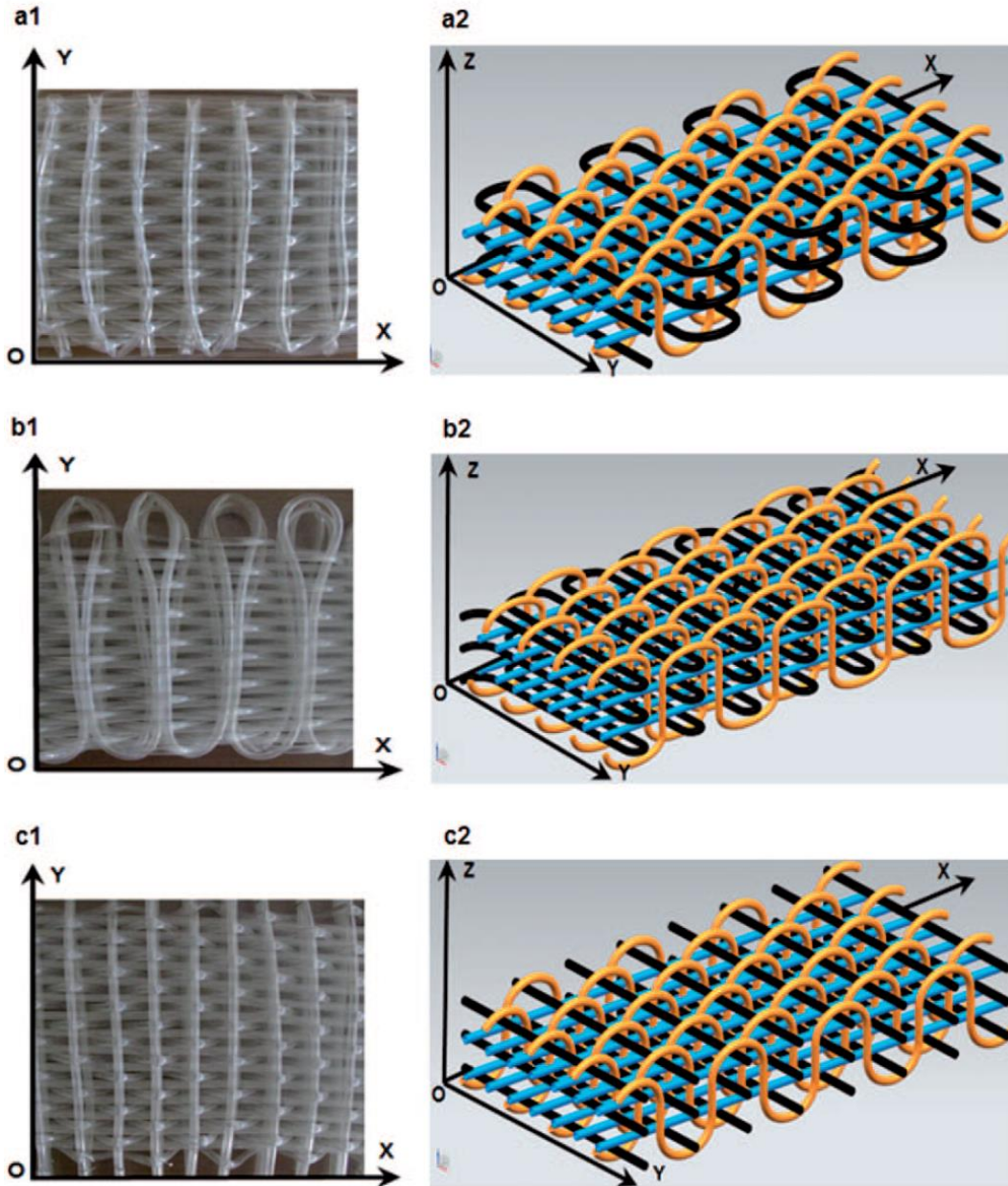


Figure 33 Bilisik et al. 3D woven structures using different insertion mechanisms, (a) pin insertion, (b) shuttle insertion, and (c) single rapier insertion [50]

In 2014 Xu et al. [51] studied the effect of Z-yarn size and density on the interlaminar shear properties of two different 3D carbon/silicon carbide composites made by chemical vapor infiltration. The first structure that was used is a needle punched cross-laid carbon fiber nonwoven with a short cut fiber lamina on the surface, using T300 carbon fibers of 1 and 6 K

as shown in Figure 34, whilst the other structure was made up of several layers of stacked 2D plain woven fabrics, which were stitched with through-thickness stitching yarns using 3K T300 carbon tows as illustrated in Figure 35. The authors found that the yarn size has a negative effect on the SiC deposition during the chemical vapor infiltration, and this effect was more apparent in the Z-stitched composite compared to the needle punched composite. They also found that in the needle punched composite there are three sources of fracture during the interlaminar shear loading, the first one was the short-cut fibers lamina, the second was the 90° ply, and the third source was the 0° ply. It was generally observed that the short-cut fiber lamina is the initial source of fracture, however, by increasing the fiber size the 0° ply fracture was more predominant, which also increased the crack extended path. On the other hand, the 3D stitched composite was found as well to have 3 sources of fractures during the interlaminar shear loading, the first source was the interlaminar region, or the Z-stitching, the second was weft yarn, and the third was the warp yarn. For this structure they found that the interlaminar region is the dominant source of fracture which further propagate to weft and warp fractures as well, and they found that increasing the yarn size increased the SiC densification in the preform, and also increasing the Z-yarn density or spacing will enhance the Z-pinning effect and the SiC densification in the interlaminar region. Thus in general increasing the yarn size increases the interlaminar shear strength of the 3D needle punched composite, and decrease the interlaminar shear strength of the 3D stitched composite, while, increasing the Z-yarn density increases the interlaminar shear strength of both composites. The work of Xu et al. has shed the light on the effect of the Z-yarn on the interlaminar shear strength of the composites, however they didn't study the effect on the in-plane properties which is an important complementary study required for optimizing the properties of the structure.

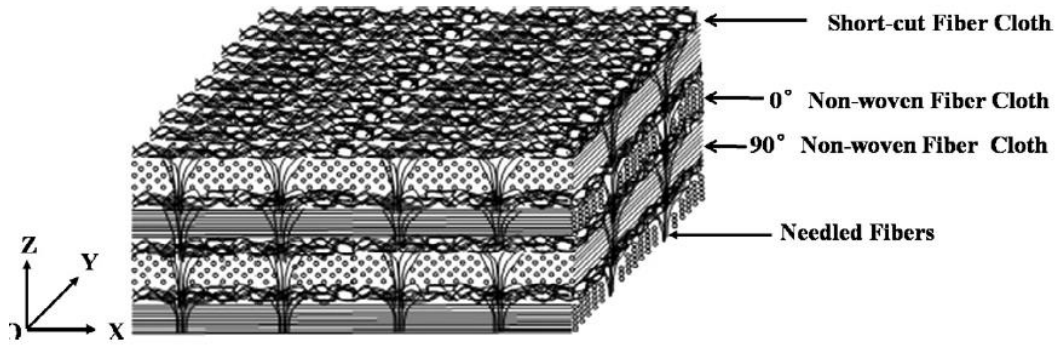


Figure 34 3D nonwoven carbon fiber needle punched web [51]

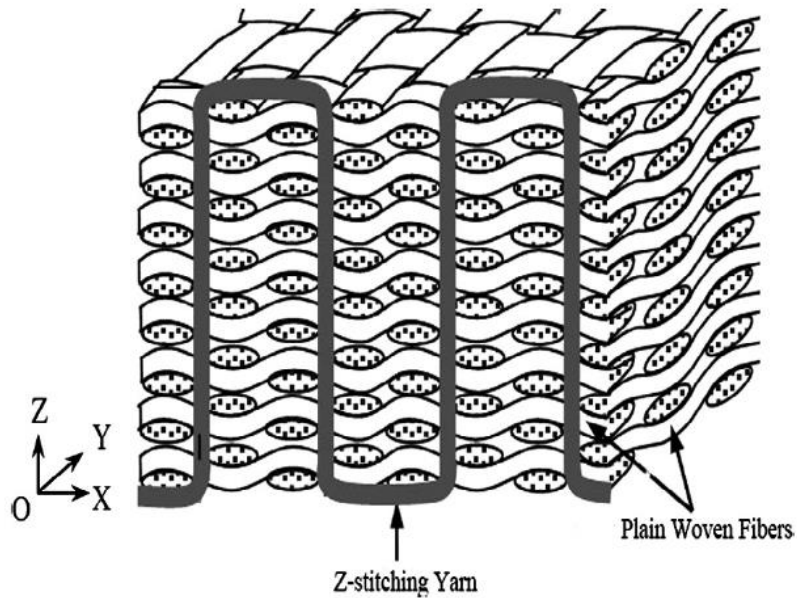


Figure 35 Stacked laminate of multi-layer plain woven preforms, Z-stitched in the through thickness direction [51]

In 2015 Dhiman et al. [52] developed a finite element analysis model to study the Influence of binder configuration on 3D woven composites. They used 2 structures with four warp layers, and same warp and filling yarns, of T700 12k, and 6k respectively, however, the first structure was composed of 3k binder yarn, and the second structure was composed of 6k binder yarn as illustrated in Figure 36. The authors developed a meso-scale finite element analysis model to simulate the properties of the composites under tensile loading, using an idealized geometry

with a hexagonal packing of the carbon tows as shown in Figure 37. They used Abaqus software to model the damage of the composite based on Hashin's and modified Von Mises criterion, whereas the composite stiffness was modeled using a homogenization and volume averaging techniques. They found that the predicted behavior was in a good agreement with the experimental results, with a slight over estimation of the properties due to the idealized geometry of the unit cells being used some of the features of this idealized geometry are the assumption that there is no crimp in the warp and weft tows, and that yarn cross section is constant along the yarn paths, and that there is perfect bonding with the matrix without any voids. They also found that increasing the size of the binder Z-yarn from 3k to 6k, resulted in a knockdown in the tensile strength and stiffness of the composite, since the Z-yarn is considered as the main source of distortion and displacement of the in-plane yarns, and under tensile loading these Z-yarns generates a compressive force at the crossover points with the weft yarns. This compressive force at crossover points force the weft yarns to pack together creating regions of high fiber volume fraction with resin rich regions between them, which is the major site of crack initiation under tensile loading and these findings are in agreement with Peerzada et al.'s [49] findings. Despite that the model that Dhiman et al. developed was verified experimentally and can be considered a relatively accurate model, but still there are many limitations to using such model, one of which is that the model is limited to plain woven jammed structure, also they didn't investigate the effect of the periodicity or spacing of the binder yarn and most importantly, didn't investigate the effect of changing the binder yarn linear density on the out-of-plane properties of the composite.

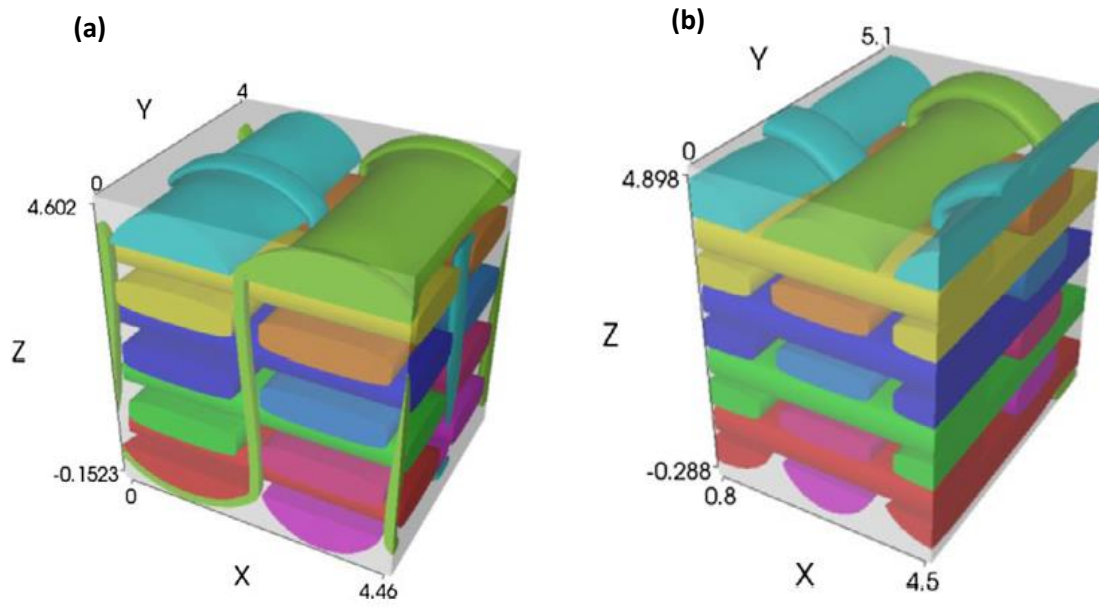


Figure 36 Dhiman representative volume element of 3DOW, (a) structure 1, and (b) structure 2 [52]

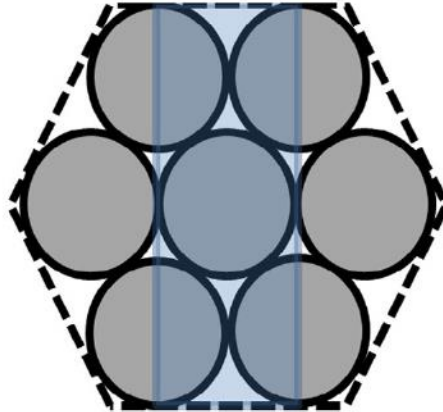


Figure 37 Hexagonal packing of individual fibers within the carbon tows [51]

In 2015 Dai et al. [53] studied the influence of fiber architecture on the tensile, compressive and flexural behavior of 3D woven composites. They used different 3DOW structures, one was a plain weave, and another 3 structures were variant of 3x3 weaves as illustrated in Figure 38. The warp, weft, and binder yarn types were consistent for all structures, further all structures had the same warp and weft yarn spacing, and the binder yarn architecture was the only

variable parameter. The composite produced thereafter was a carbon-epoxy composite using a resin-transfer-molding technique. Based on their experimental observations and analysis, the authors found that a compact binding sequence or architecture such as in plain weave, would result in a reduced waviness of the weft and warp tows, and that if the two adjacent binder tows with long floats have an opposite binding movement, this would result in an increased waviness in the weft tows. And since the waviness of the in-plane tows significantly affects the in-plane tensile properties, thus it was found that the plain weave had the highest in-plane tensile properties. They also found that the crossover points of the binder and the weft yarns are points of stress concentration, and crack initiation. On the other hand, in terms of compression properties it was found that all structures had similar compressive properties, except for W2.1, which had lower bending rigidity due to the waviness for the warp tows. Finally, in terms of delamination, they found that the longer the float of the binder yarn, the more significant the delamination would be, thus reducing the binder float was important to reduce the delamination. The work done by Dai et al. is by far one of the best in terms of investigating the effect of the binder yarn effect on the properties of the 3D woven composites, however they didn't study the effect of varying the amount of Z-yarn on the weft direction and how this would affect the in- and out-of-plane properties of the final composite.

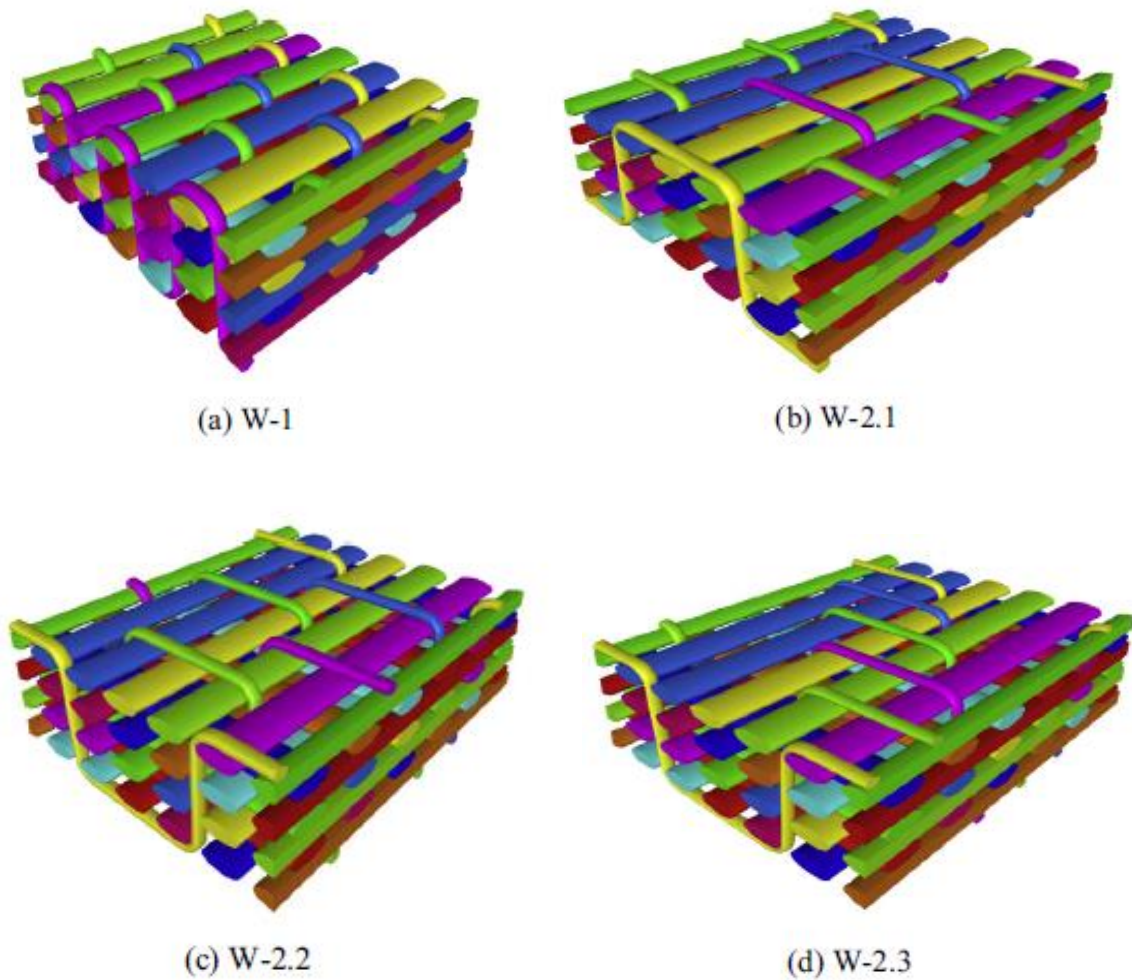


Figure 38 Dai et al. 3DOW structures with varying Z-yarn architecture, (a) W-1 plain 1x1, (b) W-2.1 3x3 weave, (c) W-2.2 3x3 weave, and (d) W-2.3 3x3 weave [53]

From the previous review, it was concluded that the research work that has been done to study the contribution of the Z-yarn on the in-plane, and out-of-plane properties of 3DOW composites are broad and diverse, many papers were comparing between 3DOW composites and other general 3D composites, such as 3D angular interlock composites, 3D needle punched composites, and 3D stacked and stitched composites. On the other hand, papers that were focused on 3DOW composites were mostly studying the effect of varying the Z-yarn thickness or linear density, and for the few papers that studied the effect of changing the Z-yarn interlacing pattern and architecture, they only investigated the in-plane properties. Because of

these limitations, there was a need to make a focused investigation on the contribution of the Z-yarn on the performance of the 3DOW composites, at various Z-yarns levels, and study how it affects the in-plane and out-of-plane properties, to be able to optimize the structure parameters for highest performance. Thus, one of the objectives of this research was to study the effect of changing the amount of Z-yarns in the structure of the 3DOW, and find the optimum Z-yarn to Y-yarn ratio that will give good out-of-plane properties, without compromising the in plane properties.

2.3. Response of 3DOW Composites under Different Modes of Impact and their Relationship

Fiber composites have high specific mechanical properties; this feature is mainly due to the synergy between the fiber and the polymer matrix. However, these mechanical properties can be significantly reduced due to impact. Thus it's important to measure the impact resistance of composite materials in different situations, and further perform post-impact tests to measure the residual properties of the composite.

Impact behavior of composites is sometimes referred to as impact resistance, which have a broad meaning, it may refer to several things, such as; the ability of the material to withstand a blow without damage, the maximum impact force necessary to rupture the composite, or the amount of energy absorbed by a given mass of the composite, etc. [54].

There are different theoretical aspects that need to be considered to understand the test theory, for example the level of impact can be changed by changing either the height of the striker in the machine which changes both the impact velocity and the impact energy, or changing the mass of the striker while keeping the velocity constant. Afterwards the forces generated during the test, the energy absorbed, and the deflection are measured [54].

This section will only cover the out-of-plane impact loading at a speed less than 10 m/s. The impact loading can be induced in several ways, for example, using a striker pendulum, or falling weight. The specimen can be mounted in several setting, for example, it could be simply supported, clamped, allowed to flex or constrained, mounted on compliant fixtures or rigid frames. There are no specific standard impact testing methods for composites, however some

of the standard tests used for plastics are adopted by the composite industry such as ASTM D3029 FA, ISO 6603/2, and BS 2782 [55].

2.3.1. Flexed beam tests

The most common pendulum striking test is the Izod and Charpy, both tests use a swinging pendulum to strike the specimen (beam). In the Izod the specimen is a beam and clamped and struck as a cantilever, while the Charpy the specimen is a simply supported beam loaded in flexure by the striker as illustrated in Figure 39. The specimen can be notched in both tests to be able to break tough specimens [55].

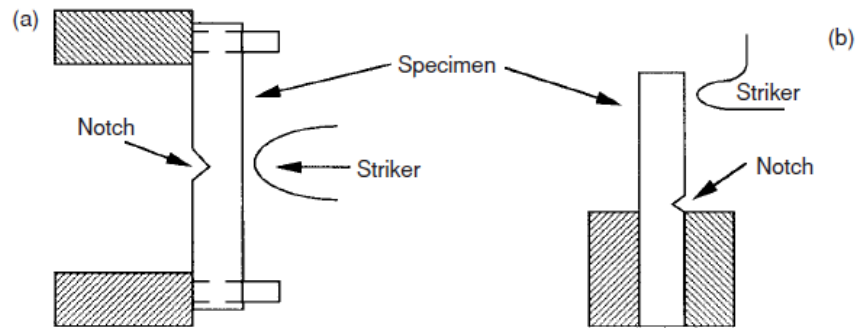


Figure 39 Schematic diagram of (a) Charpy, (b) Izod impact equipment [55]

The tests simply record the energy absorbed by the specimen, which is indicated by the angle the striker moved after striking and fracturing the specimen. The supplied energy can be changed by changing the pendulum starting position, however, most testing equipment have fixed starting positions to maintain constant velocity, so in order to change the supplied energy, the mass of the striker need to be changed. The test can be used to measure the force applied during the test, and consequently recording the strength of the composite under impact. Moreover, the specimen can be notched to measure high rate fracture toughness [55].

2.3.2. Flexed plate impact testing

In the flexed plate impact test, a projectile impacts a plate specimen as illustrated in Figure 40. There is no specific standard testing method used for such test, thus there are flexibility when deciding the specimen dimension and geometry [55].

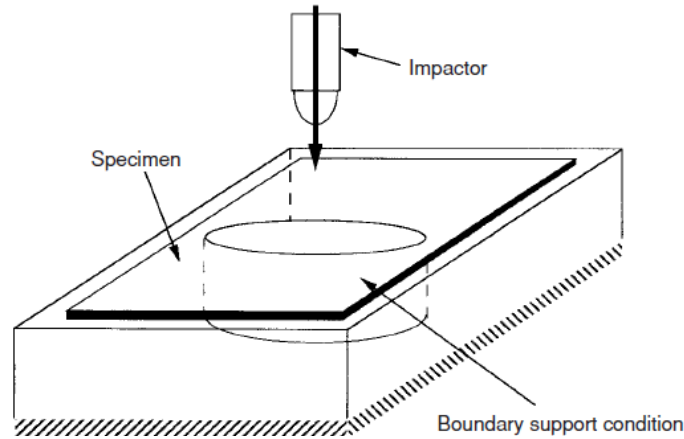


Figure 40 Schematic diagram of flexed plate impact testing [55]

The goal of such test is to measure the ultimate load resistance of the composite material and its energy absorbing capacity, the test also helps in studying the subcritical damage of the composite. The results of the test can be plotted on a force (or displacement)-time diagram and energy-time diagram as illustrated in Figure 16. The most important results of such test are the peak force and the total energy absorbed [54].

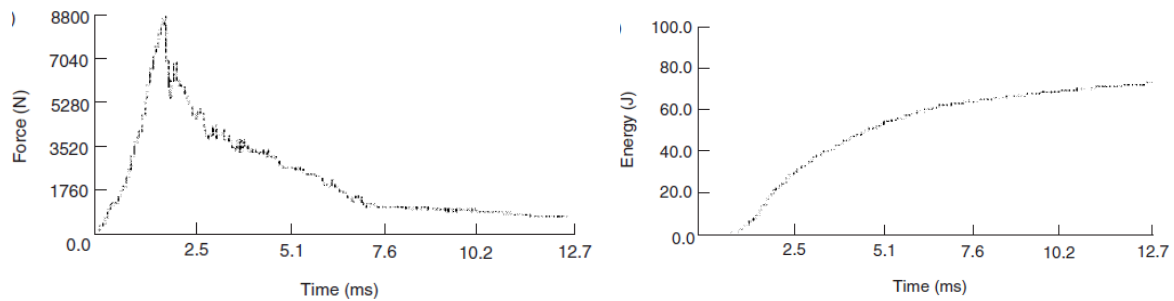


Figure 41 Force-time diagram (left) and energy- time diagram (right) [54]

In the case of high energy test the striker penetrates the plate and cause damage to the specimen. On the other hand, the damage in the low energy and low velocity test may be in the form of delamination, the area of delamination can be measured using a C-scan, and this area should be linked to the energy absorbed or peak force to be able to characterize the composite material [54].

By reviewing the available literature on impact resistance of 3DOW composites, it's found that the drop weight impact is the most popular impact test used in characterizing the impact resistance of composites. The pendulum impact testing is not very common in testing composites, it's mostly used in characterizing plastics and metals. So, if the composite materials are to replace metals and plastics in applications that require high strength and light weight, then, it should be fully characterized with all tests that simulate common failure modes in metals and plastics. Moreover, only few papers were found that did Charpy or Izod impact testing on composites, and only one papers on 3DOW composites [56], and none of the papers studied the correlation between the composites response under different modes of impact.

Thus one of the objectives of this research was to characterize the impact response of 3DOW composites under different modes of impact, namely, Tup, Charpy and Izod, and further study the correlation between the composite responses under these modes of impact.

3. OBJECTIVES

No other process than weaving, can convert sets of yarns into a well oriented and regular structure that meets performance requirements. The weaving process is very versatile, and all structural parameters can be easily tuned to match the requirements, for instance, by just changing one structural parameter, many woven structures can be produced. Any change in warp, filling or binder yarns spacing, yarn linear density, or interlacing pattern produces a new fabric structure. This fabric architecture determines the performance of the preform during the infusion process in terms of resin infiltration, and also determines the overall mechanical properties of the final composite after consolidation. Thus a deep understanding of the fabric architecture and how it affects the mechanical properties of the produced composite is very important.

From the previous review, it was found that most of the research work that has been done in modeling the mechanical behavior of 3DOW composites were focused on the linear elastic region. Whilst there hasn't been much work in predicting the behavior in the plastic region where stresses are redistributed and damage accumulation occurs, and the 3DOW composite behaves different from 2D laminates due to the presence of the Z-yarn component. Also, most of the work has been limited to jammed plain woven structures, which hindered the generalization potential of any model to be applied to any woven architecture. Moreover, all models were limited to composites with one kind of reinforcing material (i.e. one type of fibers), and failed to meet the need for modeling hybrid composites with a combination of different fiber types, linear density, spacing, etc. Secondly, only few papers were found that did Charpy or Izod impact testing on composites, and only one paper on 3DOW composites, and none of the papers studied the correlation between the composites response under different modes of impact. Thirdly, the research work that has been done to study the contribution of the Z-yarn on the in-plane, and out-of-plane properties of 3DOW were mostly studying the effect of varying the Z-yarn thickness or linear density, and for the few papers that studied the effect of changing the Z-yarn interlacing pattern and architecture, they only investigated the in-plane properties. Because of these reasons, the main objectives of the present study are addressed below.

The first objective of the present research was to develop a generalized model to predict the load-extension properties of the 3DOW composites made of spun or filament yarns, using the finite deformation approach. The model relied on the geometry of the structure, and the tensile properties of the constituent yarn components as input parameters, and the output of the model was the entire load-extension diagram of the composite, including the nonlinear regions. The model was generalized to predict the load-extension properties of any non-jammed and jammed 3DOW composite with any weave architecture, including hybrid composites. This model was used to perform a full parametric study to reveal the architecture potential of 3DOW preforms, and show how to optimize the in-plane tensile properties of the composite. The model was verified experimentally for a broad range of experimental composites, including hybrid ones. The model is discussed in details in Chapter 4.

The second objective was to investigate the effect of fabric architecture on the performance of a range of 3D orthogonally woven composites under different modes of impact, namely, Tup, Izod, and Charpy impact. For this purpose, 3D woven preforms were produced by changing the Z-yarn interlacing pattern, number of layers, and weft density. It's possible to produce preforms with the same areal density but different fabric architecture by changing the Z-yarn interlacing pattern. Previous research on 3DOW composites were generally limited to jammed plain weave. In this study, in addition to preforms with plain weave pattern (considered as reference or control), preforms with basket and twill weave patterns were produced with same areal densities and their impact resistances were compared within each mode of impact, and among the different impact modes. The question that was answered in this study is how changing the preform architecture affects the impact resistance of the produced composite, and is there a correlation between the impact resistances of this range of 3DOW composites, under different modes of impact. The composite industry is mostly interested in characterizing the impact performance of the composite based on a drop weight impact (Tup), however it's thought that if the composite materials are to replace metals in more applications, thus it's important to touch on other modes of impact damages that are used to characterize metals, such as Charpy and Izod. A thorough analysis of the impact resistances of the produced panel was done, and based on the findings, the structures with the best performance was recommended for use in the industry.

The third objective of this research was to study the effect of changing the amount of Z-yarns, on the in-plane and out-of-plane performance of the 3DOW composites. The amount of Z-yarns in the structure is reduced in terms of Z-yarn to Y-yarn ratio/y-layer, where the fully interlaced structure have 1:1 ratio, and the non-interlaced structure have 0:1 ratio (or cross-ply). The in-plane performance of the produced composite was measured through tensile, while the out-of-plane performance was measured through Tup, Charpy, and Izod impact testing. The output data was thoroughly analyzed in order to optimize the amount of Z-yarns used in the structure, so that the amount of Z-yarns used would provide sufficient interlaminar strength, and delamination resistance through the thickness, with minimal knock down in the in-plane properties. Thus, the question that was answered in this part of the research is: what is the optimum Z-yarn to Y-yarn ratio that will give good out-of-plane properties, without compromising the in-plane properties.

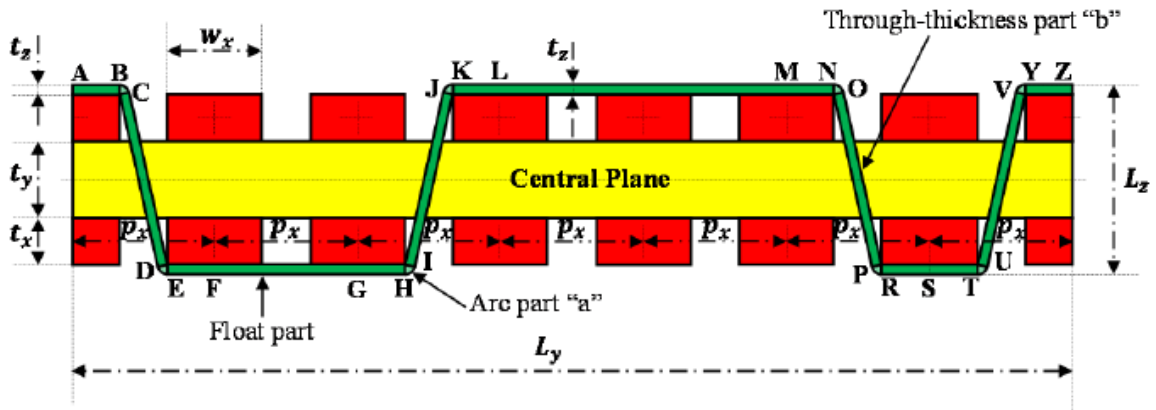
4. GENERALIZED MODEL FOR THE LOAD-EXTENSION BEHAVIOR OF 3DOW COMPOSITES

This chapter was dedicated to develop the theory for a generalized model for the load-extension behavior of 3D orthogonal woven composites, from flat continuous filament as well as spun yarns.

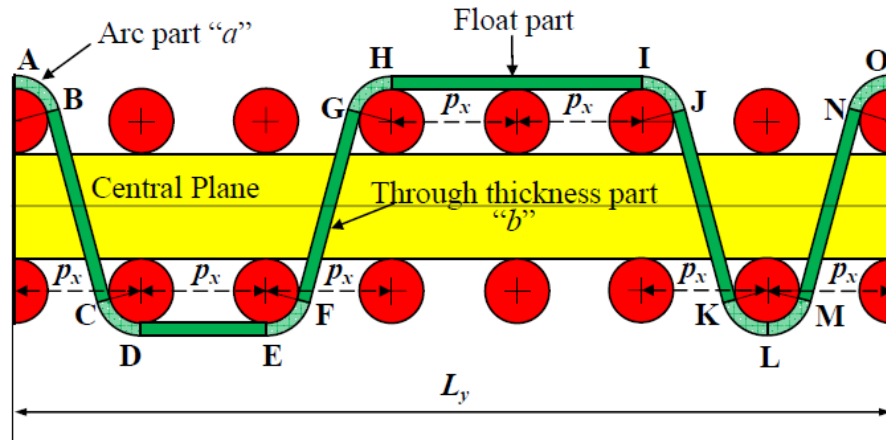
4.1. Generalized Load-Extension Model of 3DOW Preforms

Most of the advanced composite materials are produced from thermoset resin and continuous filament tows, such as glass reinforced epoxy. Flat filament yarns were assumed to have either rectangular or lenticular cross sections [57, 58], which is realistic assumption based on micrographs of 3DOW composites cross section. However, there is an increasing demand for using natural fibers in the reinforcement of Ecofriendly composites, these natural fibers are usually converted into spun yarns by twisting to bind the fibers together by friction, which causes the yarn to be round and as such the assumption of circular cross section for these yarns is valid. From the literature review it was found that most of the previous models were limited to jammed plain woven structures. The lack of research in developing a generalized model was one of the incentives to start this research. The objective here was to develop a generalized model for any 3DOW preforms, to be able to predict its entire load-extension curve under biaxial loading.

The basic approaches used in the proposed model are Kawabata's finite deformation approach [24-26], and Sun et al. generalized model [28], using the geometry of 3DOW preforms defined by Ince [59, 60]. Kawabata's finite deformation approach is simple to use and can predict the entire load-extension curve for plain and 2x2 twill weaves, while Sun et al. generalized model introduced the weave factor and can be used for any woven design, and finally the geometry developed by Ince for 3D woven preforms is simple and is used for rectangular filaments as shown in Figure 42 (a), as well as circular spun yarns as shown in Figure 42 (b).



(a)



(b)

Figure 42 Ince's generalized 3D woven preform geometry of non-jammed structure for (a) rectangular yarn cross section, and (b) circular yarns cross section [59, 60]

The proposed model employs “straight line” geometry to simplify the analytical modeling of the structure. It's designed to predict the load-extension properties over a wide range of deformations, from small strains to strains near breaking values, and it allowed the use of the nonlinear actual yarn properties. The model should predict the performance of 3D preforms of any weave architecture including hybrid, under biaxial loading which resembles the loading in composites.

The geometry of a yarn in any weave could be depicted as straight line segments, some of which are parallel to the cloth plane at yarn floats, and others are inclined to the cloth plane at yarns intersection. The local geometry of an identical unit cell of 2D plain weave used by Kawabata is depicted in Figure 43, which shows the geometry of a warp yarn at a weave intersection [24].

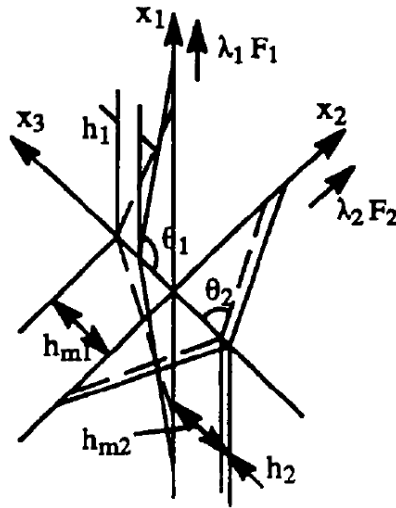


Figure 43 Kawabata's unit structure at weave intersection in the deformed state [24]

4.1.1. Nomenclature

A consistent system of nomenclature representing the 3D woven preforms geometry and tensile properties is listed here. Some of the symbols used are similar to the ones used by Kawabata, Sun et al., and Ince.

P = average yarn spacing in the straight yarn model

T = thread density

N = number of threads in the weave repeat

I = number of intersections in the weave repeat

M = weave factor = N/I

X = X-yarns direction

Y = Y-yarns direction

Z = Z-yarns direction

Θ = angle between the Z-yarn axis and the normal to the cloth plane.

L_I = Z-yarn length at intersection (slanted part)

h_m = distance between fabric neutral plane and yarn at crossover point

h = deflection of the point at which yarn axis intersects the Z-axis due to tensile deformation

n = number of layers

c = Z-yarn crimp

λ_y = stretch ratio of yarn

λ = stretch ratio of fabric along the coordinate axis, which is defined by;

$$\lambda = \frac{\text{length in the stretched state}}{\text{length in unstretched state}} = 1 + \text{strain}$$

F_T = yarn tension

F_c = Compressive force acting along Z-axis at the point of contact of the Z- and X-yarn

F = Tensile force per single yarn end on fabric along the coordinate axis X and Y

f = tensile force per unit fabric length along the coordinate axis X and Y

g_x, g_y, g_z = tensile behavior of X-, Y-, and Z-yarns

$\Phi(F_c)$ = compression of the yarn, which is the function of the normal compressive force

δ_{dZ} = decrease in thickness of Z-yarn due to tensile deformation

δ_{dX} = decrease in thickness of outermost X-yarns due to tensile deformation

$\Psi(P)$ = compressibility of the yarn

w = yarn width

t = yarn thickness

d = yarn diameter

ϕ = yarn packing factor

ρ_l = linear density of yarn (g/km or tex)

ρ_v = volumetric density of yarn material (g/cm³)

F_f = Fiber volume fraction of a yarn

a = arc part length of Z-yarn (cm)

b = through the thickness part length of Z-yarn (cm)

AR = yarn aspect ratio (ratio between width and thickness)

Suffix 0 denotes a value in the undeformed state

Suffix x denotes value of X-yarn

Suffix y denotes value of Y-yarn

Suffix z denotes value of Z-yarn

Suffix i denotes value of the ith X-yarn

Suffix j denotes value of the jth Y-yarn

Suffix k denotes value of the kth Z-yarn

Suffix t denotes total

4.1.2 Geometrical model of general weaves

The assumptions used in this model, includes assumptions used by Kawabata, Sun et al. and Ince [24, 28, 59, 60], in addition to new assumptions that are intended to simplify the analysis and make it suitable for 3DOW composites. It's assumed that during biaxial loading there is no crimp interchange between the Z- and the X-yarns, and that the Z-yarns and the outermost X-yarns are compressible, and that the X-, Y- and Z-yarns are considered perfectly flexible and hence neglecting their bending rigidities.

The X- and Y-yarns follow straight paths within the 3D preform with zero crimp, while the Z-yarns interlace with the X-yarns and follow straight path parallel to the cloth plane at weave floats, and with portions inclined to the cloth plane at weave intersections. It's assumed that the X-yarns spacing under float is equal to the spacing at the intersection. In the case of filament yarns the outermost X-yarns have a lenticular cross section, with height and width equal to that of their rectangular counterparts. As for the case of circular yarn cross section, the diameter of the yarn will be equal to the thickness and width of the yarn, where $d = t = w$.

In the case of 3D orthogonal weaving looms with rapier insertion mechanism, the filling yarn is doubled due to the nature of the mechanism, in this case the filling yarn geometry was treated as a single yarn with double the linear density.

In general, the yarns path in the structure follows straight line segments, but the case of the Z-yarns is slightly different since the Z-yarn segments can be divided into inclining segments at the weave intersections and segments parallel to the cloth plane at the weave float. The yarn length in the unit of the simplified structure is kept the same as that in the actual structure. Then the actual structure is replaced by a simplified model where X-, Y-, and Z-yarns axis are assumed to be straight lines. Figure 44 shows a schematic diagram of one repeat of a woven fabric structure, the X-, Y- and Z-yarns in the repeat could have different properties. A repeat of j^{th} Y-yarn in a 3DOW structure with rectangular yarn cross section is shown in Figure 45 (a) and with circular yarn cross section in figure 45 (b), where X-yarns are in red, y-yarns are in yellow, and Z-yarns are in green.

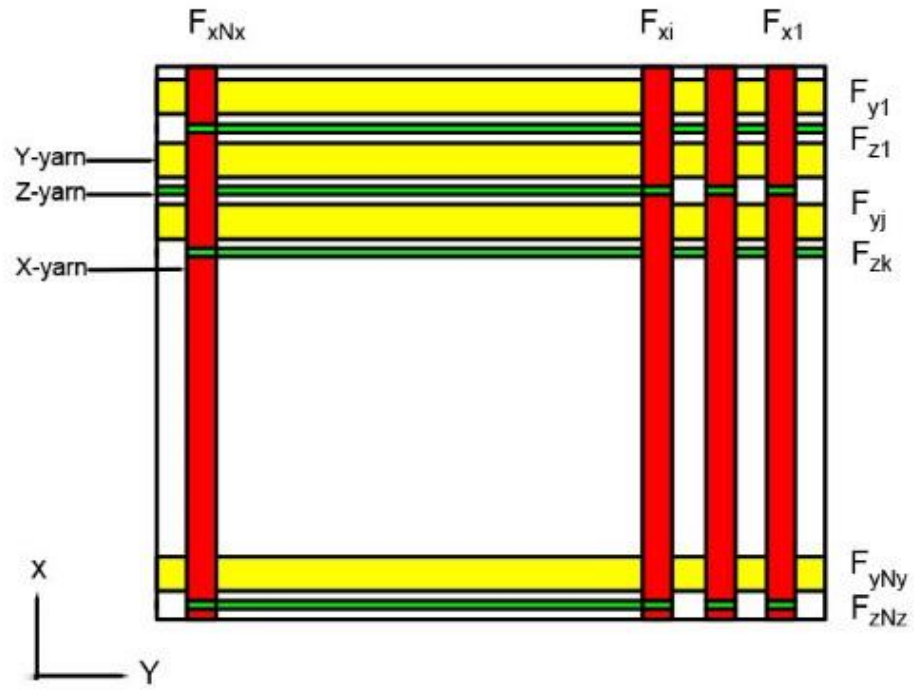
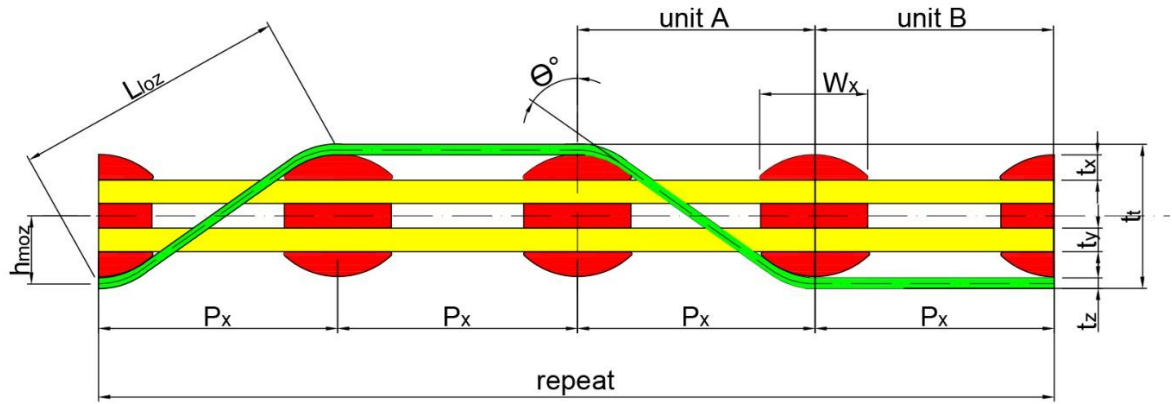
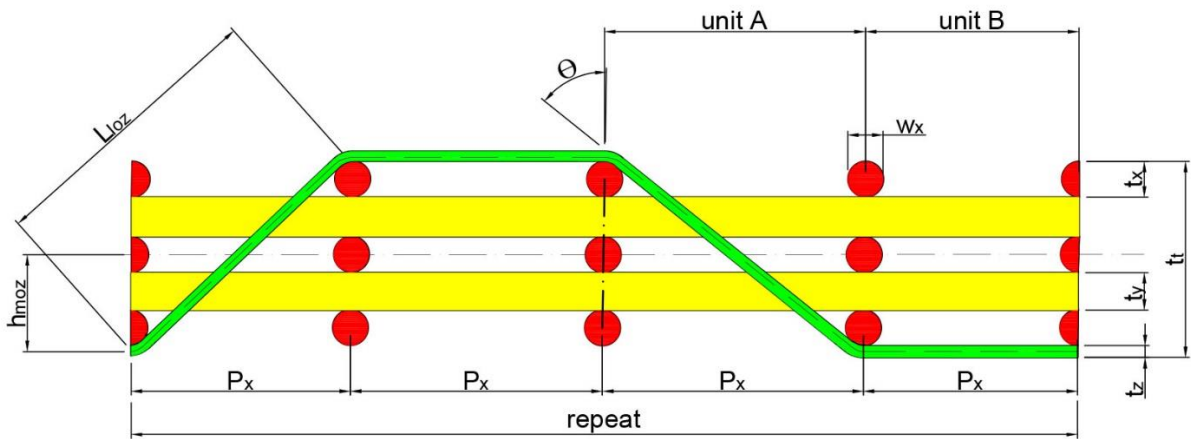


Figure 44 Schematic diagram of one construction repeat of 3DOW preform



(a)



(b)

Figure 45 Repeat of one yarn structure in the Y-direction for (a) rectangular yarn cross section, and (b) circular yarn cross section.

For convenience, the subscripts i , j , and k are eliminated from the symbols in the following equations. The structure in the undeformed state can be described by the following geometrical relationships, using the basic structural constants T_{0x} , c_{0z} , t and n .

$$P_{0x} = \frac{1}{T_{0x}} \quad (6)$$

$$\sin\theta = \frac{P_{0x}}{L_{10z}} \quad (7)$$

$$L_{10z} = \frac{P_{0x}}{\sin\theta} \quad (8)$$

$$c_{0z} = \frac{I_x L_{10z} + P_{0x} (N_x - I_x) - P_{0x} N_x}{P_{0x} N_x} \quad (9)$$

$$t_t = 2t_z + t_y n_y + t_x n_x \quad (10)$$

4.1.3. Computation of load extension properties of general weaves in biaxial loading

In this section the load-deformation behavior of the 3DOW preform can be computed. First, it's required to consider the interlacing point distribution, in order to calculate the properties of a specific weave. This approach is generalized for various interlacing patterns of the Z-yarn, and also for repeats containing different X- or Y-yarns (hybrid).

The repeat unit or the representative unit cell approach was used in this model to determine the load extension behavior of the preform. In this approach the load – extension behavior of one construction repeat containing yarns with different properties will be determined, and the load extension behavior of the entire preform will be determined by multiplying the number of construction repeats within the preform.

Each construction repeat is composed of certain number of X-, Y-, and Z-yarns, the X- and Y-yarns are considered as straight line segments in the preforms. As for the Z-yarn it will be divided into two unit structures A and B. The sum of numbers of unit structures A and B equals the number of X-yarns in the weave repeat. Unit structure A is the slanted or inclined portion of the Z-yarn at the intersection, while unit structure B is the straight portion of the Z-yarn at the float, with respect to the fabric neutral plane as illustrated in Figure 45.

There are three main steps involved in calculating the load-extension behavior of 3D woven preforms in general weaves. The first step is to determine the load-extension behavior of unit structure A at a given local fabric stretch ratio λ_{zk}^A , and obtain the fabric tensile force per Z-yarn end F_{zk} . Secondly, calculate the load-extension behavior of unit structure B, X- and Y-yarns. Thirdly, the load-extension behavior of the woven preform is computed from the behavior of individual units according to the weave pattern.

Load-extension properties of Z-yarns

Figure 46 depicts unit structure A of the k^{th} Z-yarn subjected to biaxial loading. In the following derived equations, the subscript k will be removed for convenience.

When the preform is stretched along the X- and Y-axis by stretch ratios λ_x and λ_{z-y} , four kinds of forces are induced, X-yarn tension F_{Tx} , Y-yarn tension F_{Ty} , Z-yarn tension F_{Tz} , and a compressive force F_c acting on the contact surfaces of the Z- and X-yarns.

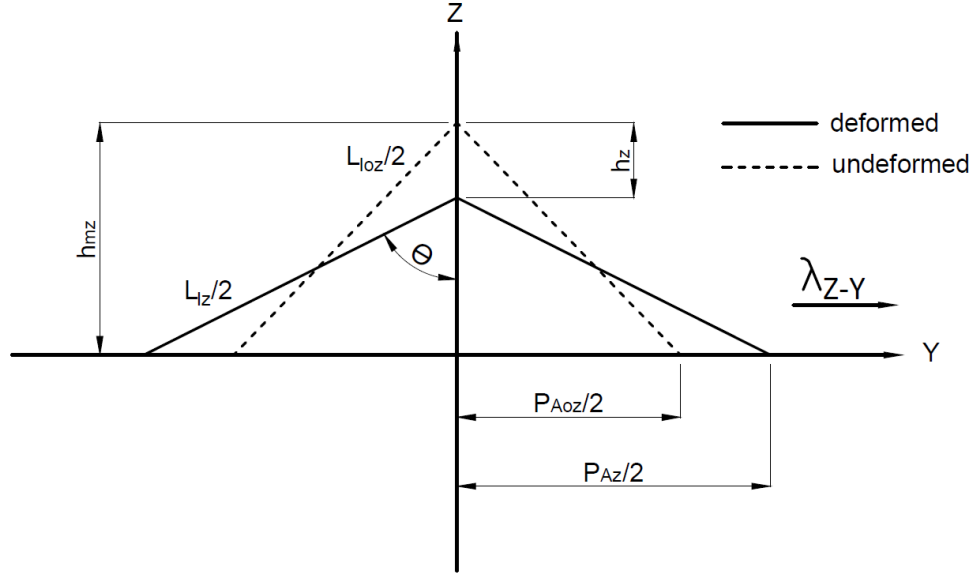


Figure 46 Z-yarn unit structure A subjected to biaxial loading

In the deformed state, the equilibrium Equation 11 must be satisfied. Where $\Phi(F_c)$ represent the compression of the Z-yarns, and the outermost X-yarns, which is a function of the normal compressive force, yet, in case of incompressible flat filament yarns h_z is equal to zero.

$$h_z = \Phi(F_c) \quad (11)$$

This means that when the preform is subjected to biaxial loading there is no crimp interchange, but rather the normal compressive force will result in compression of the Z-yarns, and the outermost X-yarns, where h_z represents the decrease in the preform thickness due to the yarns compression. And the compression of the yarns can be defined by the following equations;

$$\Phi(F_c) = \frac{1}{2} \{ \Phi_z(F_c) + \Phi_x(F_c) \} \quad (12)$$

$$\text{Where, } \Phi_z(F_c) = \delta_{dz} \quad (13)$$

$$\text{And, } \Phi_x(F_c) = \delta_{dx} \quad (14)$$

More details on measuring the compressive properties of the yarns is discussed later.

By analyzing the stresses at the cross over point of the Z-yarn with X-yarn, the compressive force F_c due to the Z-yarn tension can be defined as follow;

$$F_c = 2 F_{Tz} \cos\theta \quad (15)$$

The tensile properties of the yarns are represented by the following function, which is derived from experimental measurements.

$$F_{Tz} = g_z(\lambda_{yz}) \quad (16)$$

The following equations are derived from the geometry in Figure 4.4.

$$\text{Since, } \lambda_{yz} = \frac{L_{Iz}/2}{L_{I0z}/2} \quad (17)$$

$$\cos\theta = \frac{h_{mz}-h_z}{L_{Iz}/2} \quad (18)$$

$$P_{A0z} = P_{0x} \quad (19)$$

$$P_{Az} = \lambda_z^A P_{A0z} \quad (20)$$

$$L_{Iz} = 2 \sqrt{\left(\frac{P_{Az}}{2}\right)^2 + (h_{mz}-h_z)^2} \quad (21)$$

$$L_{I0z} = 2 \sqrt{\left(\frac{P_{A0z}}{2}\right)^2 + h_{mz}^2} \quad (22)$$

$$h_{mz} = (t_z + t_y n_y + t_x n_x)/2 \quad (23)$$

$$\text{Therefore, } \lambda_{yz} = \frac{\sqrt{(\lambda_z^A P_{A0z})^2 + 4(h_{mz}-h_z)^2}}{\sqrt{P_{A0z}^2 + 4 h_{mz}^2}} \quad (24)$$

$$\cos\theta = \frac{h_{mz}-h_z}{\sqrt{\left(\frac{\lambda_z^A P_{A0z}}{2}\right)^2 + (h_{mz}-h_z)^2}} \quad (25)$$

Thus, the compressive force can be represented by the following equations. Notice that the weave factor M is added to the equation to account for general weaves according to Sun et al. [28].

$$F_c = 2 g_z(\lambda_{yz}) \frac{2(h_{mz}-h_z)}{M\sqrt{(\lambda_z^A P_{A0z})^2 + 4(h_{mz}-h_z)^2}} \quad (26)$$

The values of the tensile force on the Z-yarn along the Y-axis F_z , can be derived as follows;

$$\text{Since, } F_z = F_{Tz} \sin\theta = \frac{F_c \sin\theta}{2 \cos\theta} = \frac{1}{2} F_c \tan\theta \quad (27)$$

$$\tan\theta = \frac{P_{Az}}{2(h_{mz}-h_z)} = \frac{\lambda_z^A P_{A0z}}{2(h_{mz}-h_z)} \quad (28)$$

$$\text{Therefore, } F_z = \frac{F_c \lambda_z^A P_{A0z}}{4(h_{mz}-h_z)} \quad (29)$$

In the case of unit structure B, the load-extension behavior is the same as that of the Z-yarn. The yarn stretch ratio λ_{yz} can be determined using the condition that $F_z = F_{Tz}$, and the yarn tensile property $F_{Tz} = g_z(\lambda_{yz})$, and therefore $\lambda_z^B = \lambda_{yz}$.

From the schematic shown in Figure 44, N_x is the number of X-yarns in the weave repeat in one layer, and also the number of unit structure A and B. Since, the stretch ratio in unit A, λ_z^A , is not equal to that in unit structure B, λ_z^B . Therefore, we calculate the average stretch ratio of the k^{th} Z-yarn, λ_{zk} as follow;

$$\lambda_{zk} = \frac{I_x \lambda_{zk}^A + (N_x - I_x) \lambda_{zk}^B}{N_x} \quad (30)$$

In case of using different Z-yarns, the stretch ratio of the Z-yarn in the direction of the Y-axis, λ_z , is the mean value of the extensions λ_{zk} of all N_x units,

$$\lambda_z = \frac{\sum_{k=1}^{N_x} \lambda_{zk}}{N_x} \quad (31)$$

To calculate the total load acting on the Z-yarn ends in the repeat unit, we calculate the load on the k^{th} Z-yarn, and multiply by the number of yarns per weave repeat as shown in the following equation;

$$F_z = \sum_{k=1}^{N_z} F_{zk} \quad (32)$$

Load-extension properties of X- and Y-yarns

In the case of X- or Y-yarns, the load-extension behavior is the same as that obtained from the experimental measurement of the yarn tensile properties, since the yarns are laid straight in the

structure without any crimp, interlacing, or waviness. The yarns stretch ratios λ_{yx} and λ_{yY} can be determined using the condition that $F_x = F_{Tx}$ and $F_y = F_{Ty}$, and the yarns tensile properties $F_{Tx} = g_x(\lambda_{yx})$ and $F_{Ty} = g_y(\lambda_{yY})$.

From the schematic shown in Figure 44, N_x is the number of X-yarns in the weave repeat in one layer, and N_y is the number of Y-yarns in the weave repeat in one layer. Therefore, we calculate the load on the i^{th} X-yarn, and j^{th} Y-yarn, and multiply by the number of yarns per weave repeat per layer N and the number of layers n to get the total load acting on the X- and Y-yarns in the repeat unit as shown in the following equation. This approach can also be used in case of using different types of X and Y-yarns.

$$F_X = n_x \sum_{i=1}^{N_x} F_{xi} \quad (33)$$

$$F_Y = n_y \sum_{j=1}^{N_y} F_{yi} \quad (34)$$

Load-extension properties of the preform

The partial tensile load acting on each yarn end in Y-axis direction, varies from Z-yarn ends to Y-yarn ends, since the interlacing pattern and yarn tensile properties will not be the same. Therefore, the Z- and the Y-yarns should be treated separately. The approach that used is defined by Hamburger in dealing with blended yarns, where the two components bear the load together until the component with the lower extension is ruptured, and then the other component bears the load individually until it ruptures, this is discussed in more details later in this chapter [62]. As for the X-axis direction, the preform load-extension properties are solely dictated by the properties of the X-yarns.

Compression properties of X- and Z-yarns

The yarn compressive properties are determined based on experimental measurements, thus it's more accurate to measure the properties of yarns that have been unraveled from the preform. The compression testing is performed on the Fast-T Compression Meter at the College of Textiles, North Carolina State University. The yarn is held by 2 clamps at a predetermined tension level before starting the compression test. An incremental compressive loading is applied to the yarn using metal weights and the corresponding thickness of the yarn is recorded. The output of the compression test is a load-displacement curve.

Since the compressional properties of the yarns depend on the applied tension, thus two levels of tensions were considered when performing the compression test. The first level of tension is zero which simulate the state of very small deformation, and the second level would be at high tension, to simulate the state of large deformation as described by Kawabata et al. [25]. The compression results from the two tension levels will be averaged for approximation as shown in the following equation.

$$\Psi(P) = \frac{1}{2}[A(P) + B(P)] \quad (35)$$

Where $A(P)$ = the compression of the yarn at zero tension,

$B(P)$ = the compression of the yarn at high tension, and

P = compressive force acting on unit yarn length

By considering the effective length L , defined by Kawabata et al. [25] which in this case is the width of the X-yarn w_x , then $\Phi(F_c)$ can be obtained as follow;

$$\Phi_z(F_c) = \Psi_z\left(\frac{F_c}{L}\right) \quad (36)$$

$$\Phi_x(F_c) = \Psi_x\left(\frac{F_c}{L}\right) \quad (37)$$

However, in case of using incompressible flat filament yarns, the decrease in preform thickness due to compression will be neglected, and h_z will be equal to zero.

4.2. Generalized Load-Extension Model of 3DOW Composites

The purpose of this section was to convert the load-extension curve of the preform into load extension-curve of the final composite. This can be achieved by applying the theory of blended yarns defined by Hamburger [62]. The theory of blended yarns requires knowing the volume fraction of each component, whether it's yarn or matrix, in addition to knowing their load-extension properties. The volume fraction of each component was calculated using Ince's generalized geometrical model of 3DOW composites [59, 60], while the load-extension properties will be calculated according to the proposed model in this research.

4.2.1. Hamburger theory of blended yarns

In this work, Hamburger theory of blended yarn was extended to be used with 3DOW composites. The main objective of Hamburger's theory of blended yarns [62] was to quantify the effect of the fiber properties and the geometrical structure of the fabric or garment end product. The problem of fiber blending when manufacturing yarns is common within the textiles industry. A blended fiber yarn or composite fabric is constructed from multiple fiber types contributing various fiber properties specific to each one. When combined however, they affect the overall structure's properties in ways that may not necessarily be expected. Hamburger's theory inputs are the physical properties of fibers and geometric forms, while, the output is the stress-elongation relation, as illustrated in Figure 47.

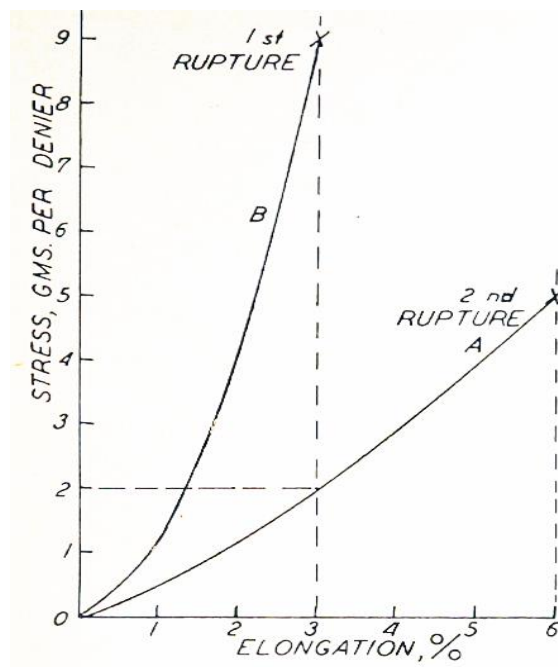


Figure 47 Effect of stress strain characteristics on blend strength [62]

By applying this principle, all components in the testing direction will bear the load together until the component with the lower extension is ruptured, and then the other component bears the load individually until it ruptures, assuming iso-strain condition. This can be applied to yarn components or resin matrix component. For instance, in the case of the Y-axis direction,

the Z- and Y-yarns bear the load together, along with the resin matrix component in this particular direction.

In order to get a quantitative measure of the contribution of each component in a specific direction, the volume fraction of each component needs to be calculated, and by assuming iso-strain condition the load-extension curve can be plotted.

4.2.2. Volume fraction of yarns and matrix components

The volume fraction of each yarn component in case of circular cross section yarns can be calculated using the following equations [59, 60]. On the other hand, the matrix component volume fraction in a specific direction can be calculated by simply subtracting the sum of the yarns volume fractions in this direction from unity, assuming no voids in the structure.

$$F_{fx} = \frac{\frac{n_x \rho_{lx}}{\rho_{vx} 10^3}}{p_x (n_y d_y + n_x d_x + 2d_z)} \quad (38)$$

$$F_{fy} = \frac{\frac{n_y \rho_{ly}}{\rho_{vx} 10^3}}{p_y (n_y d_y + n_x d_x + 2d_z)} \quad (39)$$

$$F_{fz} = \frac{\frac{[\frac{2a}{M_z} + \frac{b}{M_z} + (1 - \frac{1}{M_z}) p_x] N_z \rho_{lz}}{\rho_{vz} 10^3}}{N_y p_y p_x (n_y d_y + n_x d_x + 2d_z)} \quad (40)$$

For approximation $2a+b$ will be replaced by L_{Ioz} .

$$F_{fz} = \frac{\frac{[\frac{L_{Ioz}}{M_z} + (1 - \frac{1}{M_z}) p_x] N_z \rho_{lz}}{\rho_{vz} 10^3}}{N_y p_y p_x (n_y d_y + n_x d_x + 2d_z)} \quad (41)$$

The yarn diameter d (cm), can be calculated according to the generalized formula described below [23].

$$d = \frac{1}{280.2} * \sqrt{\frac{\rho_l}{\phi \rho_v}} \quad (42)$$

In the case of using yarns with rectangular cross section, the fiber volume fractions for the X-, Y-, and Z- yarns can be calculated from the following equations respectively [59, 60]. The terms used follow the same consistent system of nomenclature described earlier.

$$F_{fx} = \frac{\frac{n_x \rho_{lx}}{\rho_{vx} 10^3}}{p_x(n_x t_x + n_y t_y + 2t_z)} \quad (43)$$

$$F_{fy} = \frac{\frac{n_y \rho_{ly}}{\rho_{vy} 10^3}}{p_y(n_y t_y + n_x t_x + 2t_z)} \quad (44)$$

$$F_{fz} = \frac{\frac{\left(\frac{2a}{M_z} + \frac{b}{M_z} + \frac{w_x}{M_z} + \left(1 - \frac{1}{M_z}\right) p_x |N_z \rho_{lz}\right)}{\rho_{vz} 10^3}}{N_y p_y p_x (n_x t_x + n_y t_y + 2t_z)} \quad (45)$$

For approximation 2a+b will be replaced by L_{Ioz} .

$$F_{fz} = \frac{\frac{\left(\frac{L_{Ioz} + w_x}{M_z} + \left(1 - \frac{1}{M_z}\right) p_x |N_z \rho_{lz}\right)}{\rho_{vz} 10^3}}{N_y p_y p_x (n_x t_x + n_y t_y + 2t_z)} \quad (46)$$

4.3. Numerical Example

An example is given below to demonstrate the procedure used in the theoretical calculation. The structure of the 3DOW preform used is given in Table 1. The tensile properties of the X-, Y-, and Z-yarns F_{Tx} , F_{Ty} , and F_{Tz} , are shown in Figure 48.

Table 1 Structure of sample preform

Constituent	Fiber	ρ_l (tex)	ρ_v (g/cm ³)	T (cm ⁻¹)	t (mm)	w (mm)	n	N	M
X-yarn	E-glass	735x2	2.50	2.44	0.27	2.1	5	2	-
Y-yarn	E-glass	2275	2.59	2.36	0.33	2.90	4	2	-
Z-yarn	E-glass	276	2.51	2.36	0.12	0.96	-	2	1

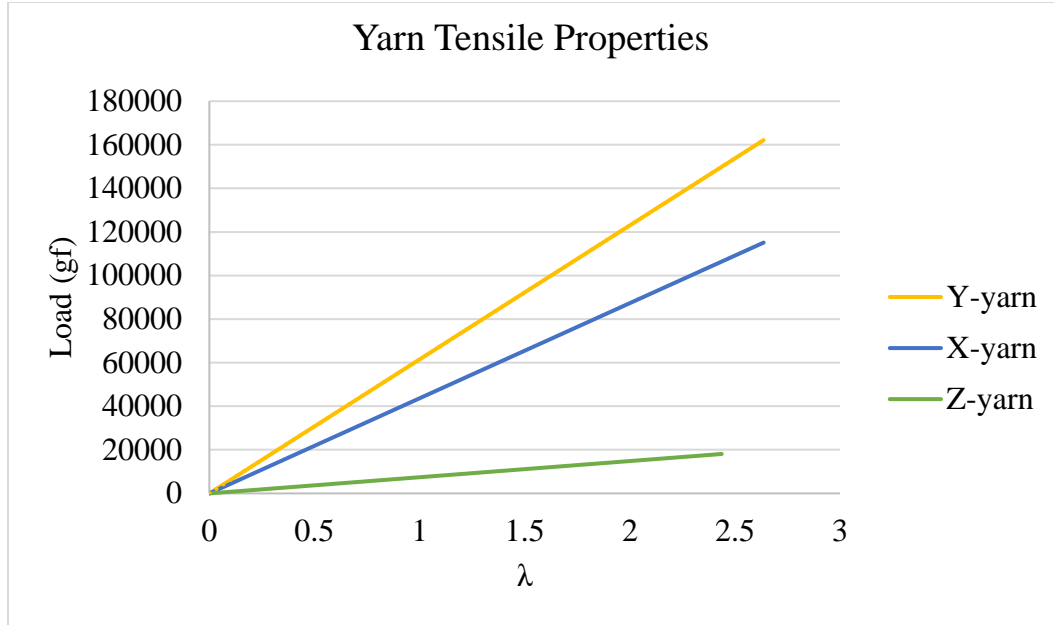


Figure 48 Tensile properties of the yarns used

4.3.1. Load-extension properties of unit structure A and B of Z-yarn

Unit structure A

The set of values of λ_{yz} can be obtained for a given set of values of (h_z, λ_z^A) from Equation 15, and the values for P_{A0z} and h_{mz} can be obtained from Equations 19 and 23 respectively. By substituting the values of λ_{yz} into Equation 16, the corresponding values of $g_z(\lambda_{yz})$ can be obtained from yarn tensile properties plotted in Figure 48. Afterwards, a group of curves can be plotted using Equation 26, which intersects with another curve from Equation 11 as illustrated in Figure 49, the first group of curves is for the relation between F_c and h_z for different values of parameter λ_z^A and the other curve is from Equation 11 which represent the yarn resistance to compression.

For uniform biaxial loading, the fabric is stretched so that the compression of the Z-yarns and the outer most X-yarns satisfies the equilibrium condition in Equation 11, which defines the condition when $F_c = F_{rc}$, where F_{rc} is the yarn resistance to compression as shown in Figure 50. From Figure 49 one can read off F_c and h_z from the intersection of the yarn compressibility curve with the compressive force curves. The locus of intersecting points gives the relation

between F_c and h_z as illustrated in Figure 51. However, in case of incompressible flat filament yarns, the decrease in preform thickness due to compression is neglected, and $h_z = 0$, and we substitute this value in the previous equations.

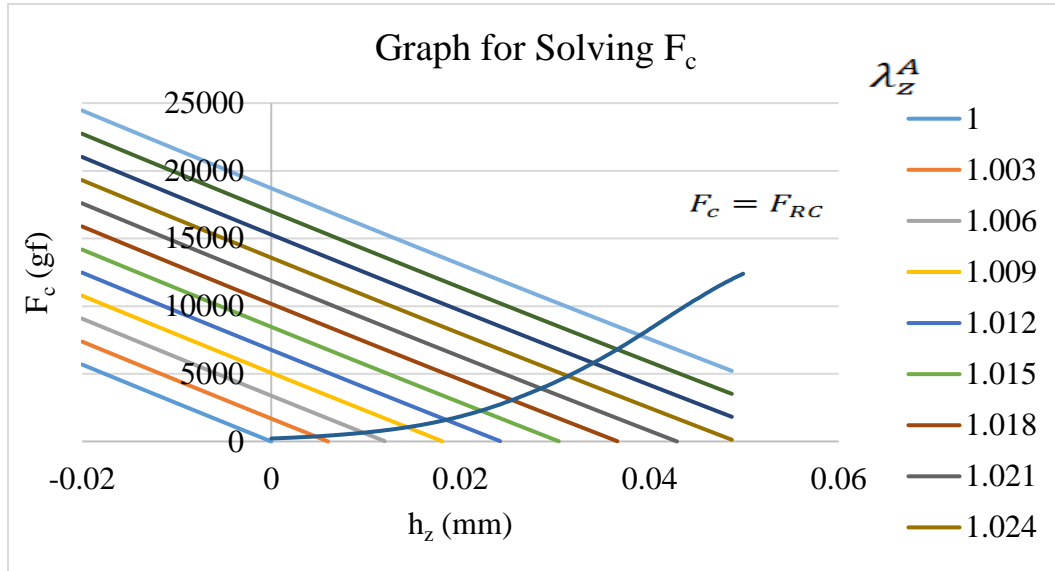


Figure 49 Graph for solving F_c

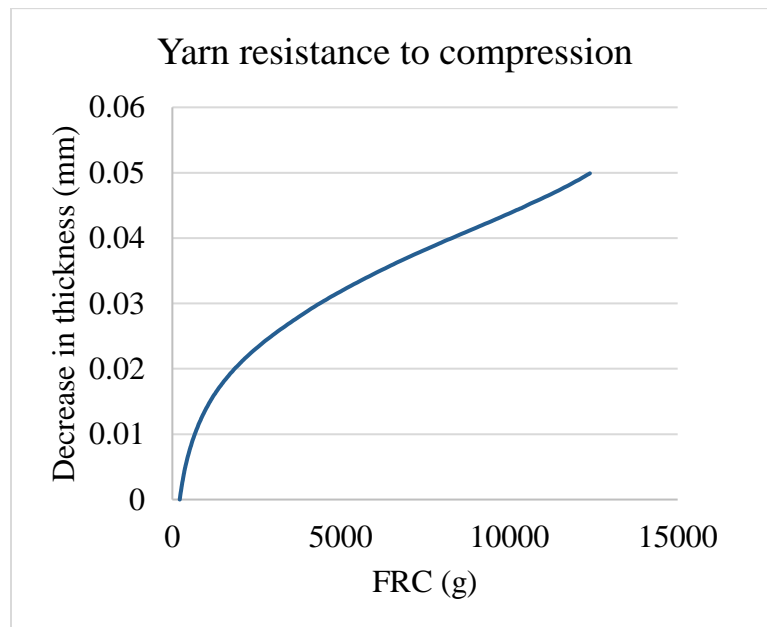


Figure 50 Average resistance to compression of Z-and X-yarns

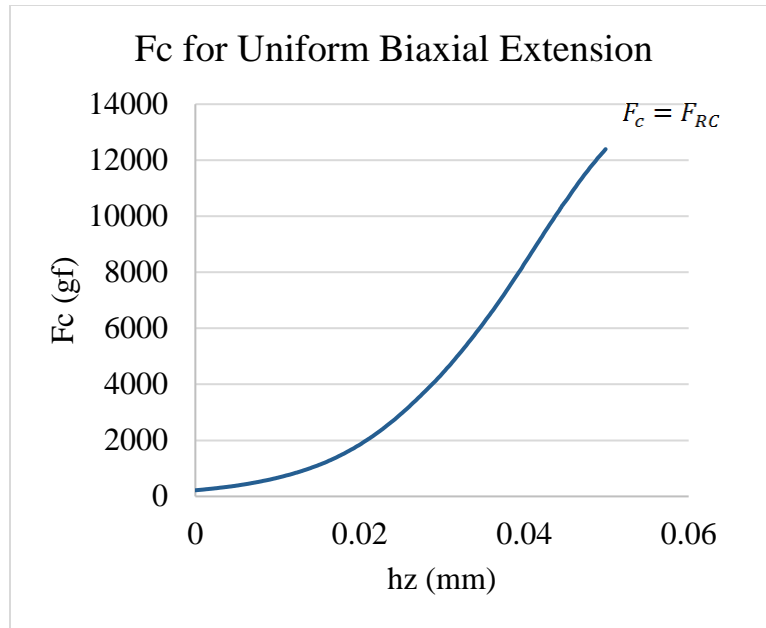


Figure 51 The parameter F_c for uniform biaxial extension

Afterwards, the set of values of F_z corresponding to the set of values of λ_z^A can be obtained from Equation 29, as shown in Figure 52.

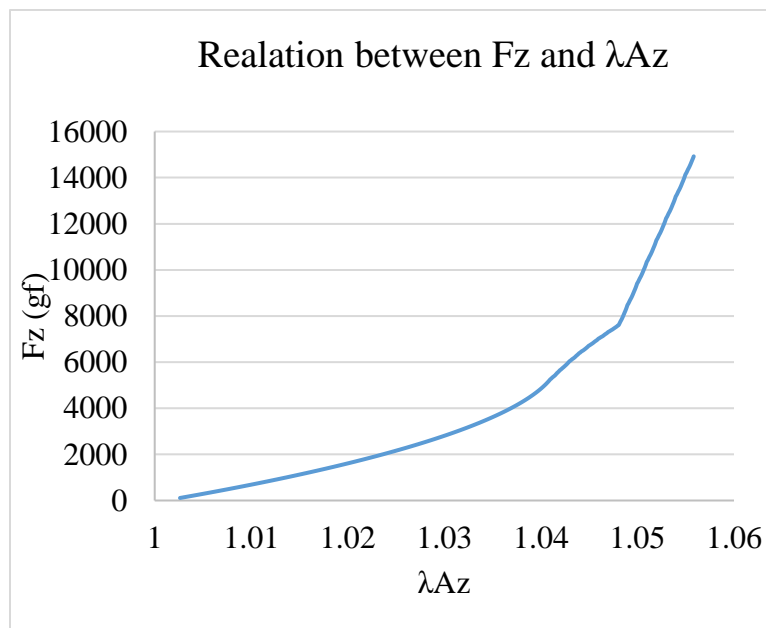


Figure 52 Relation between F_z and λ_z^A

Unit structure B

The relations between λ_{yz} and F_z can be defined by the following function,

$$\lambda_{yz} = g_z^{-1}(F_{Tz}) \quad (47)$$

Thus, by using the following relations and Equation 38, one can obtain the set of values for λ_z^B . The values of F_z and the corresponding values of λ_z^B are shown in Figure 53.

$$F_{Tz} = F_z \quad (48)$$

$$\lambda_z^B = \lambda_{yz} \quad (49)$$

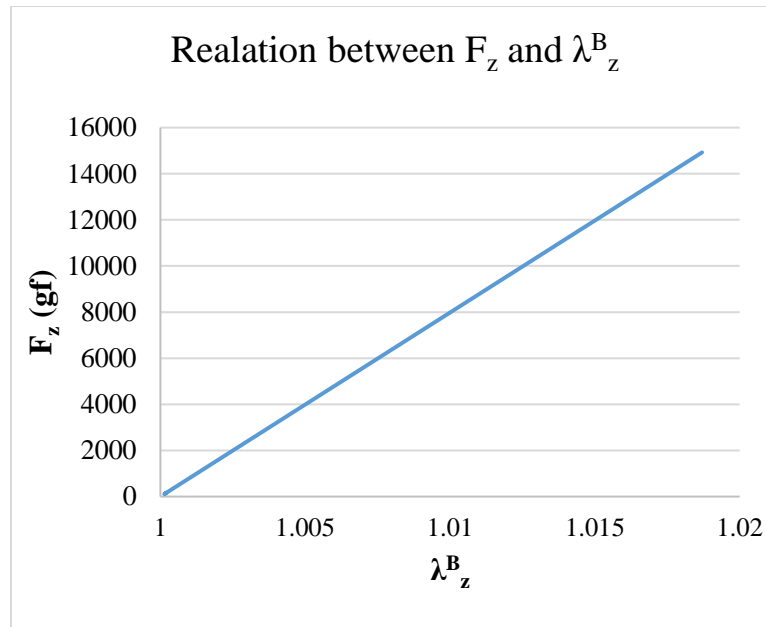


Figure 53 Relation between F_z and λ_z^B

After obtaining the values of F_z with respect to λ_z^A and λ_z^B , and by introducing the interlacing pattern of the Z-yarn from Equation 30. Therefore, the load-extension curve of the Z-yarn can be determined. In the case of using different types of Z-yarns in the structure (hybrid), Equation 31 can be used to calculate λ_z which is the mean value of the extensions λ_{zk} of all N_x units. Finally, the summation of the loads on the yarns per weave repeat are calculated from Equation 32, and the load-extension curve of the Z-yarn can be plotted as shown in Figure 54.

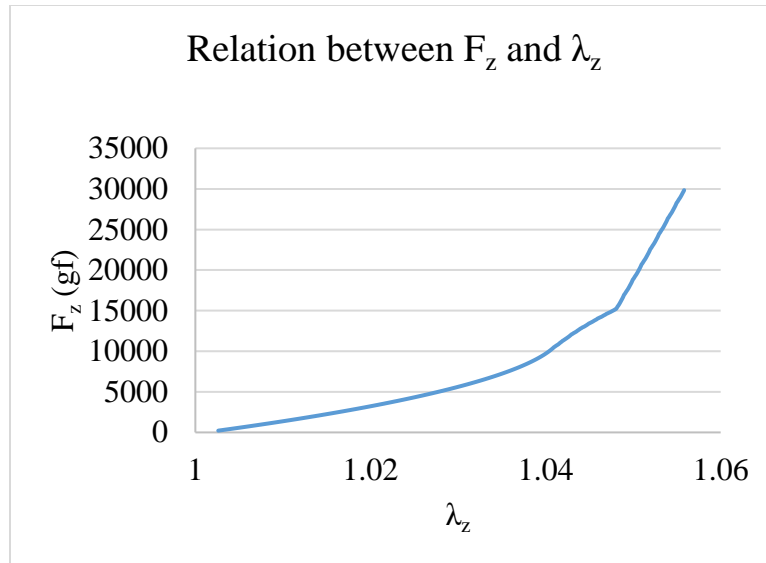


Figure 54 Relation between F_z and λ_z

4.3.2. Load-extension properties of X- and Y-yarns

The load on the X- and Y-yarns can be obtained directly from the experimental measurements in Figure 49, and then multiplying by the number of yarns per weave repeat and multiplying by the number of layers as defined in Equations 33, and 34. The values of F_x and F_y corresponding to the extensions λ_x and λ_y respectively are plotted in Figure 55.

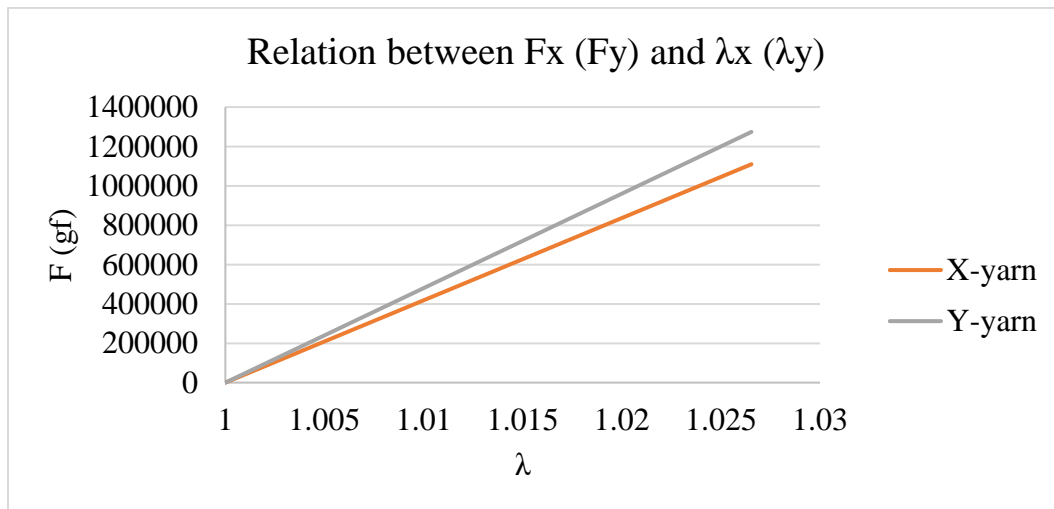


Figure 55 Relation between F_x (F_y) and λ_x (λ_y)

4.3.3. Load-extension properties of the preform

The load-extension properties of the preform in the X-axis direction are solely dictated by the X-yarns as shown in Figure 55. As for the Y-axis direction, it has two yarn components (Y- and Z-yarns), which are treated separately as described earlier. The resultant tensile curve in the Y-axis direction is plotted in Figure 56.

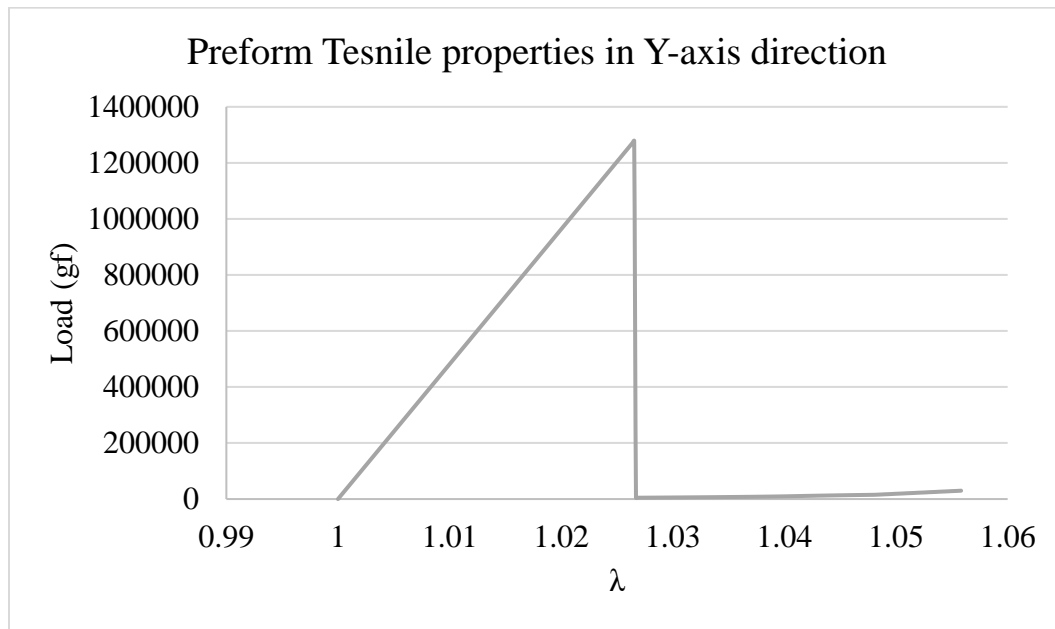


Figure 56 Preform resultant tensile properties in y-axis direction for one structural repeat

4.3.4. Load-extension properties of the composite

Once the preform load extension properties are calculated in the principle material directions (X-, and Y-axis), the contribution of the matrix can be added by using Hamburger's blended yarns theory [62].

Firstly, the volume fraction of each yarn component is calculated using Mehmet's generalized geometrical model of 3DOW composites [59, 60]. The X-, Y-, and Z-yarns volume fractions can be calculated according to Equations 38, 39, and 41 respectively in case of yarns with circular cross sections. In the circular yarn case the yarn diameter can be calculated using Equation 42. On the other hand, when using yarns with rectangular cross sections, the volume fractions of the X-, Y-, and Z-yarns can be calculated using Equations 43, 44, and 46

respectively. Secondly, the volume fraction of the matrix in the X-axis direction is calculated by subtracting the X-yarn volume fraction from unity. As for the Y-axis direction, it is calculated by subtracting the sum of the Y- and Z-yarns volume fraction from unity. Thirdly, the load-extension curve of the matrix is multiplied by the matrix volume fraction in the X- and Y-axis direction as shown in Figure 57. Finally, the load-extension curve of the matrix is added to that of the preform using the Hamburger's approach as shown in Figures 58 and 59. The resin is assumed to be linear isotropic, with perfect adhesion with the fibers, and no void content.

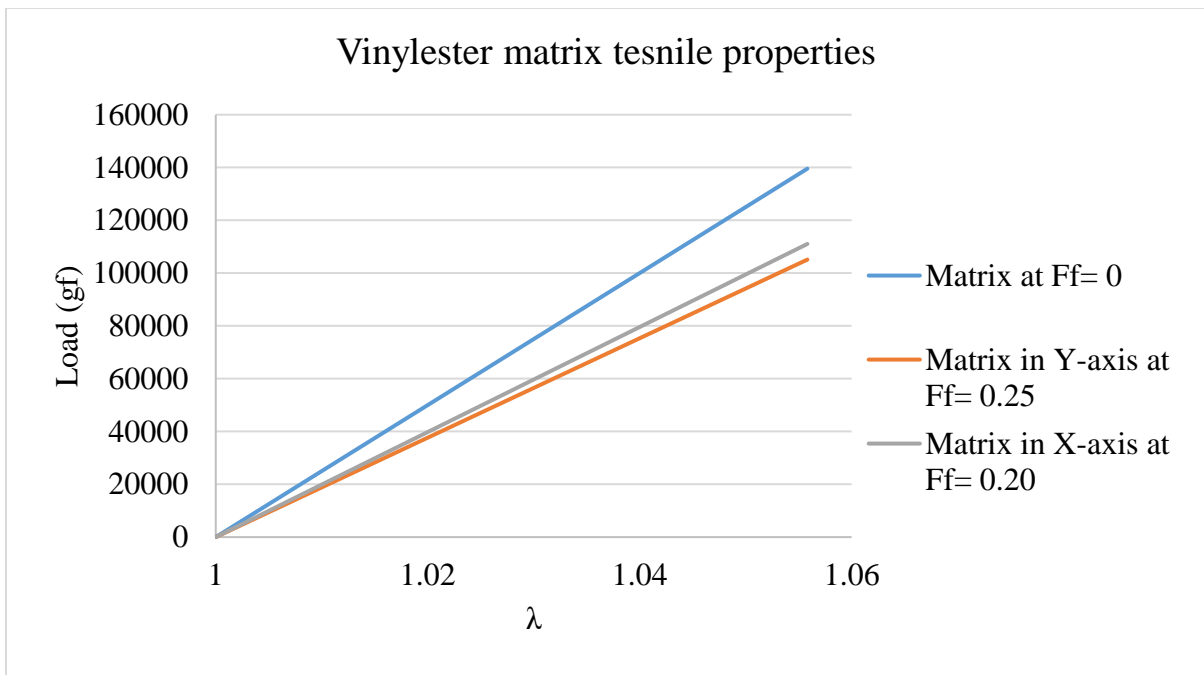


Figure 57 Tensile properties of Vinylester matrix at different fiber volume fractions for one structural repeat

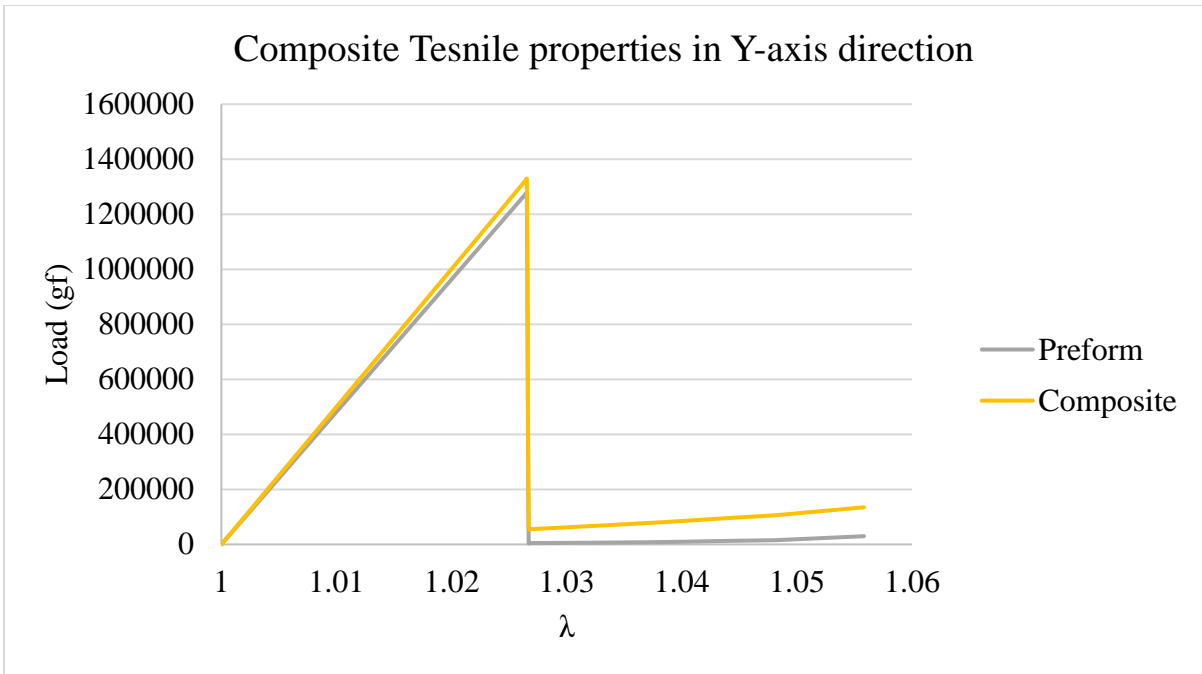


Figure 58 Composite tensile properties in Y-axis direction for one structural repeat

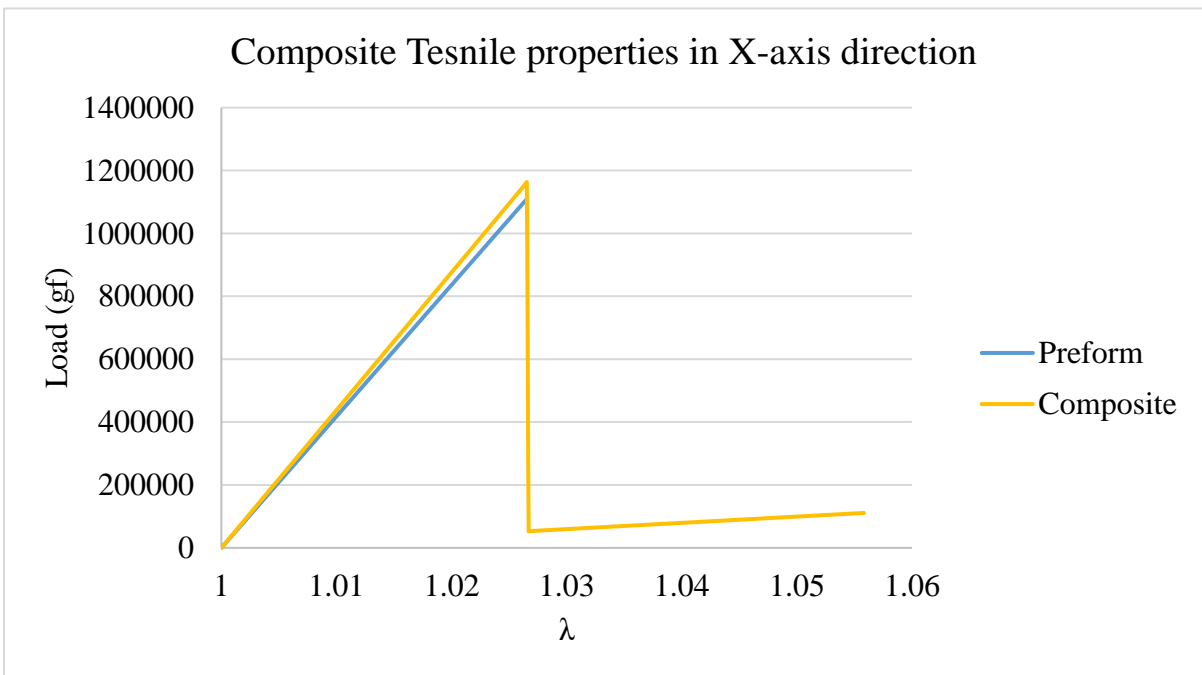


Figure 59 Composite tensile properties in X-axis direction for one structural repeat

In Figures 58 and 59, after the fiber failure the matrix continues to bear the load, which is theoretically true. However, in practice once the fiber fail and the load drops to that very low level, the composite is said to have reached its failure state. Therefore, any load bearing beyond the fiber failure should be ignored.

4.4. Experimental Verification of the Model

This part is dedicated to verifying the proposed model experimentally, and compare the predicted results from the model with the experimental results. Three different types of composites were used in the verification procedure. The first type is 3DOW E-glass composite having different construction parameters, including number of layers, Z-yarn interlacing pattern, and pick density. The second type is 3DOW hybrid composites, where the Y- and Z-yarns were E-glass, and X-yarns were from different fibers, namely Spectra, Vectran, and Zylon.

4.4.1. Composite tensile test

The objective of the composite tensile testing is to provide a basis to verify the theoretical prediction of load-extension properties. Samples were tested according to ASTM D3039 in X- and Y-axis directions. Specimen of 152.4 mm length and 35.56 mm width were used. The composite specimens were tested on the MTS hydraulic load frame located at the Composite Core Facility, College of Textiles, NC State University. Table 2 lists the composites specifications. The 3DOW E-glass composites used in the experimental verification are described in details in design of experiment A in Chapter 5 and their tensile properties are adapted from Ince's doctoral dissertation [59], whereas the hybrid composites are adapted from Xie's master thesis [63].

Table 2 3DOW composites specifications

Composite			X-Yarn			Y-Yarn			Z-Yarn		
Type	Weave	Layers	Fiber	ρ_l (tex)	T (cm ⁻¹)	Fiber	ρ_l (tex)	T (cm ⁻¹)	Fiber	ρ_l (tex)	T (cm ⁻¹)
E-glass	Plain	2, 3, 4	E-glass	735 x2	2.44, 2.74, 2.93	E-glass	2275	2.36	E-glass	276	2.36
	2x2 twill	2, 3, 4	E-glass	735 x2	2.44, 2.74, 2.93	E-glass	2275	2.36	E-glass	276	2.36
	2x2 basket	2, 3, 4	E-glass	735 x2	2.44, 2.74, 2.93	E-glass	2275	2.36	E-glass	276	2.36
Hybrid	Plain	3	Spectra	144 x2	4.965	E-glass	2275	2.36	E-glass	276	2.36
	Plain	3	Vectran	167 x2	5.5	E-glass	2275	2.36	E-glass	276	2.36
	Plain	3	Zylon	164 x2	5.825	E-glass	2275	2.36	E-glass	276	2.36

The tensile behavior of E-glass, Spectra, Vectran, and Zylon fibers/ yarns are adapted from Xie's master thesis, as illustrated in Figure 60 [63].

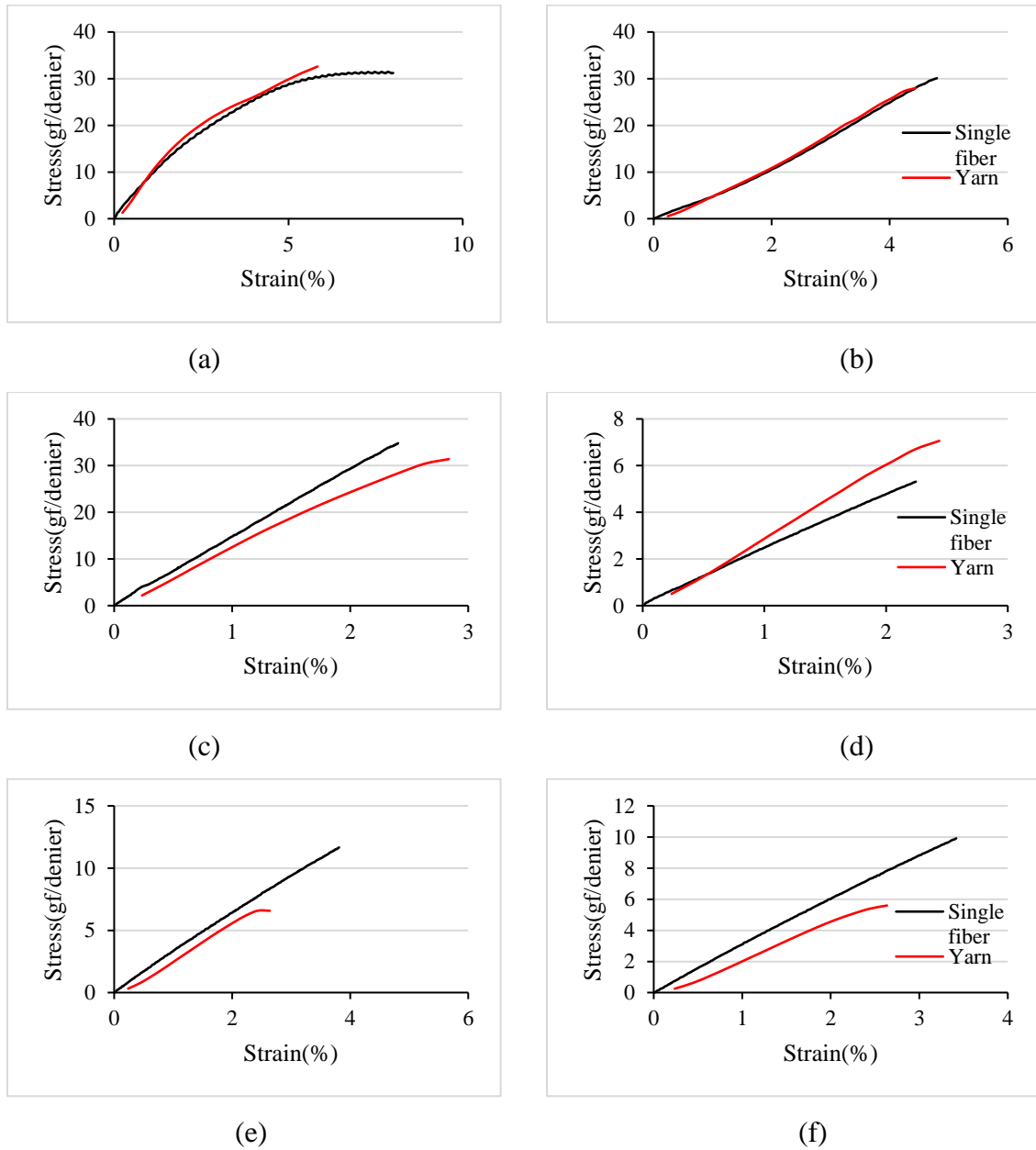
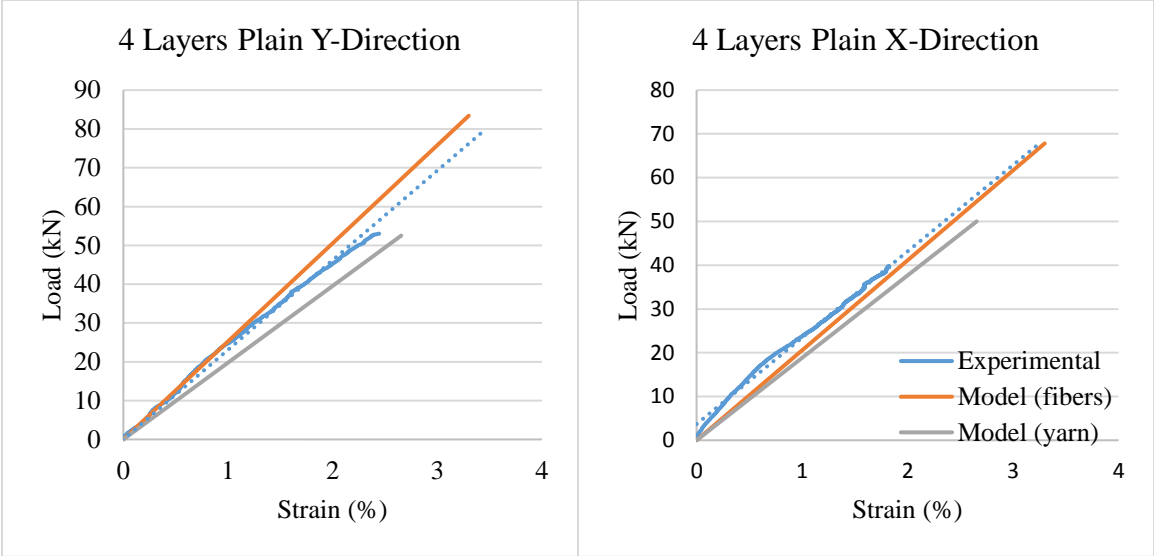


Figure 60 Yarn vs. fiber tensile properties for, (a) Spectra, (b) Vectran, (c) Zylon, (d) E-glass $\rho_1 = 275$ tex, (e) E-glass $\rho_1 = 735$ tex, and (f) E-glass $\rho_1 = 2400$ tex [63]

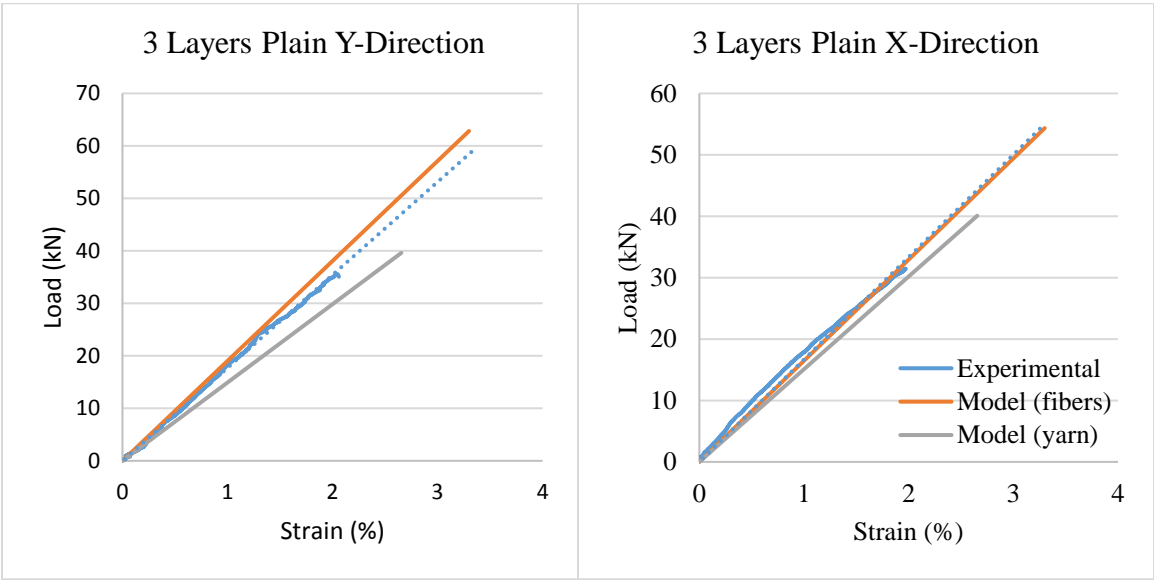
The experimental and theoretically predicted load-strain curves of the 3DOW E-glass composites in the X- and Y-axis directions are illustrated in Figures 61 through Figure 69, and the 3DOW hybrid composites in Figure 70. Each figure shows three curves, (a) measured

average load-strain curve of composites with an extrapolated trend line, (b) theoretically computed load-strain curve of the composite based on fibers properties, and (c) theoretically computed load-strain curve of the composite based on yarns properties. The fitting of the trend line was selected based on the highest coefficient of regression (e.g. linear or polynomial).

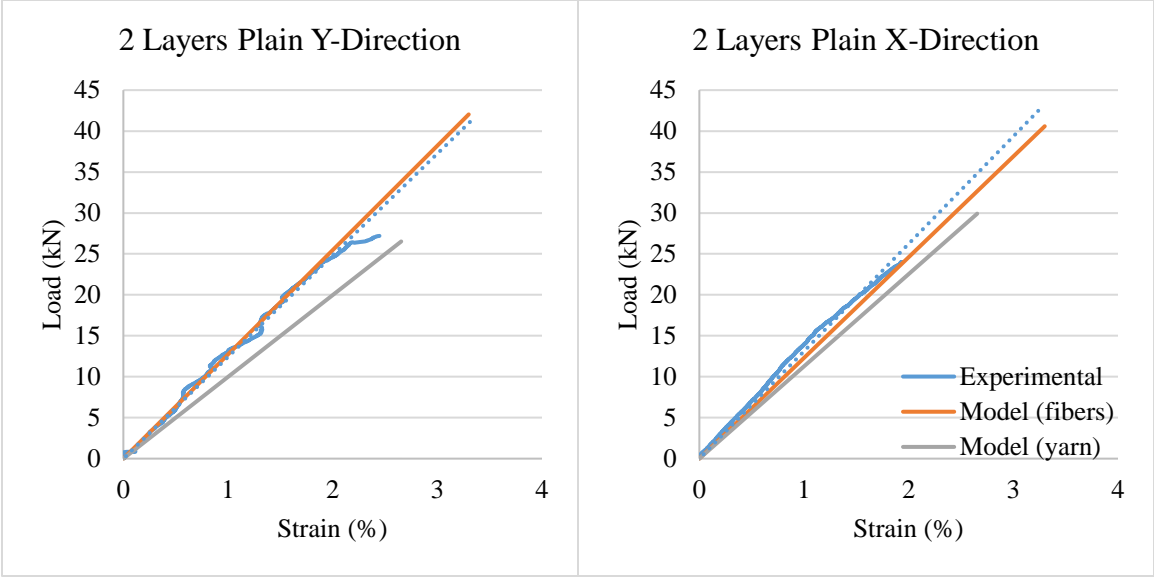
Figure 61 Experimental vs. model tensile load-strain for 3DOW plain E-glass composite with 2.44 picks/ cm in X- and Y-axis directions, (a) 4 layers, (b) 3 layers, and (c) 2 layers.



(a)

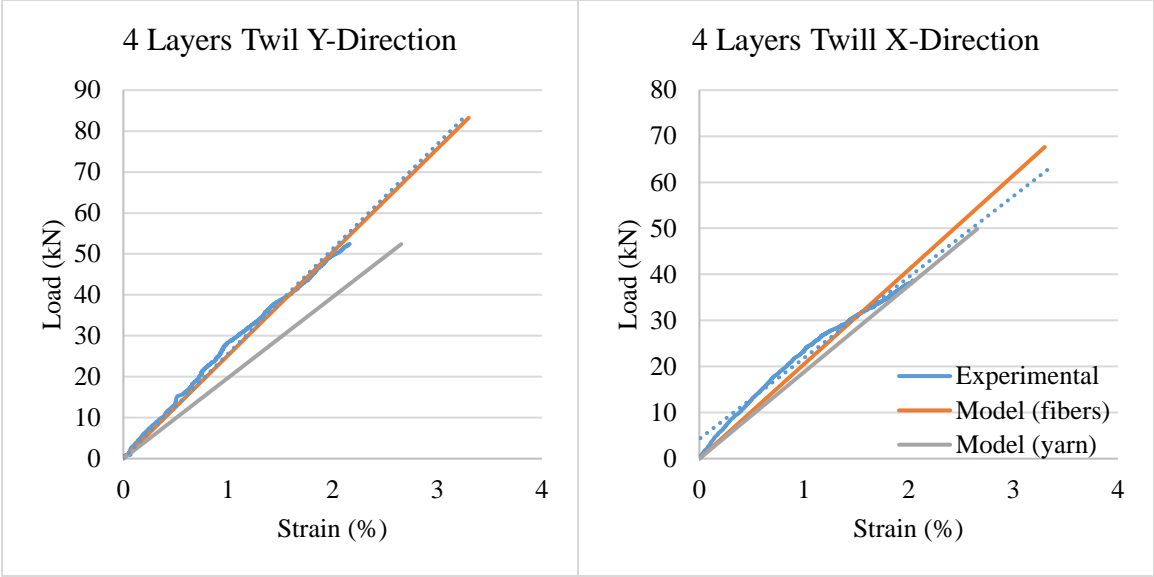


(b)

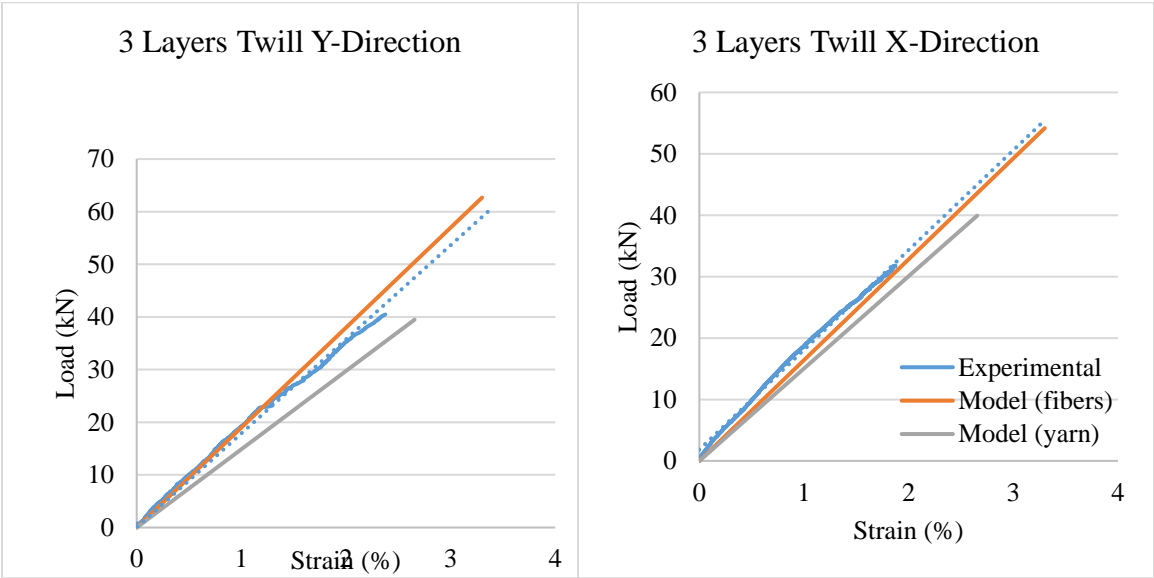


(c)

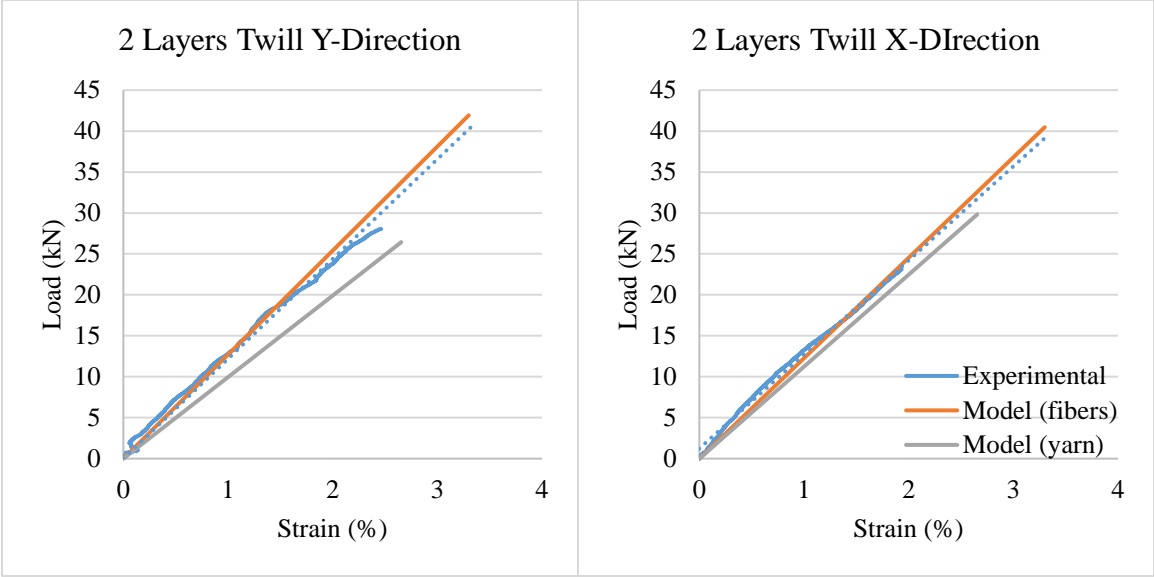
Figure 62 Experimental vs. model tensile load-strain for 3DOW 2x2 Twill E-glass composite with 2.44 picks/ cm in X- and Y-axis directions, (a) 4 layers, (b) 3 layers, and (c) 2 layers.



(a)

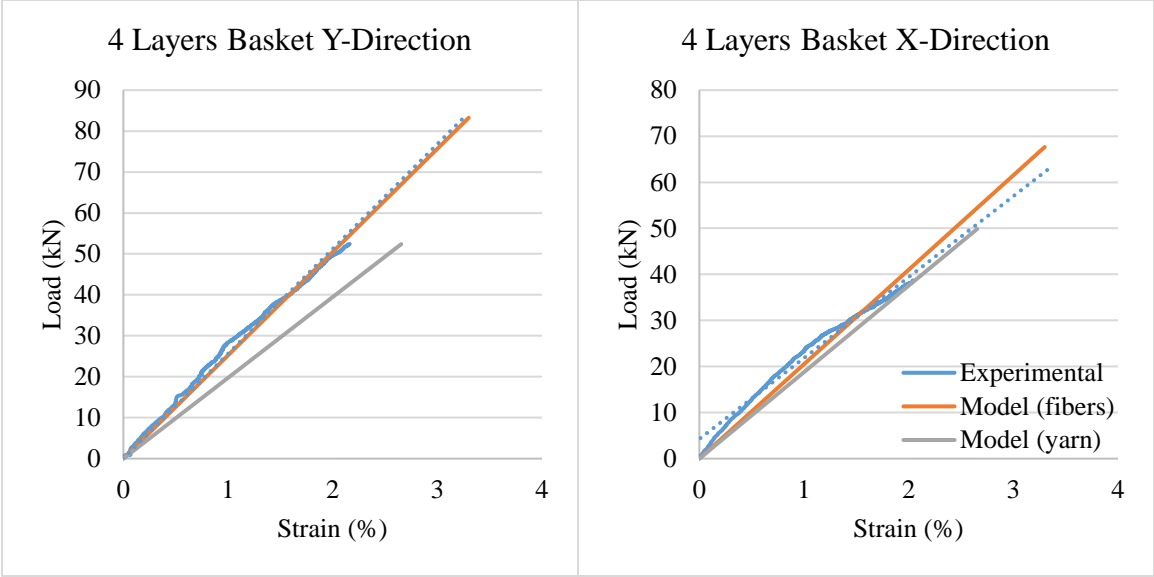


(b)

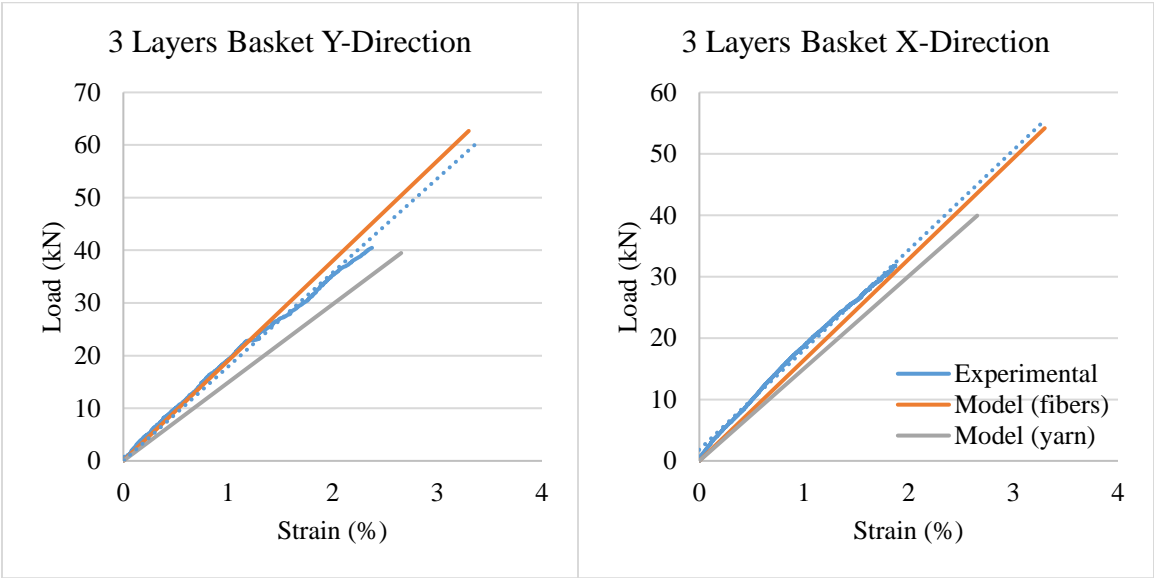


(c)

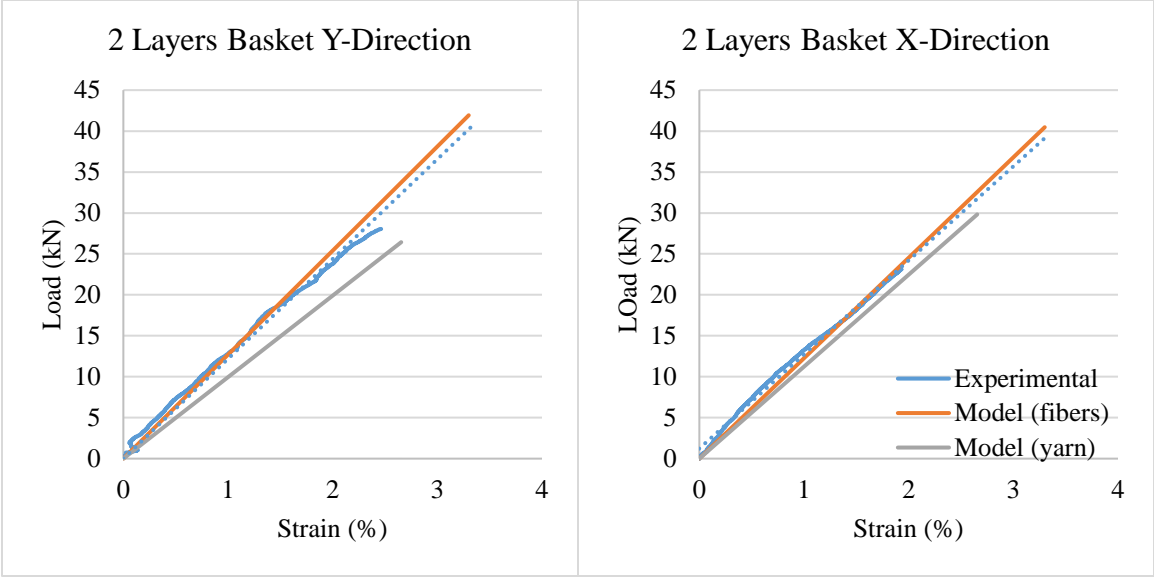
Figure 63 Experimental vs. model tensile load-strain for 3DOW 2x2 Basket E-glass composite with 2.44 picks/ cm in X- and Y-axis directions, (a) 4 layers, (b) 3 layers, and (c) 2 layers.



(a)

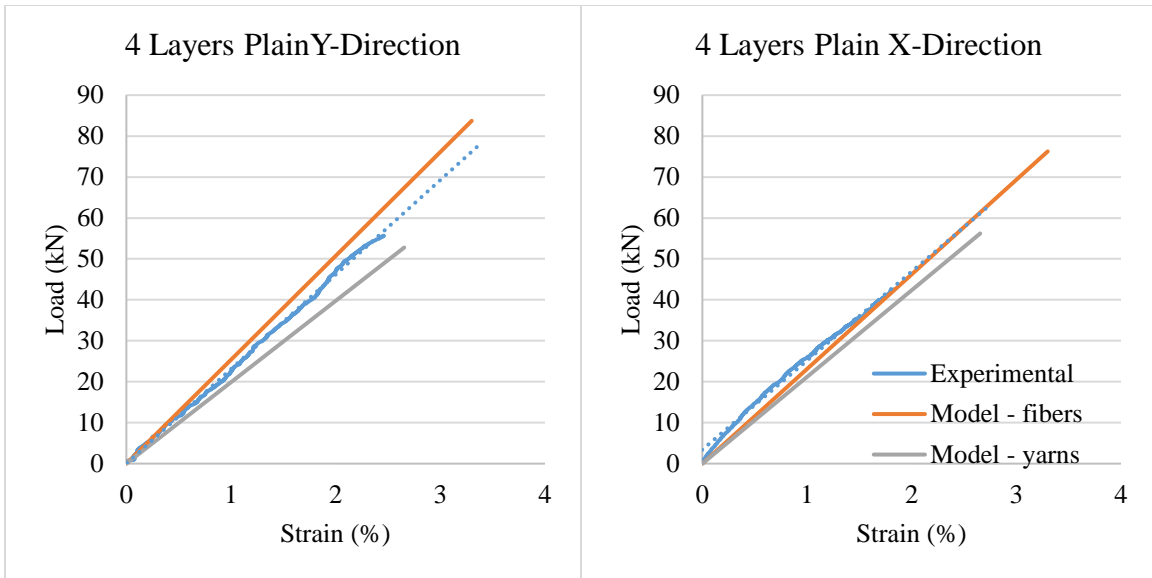


(b)

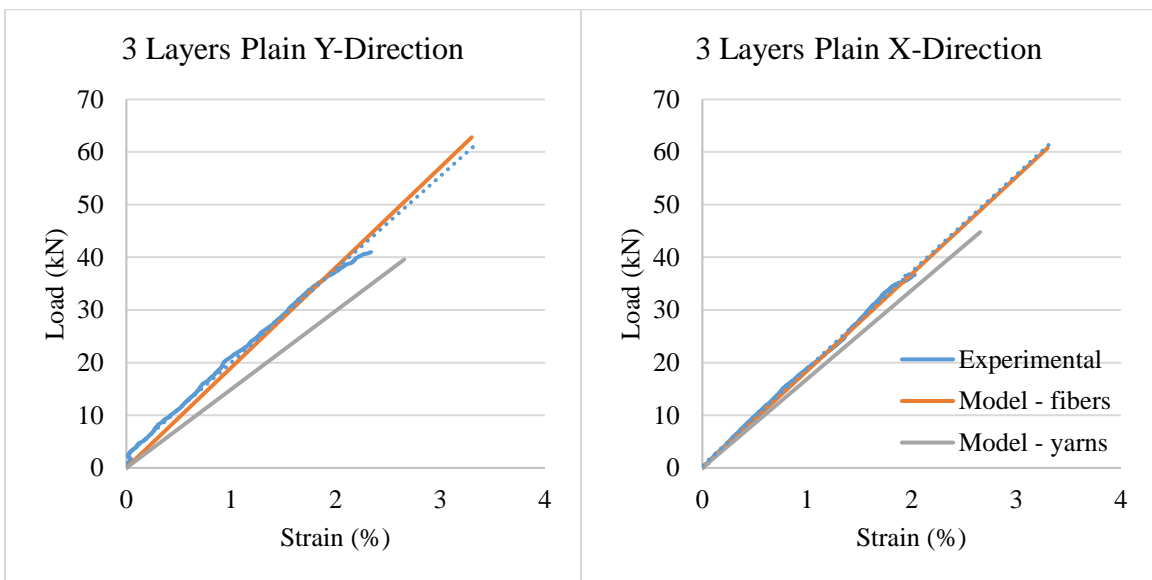


(c)

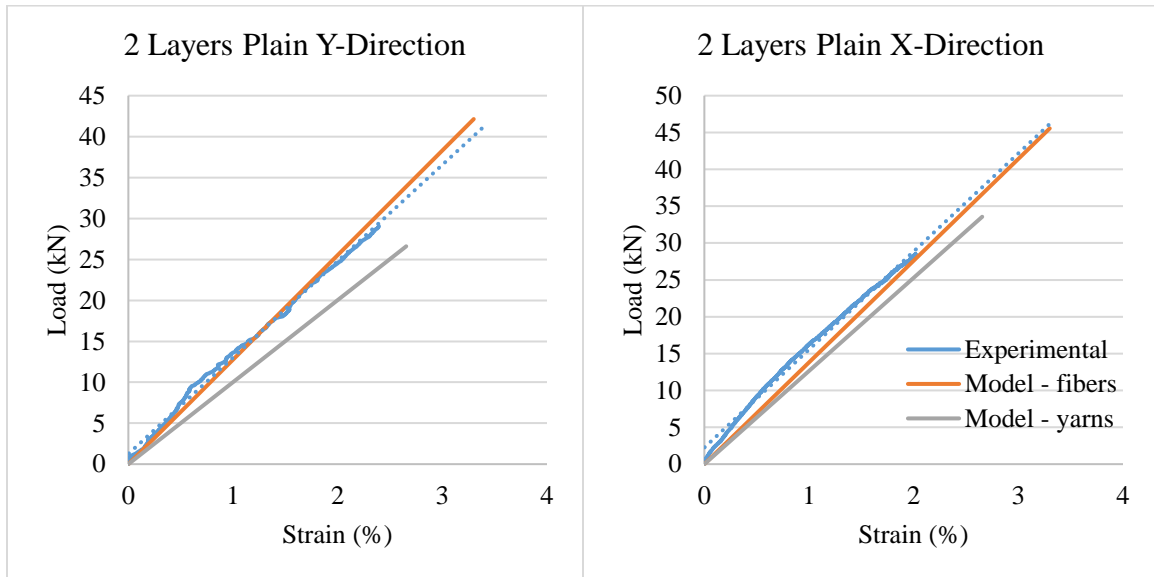
Figure 64 Experimental vs. model tensile load-strain for 3DOW plain E-glass composite with 2.74 picks/ cm in X- and Y-axis directions, (a) 4 layers, (b) 3 layers, and (c) 2 layers.



(a)

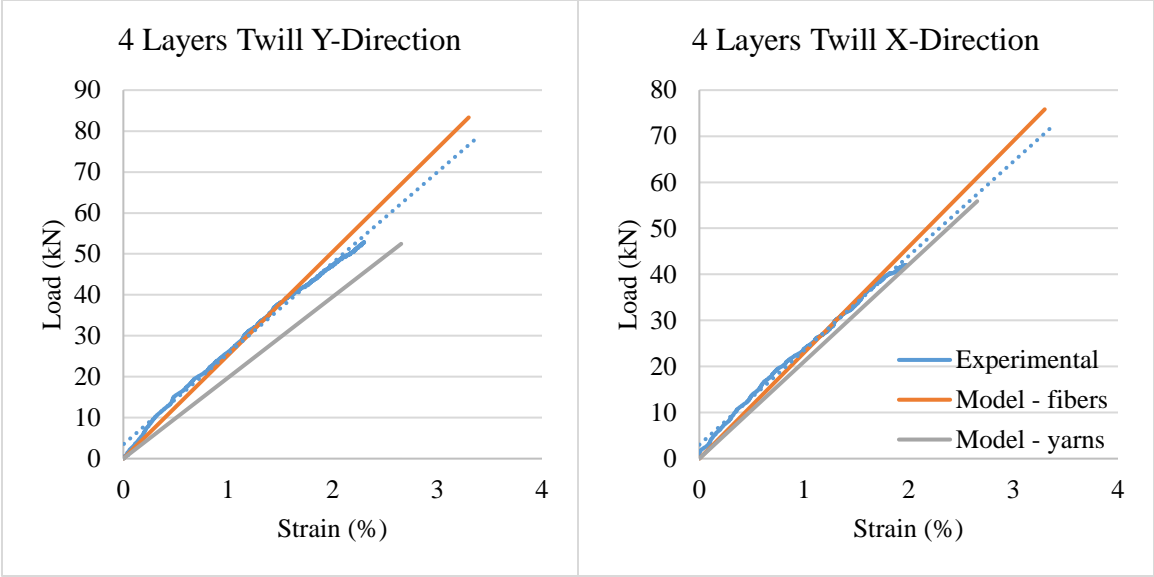


(b)

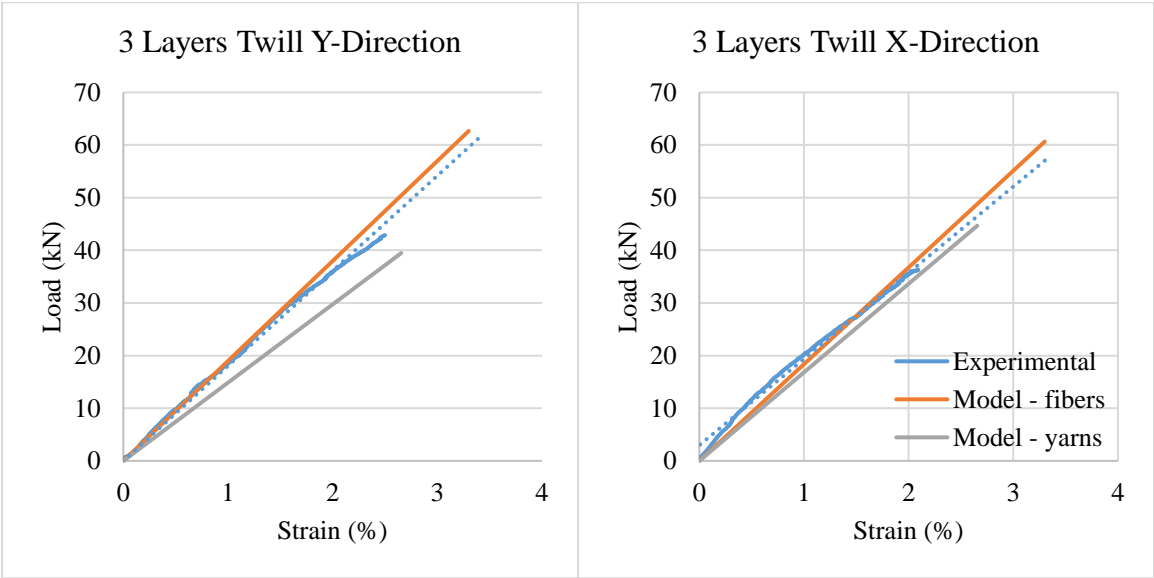


(c)

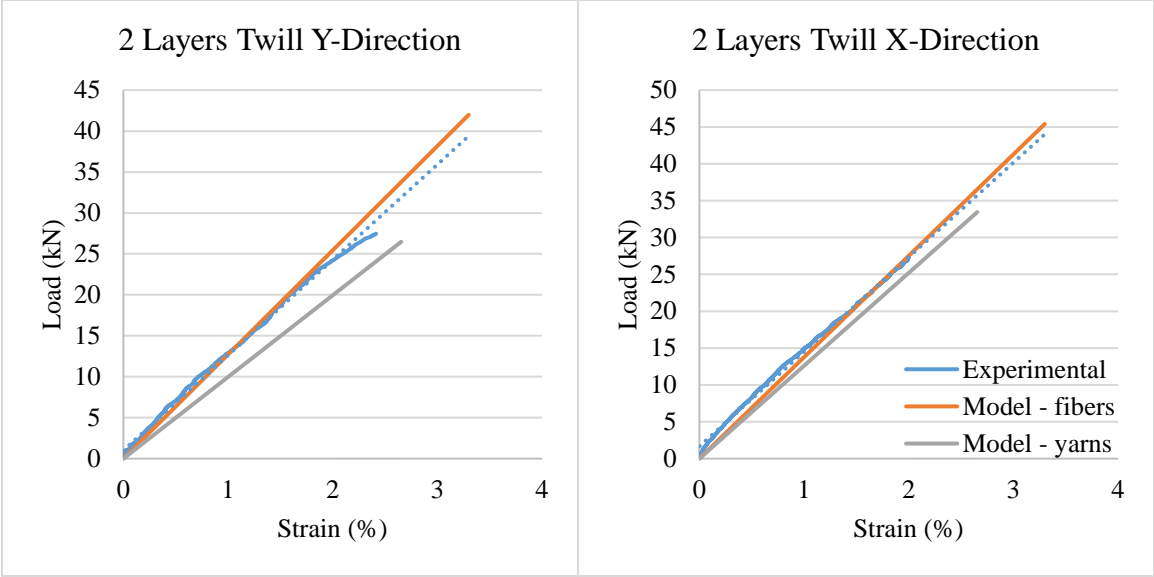
Figure 65 Experimental vs. model tensile load-strain for 3DOW 2x2 Twill E-glass composite with 2.74 picks/ cm in X- and Y-axis directions, (a) 4 layers, (b) 3 layers, and (c) 2 layers.



(a)

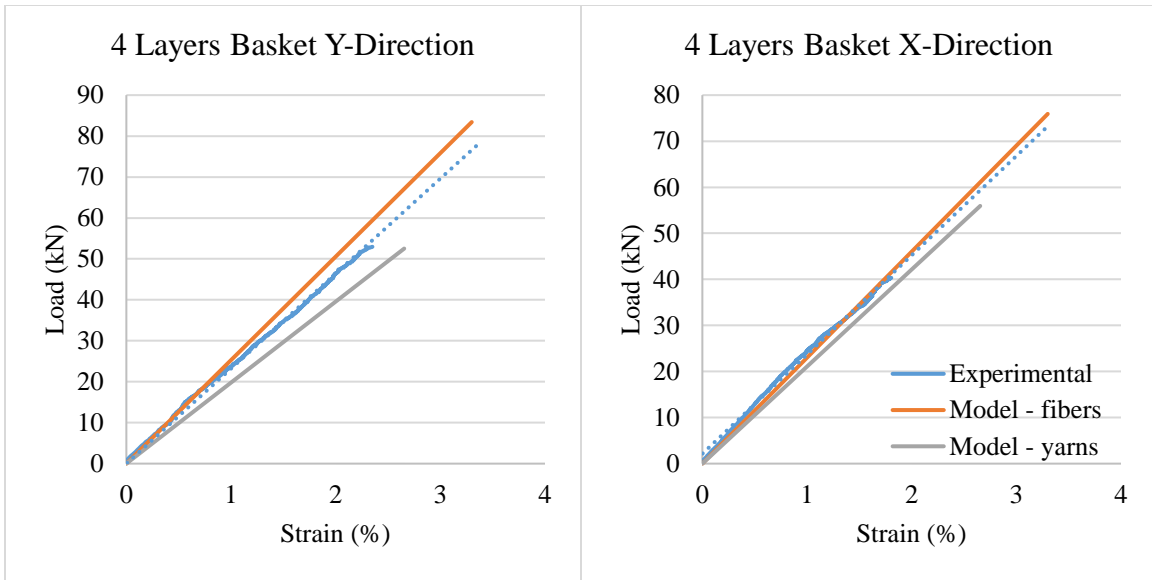


(b)

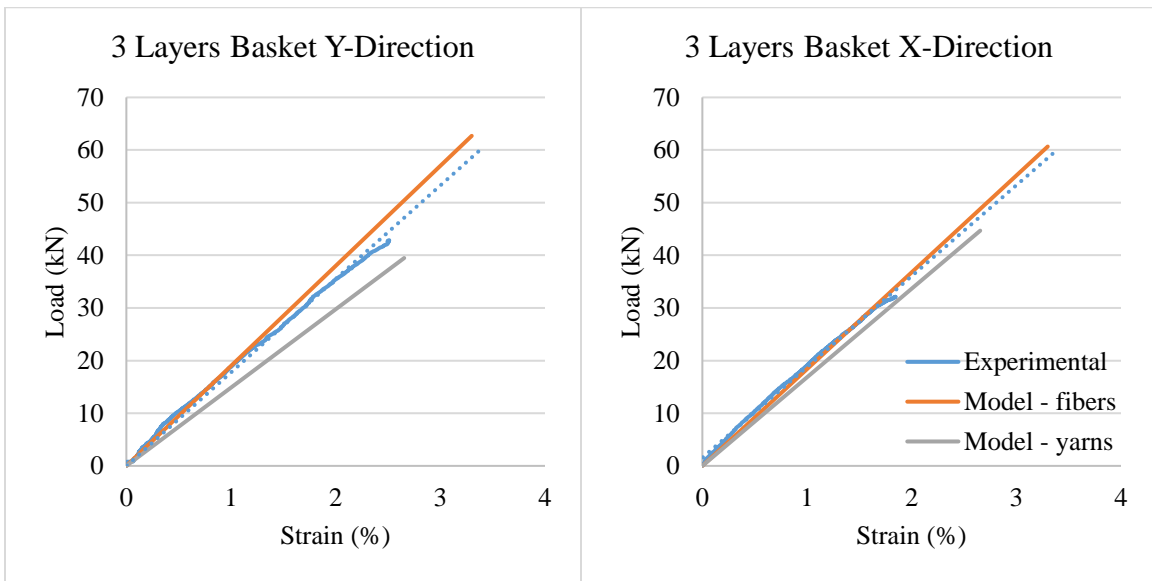


(c)

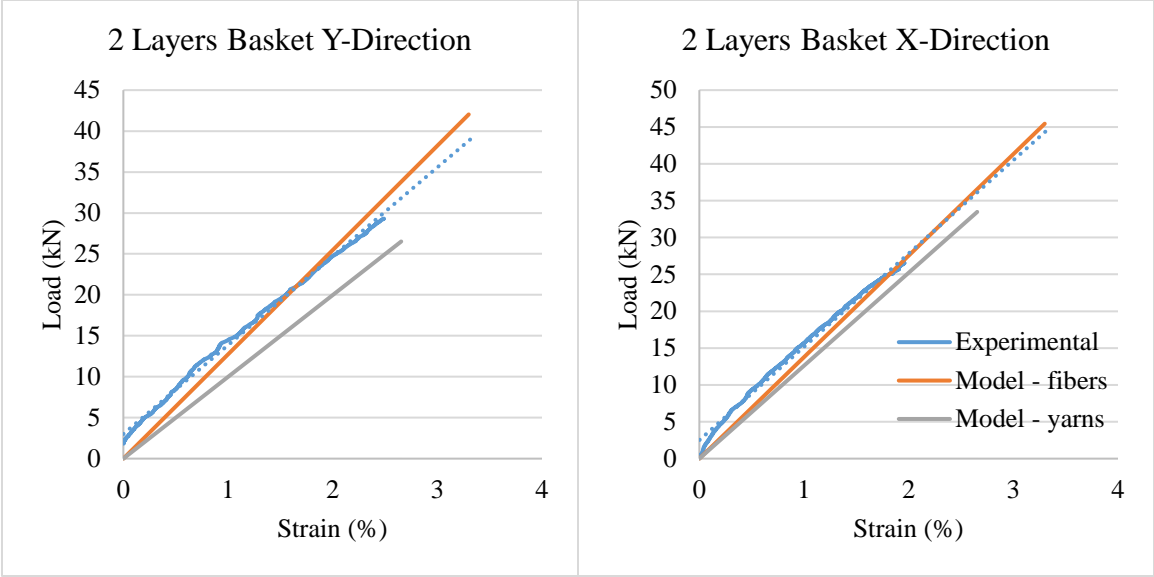
Figure 66 Experimental vs. model tensile load-strain for 3DOW 2x2 Basket E-glass composite with 2.74 picks/ cm in X- and Y-axis directions, (a) 4 layers, (b) 3 layers, and (c) 2 layers.



(a)

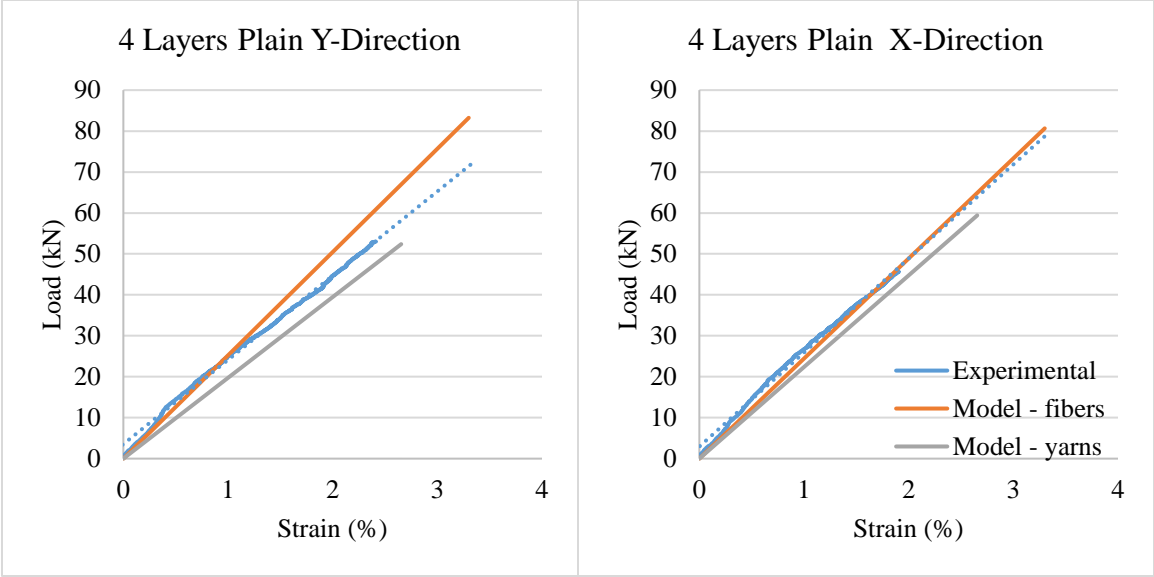


(b)

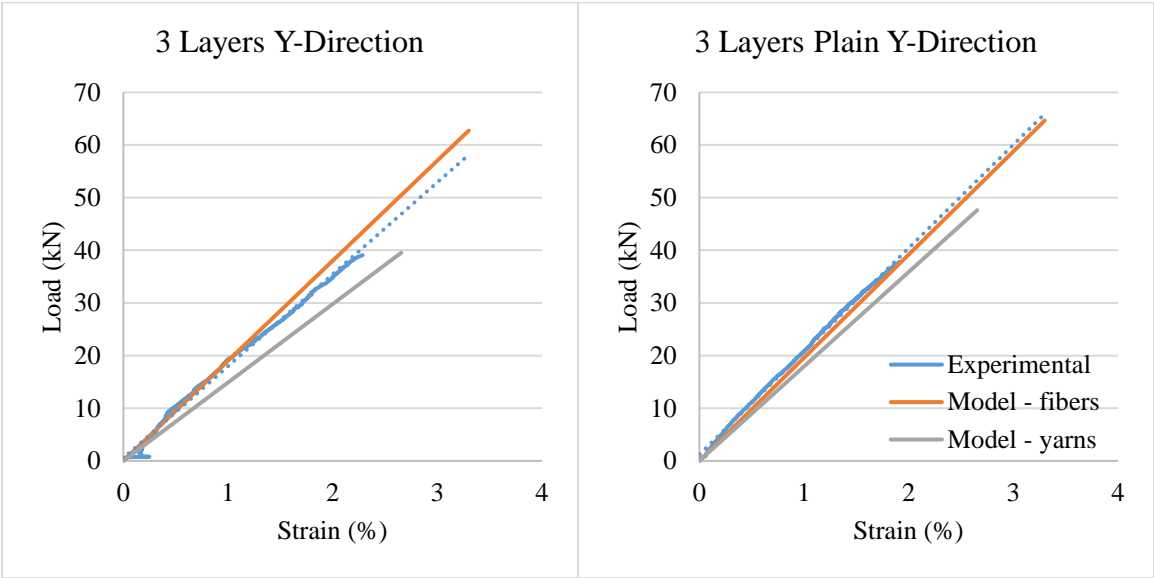


(c)

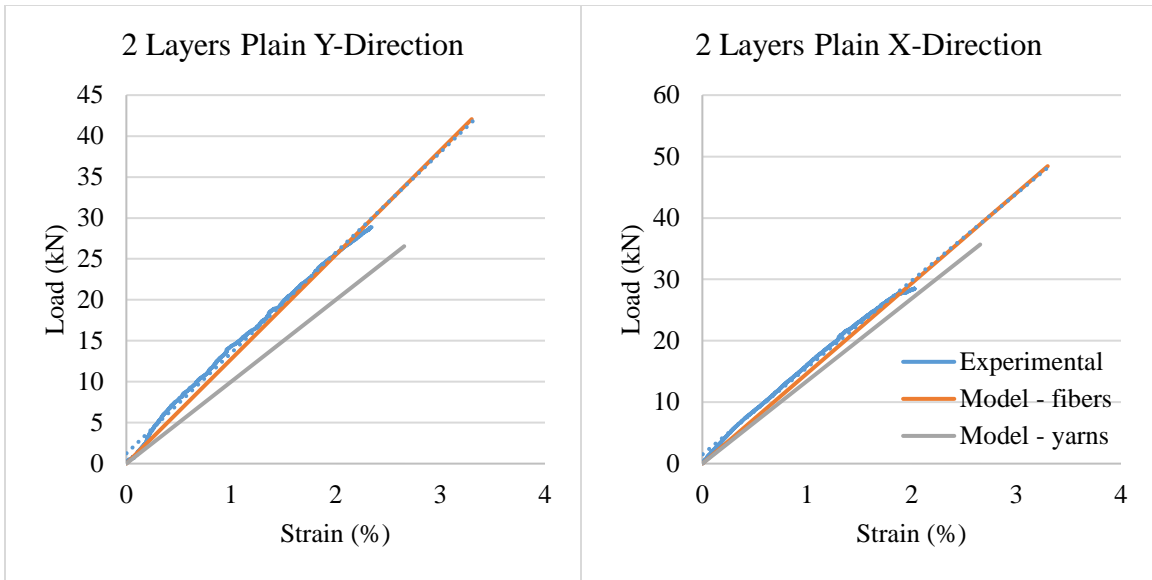
Figure 67 Experimental vs. model tensile load-strain for 3DOW plain E-glass composite with 2.925 picks/ cm in X- and Y-axis directions, (a) 4 layers, (b) 3 layers, and (c) 2 layers.



(a)

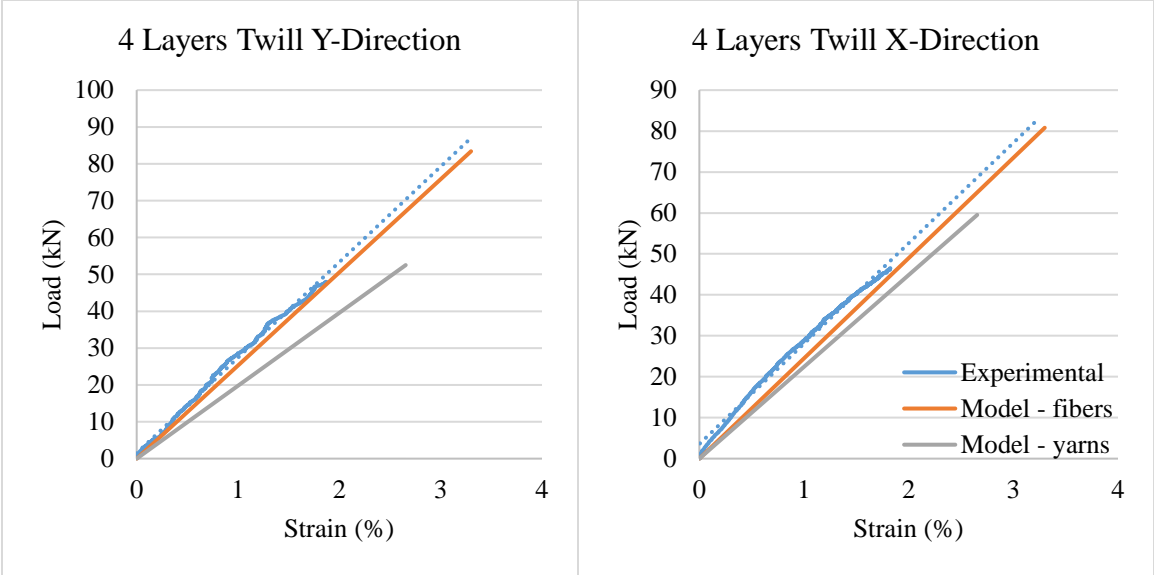


(b)

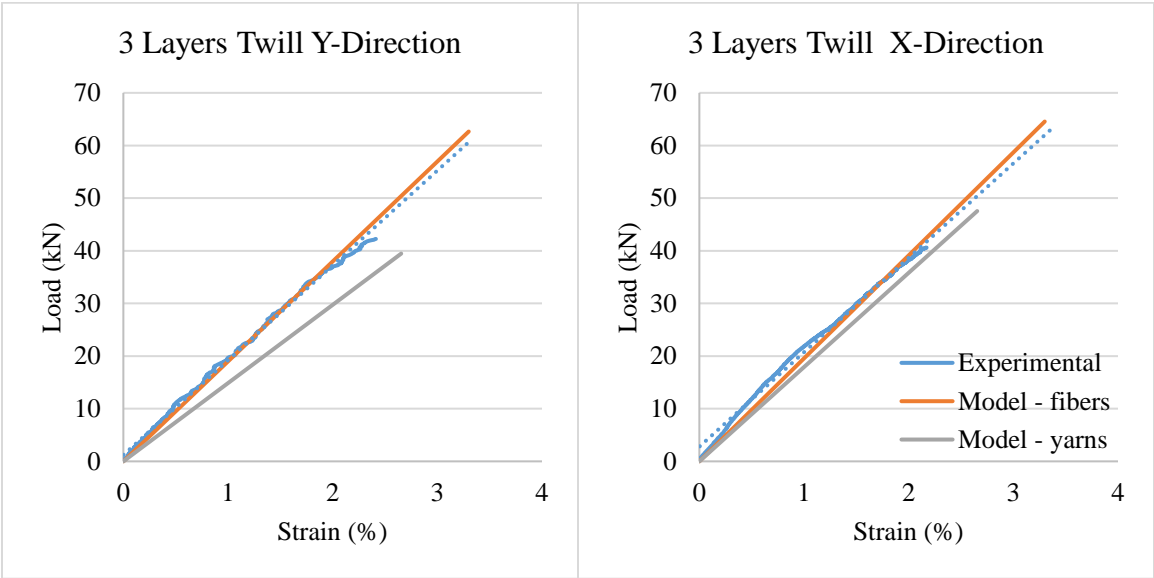


(c)

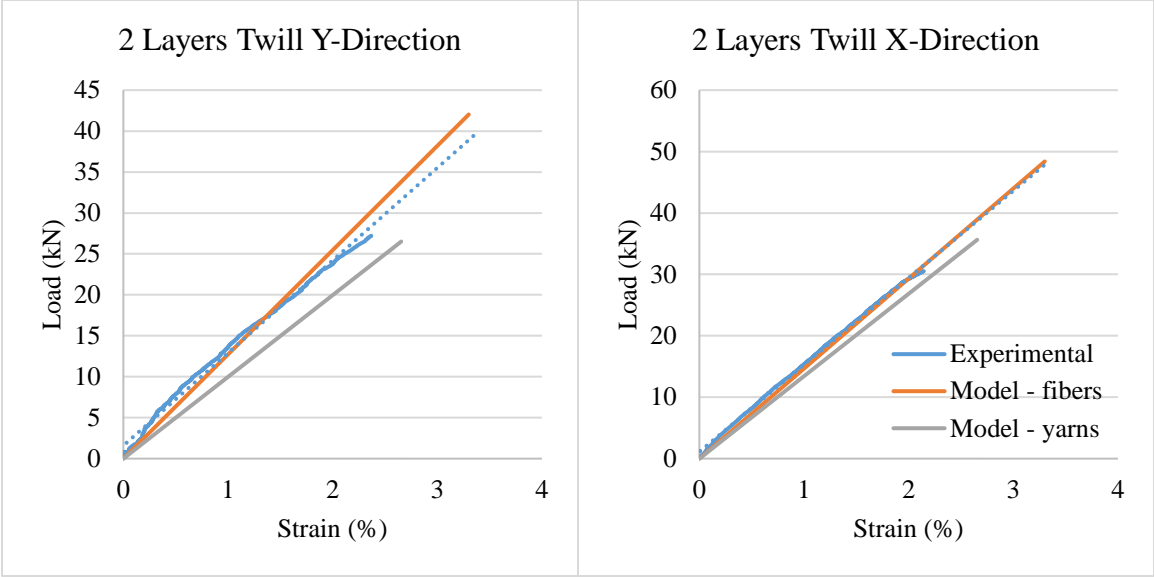
Figure 68 Experimental vs. model tensile load-strain for 3DOW 2x2 Twill E-glass composite with 2.925 picks/ cm in X- and Y-axis directions, (a) 4 layers, (b) 3 layers, and (c) 2 layers.



(a)

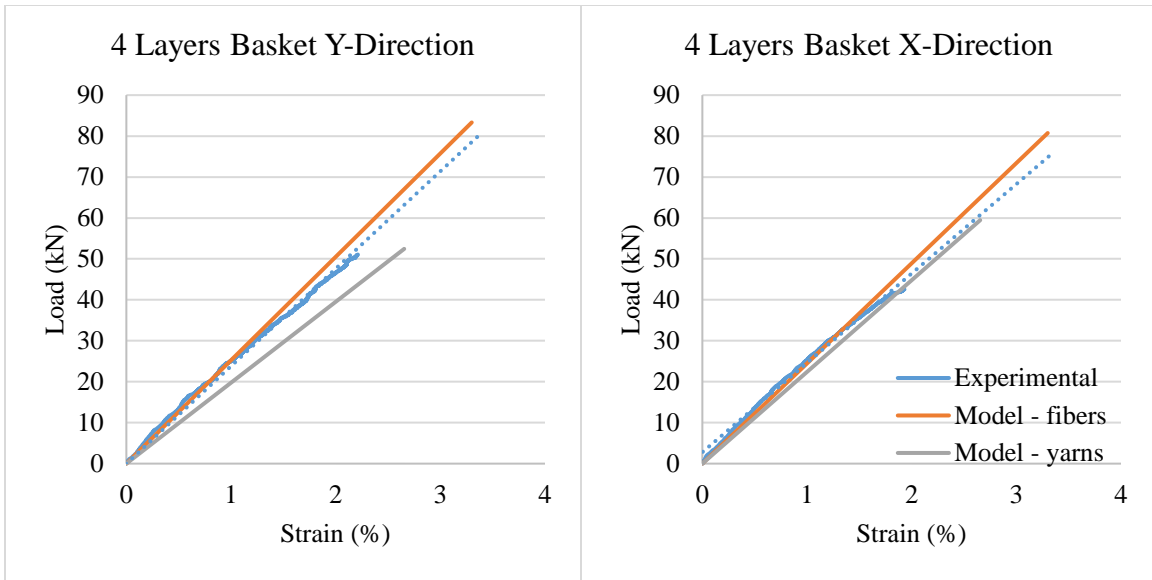


(b)

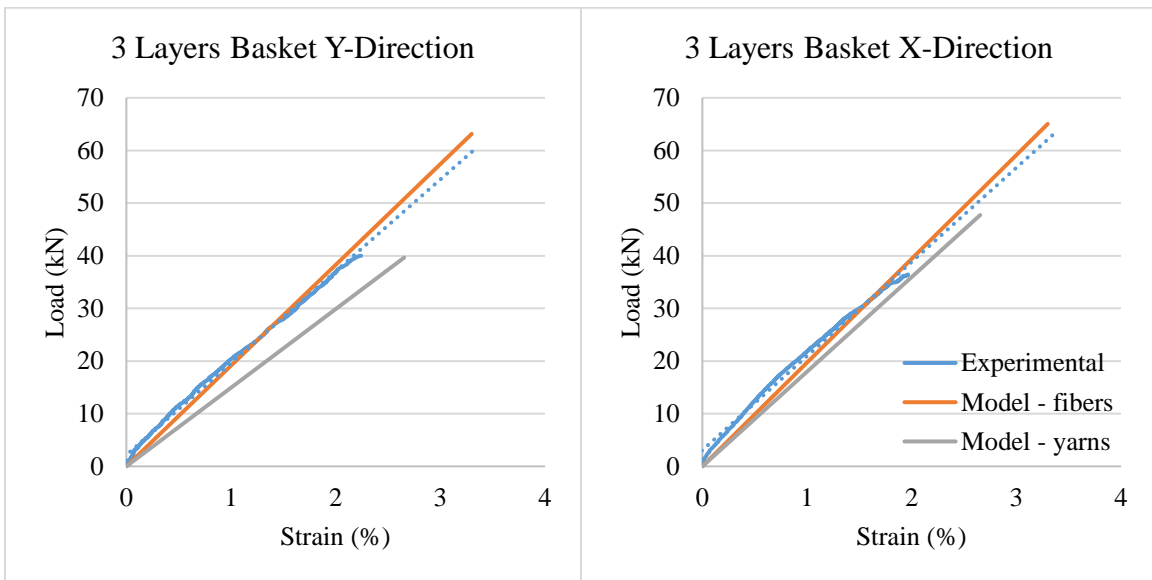


(c)

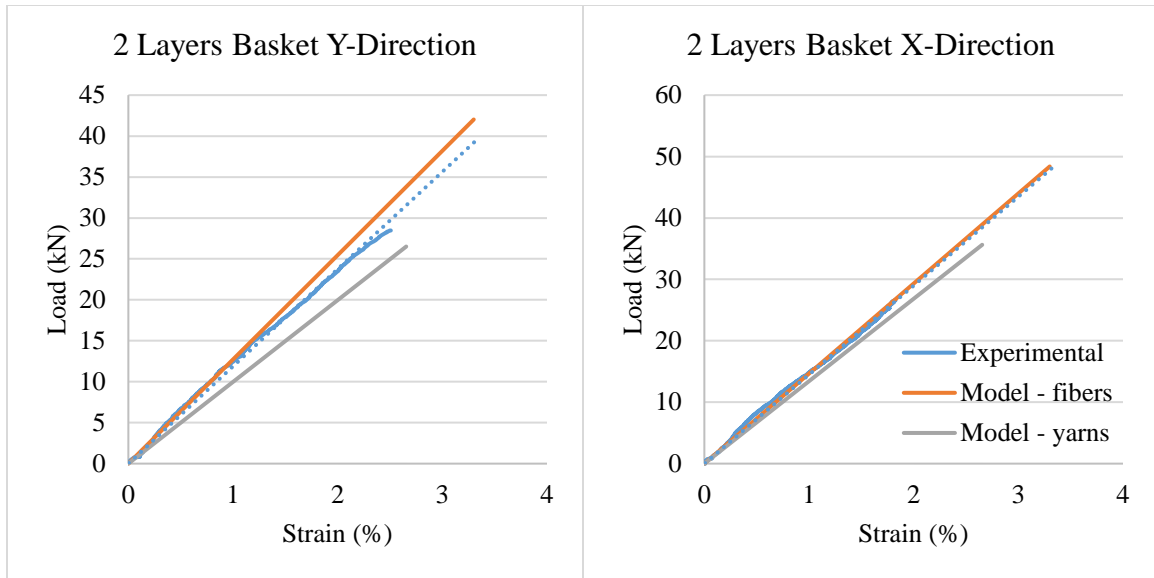
Figure 69 Experimental vs. model tensile load-strain for 3DOW 2x2 Basket E-glass composite with 2.925 picks/ cm in X- and Y-axis directions, (a) 4 layers, (b) 3 layers, and (c) 2 layers.



(a)

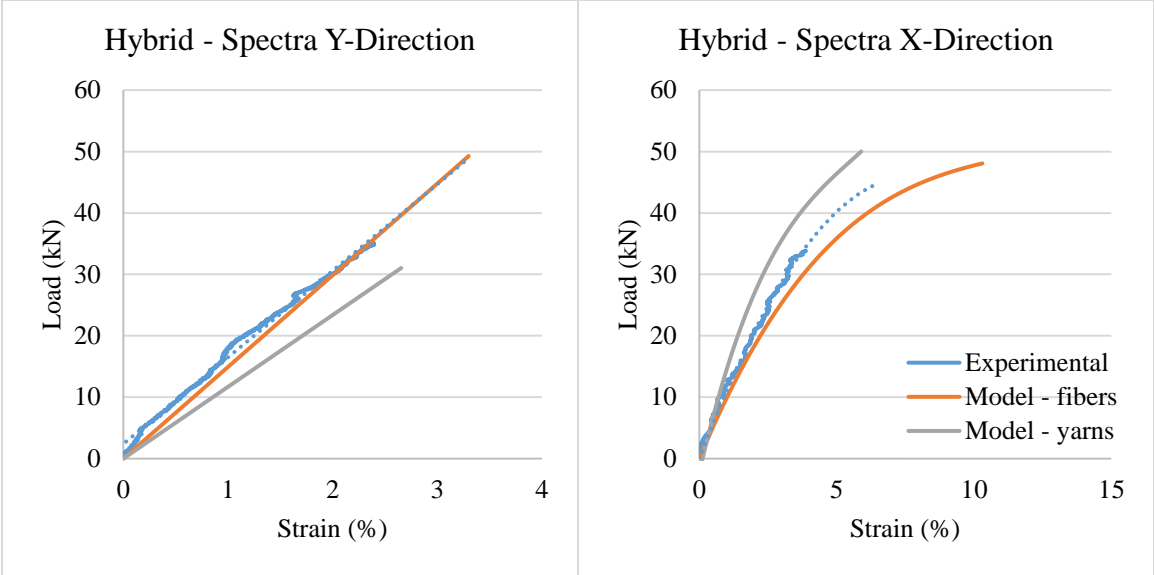


(b)

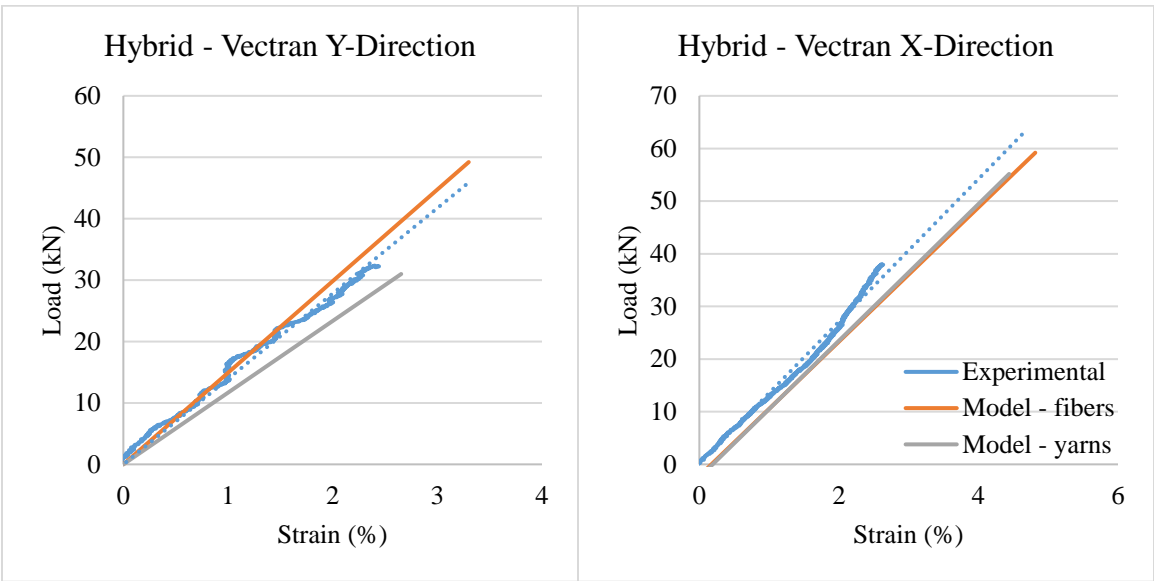


(c)

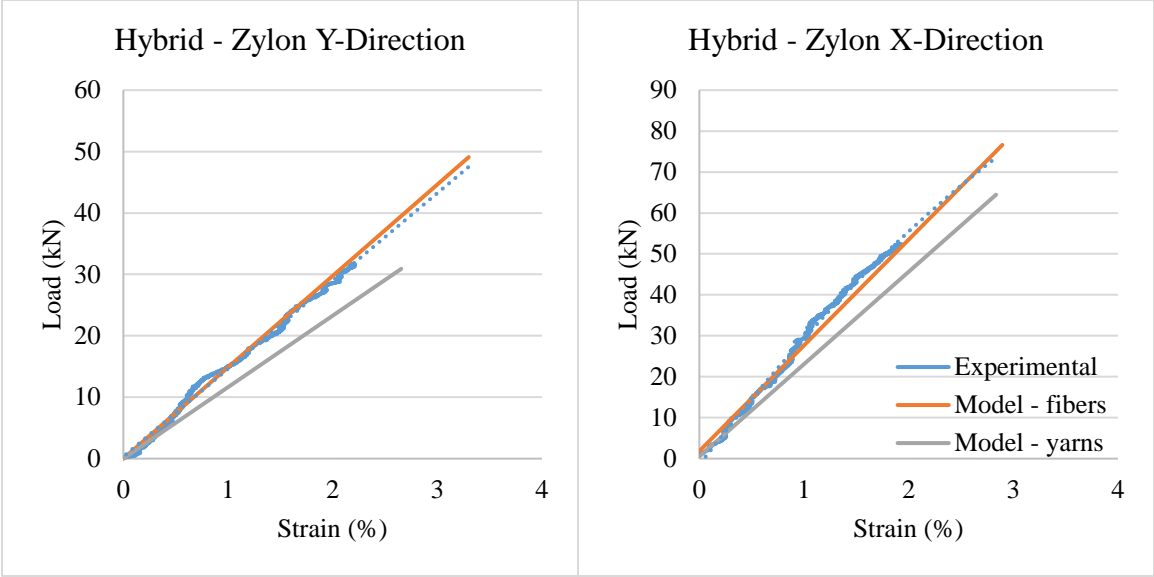
Figure 70 Experimental vs. model tensile load-strain for 3DOW plain hybrid composites in X- and Y-axis directions, (a) Spectra, (b) Vectran, and (c) Zylon.



(a)



(b)



(c)

The results show that there is a general good agreement between the experimental and theoretical curves. Some deviations are noted, which can be explained as follow.

Sources of deviation

Weak-link effect

The weak-link effect is a phenomenon commonly associated with textile materials, it indicates that the theoretical strength of any material can never be achieved in practice, due to the presence of local defects that act as nuclei for rupture initiation. Thus, the strength of textile materials decreases with increasing the gauge length, due to the higher probability of flaws and defects. [64-66]. Similarly, the strength of a specific fiber material decreases by increasing the number of fibers, from a single fiber to a fiber bundle, and this was obvious in Figure 60 [63].

However, this weak-link effect is significantly reduced when a textile material is converted into a composite, because in composites the fibers are interlocked inside the matrix, and they all bear the loads together, and this condition can be considered as a zero gauge length condition. This explains why the theoretically predicted load-strain curves that were based on the tensile properties of the single fiber had better agreement with the experimental curves, than the ones based on the tensile properties of the yarn, as can be seen in Figure 61 through Figure 70.

Strain measurement

One of the most significant deviations of the predicted curves from the experimental ones, is the lower failure strain. This can be attributed to many factors, one of which is the strain measurement method itself. In practice there are several methods used to measure the strain during testing of composite and polymer materials. Such as, electro-optical extensometer, laser vibrometer, laser extensometer, video, and strain gauges.

In this research a laser extensometer was used to measure the strain during the tensile testing. However, from previous data and research, it's clear that there are some discrepancies between the measured strains from each method [67]. For instance, the strain measured using the laser extensometer is usually lower than the measured axial strain from the MTS equipment. Each method has its own limitations, and advantages, thus it's important to understand when to use each method, given the economical, practical, quality of data, and instrumentation

considerations. For example, the measured axial strain from the MTS servo hydraulic load frame, is based on the hydraulic displacement of the grips, which is not very accurate in the case of short specimens. On the other hand, laser extensometer requires the use of retroreflective tape that is placed on the specimen to measure the strain as shown in Figure 71. However, the adhesion between the retroreflective tape and the composite specimens are not always perfect. This results in slippage of the tape during testing, which by turn results in lower strain readings.

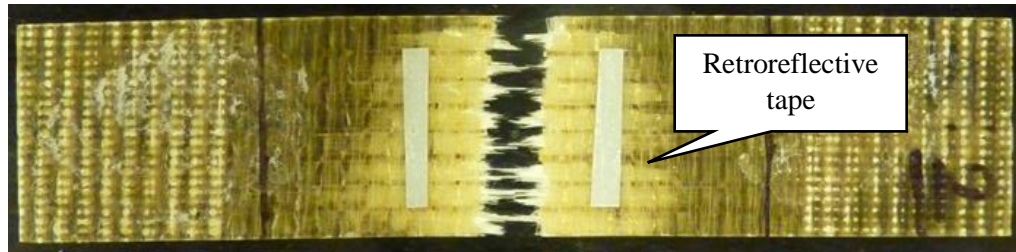


Figure 71 Tensile specimen showing retroreflective tape used for laser extensometer strain measurements

Manufacturing induced defects

The other reason for the lower failure strain is the manufacturing induced defects, that results in a premature failure, which cause the composite to fail under tensile loading at a strain level that is even lower than its constituents. Manufacturing induced defects can be categorized into weaving, Vacuum Assisted Resin Transfer Molding VARTM, and material defects.

During the weaving process the X- Y and Z-yarns are prone to abrasion, due to the friction with the weaving elements. This abrasion results in broken fibers and creates more flaws in the yarns, which by turn degrades the tensile properties. Another phenomenon that influence the tensile properties of the woven preform is the strain hardening of the yarns during weaving. This is due to the fact that the yarns undergo consecutive cycles of loading and unloading during weaving which result in a strain hardening of the yarns, hence reducing its extensibility and failure strain [68].

During the VARTM process, a high level of vacuum is applied on the preform (100 kPa), which results in compressing the preform, producing local stress concentrations at the cross

over points between the Z- and X-yarns. Moreover, these local stresses deform the outermost X-yarns, and results in an increased undulation and waviness of the X-yarns. Another form of local defects in the composite system is voids, which represents air bubbles that enter the system during the resin infusion process. These defects are considered nuclei for cracks initiation, which then propagates across the resin rich pockets in the matrix during loading, and result in a premature failure, at a lower strain level. This explains why the deviation in the failure strain between the predicted and experimental results is more significant in the X-axis direction more than the Y-axis direction.

The interfacial adhesion between the fibers and the matrix, strongly affects the load transfer and continuity of the composite system. However, the proposed model assumes that there is a perfect adhesion between the fibers and the matrix, which is not always true. This explains why the deviation in the failure strain between the theoretical curves and the experimental ones increased in the case of using hybrid composites, with untreated high performance polymeric fibers as illustrated in Figure 70. Since, untreated high performance fibers, such as Spectra, Vectran, and Zylon have very bad interfacial adhesion with thermoset resin matrix systems, which resulted in a lower failure strain [69].

4.5. Numerical parametric study

In this section, a numerical parametric study was performed using numerical results obtained from the theoretical model. In a parametric study a series of simulations is performed by changing one or more parameters, to study the effect of changing these parameters on the output of the model. This study included the effect of changing the Z-yarn linear density, weave factor, pick density and the number of layers on the peak load of the composite, as well as the Z stretch ratios. Table 3 includes a list of weave designs with different weave factors ranging from 1 to 5 which is used in this study. Additionally, four different Z-yarn linear densities 276, 1470, 2275, and 4000 tex are considered for studying the effect of Z-yarn size. The fixed parameters used in this parametric study, are listed in Table 4.

Table 3 Weaves considered for the parametric study

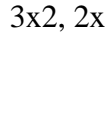
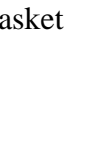
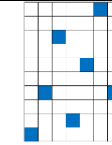
Weave	N_x	i_z	M_z	Weave design
Plain or any filling rib weave	2	2	1.00	
2x1 rib	3	2	1.50	
3x2, 2x1, 1x1 twill	10	6	1.67	
2x1, 2x2 warp rib	7	4	1.75	
3x2, 1x2, 2x1 basket	11	6	1.83	
2x2 warp rib	4	2	2.00	
3x3, 2x1 warp rib	9	4	2.25	
3x2 warp rib	5	2	2.50	
3x3 warp rib	6	2	3.00	
4x3 warp rib	7	2	3.50	
4x4 warp rib	8	2	4.00	
10-H. sateen	10	2	5.00	

Table 4 Fixed parameters used in the parametric study

$\rho_{v\ x, y, z}$	X-, Y-, Z- yarns	ρ_{lx}	ρ_{ly}	AR*	Y-yarns/layer : Z-yarns	$P_y = P_z$
2.5 g/cm ³	E-glass	1470 tex	2275 tex	7	1:1	4.23 mm

* Cross sectional aspect ratio of rectangular filament yarns

4.5.1. Effect on composite peak load

Figure 72 shows the effect of changing the Z-yarn interlacing pattern, which is represented by the weave factor M_z , and the Z-yarn linear density on the peak load of the composite in Y-axis direction. In this run the composite is assumed to have 4 Y-yarn layers and 2.44 picks/ cm/ layer. The calculation of the peak load is based on a composite coupon with 35.6 mm width, and 3, 6, 9 and 12 mm thickness for the 4, 8, 12, and 16 layers respectively.

It's clear from the graph that increasing the Z-yarn linear density increased the peak load of the composite. Moreover, increasing the weave factor, resulted in a general reduction in the peak load as can be seen from the decreasing trend, which is more significant in the case of higher Z-yarn linear density. It's important to mention that at this given conditions the Z-yarns are ruptured at weave factor equals two, this explains the sudden drop in the peak load which reaches a constant value afterwards, where the Y-yarns bear load solely. This can be further explained in the light of the effect of the weave factor on the Z-yarn stretch which will be discussed later.

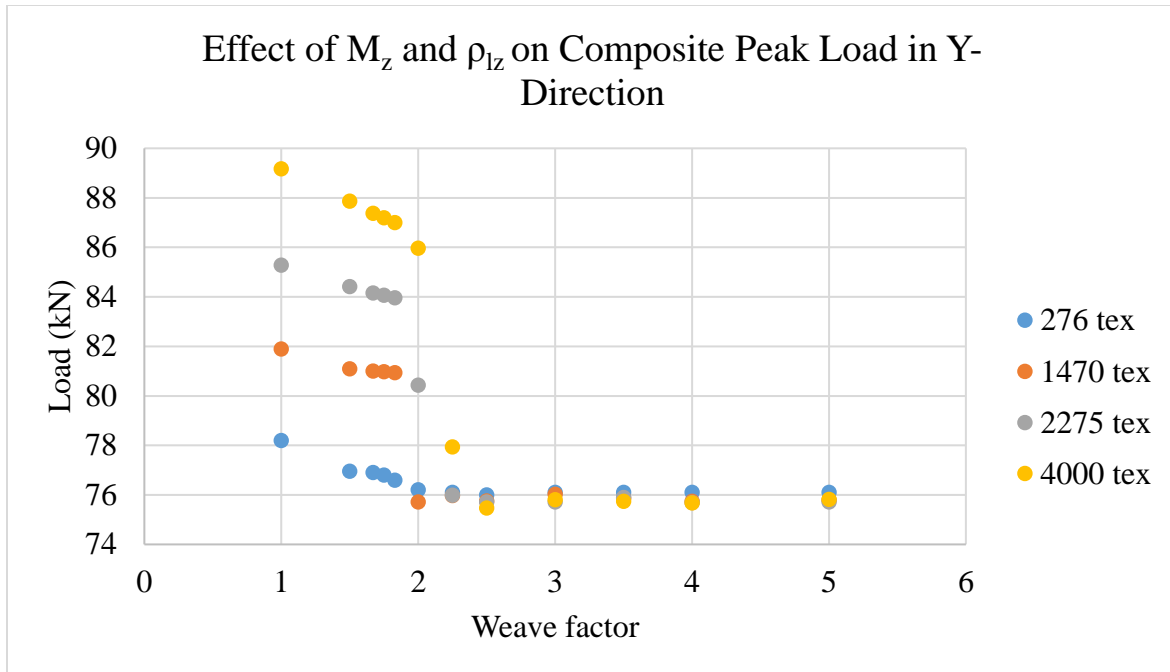


Figure 72 The effect of the Z-yarn weave factor and linear density on the peak load of the composite in the Y-axis direction.

On the other hand, Figure 73 shows the effect of changing the Z-yarn interlacing pattern and linear density on the peak load of the composite in X-axis direction. It's clear that neither changing the weave factor or the linear density have any effect on the peak load of the composite in the X-axis direction. This is due to the fact that the load bearing components in the X-axis direction are the X-yarns and the resin, which is theoretically not affected by Z-yarn changes, except for a negligible effect on the resin volume fraction in the X-axis direction.

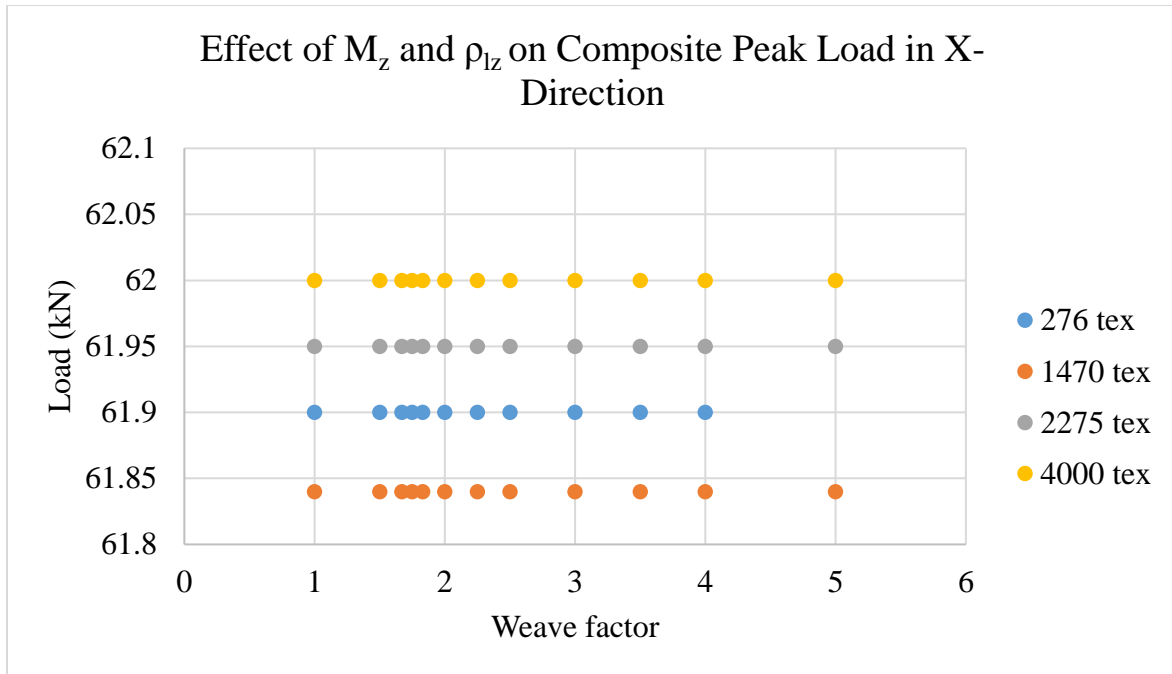


Figure 73 The effect of the Z-yarn weave factor and linear density on the peak load of the composite in the X-axis direction

Figure 74 illustrates the effect of changing the number of Y-yarn layers, and X-yarn pick density on the peak load of the composite in the Y-axis direction. In this run the weave considered is a plain weave, and the Z-yarn linear density is 1470 tex. It's obvious that increasing the number of layers increases the peak load in the Y-axis direction, however increasing the pick density has no effect. Because, X-yarn picks only contributes in the X-axis direction. On the other hand, increasing the number of Y-yarn layers and X-yarn pick density significantly increase the peak load in the X-axis direction as illustrated in Figure 75.

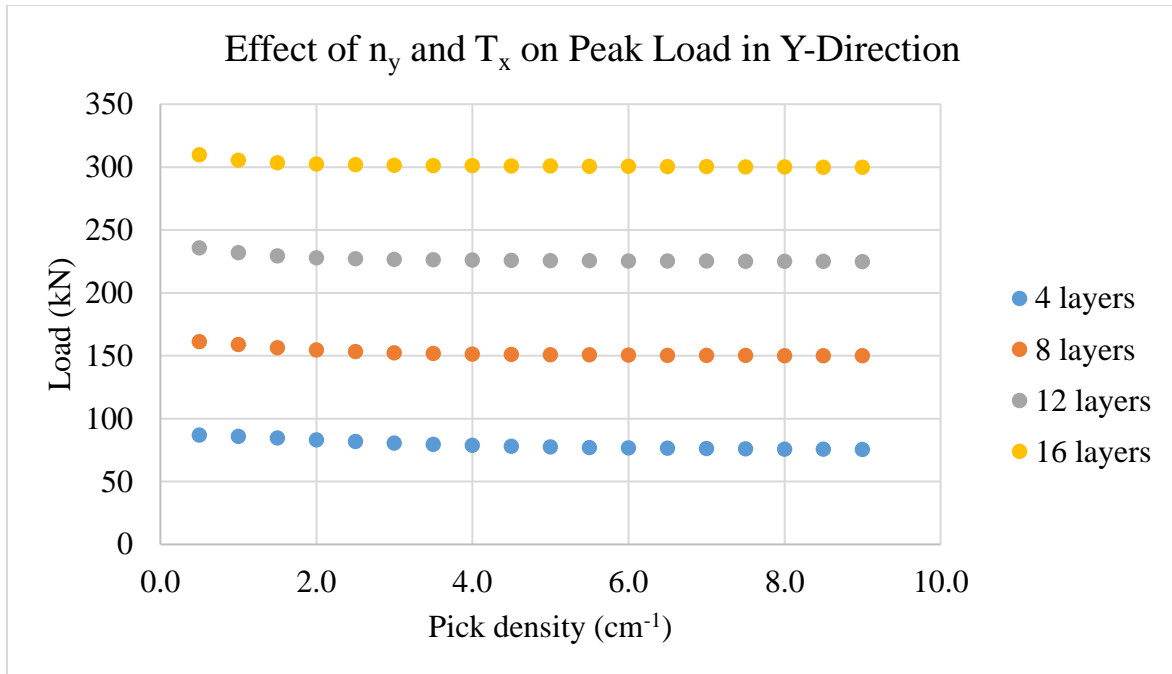


Figure 74 The effect of number of Y-yarn layers, and X-yarn pick density on the peak load of the composite in the Y-axis direction

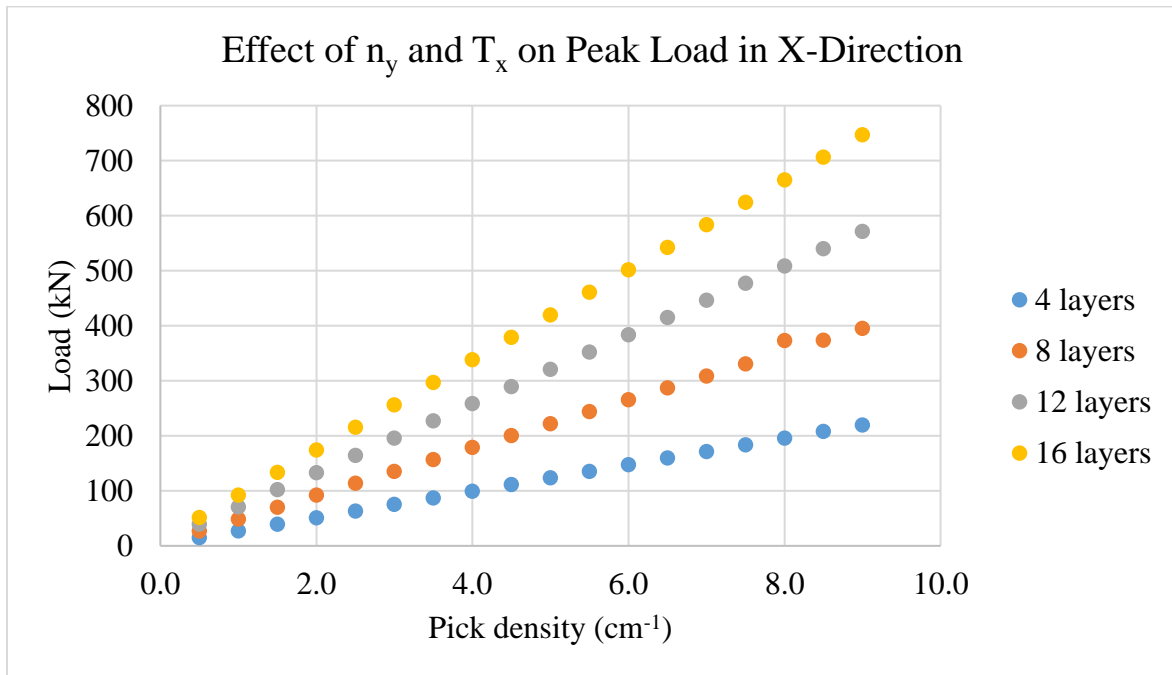


Figure 75 The effect of number of Y-yarn layers, and X-yarn pick density on the peak load of the composite in the X-axis direction

4.5.2. Effect on Z stretch ratios

The Z stretch ratios λ_{yz} , λ_z^A , λ_z^B , and λ_{zk} are the Z-yarn stretch ratio, local preform stretch ratio at unit A, local preform stretch ratio at unit B, and average preform stretch ratio of k^{th} Z-yarn, respectively. Figure 76 indicates the effect of changing the Z-yarn weave factor, Y-yarn number of layers, and X-yarn pick density on the Z-yarn stretch ratios at $\lambda_{zk}=1.03$, 4 Y-yarn layers, 2.44 X-yarn picks/ cm/ layer and Z-yarn linear density 1470 tex. Increasing the weave factor resulted in an increase in λ_{yz} , λ_z^A , and slight decrease in λ_z^B . When the weave factor was increased to 2, the Z-yarn stretch ratio λ_{yz} has reached 1.03 (3 % strain) which is the failure strain for glass fibers used in this study. This is why the peak loads in Figure 72 had a sudden drop at weave factor equals 2.

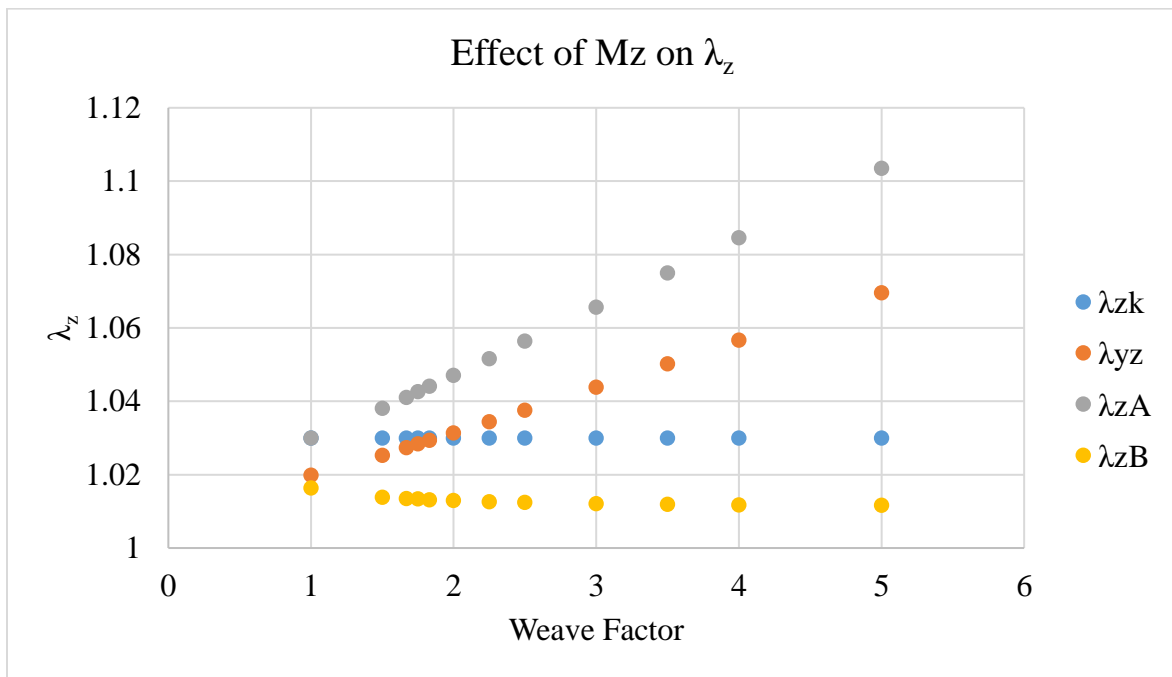


Figure 76 The effect of Z-yarn weave factor on Z stretch ratios

Figure 77 shows the effect of increasing the Y-yarn number of layers on the Z stretch ratios, at $\lambda_{zk}=1.03$, weave factor 2, 2.44 X-yarn picks/ cm/ layer and Z-yarn linear density 1470 tex. The graph shows that increasing the number of layers resulted in a decrease in λ_z^B , λ_{yz} and a slight increase in λ_z^A . This means that increasing the number of layers reduced the strain on the Z-yarn.

Similarly, increasing the X-yarn pick density resulted in a decrease in λ_z^B , λ_{yz} and a slight increase in λ_z^A at $\lambda_{zk}=1.03$, weave factor 2, 4 Y-yarn layers and Z-yarn linear density 1470 tex. Which also means that increasing the X-yarn pick density reduced the strain on the Z-yarn as illustrated in Figure 78.

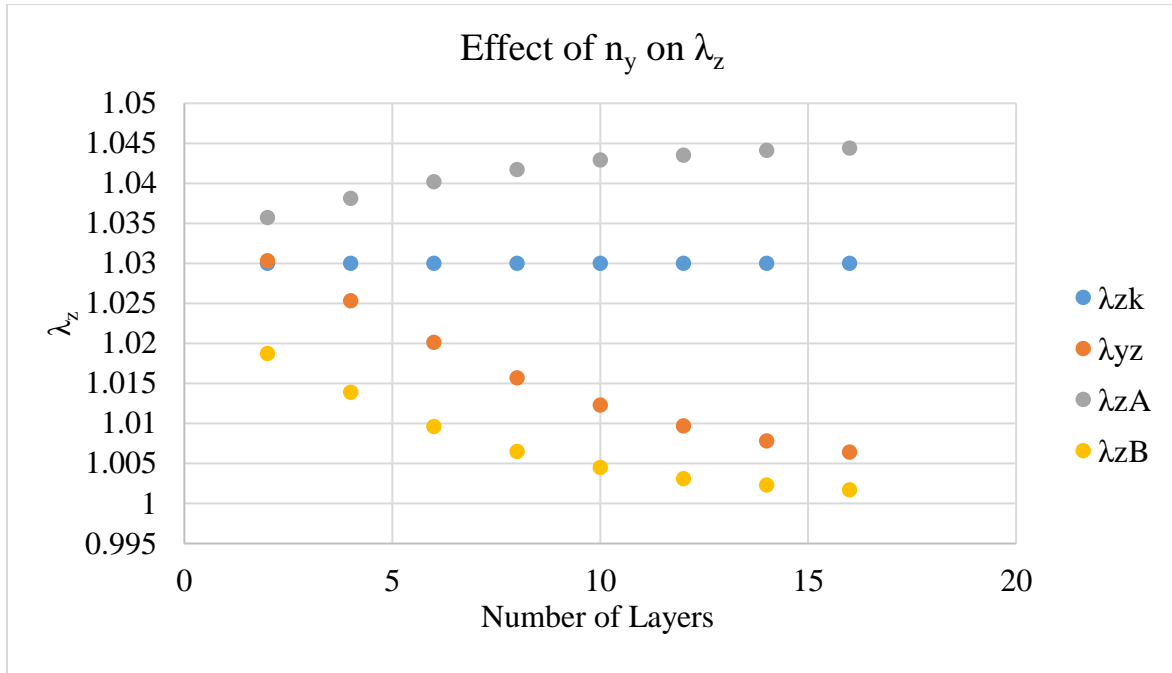


Figure 77 The effect of Y-yarn number of layers on Z stretch ratios

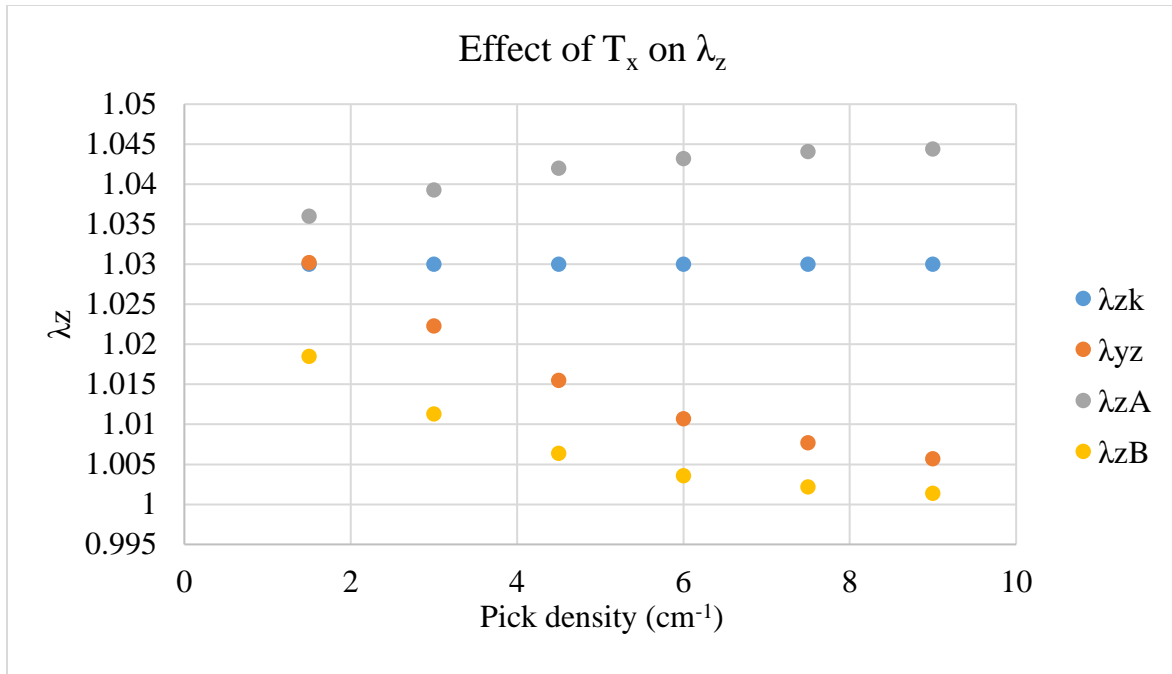


Figure 78 The effect of X-yarn pick density on Z stretch ratios

4.6. Conclusion

A generalized model to predict the load-extension properties of the 3DOW preforms and composites made of spun or filament yarns, using the finite deformation approach was developed. The model relies on the geometry of the structure, and the tensile properties of the constituent yarn and resin components as input parameters, and the output of the model is the entire load-extension diagram of the composite, including the nonlinear region. The model is generalized to predict the load-extension properties of any non-jammed and jammed 3DOW composite, that have any weave architecture, including hybrid composites.

The model was verified experimentally for a broad range of experimental composites, including hybrid ones. The results show that there is a general good agreement between the experimental and theoretical curves. The theoretical curves produced by using the fiber properties had better agreement with the experimental curves, than the ones produced using the yarn properties, due to the weak link effect. One of the significant deviations of the theoretical curves from the experimental ones, is the premature failure, or failure of the composite at a strain level lower than the theoretical. This premature failure was due to the

limitations of the strain measurement method, which was discussed in details. Additionally, this theoretical model doesn't account for defects, thus any manufacturing induced defects, such as weaving, VARTM, and material defects, would result in a premature failure of the composite at lower strain.

A full parametric study was performed to reveal the architecture potential of 3DOW preforms, and show how to optimize the in-plane tensile properties of the composite. The study included the effect of changing the Z-yarn linear density, weave factor, pick density and the number of layers on the peak load of the composite, as well as the Z stretch ratios. It was found that increasing the Z-yarn linear density slightly increases the peak load of the composite in the Y-axis direction, whereas increasing the weave factor slightly reduces it. However, the peak load in the X-axis direction wasn't affected by changing neither the Z-yarn linear density nor the weave factor. It was also observed that increasing the Y-yarn number of layers increased the peak load in both X- and Y-axis directions. Whilst, increasing the X-yarn pick density only increased the peak load in the X-axis direction. Finally, increasing the Z-yarn weave factor increased the strain on the Z-yarn, whilst, increasing the Y-yarn number of layers and X-yarn pick density reduced the strain.

This model is helpful in investigating the potential of using 3DOW preforms in applications other than composites. Since, 3DOW preforms have some attractive features for technical textiles and sports apparel. One of these features are the high drapability and low bending rigidity, due to the very low inter-fiber friction which is an inherent feature of such structure.

5. EXPERIMENTAL

This section covers in details the experimental plans used in this research. The plans were used as a guideline throughout the entire research project to achieve the research goals. The experimental plans include details on the materials being used, the experimental design, sample fabrication methods, sampling plans, and testing procedures.

5.1. Materials

The materials used in this research project can be divided into two categories, the first one is the fiber category, and the second category is the resin and curing agents.

5.1.1. Fibers

The fibers used in this research were glass fiber tows generously donated by PPG industries, in Shelby - North Carolina. The warp, weft and binder tows were Hybon® 2022 E-glass filament yarns, and they were used for all the preforms developed in this research. Each yarn component had a different linear density, the manufacturer's specifications of all 3 yarns components are listed in Table 5 [70]. Glass fibers are considered the dominant type of reinforcement in the composite industry, simply because of its versatility and excellent performance to price ratio, which when compared to carbon it would be much cheaper. Glass fibers are available in different grades, E, S and C, where E is for high modulus, and S for high strength, and C for chemical resistance, however the E-glass is much more consumed than other grades, since it has good mechanical and chemical resistance properties. For such reasons, the E-glass yarns were used to weave the 3D orthogonal preforms for this research.

Table 5 Warp, weft, and binder yarns specifications

Yarn	Linear Density (g/km)	Number of filaments	Filament Diameter (μ)	Fiber Density* (g/cm ³)
Warp (y-yarn)	2275	3920	17	2.59
Weft (x-yarn)	735	1960	14	2.50
Z-yarn (z-yarn)	276	378	14	2.51

5.1.2. Resin and curing agents

As for the, resin and the curing agents used in this study, an epoxy based Vinylester resin was used which was generously donated by Ashland Performance Materials, Kentucky. The DERAKANE® 8084 Vinylester resin was used as the matrix to produce the 3D orthogonal woven composites. The Vinylester ranks in between epoxy and polyester resin in terms of performance and price, it has a good toughness and chemical resistance. The cross linking mechanism of Vinylester is similar to polyester which is much easier than epoxy, and it can be cured at room temperature and there is no need for autoclaving, or post curing. It's being widely used in piping, tanks, home appliances that require moderate toughness, and also marine applications in which corrosion resistance is a priority. Furthermore, Vinylester has an important advantage among polyester resin, which is the lower styrene content, which makes it less hazardous. The Vinylester resin has a good interfacial adhesion with the fibers, due to the pendent OH groups on the epoxy backbone of the Vinylester which results in increased interface bond strength and enhance overall strength of the composite. During the cross-linking of the Vinylester resin, it initially forms gel, which helps all the double bonds to react at the end of the curing process, which result in a uniform glass transition temperature across the composite. This is due to the chemical nature of the Vinylester, which has easy access to the carbon-carbon double bonds, which are available at the end of the Vinylester polymer molecule [3]. Typical properties of the DERAKANE® 8084 epoxy based, and elastomer modified Vinylester resin are listed in Table 6, while the typical properties of the post cured resin are listed in Table 3 [71].

Table 6 Typical liquid resin properties of Derakane® 8084

Property	Value
Density, 25 °C	1.02 g/mL
Dynamic Viscosity, 25 °C	360 mPa·s (cP)
Kinematic Viscosity	350 cSt
Styrene Content	40%
Shelf Life, Dark, 25 °C	6 months

Table 7 Typical properties of post cured Derakane® 8084 resin clear casting

Property	Value	Test Method
Tensile Strength	76 MPa	ASTM D-638 / ISO 527
Tensile Modulus	2.9 GPa	ASTM D-638 / ISO 527
Tensile Elongation, Yield	8-10%	ASTM D-638 / ISO 527
Flexural Strength	130 MPa	ASTM D-790 / ISO 178
Flexural Modulus	3.3 GPa	ASTM D-790 / ISO 178
Density	1.14 g/cm ³	ASTM D-792 / ISO 1183
Volume Shrinkage	8.2%	
Heat Distortion Temperature	82 ⁰ C	ASTM D-648 Method A / ISO 75
Glass Transition Temperature, Tg2	115 ⁰ C	ASTM D-3419 / ISO 11359-2
IZOD Impact (unnotched)	480 J/m	ASTM D-256
Barcol Hardness	30	ASTM D-2583 / EN59

The curing agents used with the resin system include Cobalt Naphtenate-6% (promoter) and DMA (accelerator) and Peroxide type initiator, NOROX® MEKP-925H. Typical properties of the initiator are listed in Table 8 [72].

Table 8 Typical properties of initiator (NOROX® MEKP-925H)

Property	Value
Active Oxygen	9.0 %, max
Form	Liquid
Color	Water white
Specific Gravity @ 25 ⁰ /4 ⁰ C	1.10

The gelation time of the resin can be controlled by the amount of curing agents (initiator, promoter, and accelerator), and it is a very important factor when choosing a resin system, since the gelation time is considered the time window for infiltrating and fully wetting the reinforcement during consolidation. Therefore, the reinforcement has to be completely wet before the resin starts to gel, because once gelation starts the resin flow stops, and if the reinforcement is not completely infiltrated, there will be unsaturated dry spots, which will increase the scrap amount during short gelation time. On the other hand, a long gelation time increases the production time and hence reduce productivity. Thus, it was important to select the optimum gelation time that would provide a sufficient time frame to consolidate the composite, while avoiding unnecessarily prolonged cycles. Table 9 lists the typical gelation times of Derakane® 8084 at different temperatures and corresponding amount of MEKP-925H (initiator), Cobalt Naphtenate-6% (promoter) and DMA (accelerator). The temperature where the resin infusion process takes place is almost 24°C, and the time required to degas the resin and complete a resin infusion cycle, is almost 60 minutes. Therefore, the amounts of curing agents used are the ones highlighted in Table 9 [71].

Table 9 Typical gel times for Derakane® 8084 Resin

Temperature	Auxiliary Curing Chemicals	Gel Time of Resin		
		15 ±5 Minutes	30 ±10 Minutes	60 ±15 Minutes
18°C	MEKP (Initiator), wt.%	3.0	3.0	2.5
	CoNap6% (Promoter) , wt.%	0.6	0.4	0.4
	DMA (Accelerator) , wt.%	0.3	0.2	0.1
24°C	MEKP (Initiator), wt.%	2.0	2.0	1.5
	CoNap6% (Promoter) , wt.%	0.5	0.4	0.3
	DMA (Accelerator) , wt.%	0.3	0.2	0.05
30°C	MEKP (Initiator), wt.%	2.0	1.5	1.5
	CoNap6% (Promoter) , wt.%	0.3	0.3	0.3
	DMA (Accelerator) , wt.%	0.2	0.05	0.025

5.2. Experimental Design

There are two experimental plans A and B, that have been carefully designed to achieve the following objectives: (1) to experimentally verify the proposed generalized finite deformation model of the load-extension properties of 3DOW composites, (2) to study the behavior of 3DOW composites of different architectures under various modes of impact, such as, Tup, Charpy, and Izod, and test the correlation between their different impact responses, and (3) to investigate the effect and the contribution of the Z-yarn component on the in-plane and out-of-plane properties of the 3DOW composites, and optimize the amount of Z-yarns in the structure to achieve a perfect balance between in- and out-of-plane performances. Design of experiment A is for objectives (1) and (2), while design of experiment B is for objective (3).

5.2.1. Design of experiment A

In design of experiment A, it was important to vary the thickness, pick density, and Z-yarns interlacement pattern, to be able to understand how these architectural variables affect the impact resistance of the 3DOW composites under different impact modes. The thickness is controlled by the number of Y-yarn layers, and it affects the overall composite architecture, and the Z-yarn content and configuration, in addition to the resin saturation. As for the different levels of pick densities, they were chosen specifically to manufacture a volume balanced preforms in the X- and Y- directions, for the different number of Y-yarn layers. For instance, 2 y-yarn layers woven with 4.87 x-yarns/layer, 1/cm preform are volume-balanced in x-, and y- direction. Similarly, for 3 y-yarn layers preforms with 5.48 x-yarns/layers, 1/cm preforms are balanced in x- and y-direction. Since, balanced preforms tend to have better interlaminar performance than the unbalanced ones [59]. The experimental design variables and levels are listed in Table 10.

Table 10 Design of experiment A

Variable	Levels
Number of Y-yarn layers	2 ,3, 4
X-yarn density/layer, 1/cm	4.87, 5.48, 5.85
Weave	Plain, 2x2 Basket, 2x2 Twill
Total runs	27 samples (3x3x3)

5.2.2. Design of experiment B

In design of experiment B, it was important to vary the ratio of the Z- to Y-yarns in order to study the contribution of the Z-yarns, the levels were selected so that the Z-yarns percentage in the structure is systematically reduced from 1:1 which is a full interlacement, to 0:1 which is a structure with no Z-yarns interlacements. All the preforms in this experiment are plain weave, having 3 Y-yarn layers, and 5.48 X-yarns/layer/cm. The experimental design variables and levels are listed in Table 11.

Table 11 Design of experiment B

Variables	Levels
Ratio of Z-yarns to Y-yarns	1:1, 2:3, 1:3, 0:1
Total runs	4 samples

5.3. Preforms Formation

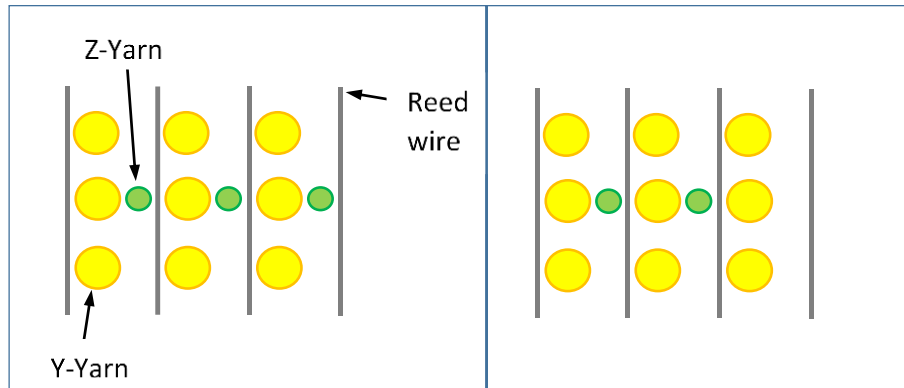
The preforms were woven using a 3D weaving loom that was generously donated by 3TEX Inc. to the composite core facility at the College of Textiles, NCSU. The loom is equipped with a creel for directly supplying the Z- and Y-yarns, the creel can hold up to 1088 yarn packages, and there is another small creel for supplying the X-yarns as shown in Figure 79. This 3D loom utilizes single rigid rapiers for the insertion of the X-yarns, the unique rapier insertion mechanism results in a double insertion/shed of the X-yarns during each insertion cycle, and also results in a continuous X-yarn.



Figure 79 3D weaving loom donated by 3TEX Inc

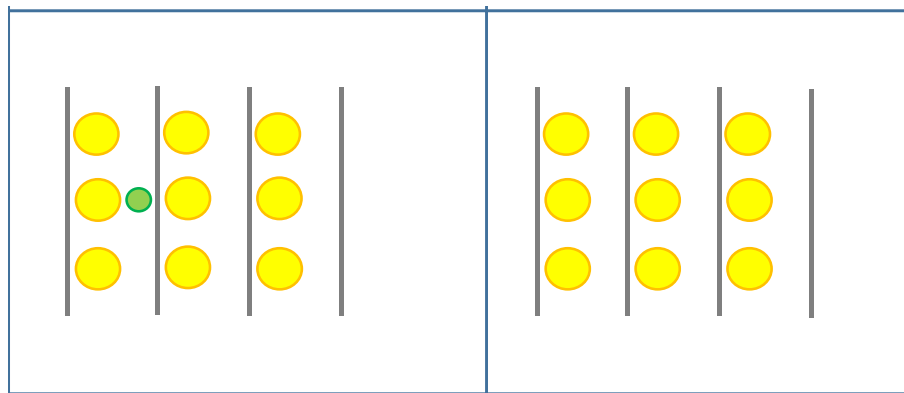
Each warp layer consisted of 102 Y-yarns, and the Y-yarns were spaced evenly using a reed with a dent density of 2.36 dents/cm (6 dents/inch), where each Y-yarn in a layer is placed in a dent. Similarly, the total number of Z-yarns were 102 for the case of full Z-yarns interlacement in which the Z- to Y-yarns ratio is 1:1, and in this case every Z-yarn end is threaded through one of the reed dents with a density of 2.36 dents/cm, the produced preform width was 43 cm excluding the selvedge. The loom includes four harnesses to be able to weave the plain and 2x2 weaves required for the experimental design, such as 2x2 twill and 2x2 basket weaves. Two extra Z-yarns are added to each side of the preform at high tension, to secure the selvedge, lock the structure and prevent unraveling. The machine is equipped with software code with user interface for the user to input x-yarn density and weave type.

A total number of 31 preforms were woven at different structural parameters and fabric architecture, 27 of which were for design of experiment A, and the other 4 were for design of experiment B. Figure 80 shows the denting plans for a 3 layers preform at various Z- to Y-yarns ratios, and Figure 81 shows the corresponding woven preforms.



(a)

(b)



(c)

(d)

Figure 80 Denting plan for a 3 layers preform at various Z- to Y-yarns/ Y-layer ratios (a) 1:1, (b) 2:3, (c) 1:3, (d) 0:1

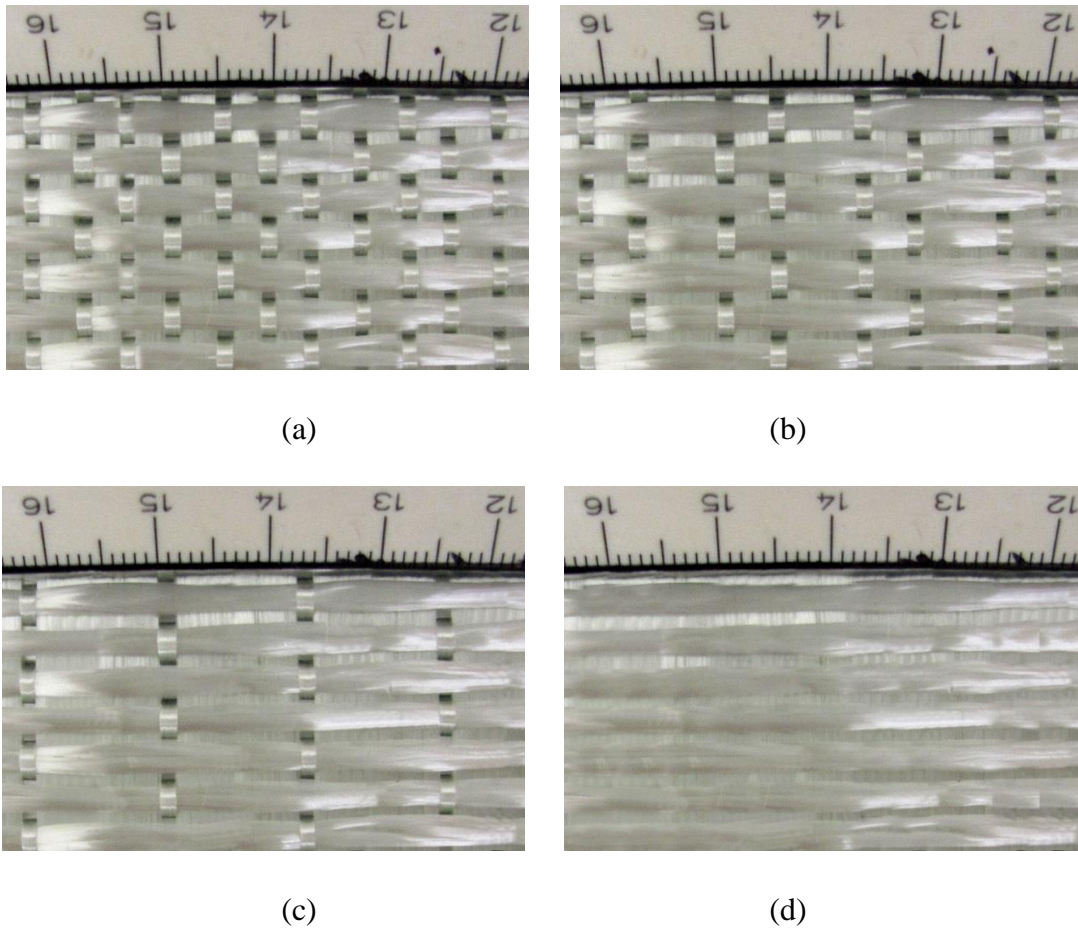


Figure 81 Woven preforms at various Z- to Y-yarns/ Y-layer ratios (a) 1:1, (b) 2:3, (c) 1:3, (d) 0:1

5.3.1. Weaving non-interlaced preforms

In design of experiment B, one of the challenges was to create a preform with no Z-yarns interlacing. One of the approaches was to weave without any Z-yarns, however, this wasn't practical, and the produced preform lacked structural integrity. Therefore, another approach was adopted, this approach utilizes few number of supporting Z-yarns (4 yarns) to hold the structure together. Additionally, it was important to have a stronger selvedge to lock the filling yarns in its place, thus, more Z-yarns were added to widen the selvedge, and an extra tension was added to these yarns as shown in Figure 82 (a). Afterwards, the produced preform are transported to the resin infusion table and the Z-yarns in the middle of the preform were pulled out of the structure to be ready for the consolidation process as shown in Figure 82 (b). The

adopted approach was very effective in producing, handling, transporting and processing non-interlaced 3DOW preforms, while maintaining its structural integrity.

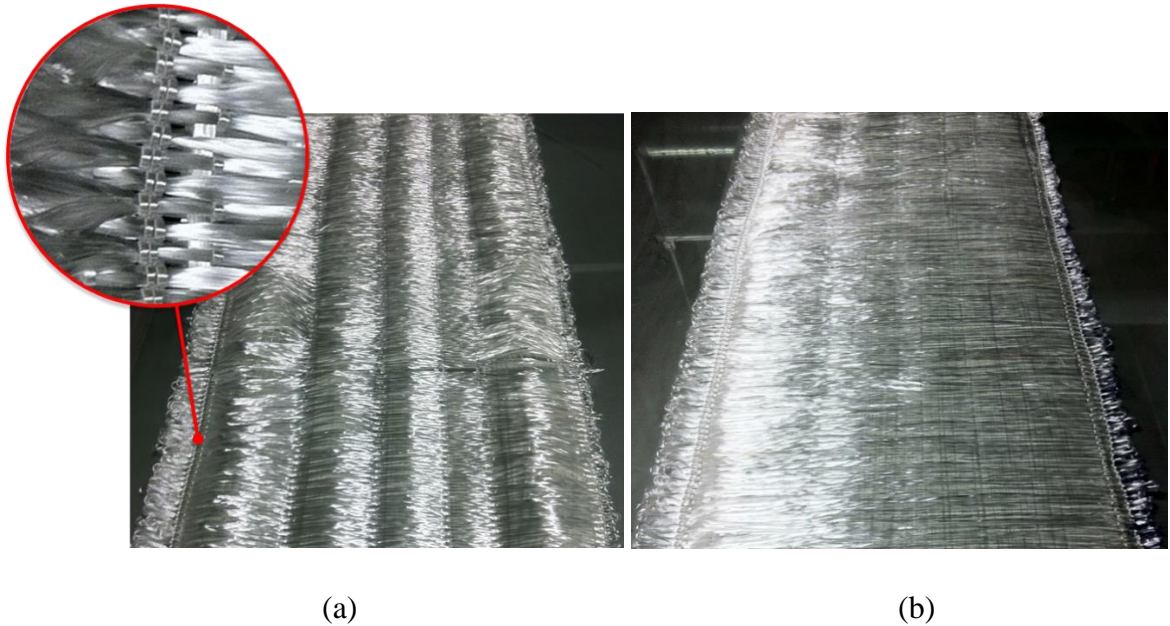


Figure 82 Non-interlaced 3DOW preform, (a) with supporting Z-yarns, and (b) Supporting Z-yarns removed

5.4. Resin Infusion

After weaving the 3D preforms they were consolidated using a vacuum assisted resin transfer molding technique VARTM. The VARTM was performed using a VacMobiles® 20/2 equipment shown in Figure 83 (a), which is available at the composite core facility, NCSU College of Textiles.

In order to reduce the resin transfer time, the width of the sample (X-direction) was chosen to be the resin flow direction since it is shorter than the length. Each dry preform is about 40 cm wide and 100 cm long. The preform is first placed over a release film that is placed over a glass top table, afterwards, the resin inlet and outlet regular and spiral tubing are placed over the preform. Another layer called peel ply is placed over the assembly, to facilitate the release of the composite after the infusion, and also a layer of flow media mesh is placed on top of the

peel ply to facilitate the resin flow. Finally, the whole assembly is sealed using a double sided tacky tape, under a final layer of vacuum bagging plastic as shown in Figure 83 (b).

Once the assembly is complete, the resin outlet is connected to the vacuum pump, and the resin inlet is connected to pressure gauge, to check for any vacuum leakage. If there is a drop in vacuum pressure due to leakage, then the source of the leakage is detected using Amprobe TMULD-300 ultra-sonic leak detector. In total 31 composite samples were produced, each was one-meter-long x 43 cm wide.

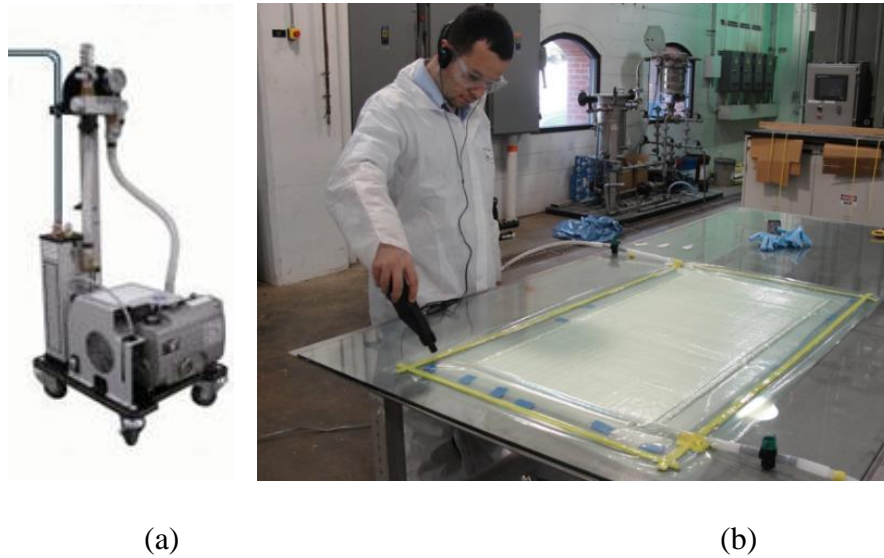


Figure 83 Consolidation using VARTM technique, (a) VacMobiles® vacuum pump, (b) vacuum bagging assembly

Specimens from the composite panel produced for design of experiment B, are show in Figure 84, which illustrates the change in the ratio of the Z-yarn to Y-yarn from 1:1 to 0:1.

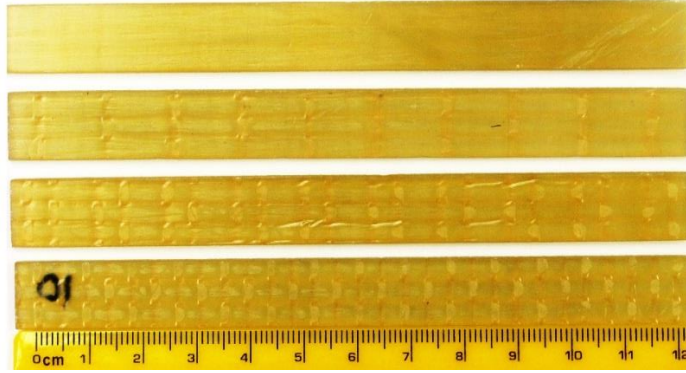


Figure 84 Specimens from the produced composites for design of experiment B

5.5. Testing and Evaluation

The testing conducted in this research, and the standard testing procedures along with the equipment being used are listed in Table 12.

Table 12 List of mechanical tests on final composite structures

Test Name	Standard	Equipment	Figure
Tensile Strength	ASTM D3039 Tensile Properties of Polymer Matrix Composite Materials	MTS Servo hydraulic 370 load frame with laser	Figure 85
Tup Impact Test	ASTM D3763: High Speed Puncture Properties of Plastics Using Load and Displacement Sensors	Instron Drop Tower Impact CEAST 9350	Figure 86 (a)
Charpy Impact	ASTM D6110 Standard Test Method for Determining the Charpy Impact Resistance of Notched Specimens of Plastics	Instron Pendulum Impactor II	Figure 86 (b)
Izod Impact	ASTM D256 Standard Test Methods for Determining the Izod Pendulum Impact Resistance of Plastics	Instron Pendulum Impactor II	Figure 86 (b)



Figure 85 MTS Servo hydraulic 370 load frame for tensile testing



Figure 86 Instron impact testing equipment, (a) drop tower impact CEAST 9350, and (b) pendulum impactor II

5.5.1. Tensile test

For testing the tensile properties of the composites, MTS Servo hydraulic 370 load frame was used. The testing device has 250 kN load capacity and it's located at the Composite Core Facility, College of Textile, NC State University.

The tensile testing was performed according to the ASTM D3039 for testing the tensile properties of the composites in the X- and Y-axis directions. The used specimen size was 152.4 mm in length, and 35.56 mm in width. In order to find the optimum gripping pressure, gripping length and gauge length, several trials were performed to make sure that the failure occurs within the gauge length area. The selected gripping pressure was 10 MPa and cross head speed was 1 mm/min. Whereas, the optimum gripping length was 40 mm, and gauge length was 72 mm. These parameters were optimum to restrain slippage and avoid crushing without the need for using end tabs.

5.5.2. Tup impact test

For testing the Tup impact properties of the composites, Instron Drop Tower Impact CEAST 9350 was used. The testing device is located at the Composite Core Facility, College of Textile, NC State University.

The Tup impact testing was performed according to ASTM D3763 to measure the impact resistance of the composites. The selected specimen size was 60 mm x 60 mm. Preliminary trials were performed to determine the required energy level to achieve full puncture, while maintaining an impact velocity of 4.4 m/s with maximum 20% change. The trials were performed on the strongest samples, which had the highest number of layers and pick density. A dead weight of 22.68 Kg was selected to satisfy these conditions, which is placed over the hemispherical striker of 12.7 mm diameter.

The specimen is pneumatically clamped and then punched by the striker, which is connected to a piezoelectric transducer to measure the force exerted on the specimen in the direction of impact. The user interface draws the force versus displacement curve, and by calculating the area under this curve, the absorbed energy can be obtained, which is also called the total puncture energy. The impact event is considered complete, once the force detected by the striker goes to zero, which indicates that full penetration is attained.

5.5.3. Charpy impact test

For testing the Charpy impact properties of the composites, Instron Pendulum Impactor II was used. The testing device is located at the Composite Core Facility, College of Textile, NC State University.

The Charpy impact testing was performed according to the ASTM D6110 for testing Charpy impact resistance of unnotched composite specimens in the X- and Y-axis directions. The used specimens size was 127 mm in length, and 12.7 mm in width. Several trials were performed in order to find the optimum striking energy. The selected striker energy was 21.6 J which was sufficient to completely break the specimen, while maintaining the absorbed energy level less than 80% of the striker energy. The trials were performed on the strongest samples, which had the highest number of layers and pick density.

5.5.4. Izod impact test

For testing the Izod impact properties of the composites, Instron Pendulum Impactor II was also used. The Izod impact testing was performed according to the ASTM D256 for testing izod impact resistance of unnotched composite specimens in the X- and Y-axis directions. The used specimens size was 63.5 mm in length, and 12.7 mm in width. Several trials were performed in order to find the optimum striking energy. The selected striker energy was 22 J which was sufficient to completely break the specimen, while maintaining the absorbed energy level less than 80% of the striker energy. The trials were performed on the strongest samples, which had the highest number of layers and pick density.

5.5.5. Measuring the fiber volume fraction

Composite specimens were placed in a muffle furnace at 600 °C to burn off the resin. Afterwards, the fiber volume fraction and the void content were calculated according to according to ISO1172 and ASTM D2734, respectively. The experiments were performed at PPG industries, Shelby, NC.

5.6. Statistical Analysis

Statistical analysis tools such as Univariate Analysis of Variance, Duncan post hoc, and Pearson's correlation were used to analyze the effect of the structural parameters of the 3DOW

composites on the mechanical properties. IBM SPSS statistical analysis software was used for this purpose. The independent structural parameters used were, the Y-yarn number of layers, X-yarn pick density, Z-yarn interlacing pattern, and Z- to Y-yarn ratio. Moreover, other response (dependent) analytical parameters were taken into consideration in the analysis, such as, composite thickness and areal density as well as preform areal density.

5.7. Sampling

A sampling plan was developed to have sufficient representative specimens in the principle material directions in accordance with the ASTM standards and guidelines. The specimens are having a staggered layout on the panel for better representation of the sample variability and to maximize the utilization of the produced composite panels as shown in Figure 87.

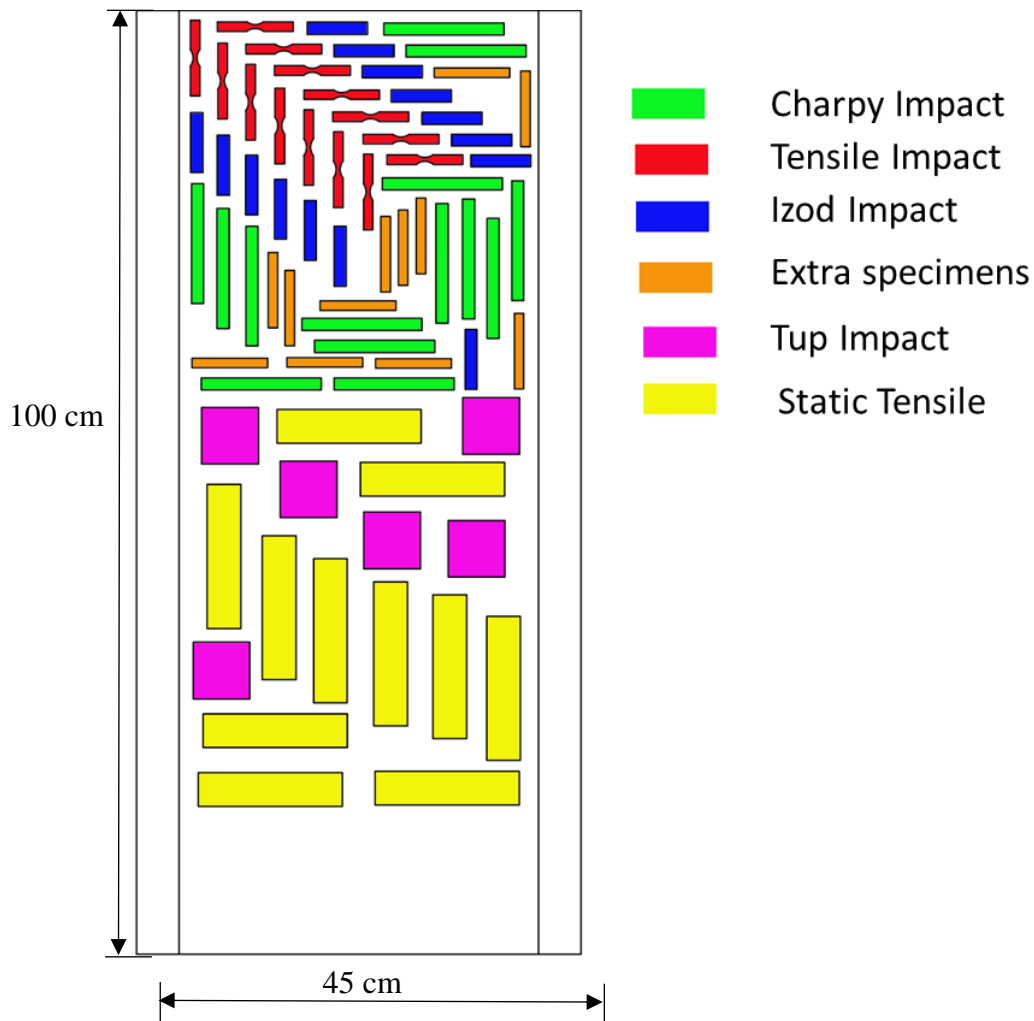


Figure 87 Specimens sampling plan

The specimens were cut using computerized waterjet cutting technology available at ADR Hydro-Cut, Inc., Morrisville, NC. The waterjet cutting are very precise in terms of dimensions, with very low coefficient of variation (less than 0.1%) as shown in Figure 88, and it doesn't cause any thermal induced damages or delamination to the composites, which are very common with the conventional CNC cutting.

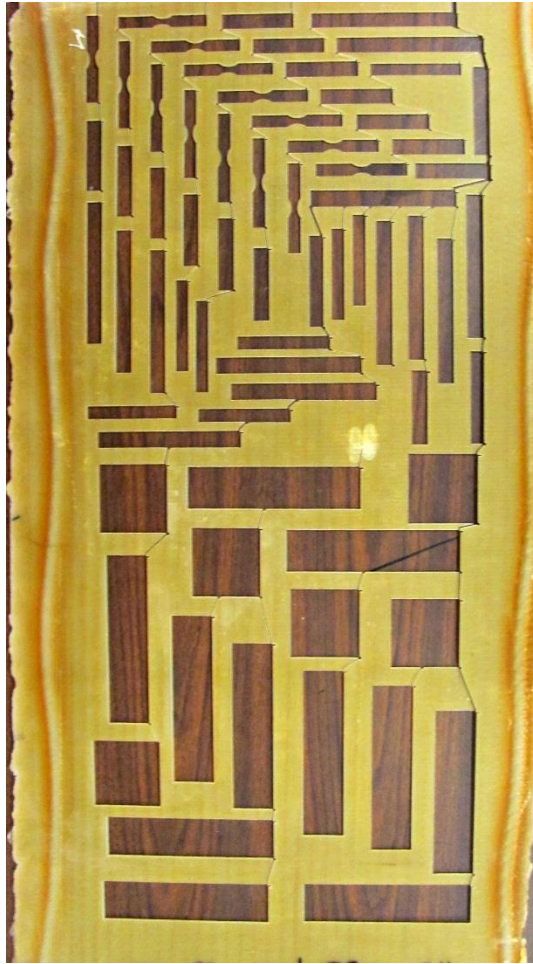


Figure 88 High precision waterjet cut composite panels

6. RESULTS AND DISCUSSION

This chapter is dedicated to presenting and discussing the effect of changing the weave and structural parameters on the properties of the 3DOW composites. The effects of the independent structural parameters of the woven preform on the tensile strength and impact resistance were analyzed statistically. The analysis is done taking into consideration, the fiber volume fraction, the composite and preform areal density, and thickness. A significance level of 5% was selected to reject the null hypothesis, if the test of significance gave a p-value lower than the selected level.

6.1. Experiment A

In Experiment A, we varied the composite thickness (number of y-yarn layers), X-yarn density, and Z-yarns interlacement pattern (weave), to be able to understand how these architectural parameters affect the impact resistance of the 3DOW composites under different impact modes. The thickness is controlled by the number of Y-yarn layers, and Z-yarn content and configuration, in addition to the resin saturation. As for the different levels of pick densities, they were chosen specifically to manufacture a volume balanced preforms in the X- and Y-directions, for the different number of Y-yarn layers. All samples used in Experiment A are listed in Table 13, showing their sample ID and their variable parameters.

Table 13 Experiment A samples ID and their variable parameters

Sample ID	Number of Y-yarn layers	Weave	X-yarn density (picks/cm/layer)
1	2	Plain	4.87
2	2	Twill	4.87
3	2	Basket	4.87
4	2	Plain	5.48
5	2	Twill	5.48
6	2	Basket	5.48
7	2	Plain	5.85
8	2	Twill	5.85
9	2	Basket	5.85
10	3	Plain	4.87
11	3	Twill	4.87
12	3	Basket	4.87
13	3	Plain	5.48
14	3	Twill	5.48
15	3	Basket	5.48
16	3	Plain	5.85
17	3	Twill	5.85
18	3	Basket	5.85
19	4	Plain	4.87
20	4	Twill	4.87
21	4	Basket	4.87
22	4	Plain	5.48
23	4	Twill	5.48
24	4	Basket	5.48
25	4	Plain	5.85
26	4	Twill	5.85
27	4	Basket	5.85

The second objective of this research was to investigate the effect of structural parameters on the performance of a range of 3D orthogonal woven composites under different modes of impact, namely, Tup, Izod, and Charpy impact. The question that was answered in this study is how changing the preform architecture affects the impact resistance of the produced composites, and is there a correlation between the impact resistances of this range of 3DOW composites, under different modes of impact.

6.1.1. Main effects of structural parameters on impact resistance

Tup impact

Tup impact is also known as Dynatup, it's intended to measure the peak load at impact, peak impact energy, as well as the total energy required to penetrate the composite material by striking it with a drop weight at a specific testing conditions. The results of the Tup impact tests for samples 1 through 27 were adapted from Ince's dissertation [59], and the results are listed in Table 14. Figure 89 shows a test specimen with a typical puncture from 3 different views.

Table 14 Tup impact results [59]

ID	Comp. Areal Density (g/m ²)	Thickness t (mm)	FVF (%)	Peak Force (kN)	CV (%)	Total Energy E (J)	CV (%)	E/ t (J/m)	E/ Comp. Areal Density (kJ/g/mm ²)	E/ Preform Areal Density (kJ/g/mm ²)
1	3516	1.87	47.3	4.67	8.8	28.1	9.4	15106	8.00	12.3
2	3271	1.76	51.0	4.40	8.1	26.2	4.2	14943	8.03	11.4
3	3273	1.91	47.3	4.67	13.0	25.8	11.6	13614	7.89	11.3
4	3692	2.03	46.5	4.63	7.4	28.8	6.9	14303	7.85	11.8
5	3395	1.83	52.8	4.78	8.3	26.0	12.6	14302	7.66	10.7
6	3462	1.88	50.0	4.64	5.6	25.9	5.5	13747	7.47	10.5
7	3708	2.01	48.7	4.87	9.2	31.1	1.7	15470	8.38	12.1
8	3609	1.94	52.2	4.92	7.7	28.3	10.1	14721	7.84	11.1
9	3536	1.93	50.6	4.86	3.6	27.1	4.9	14039	7.66	10.8
10	4776	2.62	49.0	5.93	11.5	39.2	9.9	15051	8.22	12.1
11	4650	2.60	48.7	6.20	4.5	38.9	2.8	14960	8.37	12.0
12	4577	2.49	49.4	6.29	6.2	39.0	3.1	15627	8.50	12.2
13	4990	2.76	48.6	6.60	8.2	43.0	3.8	15619	8.62	12.5
14	4834	2.59	51.7	6.61	7.4	42.4	4.7	16408	8.79	12.2
15	4734	2.59	49.7	6.26	6.3	41.2	2.5	15975	8.73	12.1
16	4958	2.70	51.4	6.68	9.3	45.0	5.9	16680	9.09	12.6
17	4985	2.64	53.0	6.91	10.6	43.3	10.0	16487	8.68	12.1
18	5193	2.86	46.3	6.84	6.9	44.1	3.2	15473	8.53	12.5
19	6042	3.36	47.5	7.09	6.4	45.2	2.2	13472	7.50	10.8
20	5898	3.19	50.6	7.59	5.8	53.0	1.7	16614	8.98	12.7
21	5787	3.07	50.5	6.93	6.0	47.9	2.8	15662	8.30	11.5
22	6383	3.71	46.2	7.94	4.7	52.6	9.8	14394	8.29	12.0
23	6563	3.49	48.9	8.37	11.8	60.6	6.6	17339	9.21	13.7
24	6174	3.37	49.9	8.40	3.3	60.8	2.8	18052	9.86	14.0
25	6388	3.50	51.5	7.58	8.1	51.8	12.0	15008	8.11	11.3
26	6597	3.57	50.2	10.31	0.0	69.7	0.0	19542	10.57	15.2
27	6199	3.20	54.7	8.80	4.7	63.3	1.7	19748	10.22	14.0

amount of fiber added to the structure by increasing the pick density is much less than the amount added by increasing the number of layers. Finally, changing the Z-yarn interlacing pattern, had controversial results based on the ANOVA and Duncan tests, this was mostly due to the higher sensitivity of the ANOVA, which is higher than the Duncan post hoc pairwise test. The ANOVA test is capable of detecting lower variation around the mean, while pairwise test hardly distinguishes between the means of the pair. Therefore, by trusting the ANOVA results, the twill had the highest energy, followed by the basket and then plain.

The importance of the normalization approach is to try to develop a design value, in which a composite designer can rely on while designing composites from 3DOW preforms. For instance, when dealing with isotropic materials like metals, one can easily obtain a design value for tensile strength, which is the breaking tensile load normalized by the cross sectional area. This design value in case of metals, can be used to design metal parts with a predetermined tensile strength irrespective of their size. Thus, the normalization approach helped in developing a design value that would eliminate the need for testing same material in different sizes and shapes. In the case of anisotropic materials, such as 3DOW composites, there are many sources of variation that make developing a design value difficult. Examples of sources of variation includes, thickness variation due to the presence of Z-yarn crowns, which is more pronounced in preforms with small number of layers, and as the number of layers increases the effect of the Z-yarn crown diminishes. Also, FVF variation, which is due to the variation in resin saturation during infusion across the composite panels from the inlet to the outlet. However, there was an endeavor in this research to compare different normalization techniques and find out which technique was able to give a reliable design value. The results of the total penetration energy were normalized using three different normalization approaches. First they were normalized by the composite thickness to eliminate the effect of the thickness from the analysis, and to avoid any errors resulting from the thickness variation within a single sample. The results of the statistical analysis of the impact energy normalized by the composite thickness are listed in Table A.12 to Table A.20 in Appendix A. The second approach was to normalize the total energy by the composite areal density, to get a fair comparison between the results of the different samples. The results of the statistical analysis of the impact energy normalized by the composite areal density are listed in Appendix A Table A.22 to Table A.30. The third approach is similar to the second one, yet, in this approach the total energy was

normalized by the preform areal density instead. The results of the statistical analysis of the impact energy normalized by the preform areal density are listed in Appendix A Table A.32 to Table A.40.

Figure 96 shows the main effect of increasing the number of Y-yarn layers on the total energy normalized by the composite thickness, it can be seen that increasing the number of layers increased the normalized energy. However, this increase became less significant after the normalization, and by performing a post hoc Duncan test it revealed that increasing from 3 to 4 layers had no significant effect as shown in Table A.14. Similarly, increasing the pick density, resulted in a statistically significant increase in the normalized energy, and it's less significant than the non-normalized results. Moreover, performing a post hoc test revealed that there was no significant difference between pick densities 4.87 and 5.48 picks/ cm/ layer, as well as between 5.48 and 5.85 picks/ cm/ layer as shown in Table A.17. On the other hand, the effect of changing the Z-yarn weave pattern became less significant with a p-value = 0.03 in Figure 98. Thus, it can be concluded that normalizing the total energy by the composite thickness generally reduced the effect of changing the structural parameters. However, the existence of a residual increasing trend by increasing the number of layers as well as increasing the pick density, indicated that these two parameters have a significant effect on the composite impact energy normalized by thickness. Additionally, it indicated that increasing the number of layers or pick densities didn't negatively affect the wettability and penetration of the resin through the preform, because if increasing the number of layers reduced the normalized impact energy, then there would be defects associated with increasing the number of layers, for instance, resin penetration.

Afterwards, the results of the total energy were normalized by the composite areal density, to eliminate the effect of the composite weight from the analysis and to have a fair comparison between samples irrespective of their weight. Figure 100 shows the main effect of increasing the number of Y-yarn layers, which is statistically significant at a confidence level of 95%. Moreover, increasing the pick density in Figure 101 resulted in a statistically significant increase in the normalized energy, yet, the post hoc test indicated that the effect of pick densities 4.87 and 5.48 picks/ cm/ layer has no significant difference, as well as between 5.48 and 5.85 picks/ cm/ layer as shown in Table A.27. Finally, the effect of changing the weave

pattern in Figure 102, became less significant, and the twill had the highest normalized energy, followed by the basket and then the plain weave. The responses in this case were very similar to the responses of the previous case, when the energy was normalized by the composite thickness. Thus, it can be concluded that the effect of the composite thickness was similar to that of the composite weight, on the total penetration energy.

The third normalization approach, was conducted by normalizing the impact energy by the preform areal density, to eliminate the effect of the preform weight from the analysis, in order to have a fair comparison between samples irrespective of their fiber weight. In this case the effect of increasing the number of layers is slightly dimmed, but it's still resulting in a statistically significant increase in the normalized energy as shown in Figure 104. As for the effect of the pick density, the ANOVA test indicated that it's slightly significant, as illustrated in Figure 105. On the other hand, the weave effect illustrated in Figure 106, had no statistical significance. The results of the total energy after being normalized by the preform areal density, indicated that this approach was the most accurate way of having a fair comparison between samples. Additionally, the results show that the number of layers had the most significant effect on the impact energy, followed by the pick density that had less effect, and finally the weave pattern.

Izod impact

In the case of Izod impact testing, the energy required to fracture the composite specimen supported as cantilever was measured, in both X- and Y-axis directions. The failure analysis of the specimens in case of X-axis direction, indicated that the X-yarns are torn during the fracture. Whereas, specimens tested in the Y-axis direction show that the Y- and Z-yarns were ruptured during the impact test. The results of the Izod impact testing in Y- and X-axis directions are listed in Tables 15 and 16 respectively.

Table 15 Izod impact results in Y-axis direction

ID	Thickness (mm)	Composite Areal Density (g/m²)	Total Energy (J)	CV (%)	Energy/ Thickness (J/m)	Energy/ Comp. Areal Density (kJ/g/mm²)	Energy/ preform Areal Density (kJ/g/mm²)
1	1.93	3236	6.06	12.8	3138	1.87	2.64
2	1.75	3285	7.51	28.6	4292	2.29	3.27
3	1.7	3262	8.67	4.6	5099	2.66	3.80
4	1.95	3434	8.04	15.6	4124	2.34	3.29
5	1.8	3412	5.54	25.8	3078	1.62	2.28
6	1.75	3504	5.41	21.7	3094	1.55	2.20
7	2	3611	6.14	17.7	3072	1.70	2.40
8	2	3584	5.59	9.7	2794	1.56	2.19
9	1.95	3337	5.76	24.7	2955	1.73	2.30
10	2.75	4750	8.27	14.1	3006	1.74	2.56
11	2.5	4618	9.86	22.2	3945	2.14	3.05
12	2.3	4426	8.32	12.5	3617	1.88	2.60
13	2.7	4856	8.16	11.5	3022	1.68	2.37
14	2.75	4892	9.42	22.6	3426	1.93	2.71
15	2.6	4774	8.07	6.5	3105	1.69	2.36
16	2.85	5104	9.85	8.9	3456	1.93	2.75
17	2.5	4860	8.71	23.0	3485	1.79	2.43
18	2.4	4769	10.59	20.8	4413	2.22	3.00
19	3.2	6005	15.43	19.3	4822	2.57	3.68
20	3.2	5891	13.35	20.3	4173	2.27	3.20
21	3.05	5788	13.97	13.7	4579	2.41	3.36
22	3.2	6072	13.39	14.4	4185	2.21	3.06
23	3.3	6122	14.55	11.0	4408	2.38	3.29
24	3.25	6013	14.64	16.5	4506	2.44	3.36
25	3.35	6487	14.06	13.5	4198	2.17	3.06
26	3.45	6495	11.17	13.1	3236	1.72	2.44
27	3.25	6478	10.05	16.3	3092	1.55	2.23

Table 16 Izod impact results in X-axis direction

ID	Thickness (mm)	Composite Areal Density (g/m²)	Total Energy (J)	CV (%)	Energy/ Thickness (J/m)	Energy/ Comp. Areal Density (kJ/g/mm²)	Energy/ preform Areal Density (kJ/g/mm²)
1	1.9	3172	9.5	26.2	4992	2.99	4.13
2	1.75	3323	9.2	8.7	5261	2.77	4.01
3	1.95	3298	8.3	3.6	4252	2.51	3.64
4	2	3408	6.8	11.1	3386	1.99	2.77
5	1.8	3352	8.7	12.2	4828	2.59	3.58
6	2	3446	7.4	23.5	3678	2.13	2.99
7	2.1	3656	7.2	17.8	3435	1.97	2.81
8	2	3564	7.7	14.1	3865	2.17	3.03
9	1.8	3341	6.5	13.5	3624	1.95	2.60
10	2.75	4776	10.0	14.6	3622	2.09	3.08
11	2.55	4634	11.1	21.8	4343	2.39	3.43
12	2.5	4485	9.1	14.3	3651	2.04	2.85
13	2.7	4823	9.5	24.6	3528	1.98	2.76
14	2.7	4899	11.2	16.3	4154	2.29	3.23
15	2.9	5049	14.6	14.9	5018	2.88	4.26
16	2.85	5272	12.5	9.6	4373	2.36	3.48
17	2.65	4902	12.5	12.3	4699	2.54	3.48
18	2.4	4726	10.5	26.2	4389	2.23	2.98
19	3.25	5946	15.1	12.7	4631	2.53	3.59
20	3.15	5872	13.0	8.8	4142	2.22	3.13
21	3.3	5958	15.7	10.7	4764	2.64	3.79
22	3.25	5944	16.3	8.2	5007	2.74	3.72
23	3.4	6108	13.4	14.1	3945	2.20	3.04
24	3.4	6049	16.6	5.8	4880	2.74	3.81
25	3.4	6385	16.1	7.4	4731	2.52	3.50
26	3.5	6612	17.0	7.5	4855	2.57	3.71
27	3.55	6409	16.8	15.1	4731	2.62	3.72

In Izod tests several types of breaks can be observed, such as complete, hinged, partial, or non-break. A list of break types and their description is shown in Table 17 which was adapted from ASTM D256. However, in this research only specimens with complete breaks were considered for the analysis. Figure 90 illustrates the Izod specimens with different types of breaks.

Table 17 Type of breaks in Izod impact specimens according to ASTM D256

Symbol	Break Type	Description
C	Complete break	A break where the specimen separate into two or more pieces
H	Hinged break	An incomplete break, such that one part of the specimen cannot support itself above the horizontal when the other part is held vertically (less than 90° included angle)
P	Partial break	An incomplete break that does not meet the definition for a hinge break but has fractured at least 90% of the distance between the vertex of the notch and the opposite side
N	Non-break	An incomplete break where the fracture extends less than 90% of the distance between the vertex of the notch and the opposite side

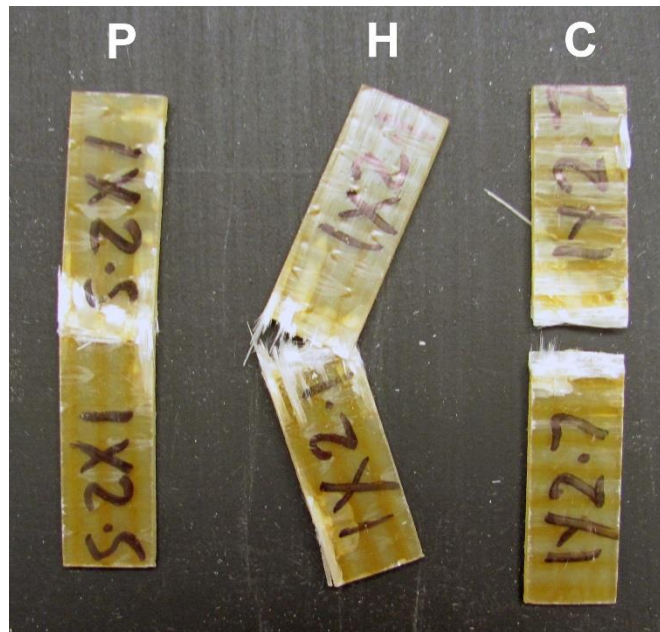


Figure 90 Types of breaks in Izod impact specimens

The results of the total energy of all the specimens, were analyzed using univariate analysis of variance to reveal the effect of the structural parameters on the total energy. The structural parameters included, Y-yarn number of layers, X-yarn pick density, and Z-yarn weave pattern. The results of the univariate analysis of variance test were confirmed using a follow up post hoc Duncan test. The statistical analysis results in the Y- and X-axis directions are listed in Appendix B and C respectively. Further, the main effects of the structural parameters are plotted in Figure 92 to Figure 107.

Firstly, the results in the Y-axis direction were analyzed. Figure 92 (a) shows that increasing the number of Y-yarn layers resulted in a significant increase in the total impact energy. On the contrary, increasing the X-yarn density resulted in a statistically significant decrease in the total energy as shown in Figure 93 (a), the effect was not very significant as the p -value=0.023. Furthermore, by performing a post hoc test, it was indicated that there is no significant difference between the pick densities 4.87 and 5.48 picks/ cm/ layer and that they belong to the same subset as shown in Table B.7. On the other hand, the Z-yarn weave pattern had no significant effect on the total energy as illustrated in Figure 94 (a). From the previous analysis, it can be roughly concluded that increasing the number of layers increased the total energy due to the increase in the amount fibers resisting the impact. However, increasing the pick density surprisingly, resulted in a slight decrease in the total energy, which could be due to the increase of number of Z-yarn interlacement per unit length, which results in more stress concentration spots, which are considered nuclei for crack initiation. Finally, changing the Z-yarn weave pattern didn't have any significant effect on the total energy, since the Z-yarns used in this experiment had very small linear density compared to the X- and Y-yarns.

The results of the total Izod energy in the Y-axis direction were normalized using three different normalization approaches, same as the ones used for Tup impact. First normalized by the composite thickness, second by composite areal density, and third by preform areal density. The results of the statistical analysis of the normalized total energy in Y-axis direction are listed in Appendix B.

In Figure 96 (a) the main effect of increasing the number of layers on the total energy normalized by composite thickness is illustrated. The analysis indicates that increasing the number of layers is statistically significant, yet it's less significant than the non-normalized

results, and by performing a post hoc test, it revealed that there is no significant difference when changing from 2 to 3 layers as shown in Table B.14. As for the effect of increasing the pick density on the normalized energy in Figure 97 (a), it's found that the decreasing trend became more significant, but still the post hoc test indicates that there is no significant difference between the pick densities 5.48 and 5.85 picks/ cm/ layer as shown in Table B.17. On the other hand, changing the weave pattern had no significant effect on the normalized energy as shown in Figure 98 (a). Thus it can be concluded that normalizing the total energy by the composite thickness, reduced the significance of the number of layers, and increased the significance of the pick density.

Furthermore, the results of the total energy were normalized by the composite areal density, Figure 100 (a) shows the main effect of increasing the number of layers in this context. There is a slight increase in energy which is statistically significant, yet by performing the post hoc test, it indicated that there is no significant difference between the results of the 2 and 3 layers and that they both belong to the same subset as shown in Table B.24. As for the effect of increasing the pick density it became more significant as illustrated in Figure 101 (a), and the decreasing trend was confirmed by the Duncan post hoc test, that indicated that all 3 level of pick densities belong to different subsets, as shown in Table B.27. Still, the analysis of the weave pattern effect on the normalized energy indicated no significance as shown in Figure 102 (a). Overall, the results of the total energy normalized by the composite areal density were similar to that of the impact energy normalized by the composite thickness, except for the increased significance of the pick density.

Finally, when the Izod energy results were normalized by the preform areal density, they similarly indicated that the number of layers had a less significant effect as depicted in Figure 104 (a). Further, the decreasing trend in the normalized energy became even more significant as shown in Figure 105 (a). As for the effect of changing the weave pattern, it was still not significant. By looking at the different results from the different normalization approaches, it can be indicated that the three methods generally produced the same results, yet the normalization by the preform areal density is the most accurate, since it eliminates the effect of the preform (fiber) weight from the analysis and results in a fair comparison between the different samples. Additionally, increasing the number of layers resulted in a slight increase in

the normalized energy, while increasing the pick density resulted in a more pronounced decrease in the total energy, and still the weave pattern has no significant effect.

Secondly, the results in the X-axis direction were analyzed. Figure 92 (b) shows that increasing the number of Y-yarn layers resulted in a significant increase in the total impact energy, that was even higher than that of the Y-direction. However, increasing the X-yarn density didn't have any significant effect on the total energy as shown in Figure 93 (b), which was different from the effect in the Y-axis direction. Similarly changing the Z-yarn weave pattern didn't have any significant effect on the Izod impact energy in the X-axis direction as shown in Figure 94 (b), which was the same case as in the Y-axis direction. From the previous analysis, it can be concluded that increasing the number of Y-yarn layers increased the total energy in the X-direction, even more significant than the Y-direction. Because, the X-yarns component is the main component that resist the impact in the case of performing the Izod test in the X-axis direction, and since the number of X-yarn layers is always one more than the Y-yarn layers. This explains why increasing the number of Y-yarn layers is more significant in the X-direction than in the Y-direction. Moreover, increasing the X-yarn pick density didn't have any significant effect, since the specimen edge is what the striker hits, thus the most significant dimension is the thickness, yet, increasing the pick density takes place in the width dimension. This explains why increasing the pick density doesn't have any significant effect on the total energy in the X-axis direction. Finally, changing the Z-yarn weave pattern didn't have any significant effect on the total energy, since the Z-yarns used in this experiment had very small linear density compared to the X- and Y-yarns.

The results of the total Izod energy in the X-axis direction were normalized using three different normalization approaches, similar to the X-axis direction. First normalized by the composite thickness, second by composite areal density, and third by preform areal density. The results of the statistical analysis of the normalized total energy in X-axis direction are listed in Appendix C.

In Figure 96 (b) the main effect of increasing the number of layers on the total energy normalized by composite thickness is illustrated. The analysis indicated that increasing the number of layers was statistically significant, yet it's less significant than the non-normalized results, and by performing a post hoc test, it revealed that there is no significant difference

when changing from 2 to 3 layers as shown in Table C.14 which is the same trend in the Y-direction. As for the effect of increasing the pick density on the normalized energy in Figure 97 (b), it's found that there is no statistical significance, and the trend is unchanged by normalizing. Similarly, changing the weave pattern had no significant effect on the normalized energy as shown in Figure 98 (B). Thus, it can be concluded that normalizing the total energy by the composite thickness, reduced the significance of the number of layers, while the pick density and the weave pattern effects are unchanged.

Furthermore, the results of the total energy were normalized by the composite areal density, Figure 100 (b) shows the main effect of increasing the number of layers in this context. There is a slight increase in energy which is statistically significant, yet by performing the post hoc test, it indicated that there is no significant difference between the results of the 2 and 3 layers and that they both belong to the same subset as shown in Table C.24. As for the effect of increasing the pick density, it had no significant effect as illustrated in Figure 101 (b). Moreover, the analysis of the weave pattern effect on the normalized energy still indicated no significance as shown in Figure 102 (b). Overall, the results of the total energy normalized by the composite areal density were similar to that of the impact energy normalized by the composite thickness.

Finally, when the Izod energy results were normalized by the preform areal density, the results were in agreement with the results normalized by the composite areal density. It's found that the number of layers had a less significant effect as depicted in Figure 104 (b). Further, neither the X-yarn pick density nor the Z-yarn weave pattern had any significant effect on the normalized total energy in the X-direction, as illustrated in Figures 105 (b) and 106 (b) respectively. By looking at the different results from the different normalization approaches, it can be indicated that the three methods generally produced the same results, yet the normalization by the preform areal density is the most accurate, since it eliminates the effect of the preform (fiber) weight from the analysis and results in a fair comparison between the different samples. Additionally, increasing the number of layers resulted in a slight increase in the normalized energy, and this was the only significant factor in the X-axis direction.

One of the findings from the previous analysis, was that the results in the X-axis direction was generally higher than that of the Y-axis direction, and it was due to the fact that the number of

X-yarn layers was always greater than the Y-yarn layers by one extra layer. Yet, in order to quantify this difference and its main effect, the results of the total energy were averaged in both directions and plotted in Figure 95 (a). It's clear that the energy in the X-axis direction was higher than the Y-axis direction, and even when normalized by composite thickness, composite areal density, and preform areal density, this significance did not change as shown in Figures 99 (a), 103 (a), and 107 (a) respectively.

Charpy impact

Similar to Izod impact testing, in the case of Charpy impact, the energy required to fracture the composite specimen supported as a simple beam until it's broken is measured, in both X- and Y-axis directions. The failure analysis of the specimens in case of X-axis direction, indicated that the X-yarns are torn during the fracture. Whereas, specimens tested in the Y-axis direction show that the Y- and Z-yarns were ruptured during the impact test. The results of the Charpy impact testing in Y- and X-axis directions are listed in Tables 18 and 19 respectively.

Table 18 Charpy impact results in Y-axis direction

ID	Thickness (mm)	Composite Areal Density (g/m²)	Total Energy (J)	CV (%)	Energy/ Thickness (J/m)	Energy/ Comp. Areal Density (kJ/g/mm²)	Energy/ Preform Areal Density (kJ/g/mm²)
1	3319	1.93	2.4	9.6	1256	0.72	1.04
2	3259	1.75	2.7	18.6	1570	0.84	1.20
3	3275	1.95	2.6	24.3	1339	0.80	1.15
4	3435	1.95	3.8	13.5	1973	1.12	1.57
5	3341	1.80	3.9	21.9	2194	1.18	1.63
6	3412	1.75	2.5	29.3	1445	0.74	1.03
7	3587	2.00	3.9	16.2	1931	1.08	1.51
8	3575	2.00	3.5	23.3	1756	0.98	1.38
9	3371	1.80	2.2	23.3	1237	0.66	0.89
10	4854	2.75	5.7	14.5	2057	1.17	1.75
11	4618	2.50	6.6	18.0	2634	1.43	2.04
12	4453	2.30	4.0	17.9	1746	0.90	1.25
13	4809	2.70	6.0	12.9	2228	1.25	1.74
14	4893	2.75	5.8	22.1	2092	1.18	1.66
15	4927	2.60	5.2	17.4	2016	1.06	1.54
16	5206	2.85	6.8	31.3	2383	1.30	1.90
17	4912	2.50	6.1	27.5	2426	1.24	1.69
18	4773	2.40	6.2	16.4	2567	1.29	1.74
19	6095	3.20	9.3	23.6	2904	1.52	2.21
20	5912	3.15	9.1	23.5	2894	1.54	2.19
21	5895	3.05	10.5	9.6	3447	1.78	2.53
22	6048	3.20	11.5	19.1	3601	1.90	2.63
23	6146	3.30	9.0	4.6	2730	1.47	2.04
24	6145	3.25	9.3	10.6	2867	1.52	2.14
25	6324	3.35	9.4	17.1	2814	1.49	2.05
26	6496	3.41	8.9	10.7	2598	1.36	1.93
27	6445	3.25	8.2	4.6	2535	1.28	1.82

Table 19 Charpy impact results in X-axis direction

ID	Thickness (mm)	Composite Areal Density (g/m²)	Total Energy (J)	CV (%)	Energy/ Thickness (J/m)	Energy/ Comp. Areal Density (kJ/g/mm²)	Energy/ Preform Areal Density (kJ/g/mm²)
1	3215	1.90	3.3	26.5	1730	1.02	1.43
2	3353	1.85	2.6	11.5	1432	0.79	1.15
3	3261	1.95	2.6	24.3	1339	0.80	1.15
4	3454	2.00	3.8	19.2	1885	1.09	1.54
5	3323	1.80	4.7	18.2	2614	1.42	1.94
6	3468	1.75	3.5	25.7	2002	1.01	1.43
7	3638	2.10	5.0	24.4	2383	1.38	1.95
8	3575	2.00	5.1	21.9	2563	1.43	2.01
9	3400	1.95	3.9	30.0	1980	1.14	1.54
10	4831	2.75	7.9	15.7	2888	1.64	2.46
11	4627	2.55	5.2	11.6	2035	1.12	1.61
12	4413	2.37	5.1	5.7	2155	1.15	1.59
13	4815	2.70	6.8	27.6	2500	1.40	1.96
14	4949	2.70	7.6	8.8	2827	1.54	2.20
15	5001	2.90	8.9	13.3	3081	1.79	2.62
16	5197	2.85	9.7	11.3	3393	1.86	2.70
17	4853	2.65	7.3	22.0	2755	1.50	2.04
18	4814	2.75	7.1	14.5	2595	1.48	2.02
19	5993	3.25	11.3	8.0	3477	1.89	2.69
20	5872	3.25	9.3	25.5	2863	1.58	2.23
21	5673	3.30	8.0	19.8	2414	1.40	1.92
22	5938	3.30	10.3	18.3	3113	1.73	2.35
23	6254	3.40	9.4	17.7	2767	1.50	2.13
24	6071	3.40	12.7	8.7	3738	2.09	2.92
25	6388	3.40	12.7	12.9	3727	1.98	2.76
26	6575	3.50	12.3	7.6	3526	1.88	2.69
27	6455	3.55	13.0	17.3	3665	2.02	2.88

Similar to Izod tests several types of breaks were observed in the Charpy impact, such as complete, hinged, partial, or non-break, which follow the same list in Table 17. However, in this research only specimens with complete and Hinged breaks were considered for the analysis. Figure 91 illustrates the Charpy specimens with different types of breaks.

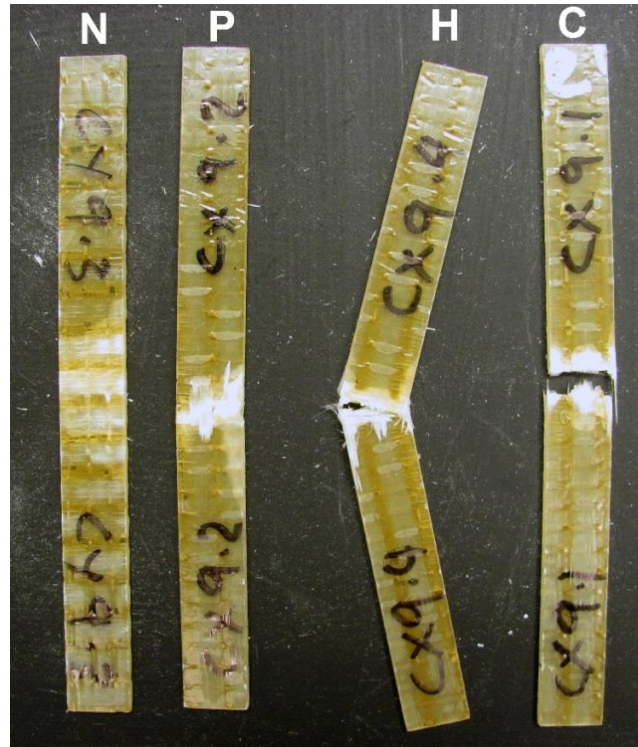


Figure 91 Types of breaks in Charpy impact specimens

The results of the Charpy total energy of all specimens were analyzed using univariate analysis of variance to reveal the effect of the structural parameters on the total energy. The structural parameters included, Y-yarn number of layers, X-yarn pick density, and Z-yarn weave pattern. The results of the univariate analysis of variance test were confirmed using a follow up post hoc Duncan test. The statistical analysis results in the Y- and X-axis directions are listed in Appendix D and E respectively. Further, the main effects of the structural parameters are plotted in Figure 92 to Figure 107.

Firstly, the results in the Y-axis direction were analyzed. Figure 92 (a) shows that increasing the number of Y-yarn layers resulted in a significant increase in the total impact energy. Whereas, increasing the X-yarn density didn't have any statistically significant effect on the total energy as shown in Figure 93 (a), this was confirmed by performing a post hoc test, which indicated that there is no significant difference between the different levels of pick densities and that they all belong to the same subset as shown in Table D.7. On the other hand, changing the Z-yarn weave pattern had shown a significant effect on the total energy as illustrated in

Figure 94 (a), and by performing a post hoc test this significance was confirmed, and it indicated that specifically the plain weave is different from the two other weaves as shown in Table D.10, and it had higher impact energy. From the previous analysis, it can be generally concluded that increasing the number of layers increase the total energy due to the increase in the amount fibers resisting the impact. However, increasing the pick density, had no significant effect on the energy, which might be due to the same reason discussed before in case of Izod impact in the X-axis direction. Finally, changing the Z-yarn weave pattern surprisingly had a significant effect on the total energy, and it was found that the plain weave is significantly higher than the twill and basket weaves.

The results of the total Charpy energy in the Y-axis direction were normalized using three different normalization approaches, same as the ones used for Tup and Izod impacts. It was first normalized by the composite thickness, then by composite areal density, and finally by preform areal density. The results of the statistical analysis of the normalized total energy in Y-axis direction are listed in Appendix D.

In Figure 96 (a) the main effect of increasing the number of layers on the total energy normalized by composite thickness is illustrated. The analysis indicated that increasing the number of layers is statistically significant, yet it's less significant than the non-normalized results, and by performing a post hoc test, this significance was confirmed as shown in Table D.14. As for the effect of increasing the pick density on the normalized energy in Figure 97 (a), it's found to be insignificant, similar to the non-normalized case. On the other hand, changing the weave pattern had a significant effect on the normalized energy as shown in Figure 98 (a), which was less significant than the non-normalized case, with $p\text{-value} = 0.008$. Further, by performing a post hoc test in Table D.20, the significance was confirmed and it indicated that specifically the plain is different from the basket, with the plain being higher. Thus it can be concluded that normalizing the total energy by the composite thickness, reduced the significance of the number of layers, and weave pattern.

Furthermore, the results of the total energy were normalized by the composite areal density, Figure 100 (a) shows the main effect of increasing the number of layers in this context. There is an increase in energy which is statistically significant, this increasing trend was similar to the results of normalizing the energy by the composite thickness. As for the effect of increasing

the pick density it's still not significant as illustrated in Figure 101 (a). Whereas, the analysis of the weave pattern effect on the normalized energy indicated even higher significance than the non-normalized results as shown in Figure 102 (a). Additionally, performing a post hoc test confirmed this increased significance of the weave pattern effect, and it indicated that each weave belongs to a distinct subset as shown in Table D.30, with the plain being the highest, followed by twill and then basket. Overall, the results of the total energy normalized by the composite areal density were similar to that of the impact energy normalized by the composite thickness, except for the increased significance of the weave pattern.

Finally, when the Charpy energy results were normalized by the preform areal density, they similarly indicated that the number of layers had a less significant effect as depicted in Figure 104 (a). While, the pick density remained insignificant as illustrated in Figure 105 (a). Whereas, the effect of changing the weave pattern had a statistically significant effect on the total energy, which is similar to that of the case normalized by the composite areal density. By looking at the different results from the different normalization approaches, it can be indicated that the normalization by composite thickness is the least accurate, whereas the normalization by the composite and preform areal density is more accurate, and produced similar results. Additionally, increasing the number of layers resulted in a slight increase in the normalized energy, while increasing the pick density had no significant effect on the total energy, while the weave pattern had a significant effect with the plain having highest impact energy. This can be due to the low weave factor of the plain weave pattern ($M=1$) and the high number of interlacements per unit length.

Secondly, the results in the X-axis direction were analyzed. Figure 92 (b) shows that increasing the number of Y-yarn layers resulted in a significant increase in the total impact energy, as in the case of the Y-direction. Similarly, increasing the X-yarn density significantly increased the total energy as shown in Figure 93 (b), which was confirmed by performing a post hoc test, which indicated that each level of pick density is distinct and belong to a different subset as shown in Table E.7. On the other hand, changing the Z-yarn weave pattern has shown a significant effect on the total energy as illustrated in Figure 94 (b) similar to the Y-axis direction, and by performing a post hoc test this significance was confirmed, and it indicated that specifically the plain weave is different from the basket weave as shown in Table E.10,

and it has higher impact energy. From the previous analysis, it can be generally concluded that increasing the number of layers increase the total energy due to the increase in the amount of fibers resisting the impact. Moreover, increasing the pick density, had a significant effect on the energy, which is due to the increase of amount of X-yarns resisting the impact in the X-axis direction. Yet, this response is not as significant as increasing the number of Y-yarn layers. Finally, changing the Z-yarn weave pattern had a significant effect on the total energy in this case, and it was indicated that the plain weave is significantly higher than the twill and basket weaves, which was the same case in the Y-direction.

The results of the total Charpy energy in the X-axis direction were normalized using three different normalization approaches, same as the ones used in Y-axis direction. It was first normalized by the composite thickness, then by composite areal density, and finally by preform areal density. The results of the statistical analysis of the normalized total energy in Y-axis direction are listed in Appendix E.

In Figure 96 (b) the main effect of increasing the number of layers on the total energy normalized by composite thickness is illustrated. The analysis indicated that increasing the number of layers was statistically significant, yet it's less significant than the non-normalized results, and by performing a post hoc test, this significance was confirmed as shown in Table E.14. As for the effect of increasing the pick density on the normalized energy in Figure 97 (b), it's found to be significant, similar to the non-normalized case. On the other hand, changing the weave pattern became less significant with a p-value = 0.045, as shown in Figure 98 (b), and by further performing a post hoc test in Table E.20, this slight significance was nullified and it indicated that all three weave patterns belong to the same subset. Thus it can be concluded that normalizing the total energy by the composite thickness, reduced the significance of the number of layers, and diminished the significance of the weave pattern.

Furthermore, the results of the total energy were normalized by the composite areal density, Figure 100 (b) shows the main effect of increasing the number of layers in this context. There is an increase in energy which is statistically significant, this increasing trend was similar to the results of normalizing the energy by the composite thickness. As for the effect of increasing the pick density, it became less significant as illustrated in Figure 101 (b), and the post hoc test revealed that the pick densities 5.48, and 5.85 have no significant difference, and both belongs

to the same subset as shown in Table E.27. Whereas, the analysis of the weave pattern effect on the normalized energy indicated higher significance than the thickness normalized results with a p-value = 0.03 as shown in Figure 102 (b). Additionally, performing a post hoc test confirmed this increased significance of the weave pattern effect, and it indicated that the twill and plain samples are significantly different and each belong to a different subset as shown in Table D.40, with the plain being the highest. Overall, the results of the total energy normalized by the composite areal density were similar to that of the impact energy normalized by the composite thickness, except for the increased significance of the weave pattern.

Finally, when the Charpy energy results in the X-axis direction were normalized by the preform areal density, they similarly indicated that the number of layers has a less significant effect as depicted in Figure 104 (b). As for the pick density effect, it was statistically significant and it was similar to the normalized results by the composite areal density as illustrated in Figure 105 (b). Moreover, the effect of changing the weave pattern had a statistically significant effect on the total energy, which is similar to that of the case normalized by the composite areal density as depicted in Figure 106 (b). By looking at the different results from the different normalization approaches, it can be indicated that the normalization by composite thickness is the least accurate, whereas the normalization by the composite and preform areal density is more accurate, and produced similar results. Additionally, increasing the number of layers and pick density resulted in a slight increase in the normalized energy, also changing the weave pattern had a significant effect with the plain having highest impact energy. This can be due to the low weave factor of the plain weave pattern ($M=1$) and the high number of interlacements per unit length.

Another finding from the previous analysis was that the results in the X-axis direction was generally higher than that of the Y-axis direction, and it was due to the fact that the number of X-yarn layers is always greater than the Y-yarn layers by one extra layer. However, this effect wasn't as significant as in the case of the Izod impact. Yet, in order to quantify this difference and its main effect, the results of the total energy were averaged in both directions and plotted in Figure 96 (a). It's clear that the energy in the X-axis direction is slightly higher than the Y-axis direction, and even when normalized by composite thickness, composite areal density,

and preform areal density, this significance did not change as shown in Figures 99 (a), 103 (a), and 107 (a) respectively.

Comparative analysis

After analyzing the main effects of the structural parameters on the impact resistance in each of the previous impact modes, next, it was important to compare the main effect of each impact mode on the total impact energy, as well as the normalized energy. This will be discussed in more details in the next section, which test the correlation between all three modes of impact.

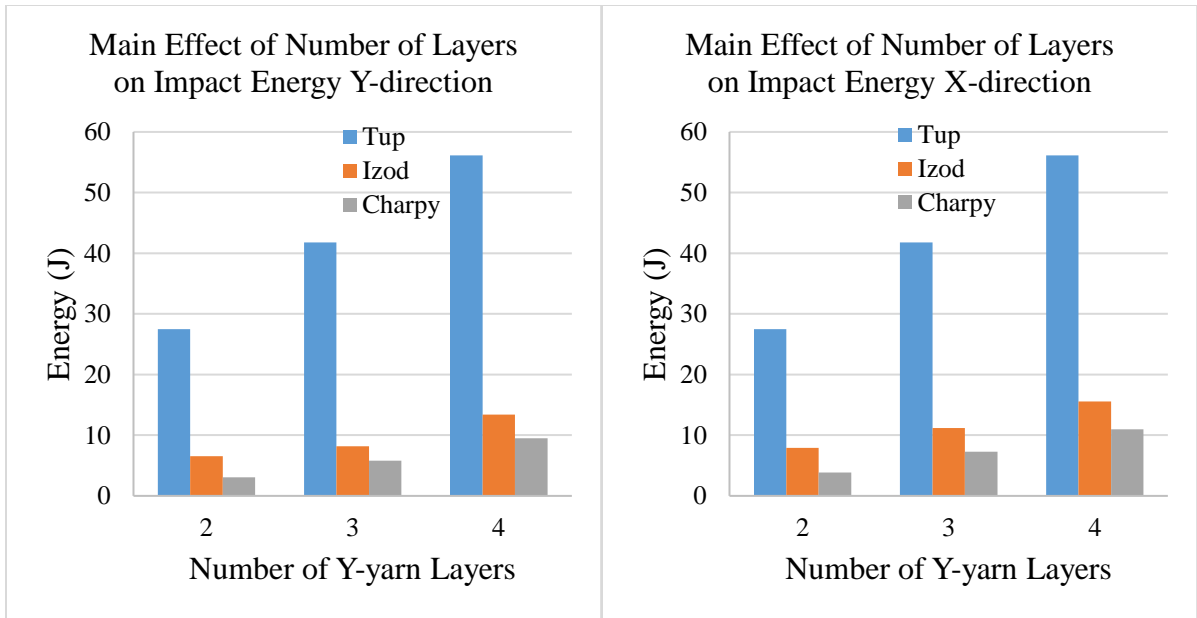
Figure 95 (b) shows the main effect of the impact mode on the total energy, and it's obvious that the Tup impact has the highest energy, followed by the Izod and then Charpy. The response of the Tup impact is significantly higher than the Izod and the Charpy. This is because the Tup impact is a flexed plate impact test, where the sample is supported as a flat plate laying horizontally, and then a falling Tup strikes its face. The Tup impact specimen is square and it's independent of the yarns orientation within the specimen, and all yarn components resist the impact collectively. Hence, the energy required to puncture the specimen is high, due to the synergetic effect between the different yarn components, and especially the Z-yarn component which plays an important role in this context, since it significantly increases the through thickness properties and the delamination resistance of the 3DOW composite. On the other hand, the Charpy and Izod are flexed beam tests, where the sample is either supported as a simple beam (Charpy), or a cantilever (Izod), and then a swinging pendulum strikes the specimen from the edge, and in this case specific yarn components resist the puncture, depending on the specimen direction. For example, specimens in X-axis direction, indicated that the X-yarns are torn during the fracture, whilst, specimens tested in the Y-axis direction showed that the Y- and Z-yarns were ruptured during the impact test.

Moreover, the Izod impact resistance is always higher than the Charpy, despite that for the same sample, both specimens had the same thickness and width. This is because the total impact energy in both cases, is equivalent to the energy lost by the pendulum during the breakage of the specimen, which is the sum of energy required to initiate fracture within the thickness of the specimen, energy required to propagate the fracture across the width of the specimen, and energy required to throw or toss the free ends of the broken specimen. Yet, in case of using rigid material like composites, the fracture is brittle, therefore, the energy

required to propagate the fracture is very small compared to the energy required to initiate the fracture, and it could be neglected. With this being said, the only difference between the two modes would be the energy required to throw the free ends of the broken specimen (toss energy). Thus, when comparing the toss energy in both cases, we found that the energy required to throw the broken ends in case of Izod is higher since one of the specimen ends is being rigidly clamped, whereas, in case of Charpy both ends are simply supported without clamping, hence the energy required to toss the broken ends is lower.

The main effect of each impact mode on the total energy was normalized by the composite thickness in Figure 99 (b), composite areal density in Figure 103 (b), and preform areal density in Figure 107 (b). The plots show that the main effects of the different modes of impact, still have the same significance even after the normalization.

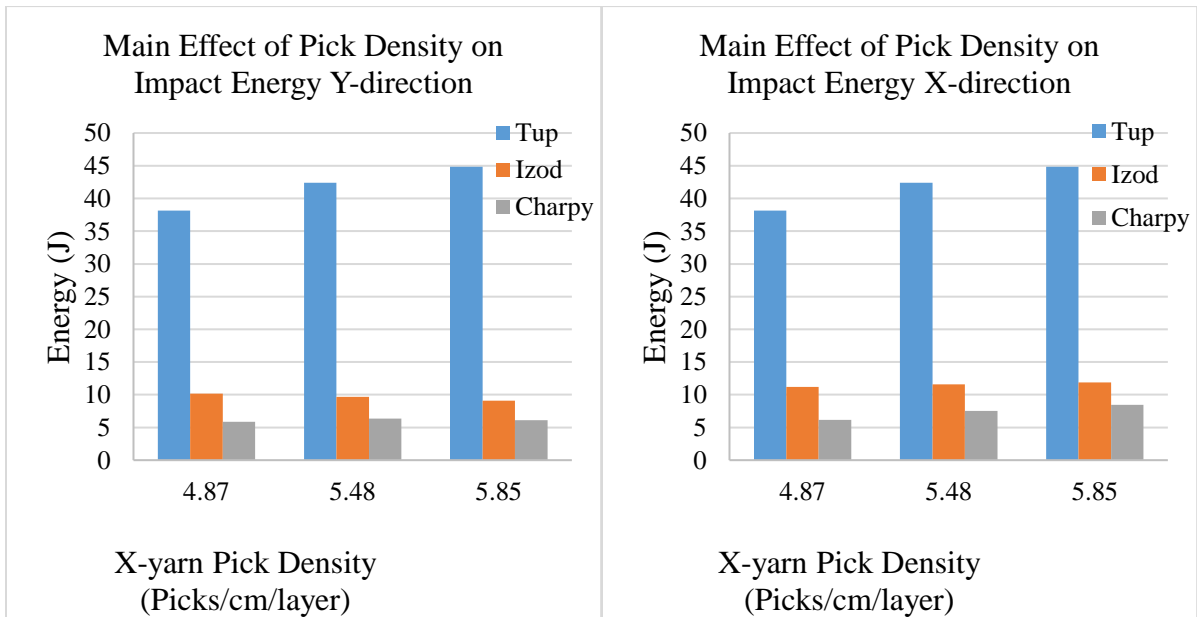
In conclusion, the Tup results has significantly higher impact energy than both, the Charpy and Izod, because all the yarn components in the case of Tup resist the puncture collectively. On the other hand, the Charpy impact results are always lower than the Izod results, because the toss energy required to throw the broken ends of the specimen is always lower in case of Charpy. Moreover, the significance of the main effects of the three different impact modes remained unchanged after normalizing the results by thickness, composite areal density, and preform areal density.



(a)

(b)

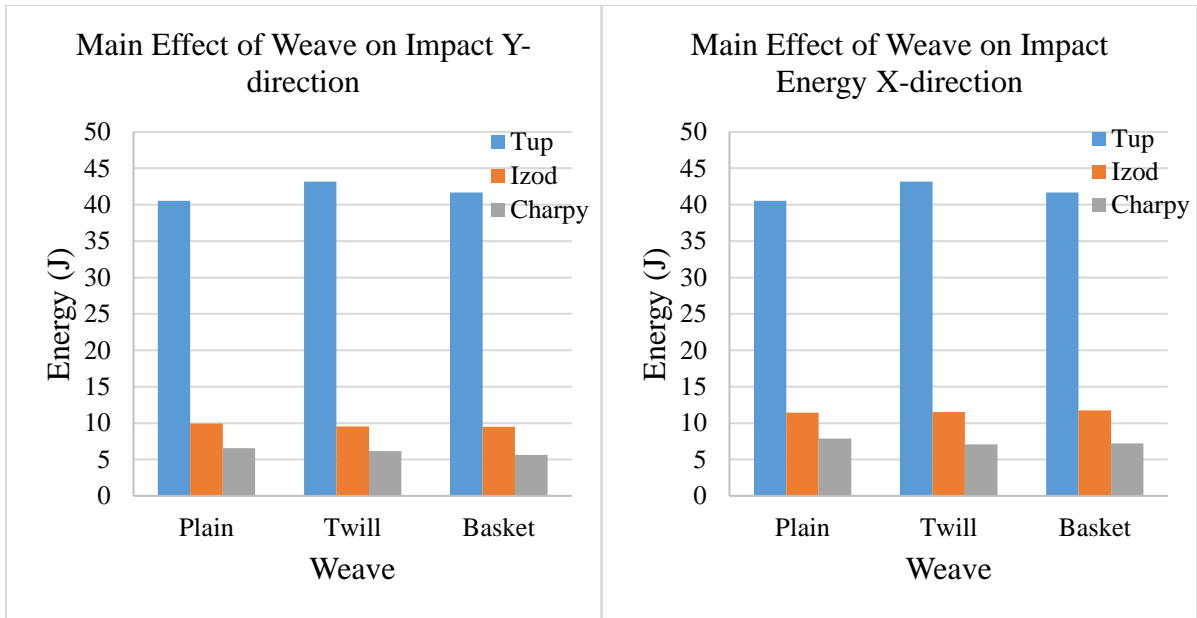
Figure 92 Main effect of number of layers on impact energy, (a) Y-direction, and (b) X-direction



(a)

(a)

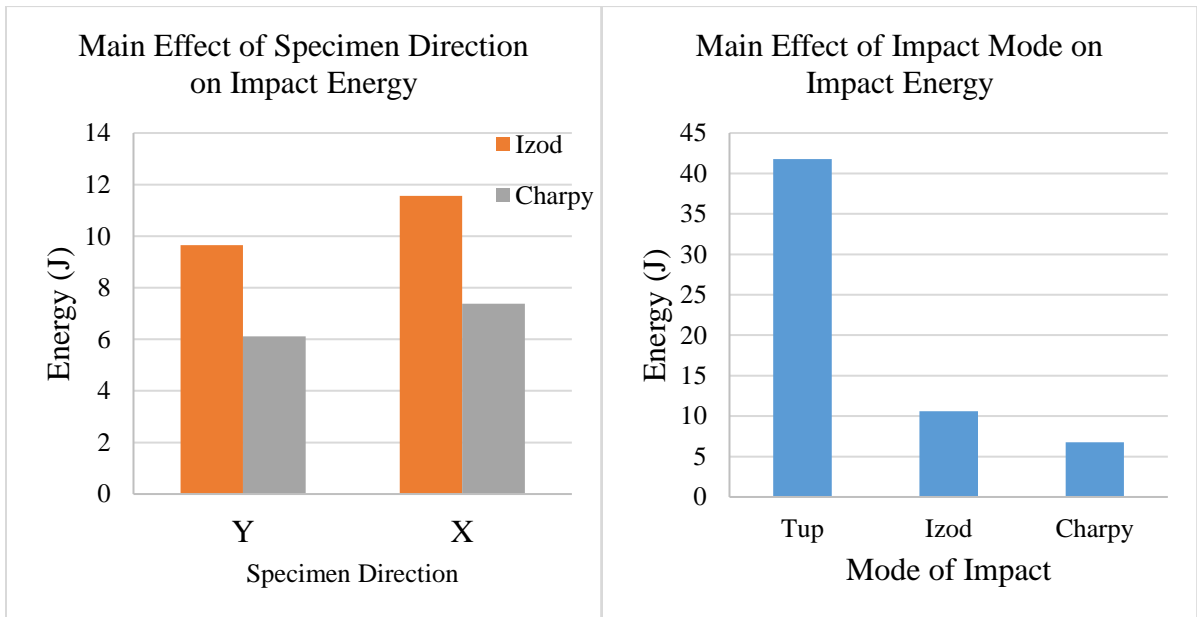
Figure 93 Main effect of X-yarn density on impact energy, (a) Y-direction, and (b) X-direction



(a)

(b)

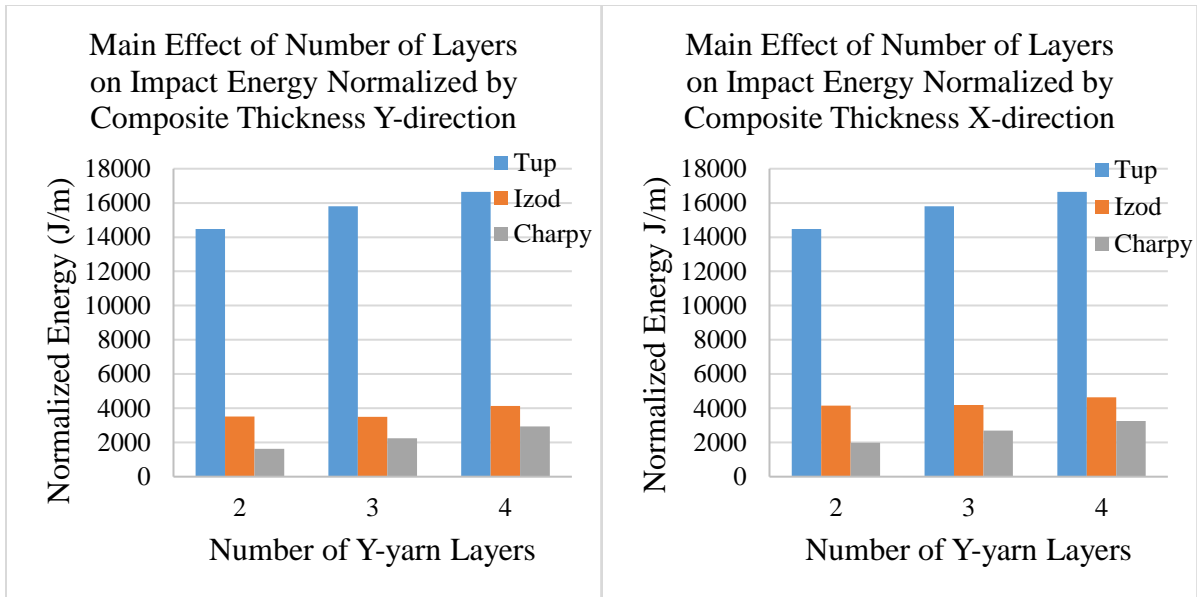
Figure 94 Main effect of weave pattern on impact energy, (a) Y-direction, and (b) X-direction



(a)

(b)

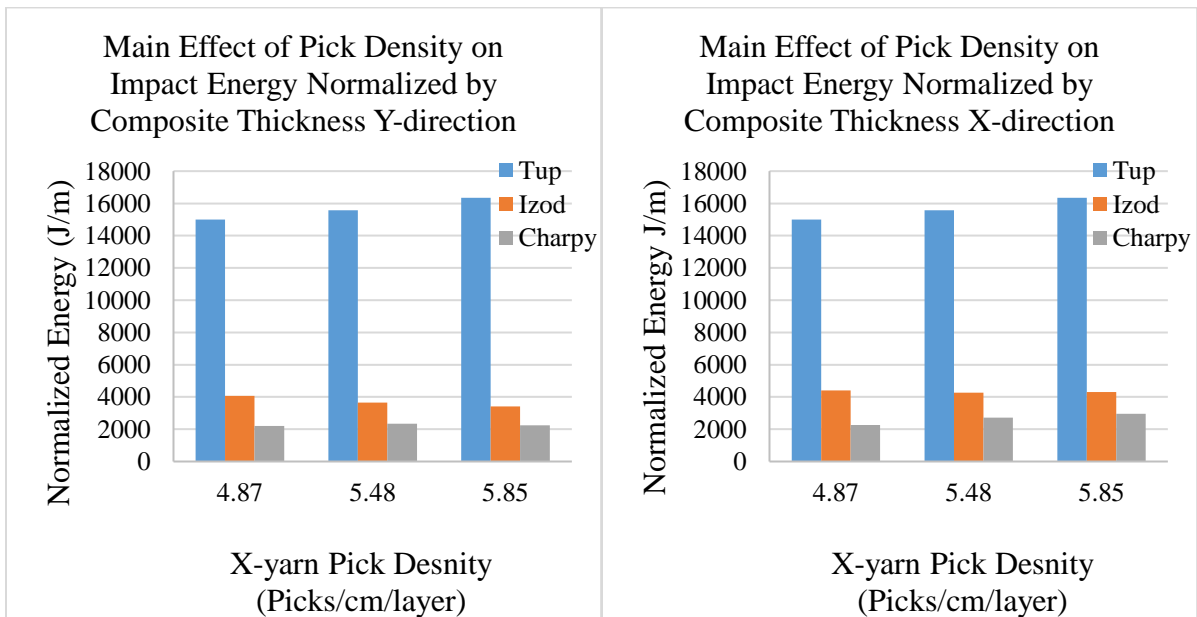
Figure 95 Main effect of (a) specimen direction, and (b) impact mode, on impact energy



(a)

(b)

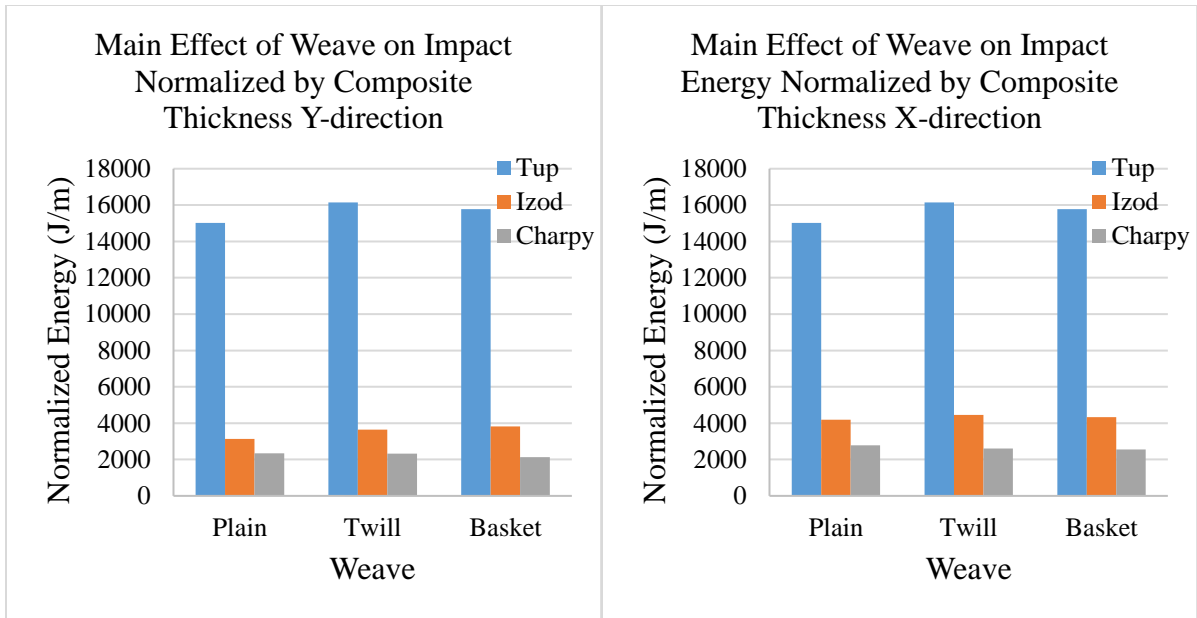
Figure 96 Main effect of number of layers on impact energy normalized by composite thickness, (a) Y-direction, and (b) X-direction



(a)

(b)

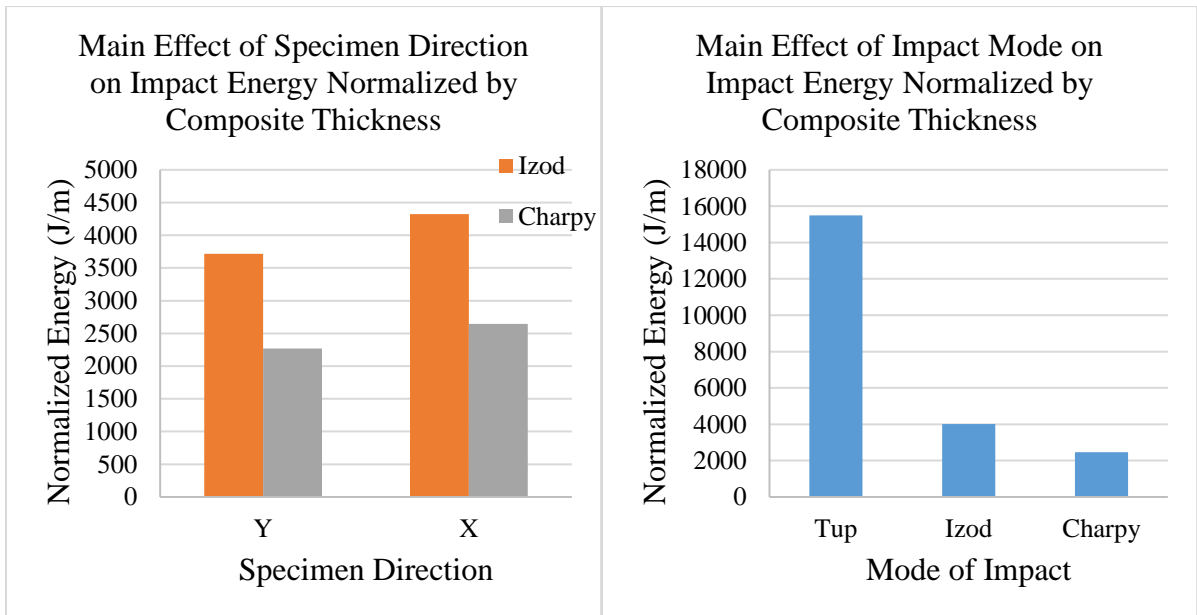
Figure 97 Main effect of X-yarn density on impact energy normalized by composite thickness, (a) Y-direction, and (b) X-direction



(a)

(b)

Figure 98 Main effect of weave pattern on impact energy normalized by composite thickness, (a) Y-direction, and (b) X-direction



(a)

(b)

Figure 99 Main effect of (a) specimen direction, and (b) impact mode, on impact energy normalized by composite thickness

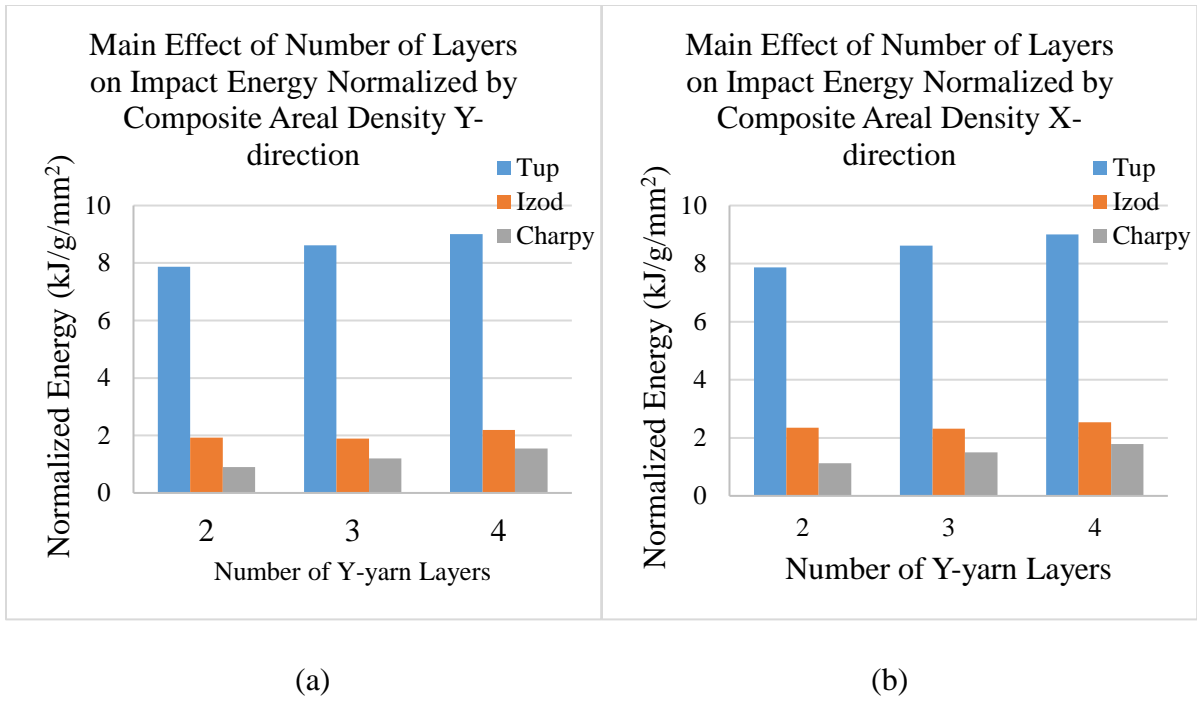


Figure 100 Main effect of number of layers on impact energy normalized by composite areal density, (a) Y-direction, and (b) X-direction

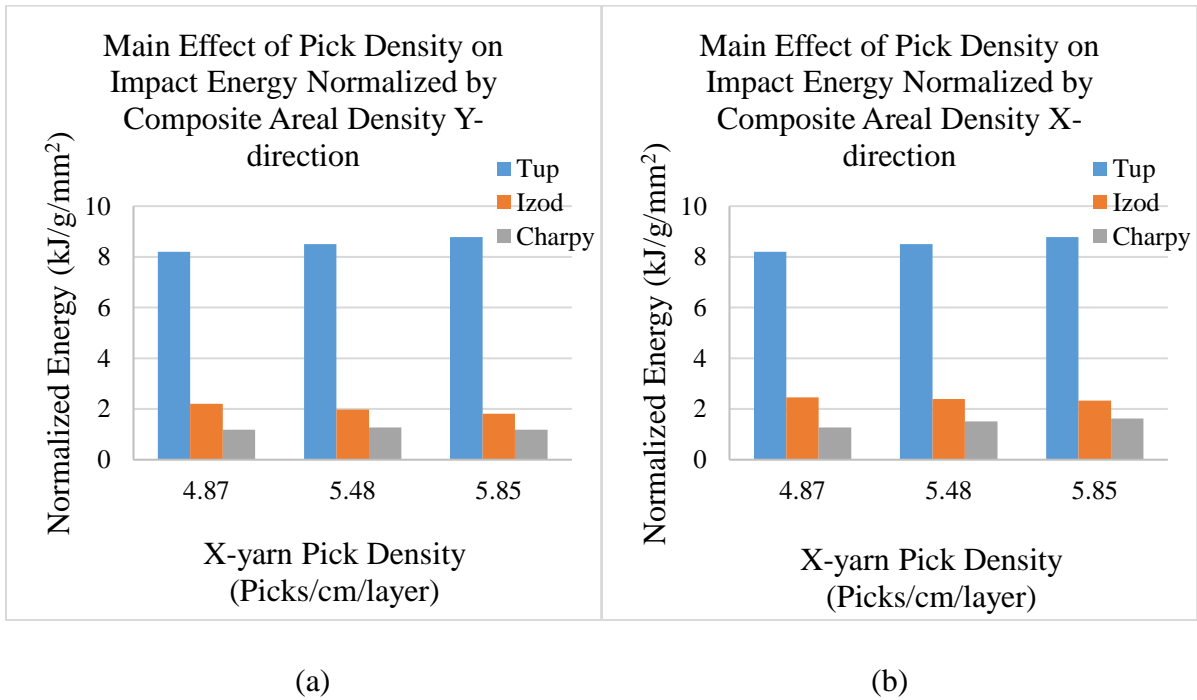
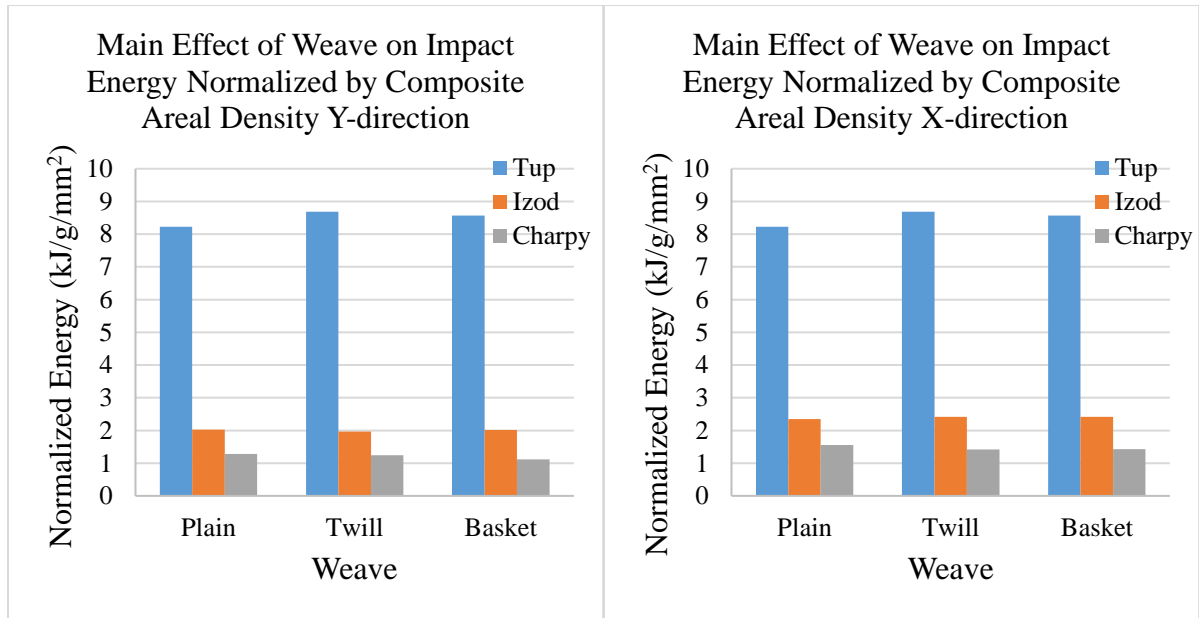


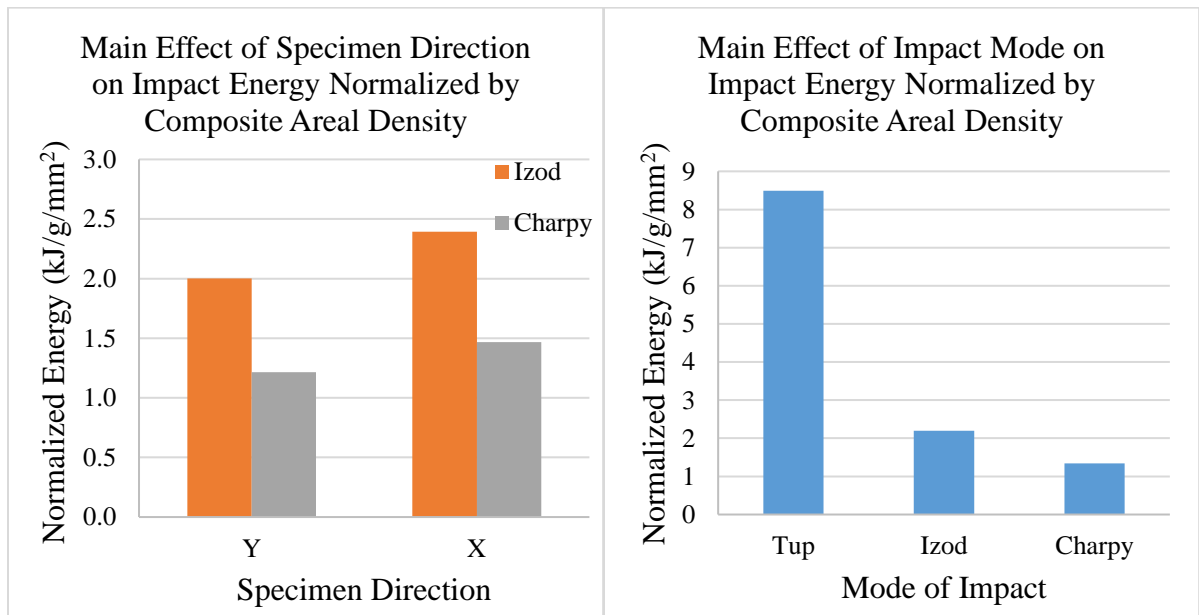
Figure 101 Main effect of X-yarn density on impact energy normalized by composite areal density, (a) Y-direction, and (b) X-direction



(a)

(b)

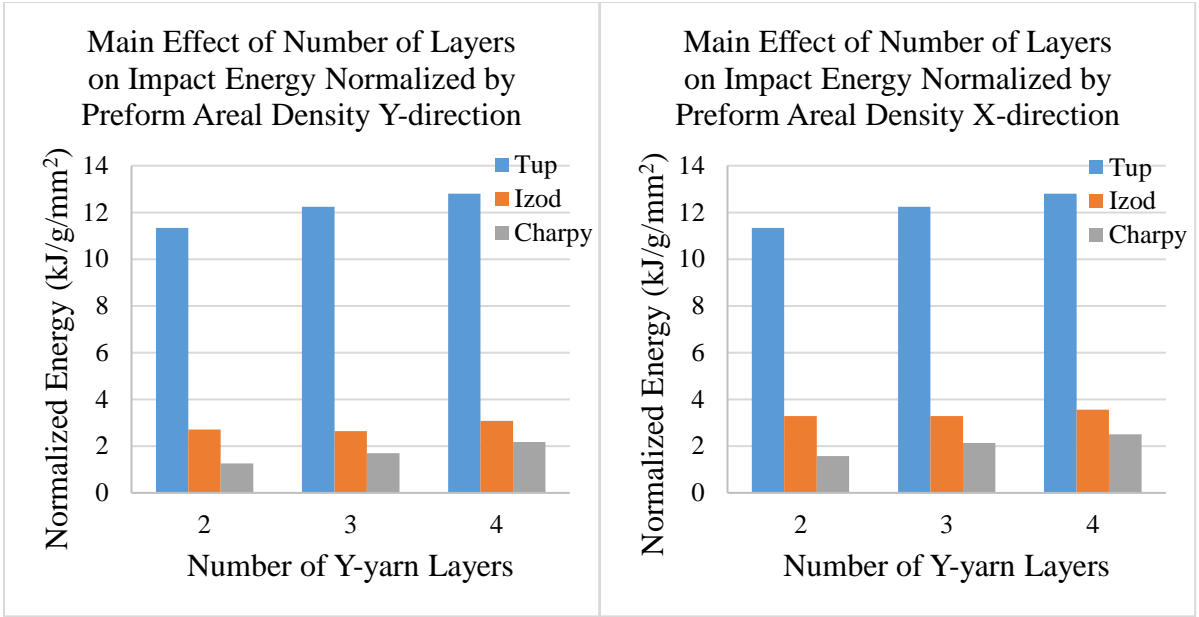
Figure 102 Main effect of weave pattern on impact energy normalized by composite areal density, (a) Y-direction, and (b) X-direction



(a)

(b)

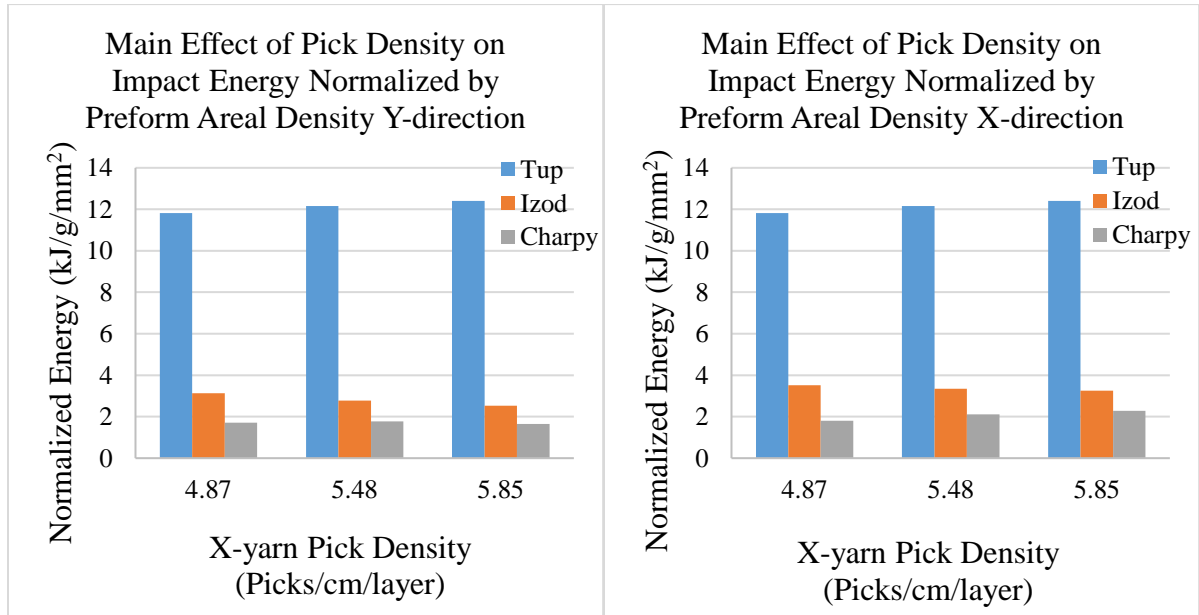
Figure 103 Main effect of (a) specimen direction, and (b) impact mode, on impact energy normalized by composite areal density



(a)

(b)

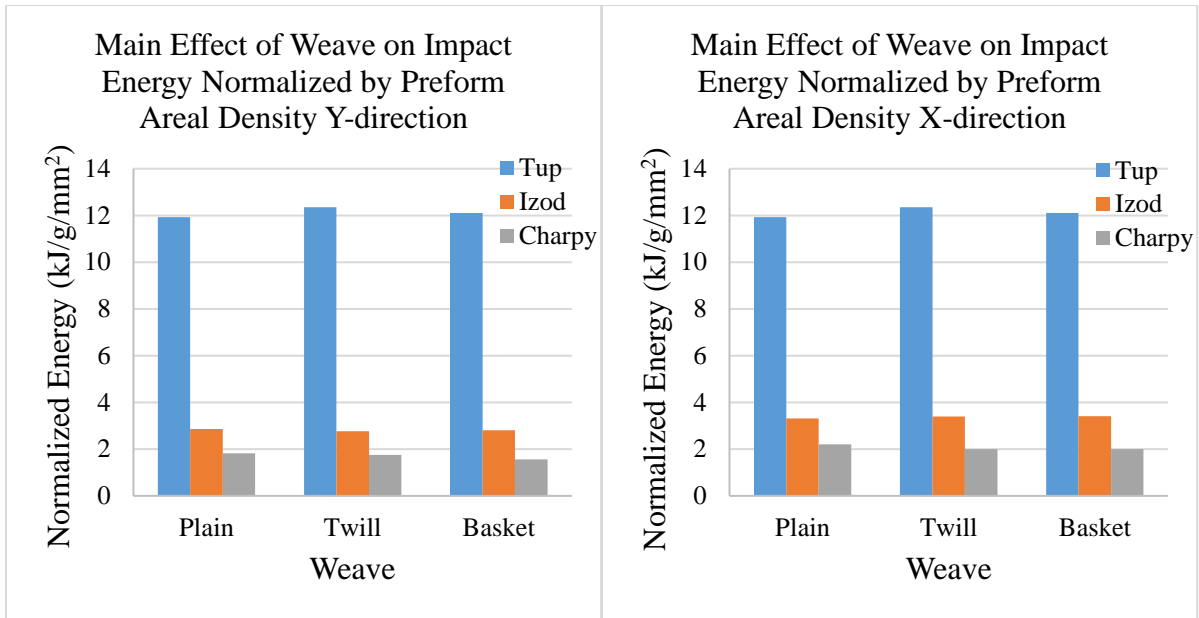
Figure 104 Main effect of number of layers on impact energy normalized by preform areal density, (a) Y-direction, and (b) X-direction



(a)

(b)

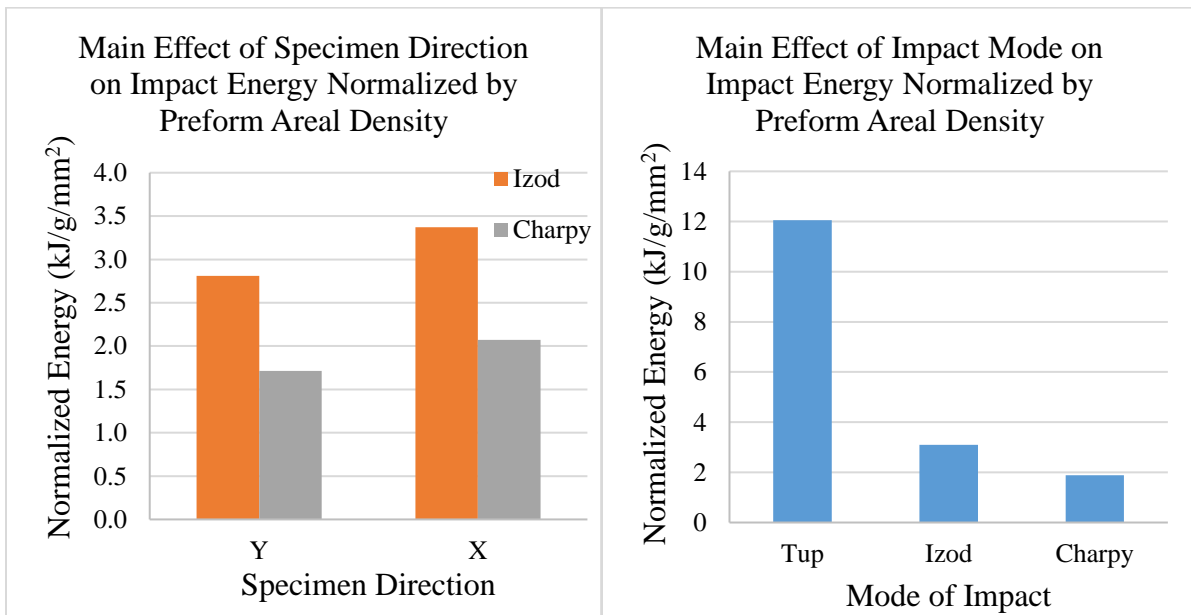
Figure 105 Main effect of X-yarn density on impact energy normalized by preform areal density, (a) Y-direction, and (b) X-direction



(a)

(b)

Figure 106 Main effect of weave pattern on impact energy normalized by preform areal density, (a) Y-direction, and (b) X-direction



(a)

(b)

Figure 107 Main effect of (a) specimen direction, and (b) impact mode, on impact energy normalized by preform areal density

6.1.2 Correlation between different modes of impact

This section is dedicated to study the correlation between the impact energies of the various composite samples in Experiment B, when subjected to different modes of impact, namely Tup, Izod, and Charpy. As mentioned previously, the Tup impact is independent of the test direction, however, a comparison has been made between the same results of the Tup impact once with the Izod and Charpy results in the Y-axis direction, and another time in the X-axis direction.

In a bivariate Pearson correlation test, the coefficient of correlation is calculated (r), which is a measure of the strength and direction of the linear relation between two data sets. Generally, if the coefficient of correlation is higher than 0.8 than there is a strong correlation, and if it's lower than 0.5 than there is a weak correlation. The coefficient of correlation could be positive or negative, positive values indicate a direct correlation, while negative values indicate indirect correlation.

Overall results

First, an overall correlation was performed between the energies of Tup, Izod, and Charpy impacts of all the samples in Experiment A. The statistical tests and correlation matrices are listed in Appendix F. The Y-axis direction results in Table F.1 show that there is a strong correlation between the results of the Charpy and Tup impacts, with $r = 0.886$. While, the Izod results had an intermediate correlation with the Tup results, $r = 0.776$. Yet, the correlation between the Izod and Charpy results had the highest correlation with $r = 0.910$. On the other hand, Table F.2 shows the correlation results in the X-axis direction, which indicated higher correlation between the results of the Charpy and Tup impacts, with $r = 0.912$. Similarly, the correlation between the Izod and Tup impacts results became stronger, with $r = 0.882$. While, the correlation between the Izod and Charpy results remained strong, with $r = 0.909$, which is almost the same value as the Y-axis direction. This means that, there is a strong correlation between impact energies of all three impact modes. The correlation between the Charpy and Izod was the highest, since both tests are flexed beam pendulum tests. Additionally, the correlation became even stronger in the X-axis direction.

Afterwards, the results of the three impact modes were normalized by the composite thickness, and the correlation results in the Y-axis direction are listed in Table F.3. One can notice that, the correlation between the Charpy and Tup results became weak, with $r = 0.338$, whilst, the correlation between the Izod and Tup results became very weak, with $r = -0.147$. Yet, the correlation between the Izod and Charpy results is still the highest, but it's significantly reduced to $r = 0.438$. On the other hand, Table F.4 shows the correlation results in the X-axis direction, which indicated higher correlation between the results of the Charpy and Tup impacts, with $r = 0.575$. Similarly, the correlation between the Izod and Tup impacts results became higher, with $r = 0.252$. While, the correlation between the Izod and Charpy results was surprisingly reduced to $r = 0.307$. From the previous results, it can be concluded that the correlation was significantly reduced after normalizing by the composite thickness. Additionally, the correlation slightly increased in the X-axis direction. This significant drop in the correlation after normalizing by the composite thickness, indicated that the thickness was a strong factor that influenced the results, and yielded a high correlation in the non-normalized case.

Further, the results were normalized by the composite areal density, and the correlation matrix in the Y-axis direction is shown in Table F.5. Generally, the results in this case, were very similar to the case normalized by the composite thickness. The correlation between the Charpy and Tup results was weak, with $r = 0.368$, while, there was no correlation between the Izod and Tup results, since $r = -0.091$. Moreover, the correlation between the Izod and Charpy results was still the highest, but it's a weak correlation, with $r = 0.406$. On the other hand, Table F.6 shows the correlation results in the X-axis direction, which indicated slight increase in correlation between the results of the Charpy and Tup impacts, over the Y-axis direction, with $r = 0.591$. Similarly, the correlation between the Izod and Tup impacts results became slightly higher, with $r = 0.195$. While, the correlation between the Izod and Charpy results was reduced to $r = 0.230$, similar to the case normalized by thickness. From the previous results, it can be concluded that the correlation was significantly reduced after normalizing by the composite areal density. Additionally, the correlation slightly increased in the X-axis direction. This significant drop in the correlation after normalizing by the composite areal density, indicated that the composite weight was a strong factor that influenced the results, and yielded a high correlation in the non-normalized case.

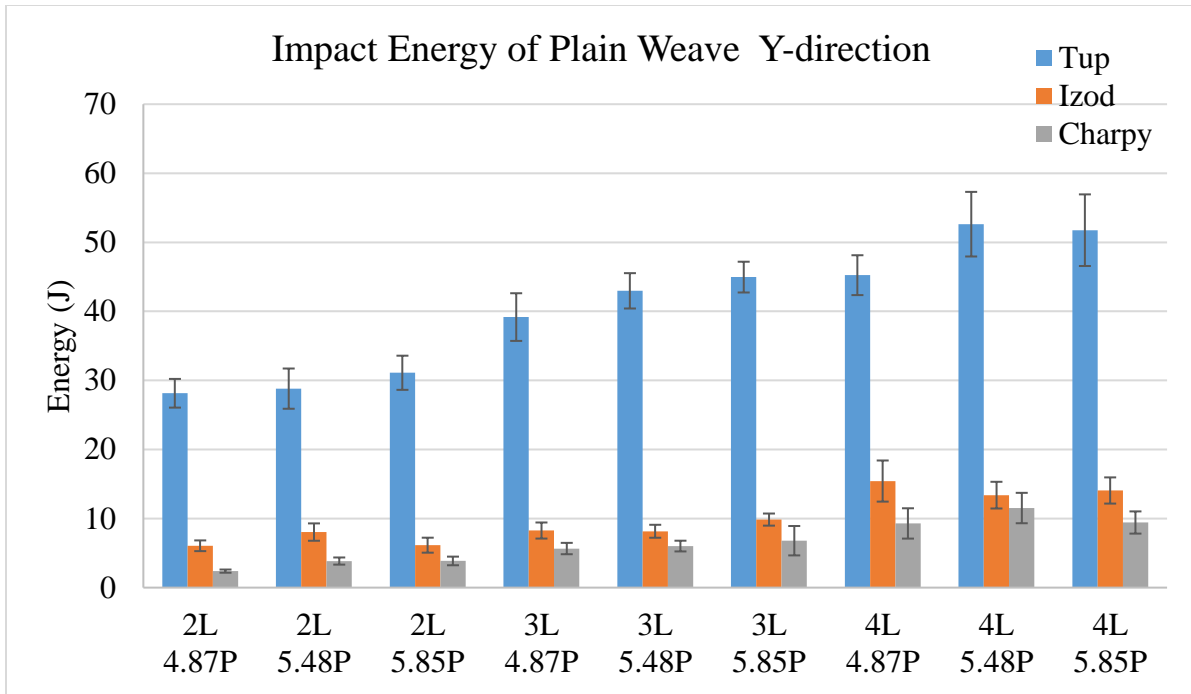
Finally, the results were normalized by the preform areal density, and the correlation matrix in the Y-axis direction is shown in Table F.7. Generally, the results in this case, are very similar to the case normalized by the composite areal density. The correlation between the Charpy and Tup results was weak, with $r = 0.345$, while, there was no correlation between the Izod and Tup results, since $r = -0.026$. Moreover, the correlation between the Izod and Charpy results is still the highest, but it's a weak correlation, with $r = 0.409$. On the other hand, Table F.8 shows the correlation results in the X-axis direction, which indicated a slight increase in correlation over the Y-axis direction, between the results of the Charpy and Tup impacts, with $r = 0.500$. Similarly, the correlation between the Izod and Tup impacts results became slightly higher, with $r = 0.162$. While, the correlation between the Izod and Charpy results was reduced to $r = 0.244$, similar to the case normalized by composite areal density. From the previous results, it can be concluded that the correlation became significantly reduced after normalizing by the preform areal density, similar to the case normalized by composite areal density. Additionally, the correlation slightly increased in the X-axis direction. This significant drop in the correlation after normalizing by the preform areal density, indicated that the preform weight was a strong factor that influenced the results, and yielded a high correlation in the non-normalized case.

From the overall analysis of the entire 27 samples, it can be concluded that, there was a strong correlation between the results of all three impact modes, in the non-normalized case. However, after normalizing by any of the three normalization approaches, the correlations were significantly reduced. Which indicated that the composite thickness, composite weight, and preform weight are factors that have a strong effect on the correlation. Thus, the analysis after normalization became more accurate and realistic. The normalized analysis indicated that there is a weak correlation between the Tup and Charpy impact results, very weak correlation between Charpy and Izod results, and no correlation between Izod and Tup results.

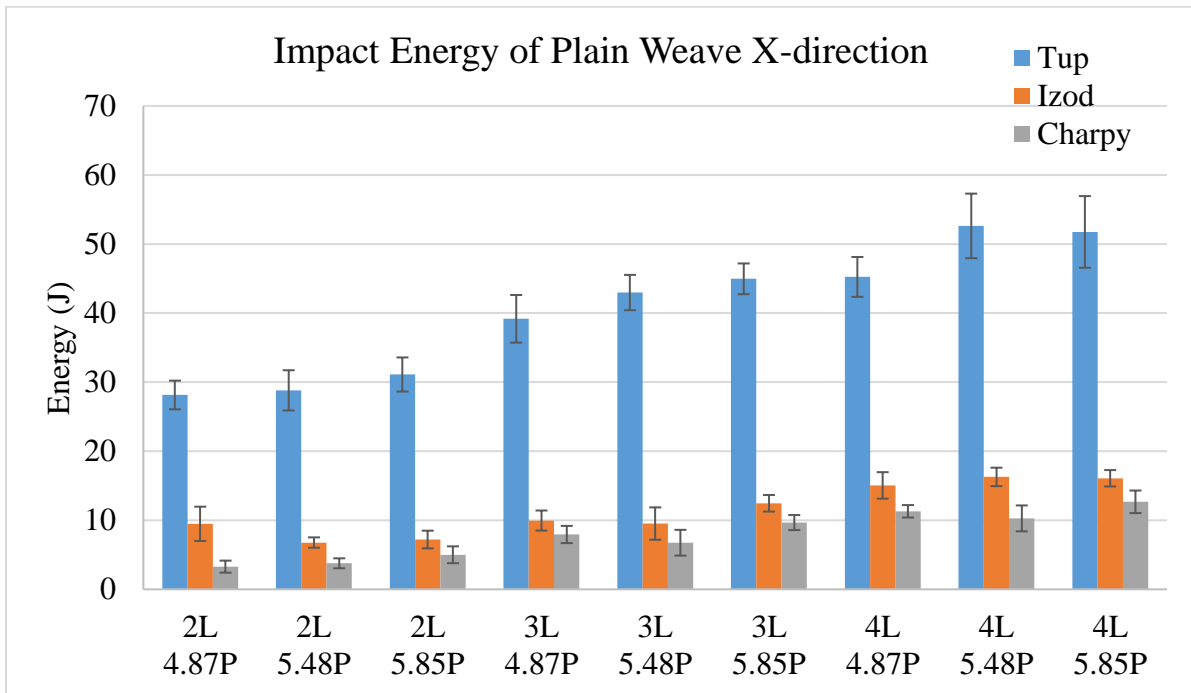
In order, to check if this general conclusion is valid in all cases, a further analysis was performed on separate samples, to see if the results would change. The samples were divided into four groups, plain samples, twill samples, basket samples, and balanced samples. The analysis of each group will be discussed separately next.

Plain weave samples

First, a correlation test was performed between the energies of Tup, Izod, and Charpy impacts of all plain weave samples in Experiment A. The statistical tests and correlation matrices are listed in Appendix G. The Y-axis direction results in Table G.1 show that there is a very strong correlation between the results of the Charpy and Tup impacts, with $r = 0.946$. Similarly, the Izod results had a strong correlation with the Tup results, $r = 0.829$. Moreover, the correlation between the Izod and Charpy results was also very strong with $r = 0.918$ as illustrated in Figure 108 (a). On the other hand, Table G.2 shows the correlation results in the X-axis direction, which were very similar to the Y-axis direction. It indicated very strong correlation between the results of the Charpy and Tup impacts, with $r = 0.934$, and a strong correlation between the Izod and Tup impacts results as well as the Izod and Charpy, with $r = 0.900$ and 0.910 respectively as illustrated in Figure 108 (b). This means that, there is a strong correlation between impact energies of all three impact modes. The correlation between the Charpy and Tup is the highest. Additionally, the correlation is almost the same in the Y- and X-axis directions.



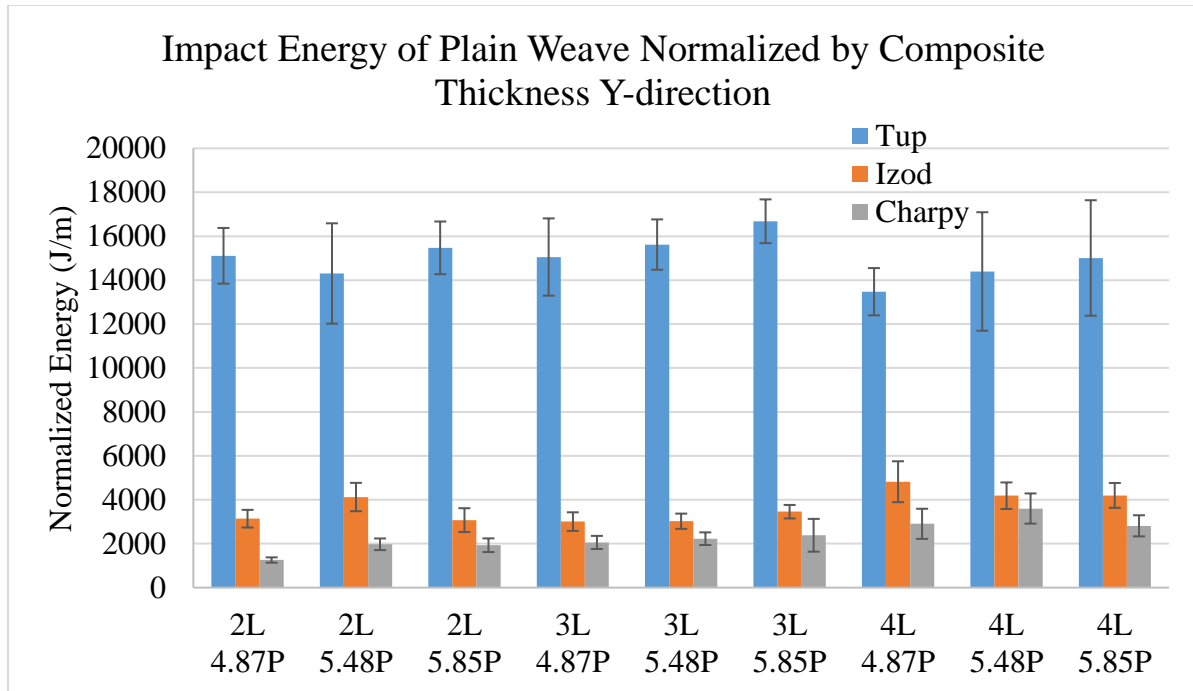
(a)



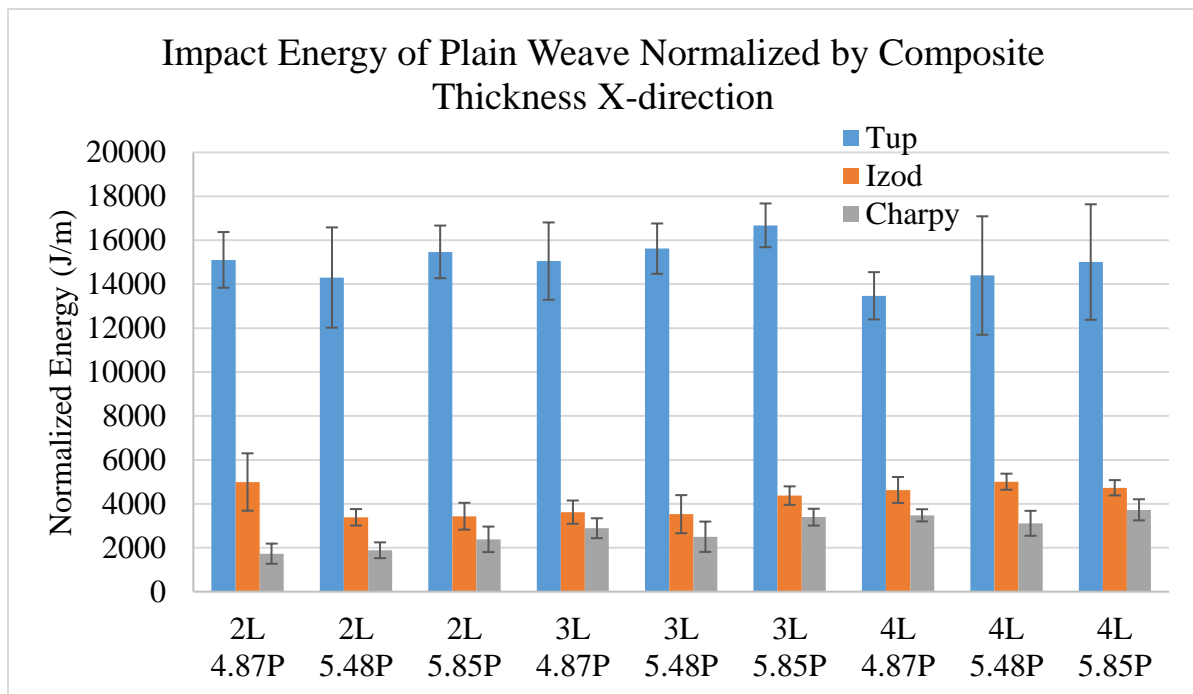
(b)

Figure 108 Impact energies of plain weave samples in, (a) Y-axis direction, and (b) X-axis direction

Afterwards, the results of the three impact modes were normalized by the composite thickness, and the correlation results in the Y-axis direction are listed in Table G.3. One can notice that, the correlation between the Charpy and Tup results became weak and indirect, with $r = -0.340$, whilst, the correlation between the Izod and Tup results became intermediate and indirect, with $r = -0.718$. Additionally, the correlation between the Izod and Charpy results was reduced, but it still has an intermediate direct strength, with $r = 0.670$ as shown in Figure 109 (a). On the other hand, Table G.4 shows the correlation results in the X-axis direction, which is even lower than the Y-direction. The correlation between the Charpy and Tup impacts was negligible, with $r = -0.014$, while, the correlation between the Izod and Tup impacts was very weak and indirect, $r = -0.200$. Additionally, the correlation between the Izod and Charpy results was reduced to $r = 0.385$ as shown in Figure 109 (b). From the previous results, it can be concluded that the correlation became significantly reduced after normalizing by the composite thickness. Additionally, the correlation became indirect between the Tup and the two other modes of impact. In the X-axis direction, the correlations were further weakened. This significant change in the correlation after normalizing by the composite thickness, indicated that the thickness was a strong factor that influenced the results, and yielded a strong direct correlation in the non-normalized case.



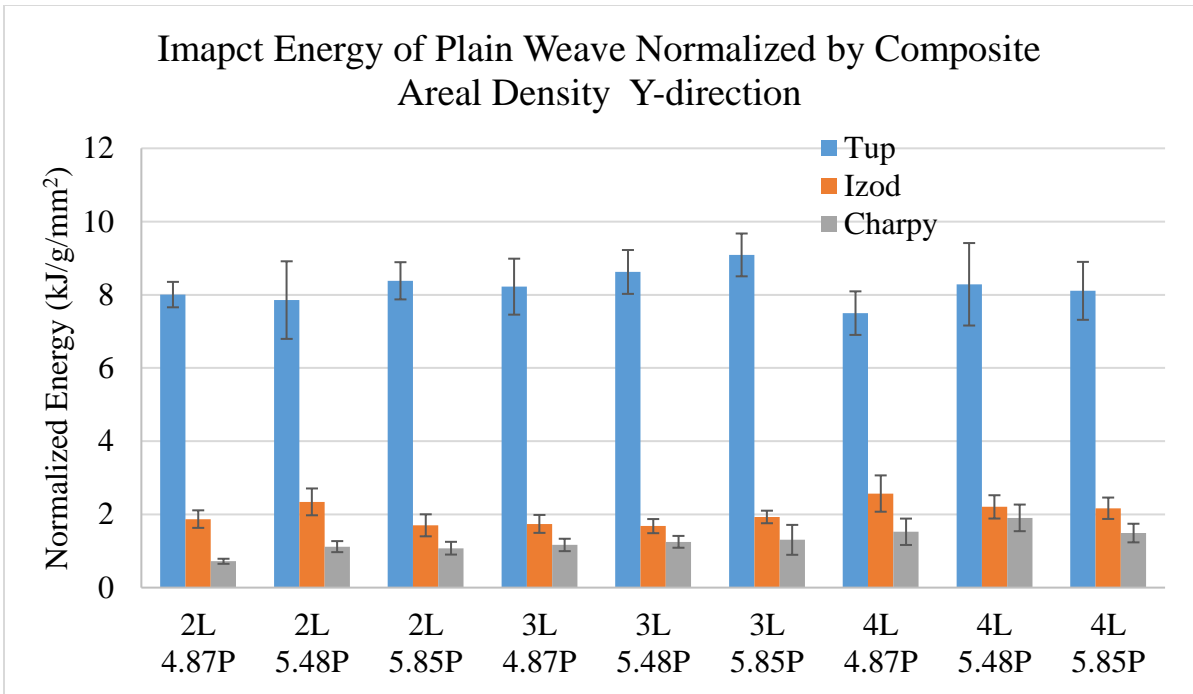
(a)



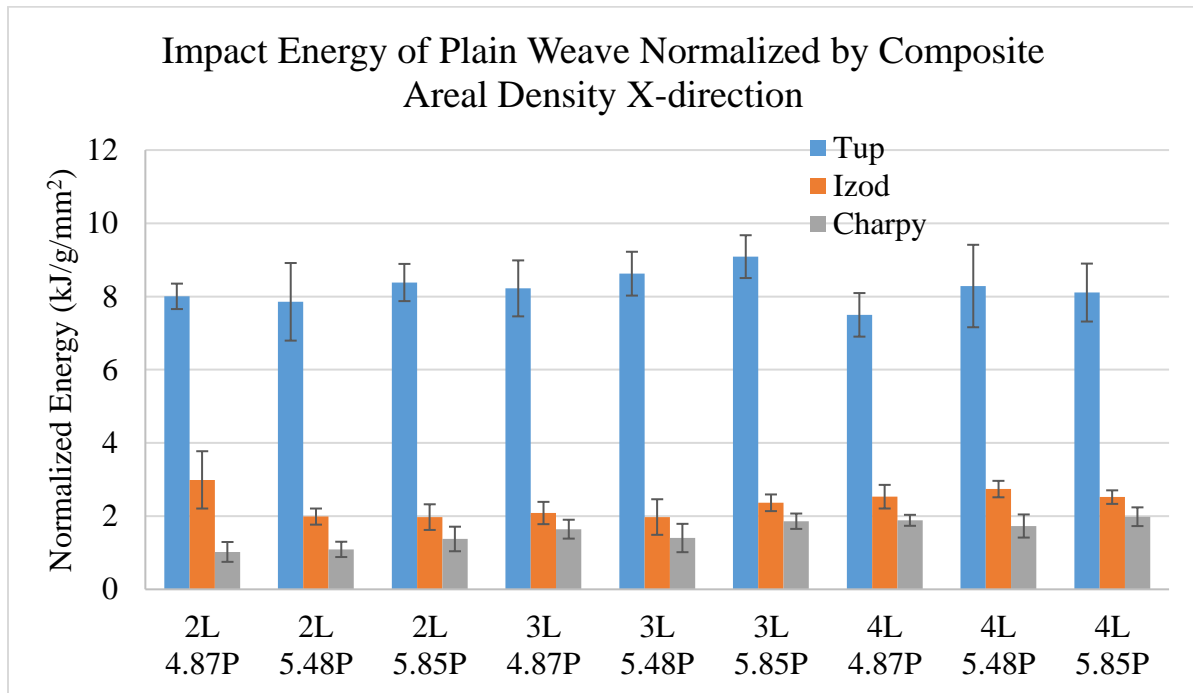
(b)

Figure 109 Impact energies normalized by composite thickness of plain weave samples in, (a) Y-axis direction, and (b) X-axis direction

Further, the results were normalized by the composite areal density, and the correlation matrix in the Y-axis direction is shown in Table G.5. Generally, the results in this case, are close to the case normalized by the composite thickness. There was no correlation between the Charpy and Tup results, with $r = -0.003$, while there was intermediate indirect correlation between the Izod and Tup results, since $r = -0.660$. Moreover, the correlation between the Izod and Charpy results was weak, with $r = 0.499$ as shown in Figure 110 (a). On the other hand, Table G.6 shows the correlation results in the X-axis direction, which indicated slight increase in correlation between the results of the Charpy and Tup impacts, over the Y-axis direction, with $r = 0.144$, while, the correlation between the Izod and Tup impacts results became weaker, with $r = -0.243$. Moreover, the correlation between the Izod and Charpy results was very weak, with $r = 0.128$ as illustrated in Figure 110 (b). From the previous results, it can be concluded that the correlation became significantly reduced after normalizing by the composite areal density. This significant drop in the correlation after normalizing by the composite areal density, indicated that the composite weight was a strong factor that influenced the results, and yielded a high correlation in the non-normalized case.



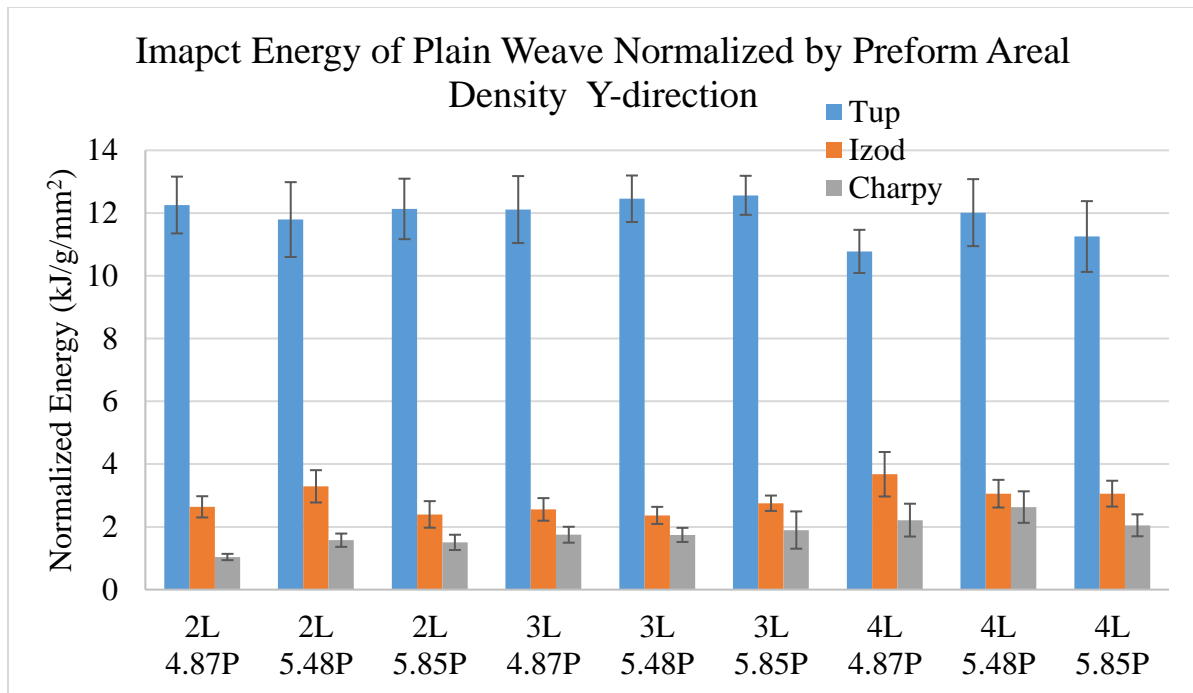
(a)



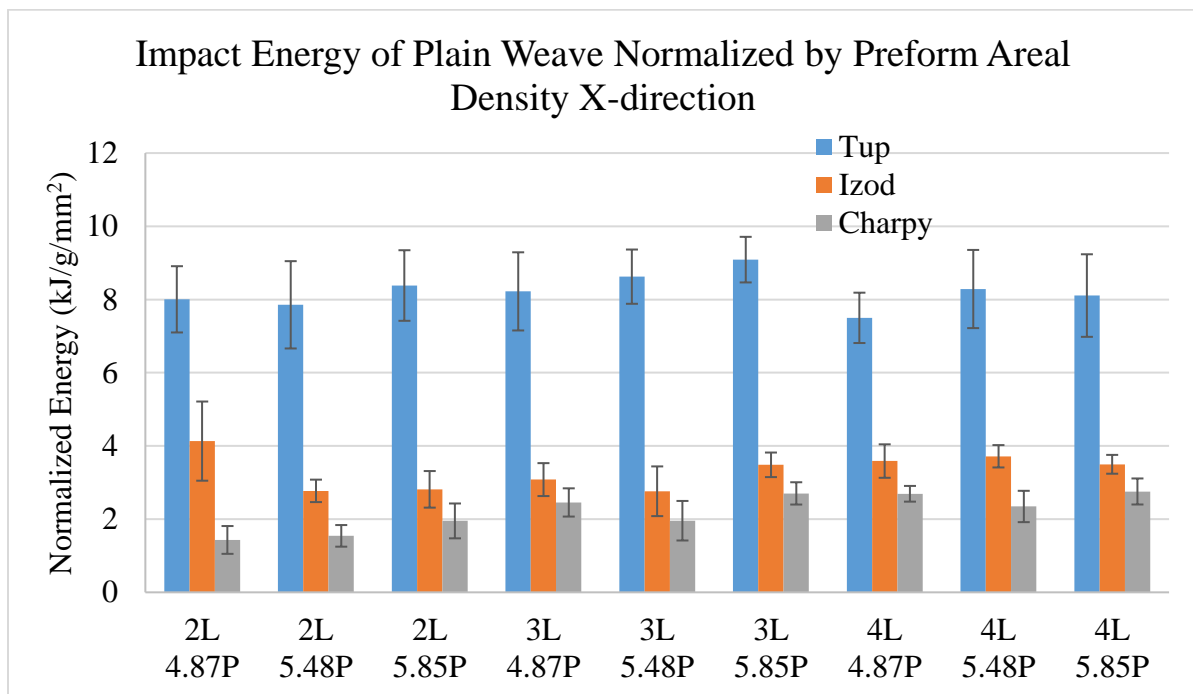
(b)

Figure 110 Impact energies normalized by composite areal density of plain weave samples in, (a) Y-axis direction, and (b) X-axis direction

Finally, the results were normalized by the preform areal density, and the correlation matrix in the Y-axis direction is shown in Table G.7. Generally, the results in this case, are very similar to the case normalized by the composite thickness. The correlation between the Charpy and Tup results was weak, with $r = 0.395$, while, there was a strong indirect correlation between the Izod and Tup results, since $r = -0.821$. Moreover, the correlation between the Izod and Charpy results was weak, with $r = 0.496$ as shown in Figure 111 (a). On the other hand, Table G.8 shows the correlation results in the X-axis direction, which indicated weak correlation between the results of the Charpy and Tup impacts, with $r = -0.388$, while the correlation between the Izod and Tup impact results became weaker, with $r = 0.174$, and between the Izod and Charpy was reduced to $r = 0.157$ as shown in Figure 111 (b). From the previous results, it can be concluded that the correlation was significantly reduced after normalizing by the preform areal density, similar to the case normalized by composite thickness. Additionally, the correlation was slightly weaker in the X-axis direction. This significant drop in the correlation after normalizing by the preform areal density, indicated that the preform weight was a strong factor that influenced the results, and yielded a high correlation in the non-normalized case.



(a)



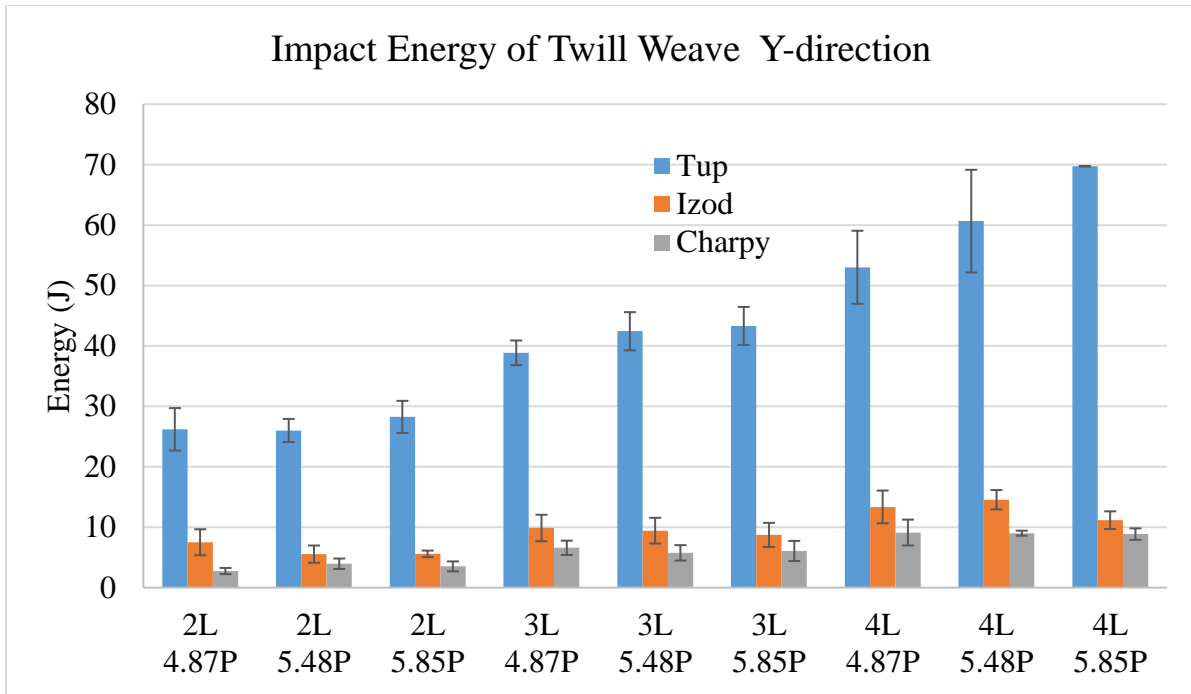
(b)

Figure 111 Impact energies normalized by preform areal density of plain weave samples in, (a) Y-axis direction, and (b) X-axis direction

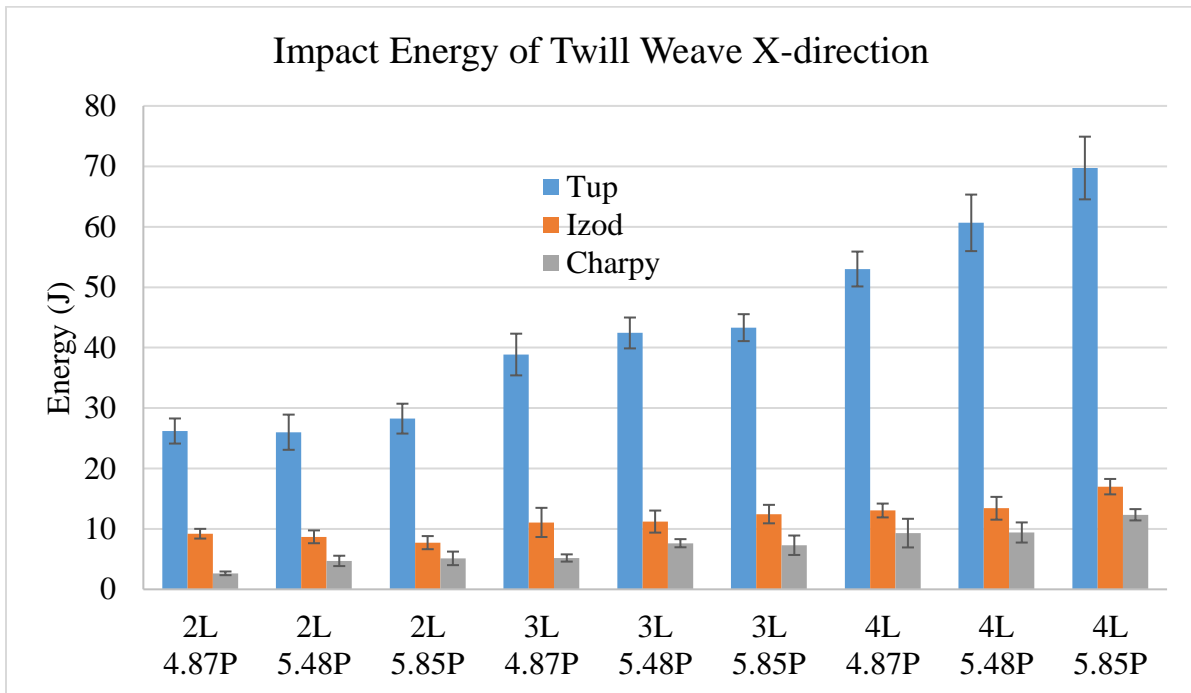
In the analysis of the plain weave samples, it can be concluded that, there was a strong correlation between the results of all three impact modes, in the non-normalized case. However, after normalizing by any of the three normalization approaches, the correlation was significantly reduced. Which indicated that the composite thickness, composite weight, and preform weight are factors that have a strong effect on the correlation. Thus, the analysis after normalization became more accurate and realistic. The normalized analysis indicated that there is an intermediate negative correlation between the Tup and Izod impact results in Y-axis direction, weak or no correlation between Charpy and Tup results, and weak correlation between Izod and Tup results.

Twill weave samples

First, a correlation test was performed between the energies of Tup, Izod, and Charpy impacts of all twill weave samples in Experiment A. The statistical tests and correlation matrices are listed in Appendix H. The Y-axis direction results in Table H.1 show that there was a very strong correlation between the results of the Charpy and Tup impacts, with $r = 0.933$. Similarly, the Izod results had a strong correlation with the Tup results, $r = 0.843$. Moreover, the correlation between the Izod and Charpy results was also very strong with $r = 0.917$ as illustrated in Figure 112 (a). On the other hand, Table H.2 shows the correlation results in the X-axis direction, which were very similar to the Y-axis direction. It indicated very strong correlation between the results of the Charpy and Tup impacts, as well as between the Izod and Tup, with $r = 0.959$ and 0.962 respectively. Also, it indicated a strong correlation between the Izod and Charpy impact results, with $r = 0.912$ as illustrated in Figure 112 (b). This means that, there was a strong correlation between impact energies of all three impact modes. The correlation between the Charpy and Tup is the highest. Additionally, the correlation was almost the same in the Y- and X-axis directions.



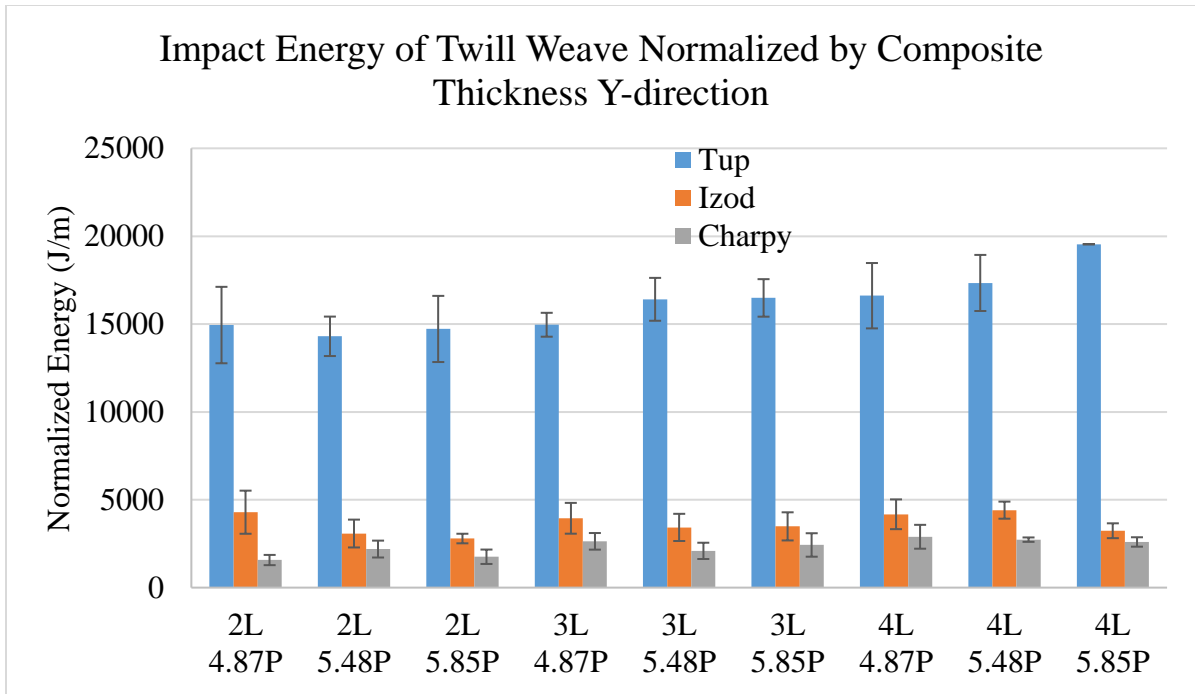
(a)



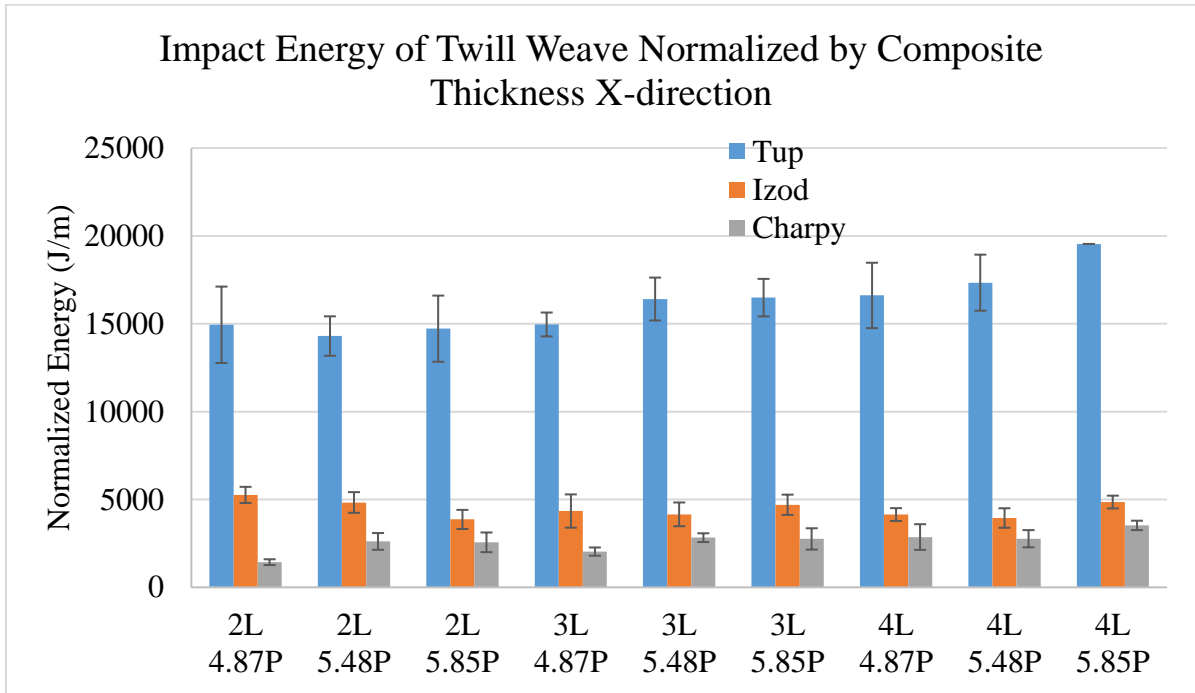
(b)

Figure 112 Impact energies of twill weave samples in, (a) Y-axis direction, and (b) X-axis direction

Afterwards, the results of the three impact modes were normalized by the composite thickness, and the correlation results in the Y-axis direction are listed in Table H.3. One can notice that, the correlation between the Charpy and Tup results became intermediate, with $r = 0.545$, whilst, the correlation between the Izod and Tup results became very weak, with $r = 0.103$. Additionally, the correlation between the Izod and Charpy results was reduced, and the correlation became weak, with $r = 0.334$ as shown in Figure 113 (a). On the other hand, Table H.4 shows the correlation results in the X-axis direction, which is different from the Y-direction. The correlation between the Charpy and Tup was intermediate, with $r = 0.741$, while, there was no correlation between the Izod and Tup impacts, $r = -0.012$. Additionally, there was a weak indirect correlation between the Izod and Charpy results, with $r = 0.306$ as shown in Figure 113 (b). From the previous results, it can be concluded that the correlation became significantly reduced after normalizing by the composite thickness. However, there was still an intermediate correlation between the Charpy and Tup impact in both Y- and X-axis direction. This significant reduction in the correlation after normalizing by the composite thickness, indicated that the thickness was a strong factor that influenced the results, and yielded a strong direct correlation in the non-normalized case.



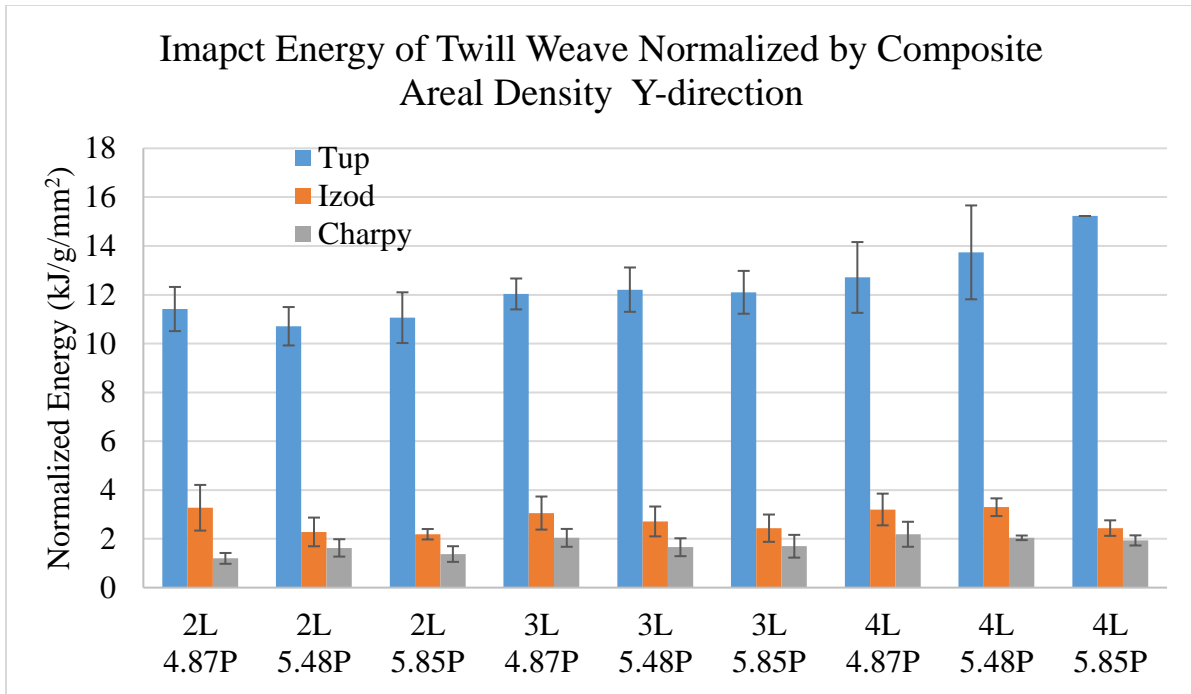
(a)



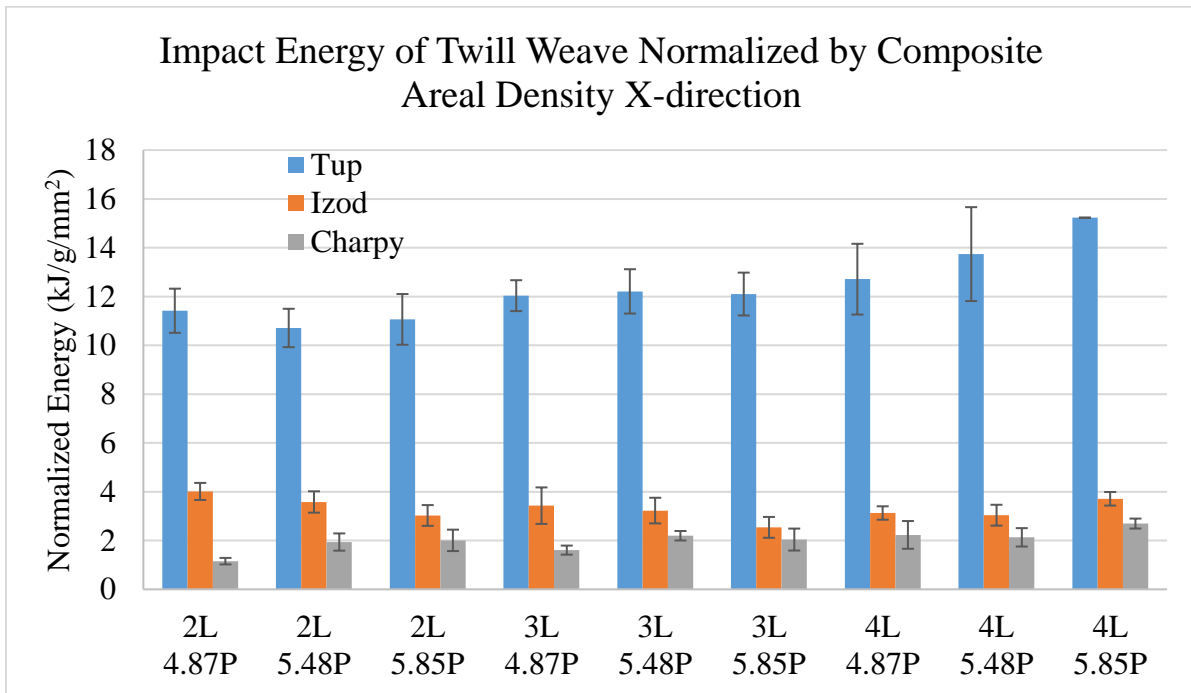
(b)

Figure 113 Impact energies normalized by composite thickness of twill weave samples in, (a) Y-axis direction, and (b) X-axis direction

Further, the results were normalized by the composite areal density, and the correlation matrix in the Y-axis direction is shown in Table H.5. Generally, the results in this case, were very close to the case normalized by the composite thickness. There was intermediate correlation between the Charpy and Tup results, with $r = 0.563$, while there was a very weak correlation between the Izod and Tup results, since $r = 0.122$. Moreover, the correlation between the Izod and Charpy results was weak, with $r = 0.326$, as shown in Figure 114 (a). On the other hand, Table H.6 shows the correlation results in the X-axis direction, which indicated slight increase in correlation between the results of the Charpy and Tup impacts, over the Y-axis direction, with $r = 0.679$, while, the correlation between the Izod and Tup impacts results became negligible, with $r = -0.063$. Moreover, the correlation between the Izod and Charpy results was indirect and weak, with $r = -0.394$ as illustrated in Figure 114 (b). From the previous results, it can be concluded that the correlation became significantly reduced after normalizing by the composite areal density. This significant drop in the correlation after normalizing by the composite areal density, indicated that the composite weight was a strong factor that influenced the results, and yielded a high correlation in the non-normalized case. Additionally, there was a significant intermediate direct correlation between the Charpy and Tup impact results, in both Y- and X-axis directions.



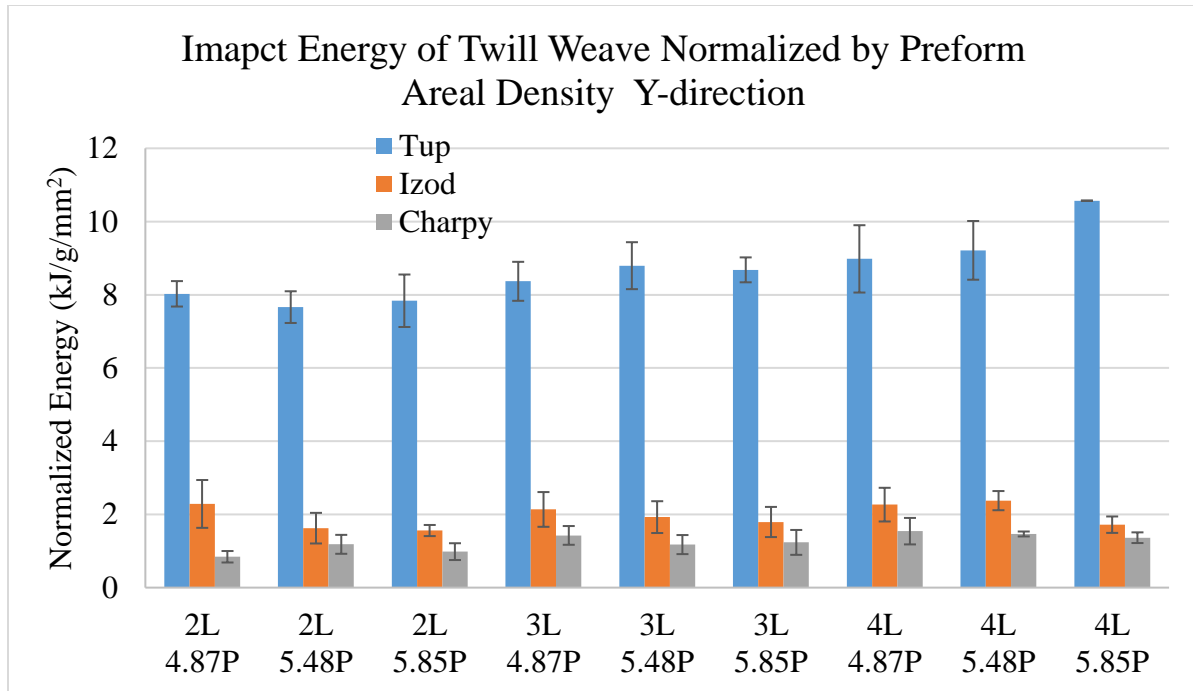
(a)



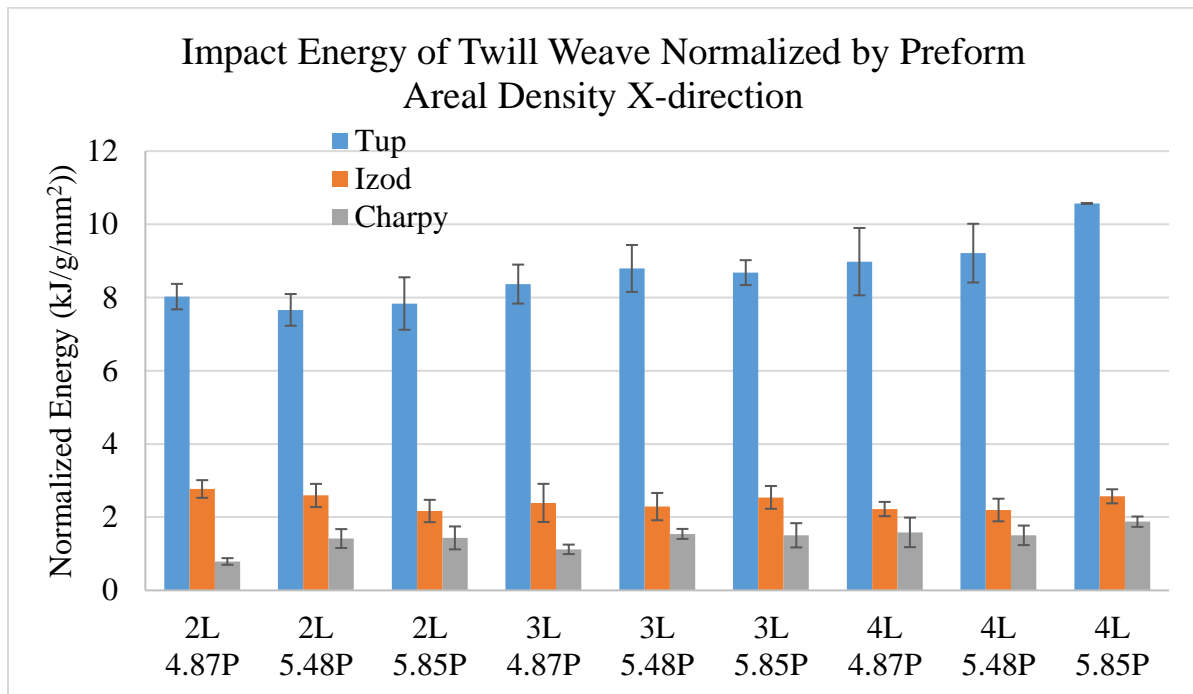
(b)

Figure 114 Impact energies normalized by composite areal density of twill weave samples in, (a) Y-axis direction, and (b) X-axis direction

Finally, the results were normalized by the preform areal density, and the correlation matrix in the Y-axis direction is shown in Table H.7. Generally, the results in this case, were very similar to the case normalized by the composite thickness. The correlation between the Charpy and Tup results was intermediate, with $r = 0.603$, while, there was a weak correlation between the Izod and Tup results, as well as the Izod and Charpy results, with $r = 0.202$ and 0.328 respectively as shown in Figure 115 (a). On the other hand, Table H.8 shows the correlation results in the X-axis direction, which indicated an intermediate correlation between the results of the Charpy and Tup impacts, with $r = 0.673$, similar to the Y-direction case. While, there was no correlation between the Izod and Tup impact results, since $r = -0.025$, and between the Izod and Charpy results there was a negative weak correlation, $r = -0.411$ as shown in Figure 115 (b). From the previous results, it can be concluded that the correlation was significantly reduced after normalizing by the preform areal density, similar to the case normalized by composite areal density. Additionally, there was an intermediate correlation between the Tup and Charpy impact results in both directions, and a weak correlation between the Charpy and Izod results with positive correlation in Y-direction, and negative correlation in X-direction. This significant drop in the correlation after normalizing by the preform areal density, indicates that the preform weight was a strong factor that influenced the results, and yielded a high correlation in the non-normalized case.



(a)



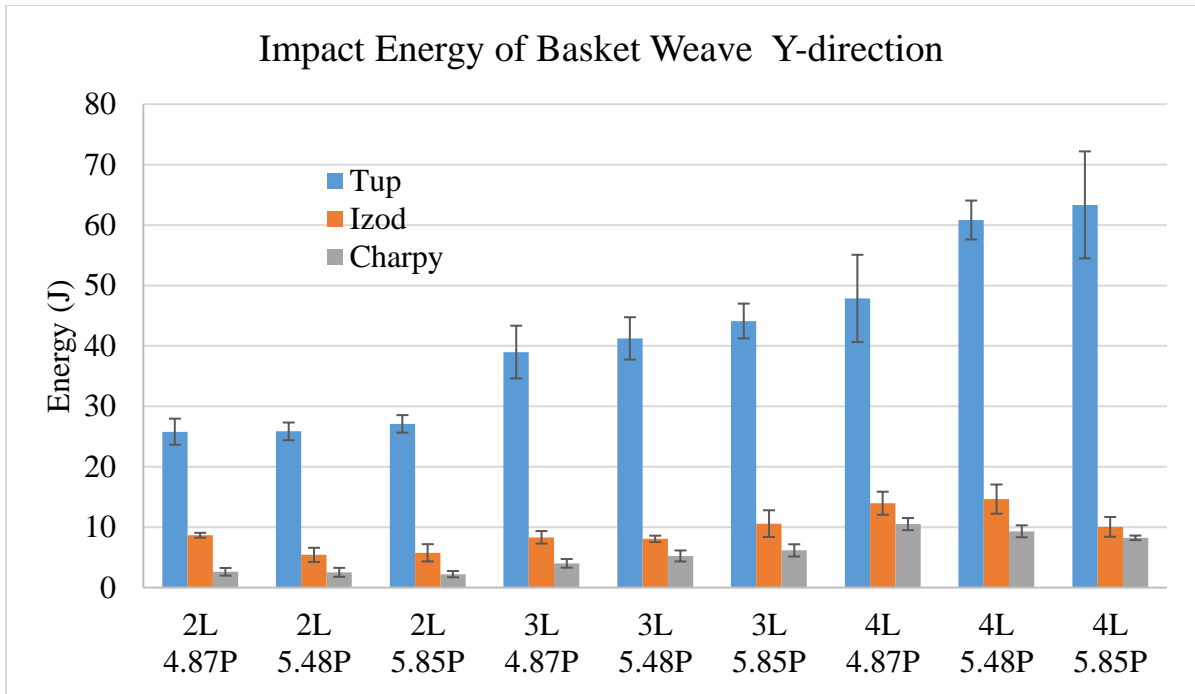
(b)

Figure 115 Impact energies normalized by preform areal density of twill weave samples in, (a) Y-axis direction, and (b) X-axis direction

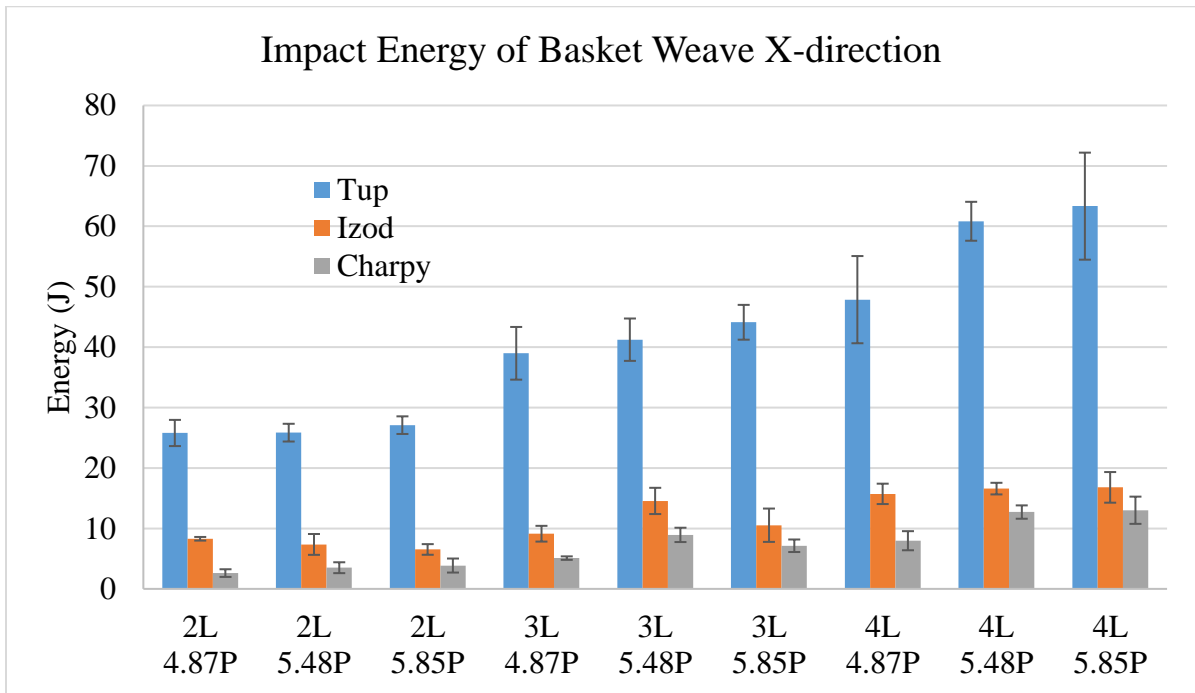
From the analysis of the twill weave samples, it can be concluded that, there was a strong correlation between the results of all three impact modes, in the non-normalized case. However, after normalizing by any of the three normalization approaches, the correlations were significantly reduced. Which indicated that the composite thickness, composite weight, and preform weight are factors that have a strong effect on the correlation. Thus, the analysis after normalization became more accurate and realistic. The normalized analysis indicated that there was an intermediate direct correlation between the Tup and Charpy impact results in both Y- and X-axis directions, weak or no correlation between Izod and Tup results, and weak correlation between Izod and Charpy results.

Basket weave samples

First, a correlation test was performed between the energies of Tup, Izod, and Charpy impacts of all basket weave samples in Experiment A. The statistical tests and correlation matrices are listed in Appendix I. The Y-axis direction results in Table I.1 show that there is a strong correlation between the results of the Charpy and Tup impacts, with $r = 0.878$. While, the Izod results had an intermediate correlation with the Tup results, $r = 0.761$. Moreover, the correlation between the Izod and Charpy results was also strong with $r = 0.913$ as illustrated in Figure 116 (a). On the other hand, Table I.2 shows the correlation results in the X-axis direction, which was slightly stronger than the Y-axis direction. It indicated very strong correlation between the results of the Charpy and Tup impacts, with $r = 0.968$. Also, it indicated strong correlation between Izod as well as Izod and Charpy, with $r = 0.912$ and 0.928 respectively, as illustrated in Figure 116 (b). This means that, there was a strong correlation between impact energies of all three impact modes. The correlation between the Charpy and Tup was the highest. Additionally, the correlation was stronger in the X-axis direction.



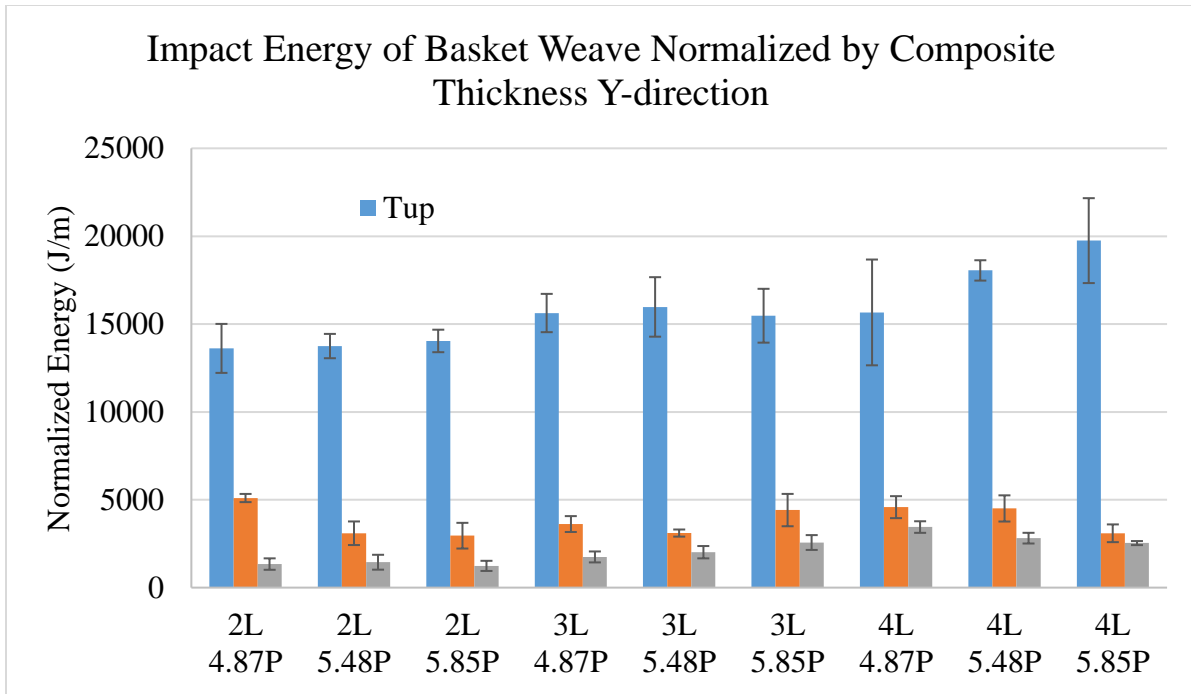
(a)



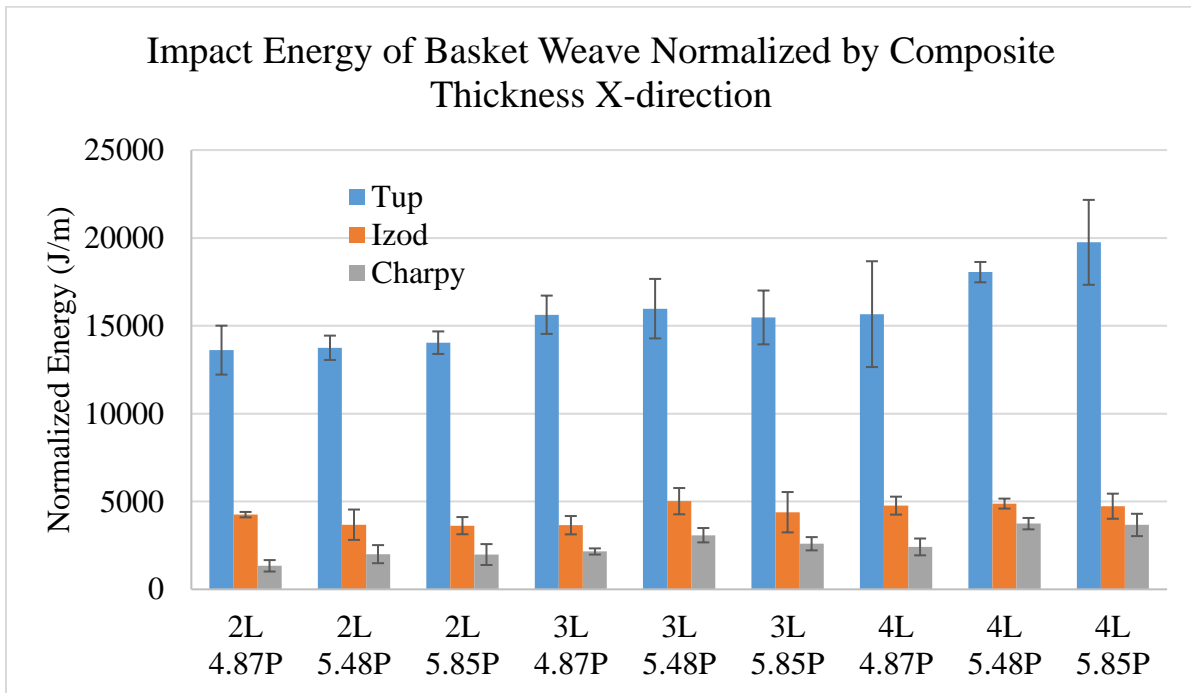
(b)

Figure 116 Impact energies of basket weave samples in, (a) Y-axis direction, and (b) X-axis direction

Afterwards, the results of the three impact modes were normalized by the composite thickness, and the correlation results in the Y-axis direction are listed in Table I.3. One can notice that, the correlation between the Charpy and Tup results became intermediate, with $r = 0.619$, whilst, the correlation between the Izod and Tup results became very weak, with $r = -0.112$. Additionally, the correlation between the Izod and Charpy results was reduced, and the correlation became weak, with $r = 0.376$ as shown in Figure 117 (a). On the other hand, Table I.4 shows the correlation results in the X-axis direction, which is much stronger than the Y-direction. The correlation between the Charpy and Tup is surprisingly strong, with $r = 0.918$, while, there was an intermediate correlation between the Izod and Tup results, as well as between the Izod and Charpy results, with $r = 0.630$ and 0.699 respectively, as shown in Figure 117 (b). From the previous results, it can be concluded that the correlation was reduced after normalizing by the composite thickness. However, there was still a strong correlation between the Charpy and Tup results in the X-axis direction, and an intermediate correlation between the Charpy and Tup impact in both Y- and X-axis direction. This significant reduction in the correlation after normalizing by the composite thickness, indicates that the thickness was a strong factor that influenced the results, and yielded a strong direct correlation in the non-normalized case.



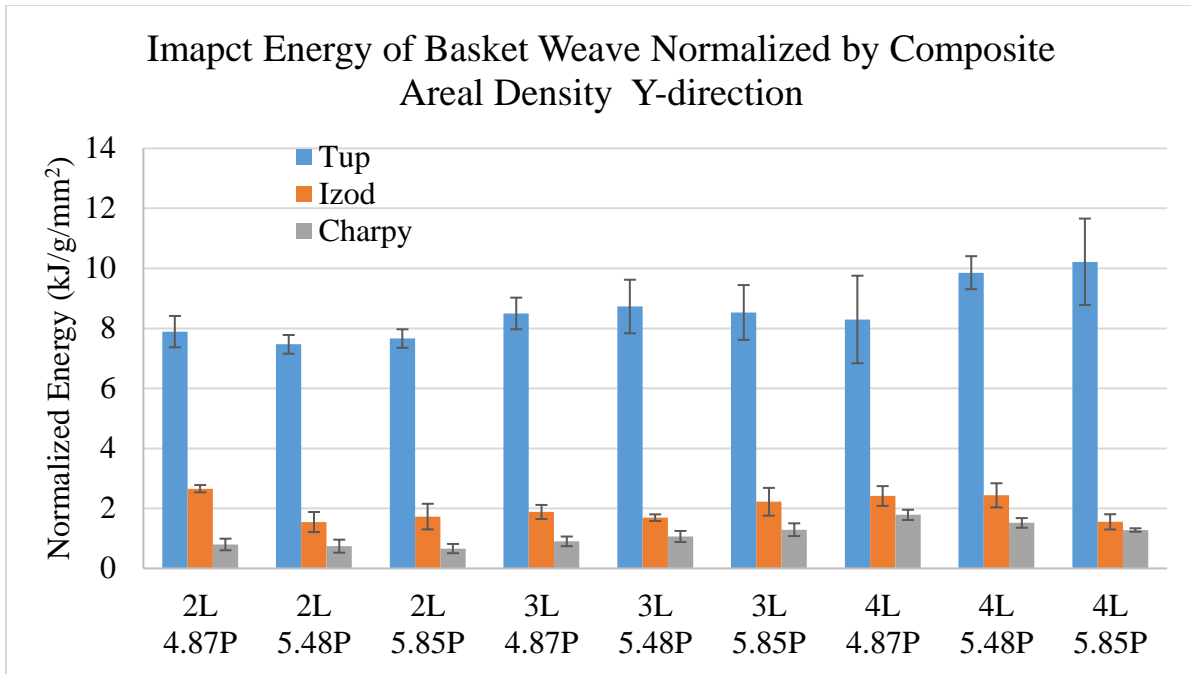
(a)



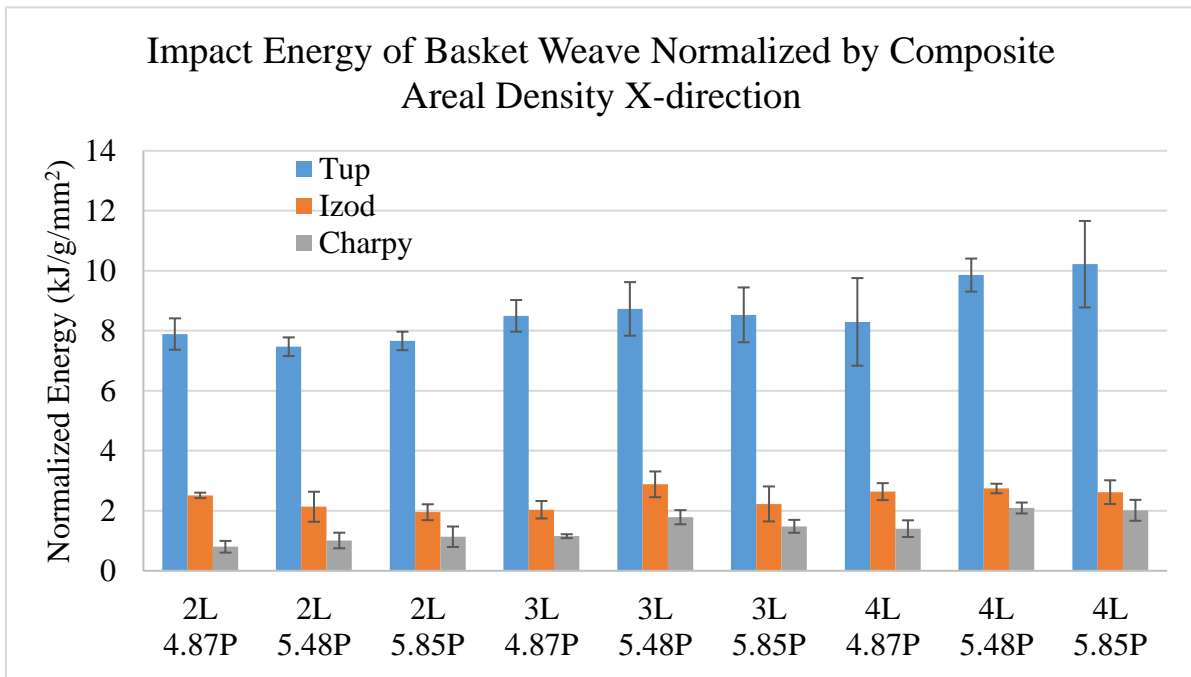
(b)

Figure 117 Impact energies normalized by composite areal density of basket weave samples in, (a) Y-axis direction, and (b) X-axis direction

Further, the results were normalized by the composite areal density, and the correlation matrix in the Y-axis direction is shown in Table I.5. Generally, the results in this case, were very close to the case normalized by the composite thickness. There was intermediate correlation between the Charpy and Tup results, with $r = 0.577$, while there was no correlation between the Izod and Tup results, since $r = -0.012$. Moreover, the correlation between the Izod and Charpy results was weak, with $r = 0.421$, as shown in Figure 118 (a). On the other hand, Table I.6 shows the correlation results in the X-axis direction, which indicated a significant increase in correlation between the results of the Charpy and Tup impacts, over the Y-axis direction, with $r = 0.901$. Whereas, the correlation between the Izod and Tup impacts results became intermediate, as well as correlation between the Izod and Charpy results, with $r = 0.587$ and 0.645 respectively, as illustrated in Figure 118 (b). From the previous results, it can be concluded that the correlation was significantly reduced after normalizing by the composite areal density, except for the correlation between the Charpy and Tup results in the X-axis direction. Additionally, there was an intermediate correlation between the Charpy and Tup impact results, in both Y- and X-axis directions. This drop in the correlation after normalizing by the composite areal density, indicated that the composite weight was a strong factor that influenced the results, and yielded a high correlation in the non-normalized case.



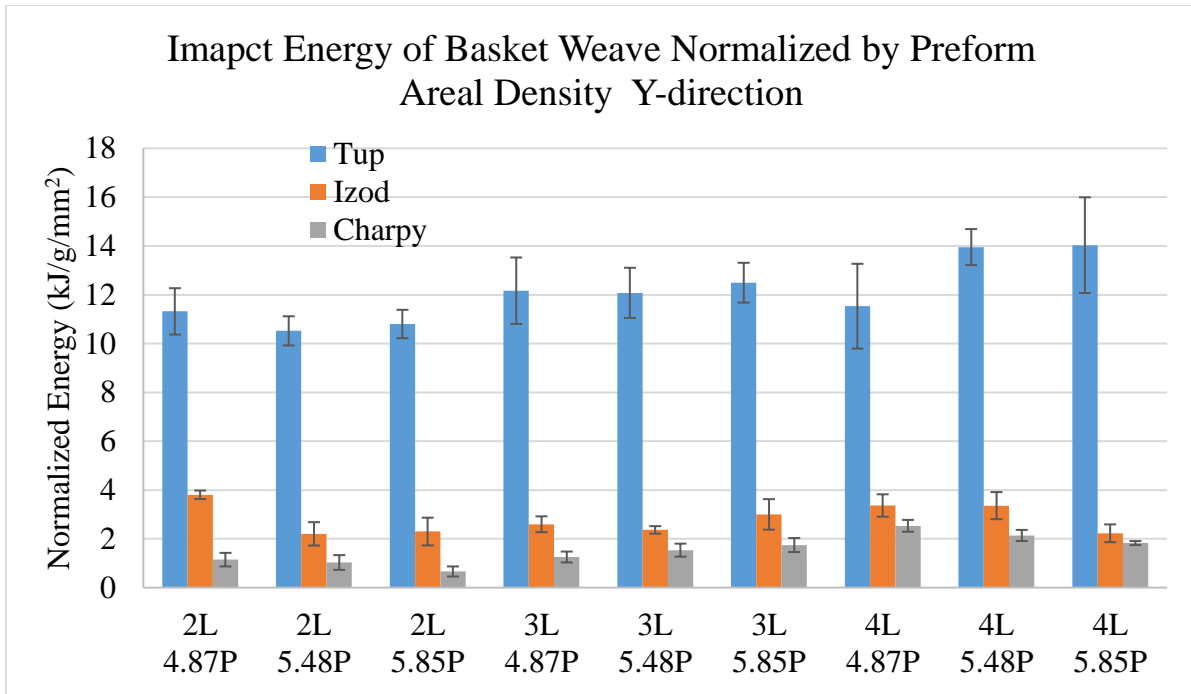
(a)



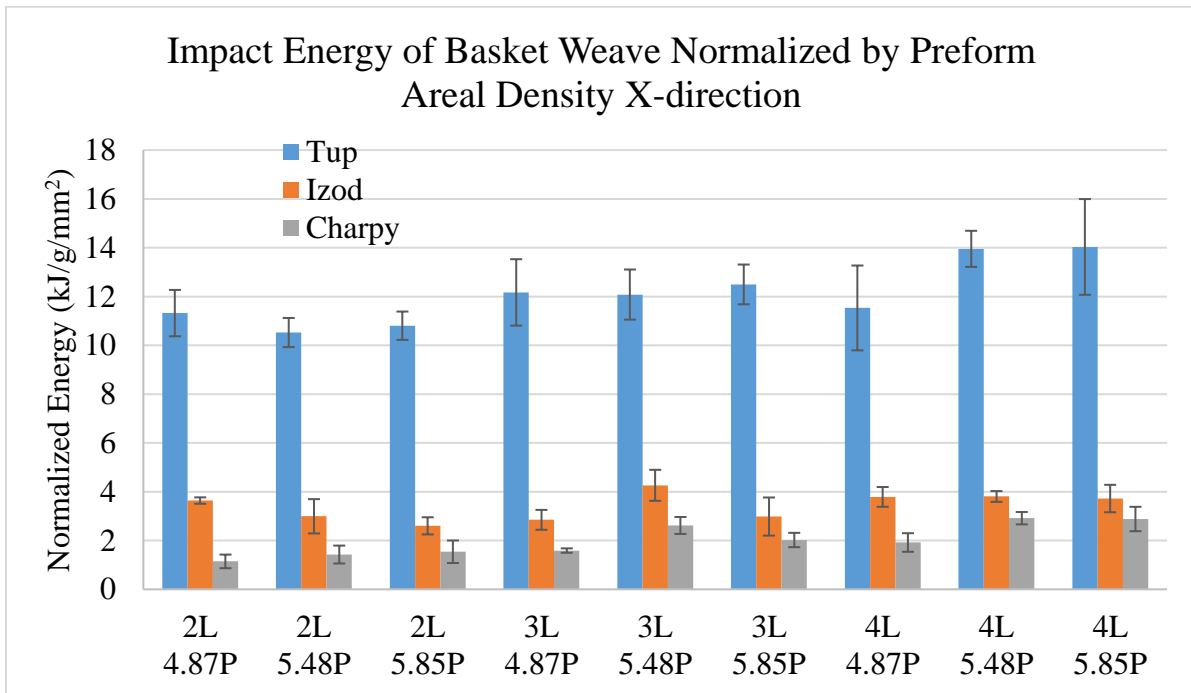
(b)

Figure 118 Impact energies normalized by composite areal density of basket weave samples in, (a) Y-axis direction, and (b) X-axis direction

Finally, the results were normalized by the preform areal density, and the correlation matrix in the Y-axis direction is shown in Table I.7. Generally, the results in this case, were very similar to the case normalized by the composite areal density. The correlation between the Charpy and Tup results were intermediate, with $r = 0.572$, while, there was a weak correlation between the Charpy and Izod results, $r = 0.410$, and there was no correlation between the Izod and Tup results, as shown in Figure 119 (a). On the other hand, Table I.8 shows the correlation results in the X-axis direction, which indicated a strong correlation between the results of the Charpy and Tup impacts, with $r = 0.853$, similar to the Y-direction case. While, there was a weak correlation between the Izod and Tup impact results, since $r = 0.435$. Whereas, the correlation between the Izod and Charpy results was intermediate, with $r = 0.604$, as shown in Figure 119 (b). From the previous results, it can be concluded that the correlation was significantly reduced after normalizing by the preform areal density, similar to the case normalized by composite areal density, except for the correlation between the Charpy and Tup in the X-axis direction which remained strong. Additionally, there was an intermediate correlation between the Charpy and Izod results both directions. This significant drop in the correlation after normalizing by the preform areal density, indicated that the preform weight was a strong factor that influenced the results, and yielded a high correlation in the non-normalized case.



(a)



(b)

Figure 119 Impact energies normalized by preform areal density of basket weave samples in, (a) Y-axis direction, and (b) X-axis direction

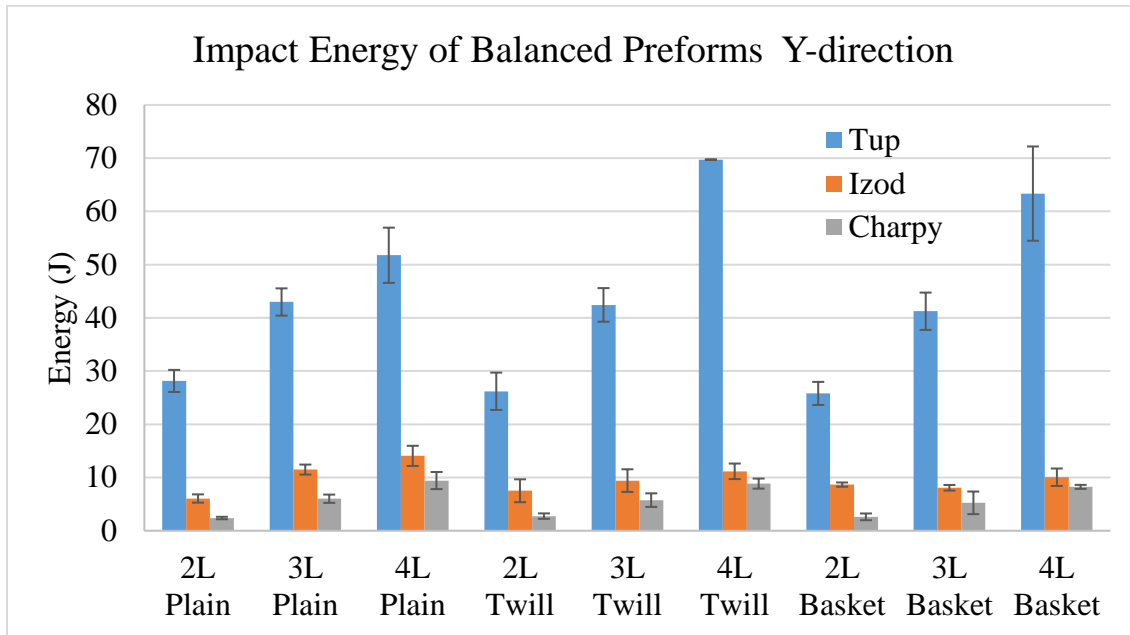
In the analysis of the basket weave samples, it can be concluded that, there was a strong correlation between the results of all three impact modes, in the non-normalized case. However, after normalizing by any of the three normalization approaches, the correlations were significantly reduced except for the correlation between the Charpy and Tup results in the X-direction. This led to the conclusion that the composite thickness, composite weight, and preform weight are factors that have a strong effect on the correlation. Thus, the analysis after normalization became more accurate and realistic. The normalized analysis indicated that there was an intermediate to strong direct correlation between the Tup and Charpy impact results, weak or no correlation between Izod and Tup results, and weak to intermediate correlation between Izod and Charpy results.

Balanced weave samples

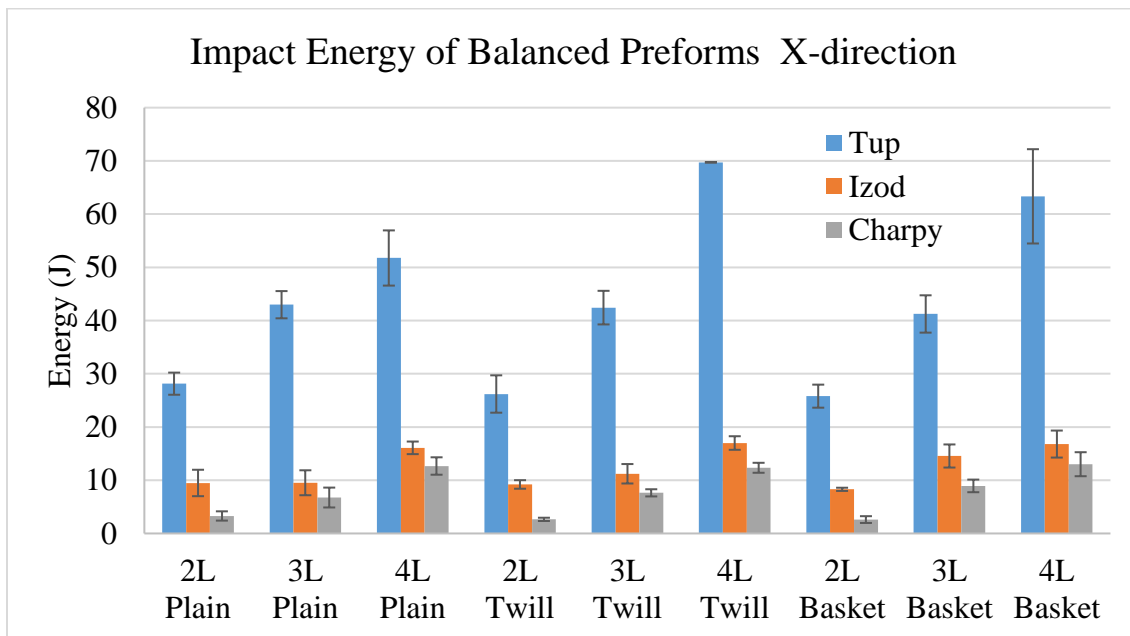
The final correlation analysis was performed on balanced samples, which are made of volume balanced preforms in the X- and Y- directions, for the different number of Y-yarn layers. For example, 2 Y-yarn layers woven with 4.87 X-yarns/ cm/ layer preform are volume-balanced in X-, and Y- directions. Similarly, for 3 y-yarn layers preforms with 5.48 X-yarns/ cm/ layer preforms are balanced in X- and Y-directions. Balanced preforms tend to have better interlaminar performance than the unbalanced ones, thus it was important to test the correlation between the three impact modes, for this group of samples.

First, a correlation test was performed between the energies of Tup, Izod, and Charpy impacts of all balanced weave samples in Experiment A. The statistical tests and correlation matrices are listed in Appendix J. The Y-axis direction results in Table J.1 show that there was a very strong correlation between the results of the Charpy and Tup impacts, with $r = 0.928$. While, the Izod results had an intermediate correlation with the Tup results, $r = 0.671$. Moreover, the correlation between the Izod and Charpy results was also strong with $r = 0.856$ as illustrated in Figure 120 (a). On the other hand, Table J.2 shows the correlation results in the X-axis direction, which is slightly stronger than the Y-axis direction. It indicated very strong correlation between the results of the Charpy and Tup impacts, with $r = 0.939$. Also, it indicated strong correlation between Izod as well as Izod and Charpy, with $r = 0.896$ and 0.955 respectively, as illustrated in Figure 120 (b). This means that, there was a strong correlation

between impact energies of all three impact modes. The correlation between the Charpy and Tup was the highest. Additionally, the correlation was stronger in the X-axis direction.



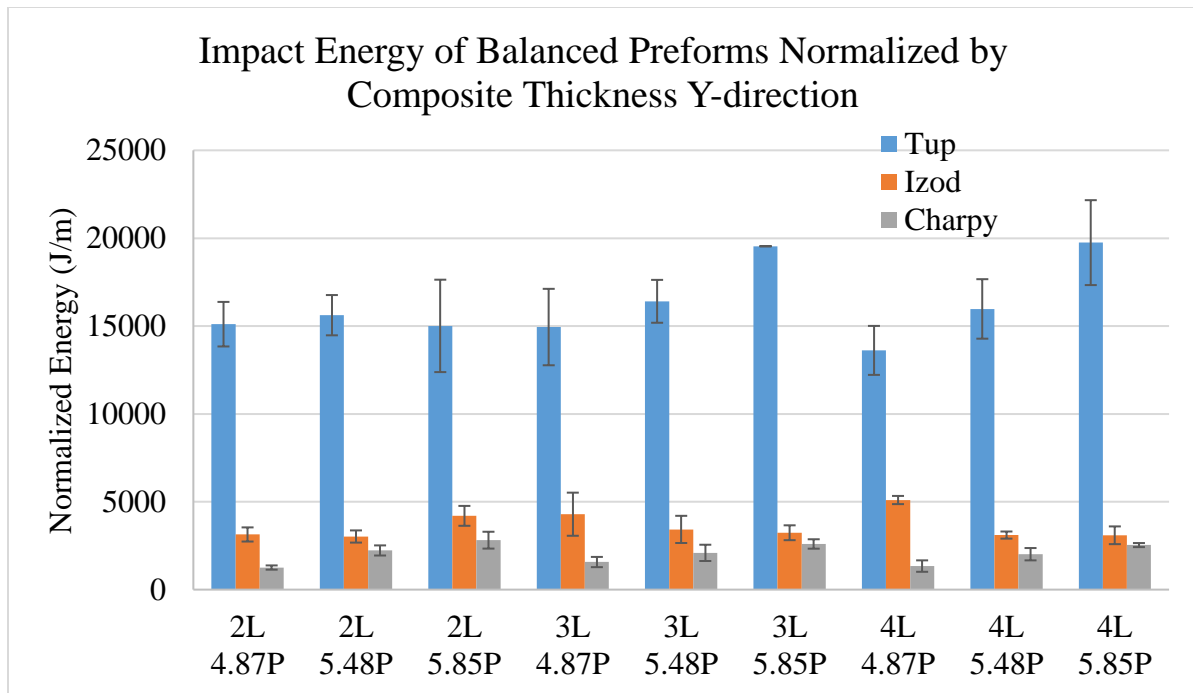
(a)



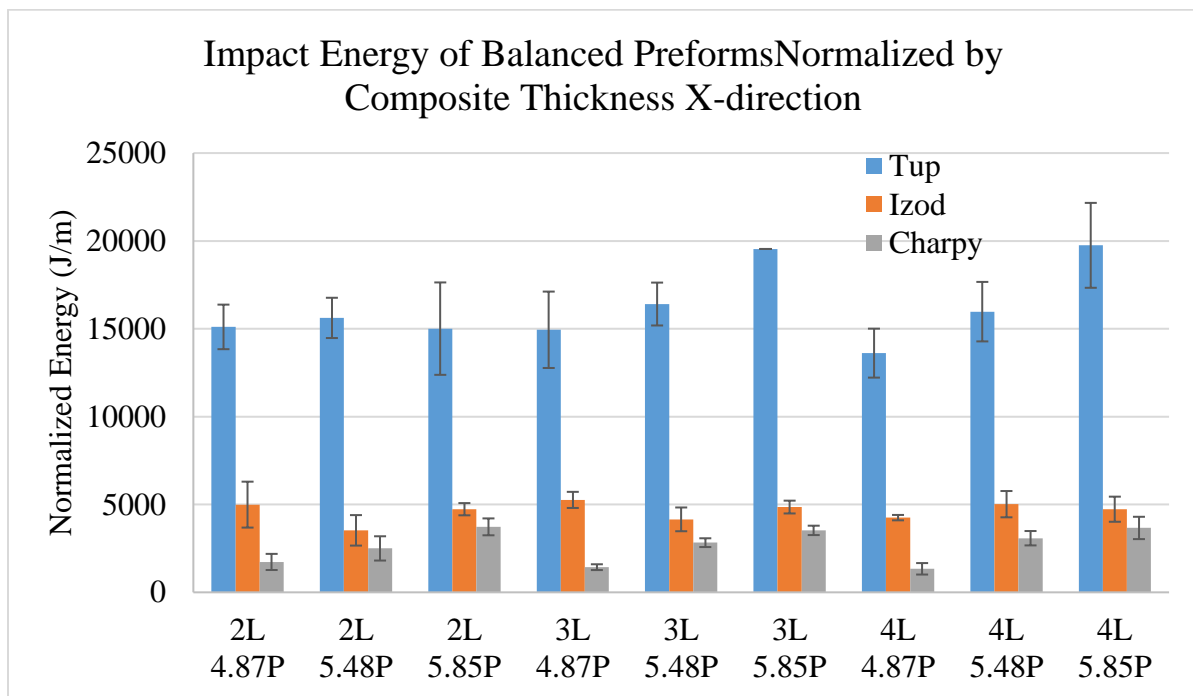
(b)

Figure 120 Impact energies of balanced samples in, (a) Y-axis direction, and (b) X-axis direction

Afterwards, the results of the three impact modes were normalized by the composite thickness, and the correlation results in the Y-axis direction are listed in Table J.3. One can notice that, the correlation between the Charpy and Tup results became intermediate, with $r = 0.624$, whilst, the correlation between the Izod and Tup results became intermediate and indirect, with $r = -0.617$. Additionally, the correlation between the Izod and Charpy results was reduced, and the correlation became weak, with $r = -0.339$ as shown in Figure 121 (a). On the other hand, Table J.4 shows the correlation results in the X-axis direction, which was different from the Y-direction. The correlation between the Charpy and Tup is intermediate, with $r = 0.703$, while, there was a very weak correlation between the Izod and Tup results, with $r = 0.137$. Moreover, there was no correlation between the Izod and the Charpy results, with $r = -0.012$ as shown in Figure 121 (b). From the previous results, it can be concluded that the correlation was reduced after normalizing by the composite thickness. However, there was still an intermediate correlation between the Charpy and Tup results in the both X- and Y-axis directions. This significant reduction in the correlation after normalizing by the composite thickness, indicated that the thickness was a strong factor that influenced the results, and yielded a strong direct correlation in the non-normalized case.



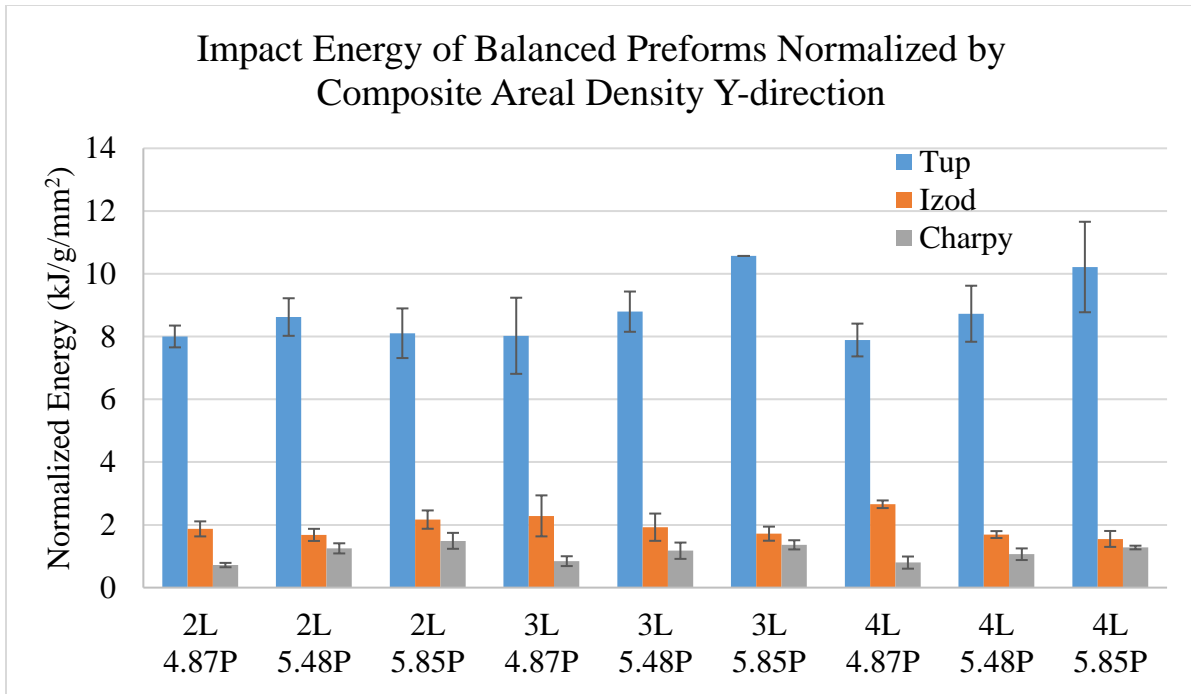
(a)



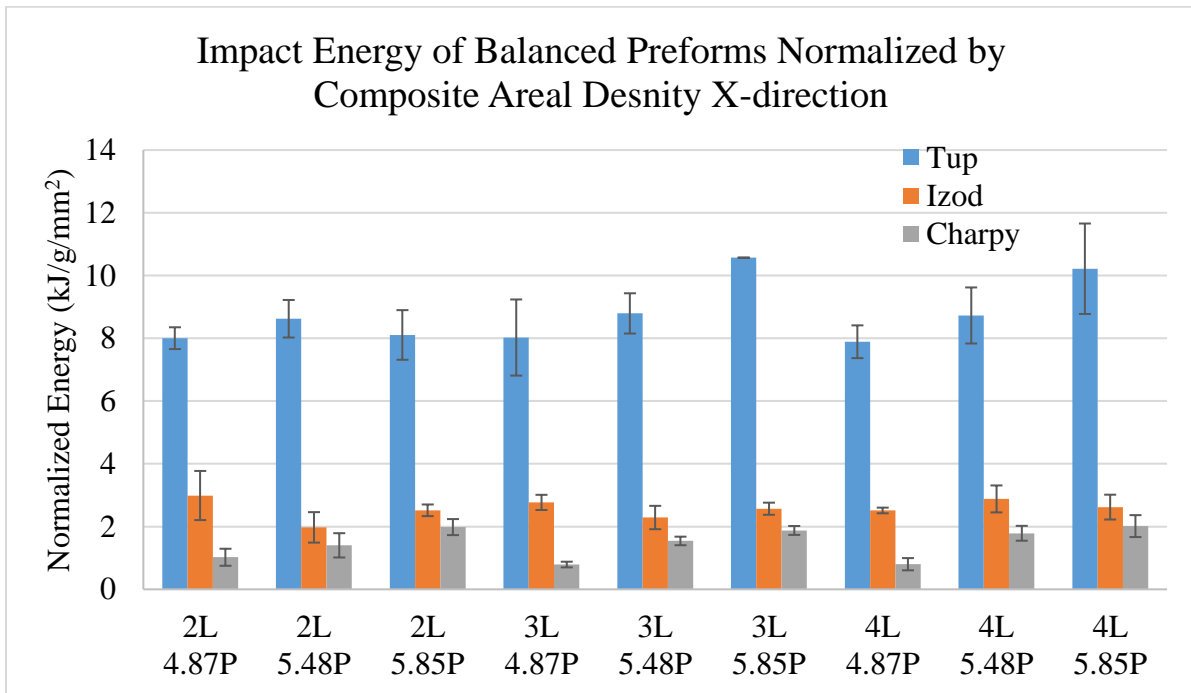
(b)

Figure 121 Impact energies normalized by composite thickness of balanced samples in, (a) Y-axis direction, and (b) X-axis direction

Further, the results were normalized by the composite areal density, and the correlation matrix in the Y-axis direction is shown in Table J.5. Generally, the results in this case, were very close to the case normalized by the composite thickness. There was intermediate correlation between the Charpy and Tup results, with $r = 0.566$, as well as between the Izod and Tup results, $r = -0.677$. Moreover, the correlation between the Izod and Charpy results was weak, with $r = 0.454$, as shown in Figure 122 (a). On the other hand, Table J.6 shows the correlation results in the X-axis direction. There is still an intermediate correlation between the results of the Charpy and Tup impacts, similar to the Y-axis direction, with $r = 0.675$. Whereas, the correlation between the Izod and Tup impacts results became very weak, as well as correlation between the Izod and Charpy results, with $r = -0.102$ and -0.137 respectively, as illustrated in Figure 122 (b). From the previous results, it can be concluded that the correlation was significantly reduced after normalizing by the composite areal density, except for the correlation between the Charpy and Tup results in both X- and Y-axis directions. Additionally, there was an indirect intermediate correlation between the Izod and Tup impact results, in Y-axis direction. This drop in the correlation after normalizing by the composite areal density, indicated that the composite weight was a strong factor that influenced the results, and yielded a high correlation in the non-normalized case.



(a)

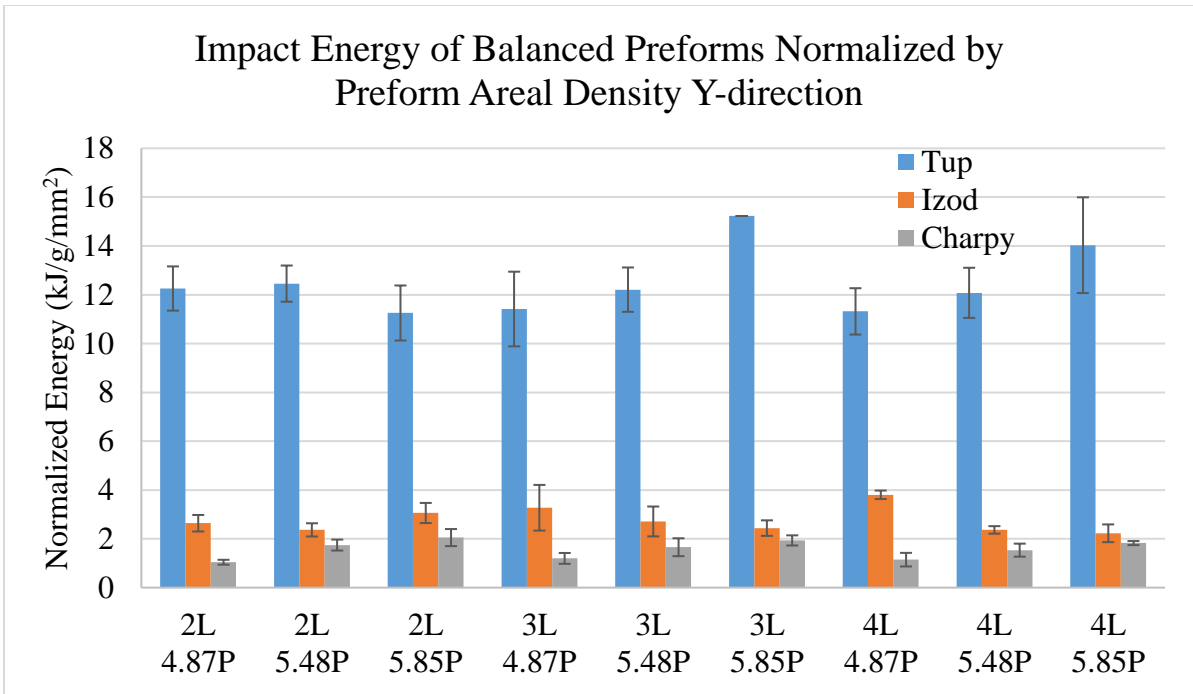


(b)

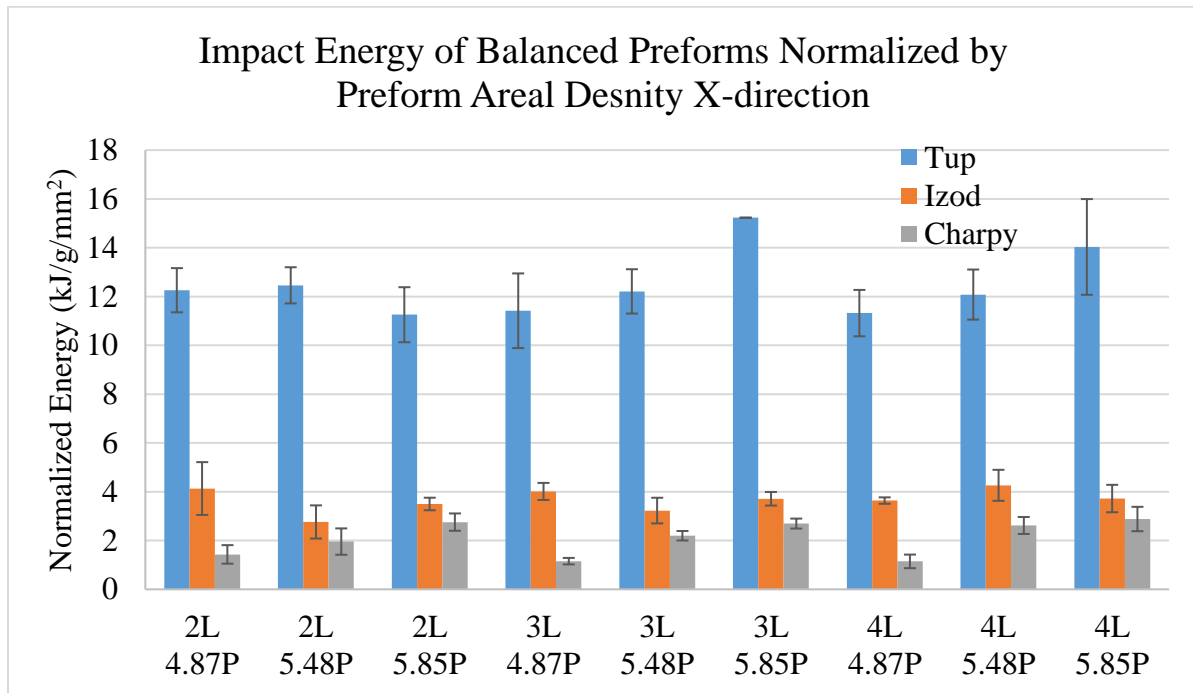
Figure 122 Impact energies normalized by composite areal density of balanced samples in, (a) Y-axis direction, and (b) X-axis direction

Finally, the results were normalized by the preform areal density, and the correlation matrix in the Y-axis direction is shown in Table J.7. Generally, the results in this case, were similar to the case normalized by the composite areal density. The correlation between the Charpy and Tup results was weak and direct, with $r = 0.463$, whereas here correlation between the Izod and the Charpy results was weak and indirect. Yet, there was an intermediate indirect correlation between the Tup and Izod results, $r = -0.654$, as shown in Figure 123 (a). On the other hand, Table J.8 shows the correlation results in the X-axis direction, which indicated an intermediate correlation between the results of the Charpy and Tup impacts, with $r = 0.544$. While, there was no correlation between the Izod and Tup impact results, $r = -0.025$, as well as between the Izod and Charpy results, with $r = -0.098$, as shown in Figure 123 (b).

From the previous results, it can be concluded that the correlation was significantly reduced after normalizing by the preform areal density, similar to the case normalized by composite areal density. However, there was still a direct intermediate correlation between the Charpy and Tup results in the X-axis direction. This significant drop in the correlation after normalizing by the preform areal density, indicated that the preform weight was a strong factor that influenced the results, and yielded a high correlation in the non-normalized case.



(a)



(b)

Figure 123 Impact energies normalized by preform areal density of balanced samples in, (a) Y-axis direction, and (b) X-axis direction

From the analysis of the balanced samples, it can be concluded that, there was a strong correlation between the results of all three impact modes, in the non-normalized case. However, after normalizing by any of the three normalization approaches, the correlations were significantly reduced. This led to the conclusion that the composite thickness, composite weight, and preform weight are factors that have a strong effect on the correlation. Thus, the analysis after normalization became more accurate and realistic. The normalized analysis indicated that there was an intermediate direct correlation between the Tup and Charpy impact results, weak or no correlation between Izod and Tup results, and weak correlation between Izod and Charpy results.

6.1.3. Conclusion on Experiment A

In the Tup impact test, it was concluded that increasing the Y-yarn number of layers and X-yarn density significantly increased the impact energy, yet increasing the pick density was generally not as significant as increasing the number of layers, while changing the Z-yarn interlacing pattern had a slight significant effect on the total energy with the twill being the highest, followed by basket, and then plain. Further, after normalizing the total penetration energy, the effects of the structural parameters became less significant. However, the existence of a residual increasing trend by increasing the number of layers as well as increasing the pick density, and changing the weave indicated that those three parameters have a significant effect on the composite impact energy irrespective of composite thickness, composite weight, or preform weight.

As for the Izod impact energy, it was concluded that increasing the number of layers increased the total energy in both directions. However, increasing the pick density surprisingly, resulted in a slight decrease in the total energy in the Y-direction, and no effect in the X-direction. Additionally, changing the Z-yarn weave pattern didn't have any effect on the total energy in both directions. Further, after normalization, it was found that increasing the number of layers resulted in a slight increase in the normalized energy in both directions, while increasing the pick density resulted in a more pronounced decrease in the total energy in the Y-direction, and didn't have any effect in the X-direction, and still the weave pattern had no significant effect in either direction. The energy in the X-direction was always higher than the Y- direction, even after normalization.

In the case of Charpy impact energy, it can be concluded that increasing the number of layers increased the total energy in both directions, and changing the weave pattern surprisingly had a significant effect as well. Yet, increasing the pick density, was the only significant factor in the X-direction. Further, after normalization the significance of the number of layers, and weave pattern effects were reduced. Moreover, the results in the X-axis direction were generally higher than that of the Y-axis direction, and they remained significant even after the normalization. However, this effect wasn't as significant as in the case of the Izod impact.

By comparing the main effect of the three impact tests, the Tup results had significantly higher impact energy than both, the Charpy and Izod, and the Charpy impact results were always lower than the Izod results, and this trend remained the same even after normalization.

Additionally, when testing the overall correlation between the three impact energies, it was concluded that, there was a strong correlation between the results of all three impact modes. However, after normalizing by any of the three normalization approaches, the correlations were significantly reduced. The analysis after normalization became more accurate and realistic, it indicated that there was a weak correlation between the Tup and Charpy impact results, very weak correlation between Charpy and Izod results, and no correlation between Izod and Tup results.

Moreover, by looking at the correlation between the normalized results of the plain weave samples, the normalized analysis indicated that there was an intermediate negative correlation between the Tup and Izod impact results in Y-axis direction, weak or no correlation between Charpy and Tup results, and weak correlation between Izod and Tup results. As for the twill samples, there was an intermediate direct correlation between the Tup and Charpy impact results in both Y- and X-axis directions, weak or no correlation between Izod and Tup results, and weak correlation between Izod and Charpy results. While, in case of basket samples there was an intermediate to strong direct correlation between the Tup and Charpy impact results, weak or no correlation between Izod and Tup results, and weak to intermediate correlation between Izod and Charpy results. Finally, in case of balanced samples there was still a direct intermediate correlation between the Charpy and Tup results in the X-axis direction.

6.2. Experiment B

In Experiment B, it was important to vary the ratio of the Z- to Y-yarns/ layer in order to study the effect of the Z-yarn on the in- and out-of-plane properties of the 3DOW. The levels were selected so that the Z-yarns percentage in the structure is systematically reduced from 1:1 which is a full interlacement, to 0:1 which is a structure with no Z-yarns interlacements. All the preforms in this experiment are plain weave, having 3 Y-yarn layers, and 5.48 X-yarns/layer/cm. All samples used in Experiment B are listed in Table 20, showing their sample ID and their variable parameter.

Table 20 Experiment B samples ID and their variable parameter

Sample ID	Z : Y-yarn/ layer
13	1:1
28	1:2
29	1:3
30	0:1

6.2.1 Effect of Z: Y-yarn/ layer ratio on mechanical properties

In this section the effect of varying the amount of Z-yarns in the 3DOW composite structure, on the in- and out-of-plane properties was investigated. The in-plane properties were represented by the quasi static tensile responses, in addition to the Izod, and Charpy impact. Whereas, the out-of-plane properties were represented by the Tup impact responses.

Tup Impact

The Tup impact responses included, peak load, load – deflection curves, total penetration energy, and normalized total energy. The results of the Tup impact tests are listed in Tables 21. The results were analyzed using one-way ANOVA test to reveal the effect of the Z: Y-yarn/ layer ratio on the Tup impact properties of the composites. The results of the one-way ANOVA test were confirmed using a follow up post hoc Duncan test. The statistical analysis results are listed in Appendix L.

Table 21 Tup impact results

ID	Comp. Areal Density (g/m ²)	Thickness t (mm)	FVF (%)	Peak Force (kN)	CV (%)	Total Energy E (J)	CV (%)	E/ t (J/m)	E/ Comp. Areal Density (kJ/g/mm ²)	E/ Preform Areal Density (kJ/g/mm ²)
13	4990	2.76	48.6	7.76	2.09	54.04	1.6	18876	10.96	15.66
28	5008	2.89	48.0	7.74	11.6	53.4	8.5	18483	10.7	15.6
29	4824	2.69	47.5	7.74	5.5	51.4	4.2	19066	10.6	15.2
30	4205	2.45	47.2	5.94	14.3	39.9	20.3	16303	9.5	11.9

Figure 124 (a) indicates that there is no statistically significant difference between the impact peak loads of the composite samples, due to changing the Z: Y-yarn/ layer ratio, however, by looking at the mean values, one can see a decrease in the peak load in the sample that had no Z-yarns. Further, by looking at the typical load – deflection curves of the samples in Figure 124 (b), this finding was confirmed. Figure 124 (b) also indicated that despite that the peak loads of the samples with Z: Y ratios 1:1, 1:2 and 1:3 are very close, yet their failure mechanisms are different, since, some curves indicated fiber breakage, while other indicated progressive delamination, and this will be discussed in more details later in section 6.2.2.

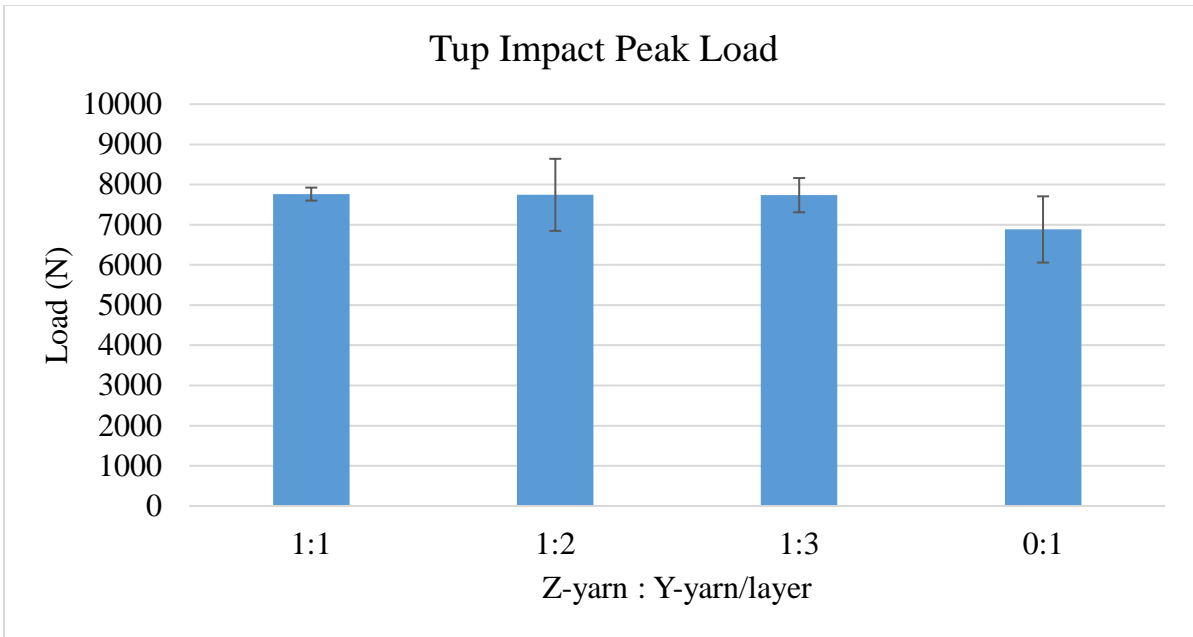
Moreover, by plotting the total penetration energies of the different samples in Figure 125 (a), the previous decreasing trend became more significant, and by performing an ANOVA test it indicated that there was a statistically significant difference as shown in Table L.4. Moreover, performing a post hoc Duncan test indicated that that the samples with Z: Y ratios 1:1, 1:2, and 1:3 are similar to each other and they belong to the same subset, while the sample with Z: Y ratio 1:0 was significantly different, and it had a lower total energy as shown in Table L.6.

Afterwards, the total penetration energy was normalized by several normalization approaches, in order to segregate the effect of some dependent parameters from the analysis and to have a fair comparison between the samples. Hence, it was normalized by the composite thickness, composite areal density, and preform areal density.

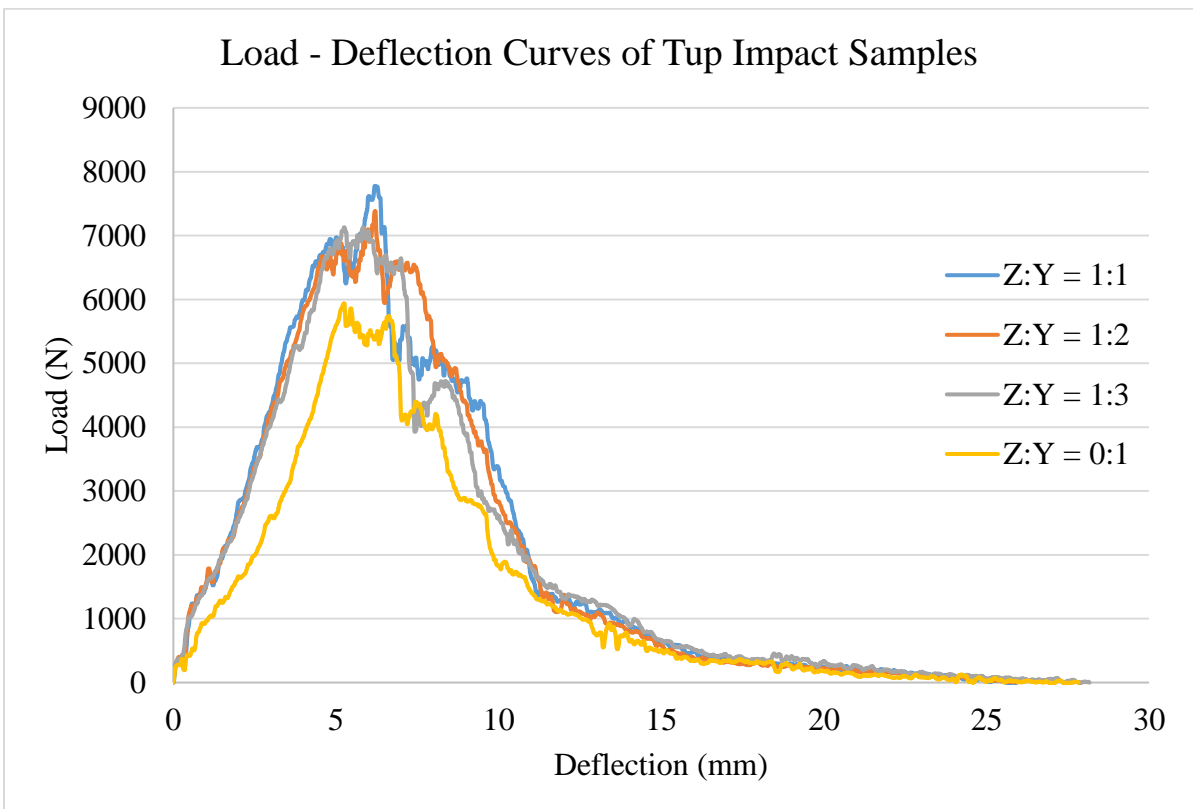
When the total energy was normalized by the composite thickness in Figure 125 (b) the effect of changing the Z: Y ratio became insignificant as shown in Table L.7. Similarly, when the total energy was normalized by the composite areal density, there was no significant difference

between the responses of the four samples as illustrated in Figure 125 (c). However, when the total energy was normalized by the preform areal density in Figure 125 (d), it indicated a significant decreasing trend, due to the decrease in the amount of Z-yarns in the structure, and this decreasing trend was even more obvious than the non-normalized case. By performing a post hoc test, it indicated that the responses of the samples with Z: Y ratios 1:1, 1:2 are 1:3 are similar, and that they belong to the same subset, while the response of the sample with Z: Y ratio 0:1 is different and it belongs to a different subset, and it had the lowest normalized total energy as shown in Table K.15.

From the analysis of the Tup impact responses, it can be concluded that changing the Z: Y ratio didn't have any significant effect on the peak impact load, except for the sample with Z: Y ratio 0:1 which had slightly lower peak load. Moreover, the total penetration energy significantly decreased by decreasing the amount of Z-yarns in the structure, and this decrease was more pronounced in the structure that had no Z-yarn interlacements. This indicated that even a very small amount of Z-yarns in the structure resulted in a composite with higher out-of-plane properties. Further, when the total energy was normalized by the composite thickness and areal density, the normalized energies had no significant difference, which indicated that the thickness and areal density of the composite had a significant effect on its total penetration energy. However, when the total energy was normalized by the preform areal density, which is a more accurate and realistic way of normalization, it confirmed the trend from the non-normalized case, and it indicated that the structure with no Z-yarn interlacements had significantly lower normalized energy.

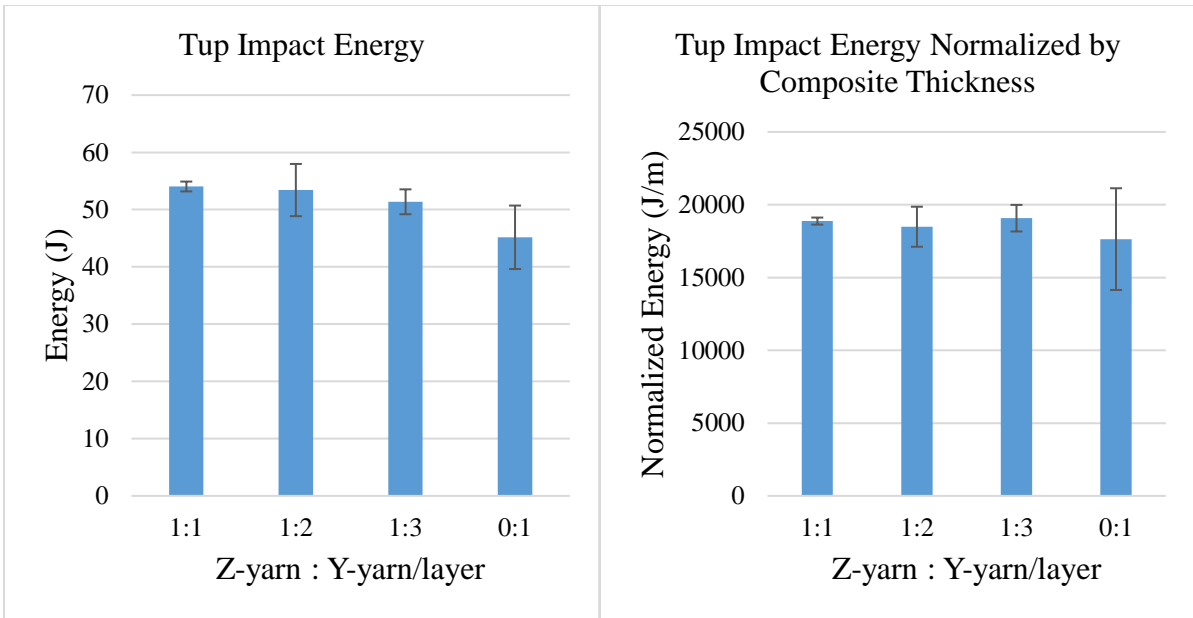


(a)



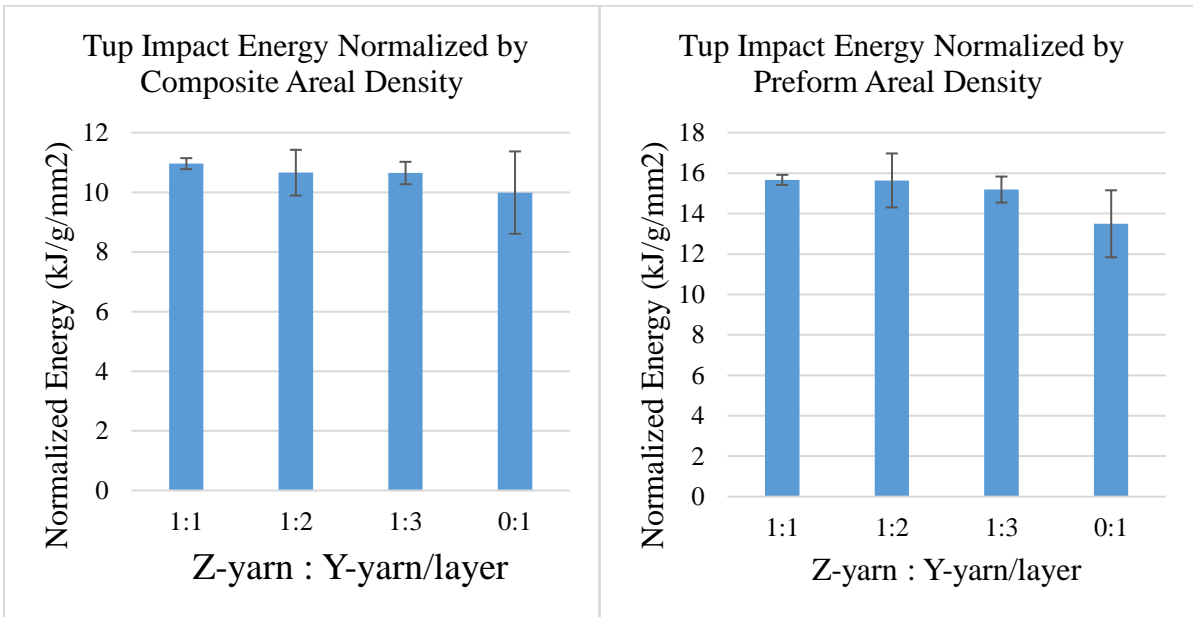
(b)

Figure 124 Tup impact, (a) peak loads, and (b) typical load - deflection curves



(a)

(b)



(c)

(d)

Figure 125 Top impact energy in X- and Y- directions, (a) non-normalized, (b) normalized by composite thickness, (c) by composite areal density, and (d) by preform areal density

Tensile

The tensile responses included, peak load, failure strain, modulus, load-strain curves, and normalized peak load in both X- and Y-directions. The results of the tensile testing in the Y- and X-axis directions are listed in Tables 22 and 23 respectively. The composites used in this experiment exhibited brittle failure, since they are made of E-glass fibers, and thermoset resin. One of the characteristics of brittle failure is that the material doesn't yield, and it has no plastic region, moreover, the peak point and the breaking load corresponded to the same point as illustrated in Figure 126 (d). Therefore, the peak load was generally used to characterize the tensile behavior of the composite in this analysis.

Table 22 Tensile test results in Y-axis direction

ID	Tensile Modulus	Failure Strain (%)	Peak Load (kN)	CV (%)	Total Tex (Tex)	Load/ Thickness (kN/m)	Load/ Comp. Areal Density (N/g/mm ²)	Load/ Preform Areal Density (N/g/mm ²)	Load/ Total Tex (N/Tex)
13	16.8	2.2	38632	7.0	59843	13730	7.5	11.2	0.65
28	20.4	2.5	39294	5.6	59067	13626	7.9	11.5	0.67
29	22.4	2.2	38120	4.7	58291	13783	7.7	11.3	0.65
30	23.3	1.9	38760	11.2	57515	12988	7.3	11.6	0.67

Table 23 Tensile test results in X-axis direction

ID	Tensile Modulus	Failure Strain (%)	Peak Load (kN)	CV (%)	Total Tex (Tex)	Load/ Thickness (kN/m)	Load/ Composite Areal Density (N/g/mm ²)	Load/ Preform Areal Density (N/g/mm ²)	Load/ Total Tex (N/Tex)
13	21.0	2.0	35805	3.8	57824	13339	7.2	10.4	0.62
28	22.1	2.1	35679	3.5	57824	12312	7.0	10.4	0.62
29	20.5	2.0	34230	3.6	57824	12564	7.1	10.1	0.59
30	20.6	1.9	33215	9.1	57824	12149	7.0	9.9	0.57

The results were analyzed using one-way ANOVA test to reveal the effect of the Z: Y-yarn/ layer ratio on the tensile properties of the composites. The results of the one-way ANOVA test

were confirmed using a follow up post hoc Duncan test. The statistical analysis results are listed in Appendix K.

Figure 126 (a) shows the effect of the Z: Y ratio on the tensile peak load in the X- and Y-directions, the graph indicated that there was no significant difference between the samples, and this was also confirmed by the ANOVA test in Y- and X-directions in Table K.7 and K28 respectively. Further, the typical load - strain curves in Y- and X-directions illustrated in Figure 127, indicated that there was no significant difference between the tensile behaviors of the samples in either direction, except for the sample with Z: Y ratio 1:2 which consistently had higher failure strain.

Moreover, when looking at the effect of the Z: Y ratio on the failure strain in Figure 126 (b), it indicated that the failure strain slightly decreased by reducing the amount of Z-yarns in the structure in the Y-direction, and this was significant at 95% confidence level with p-value =0.013 in Table K.4, and by performing a post hoc Duncan test, it indicated that specifically the samples with Z: Y ratios 1:2 and 0:1 are significantly different, with the 0:1 having the lowest failure strain as shown in Table K.6. However, changing the Z: Y ratio didn't have any significant effect on the failure strain in the X-direction as shown in Table K.25.

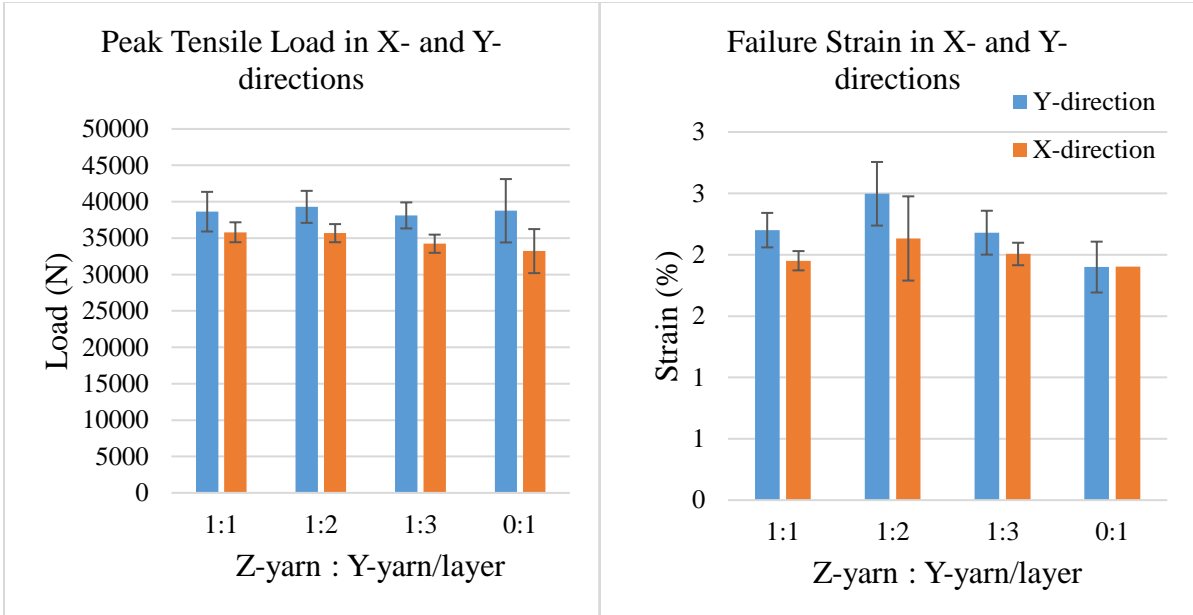
As for the tensile modulus in Figure 126 (c), it didn't significantly change by changing the Z: Y ratio in the Y-direction, yet, performing a post hoc test indicated that specifically the samples with Z: Y ratio 1:1 and 0:1 are significantly different, with 0:1 having higher tensile modulus as shown in Table K.3. Additionally, by looking at the means, one can easily see a slight increasing trend in the tensile modulus by reducing the amount of Z-yarn. However, that wasn't the case in the X-direction, since changing the Z: Y ratio, didn't have any significant effect in that case.

The peak load of all the samples in the Y-direction was consistently higher than that in the X-direction, despite that the samples are made out of balanced preforms, which means that the amount of fibers in the Y-direction is equal to the amount of fibers in the X-direction. This is because the failure strain in the X-direction was always lower, which means that the samples suffered premature failure due to defects, and by looking at Figure 126 (d) which shows a typical tensile load – strain curve for one of the samples in the X- and Y-directions, one can see that both curves behaved similarly except that the samples in the X-direction failed first.

Afterwards, the peak load was normalized by several normalization approaches, in order to segregate the effect of some dependent parameters from the analysis and to have a fair comparison between the samples. Hence, it was normalized by the composite thickness, composite areal density, preform areal density, and total fiber Tex.

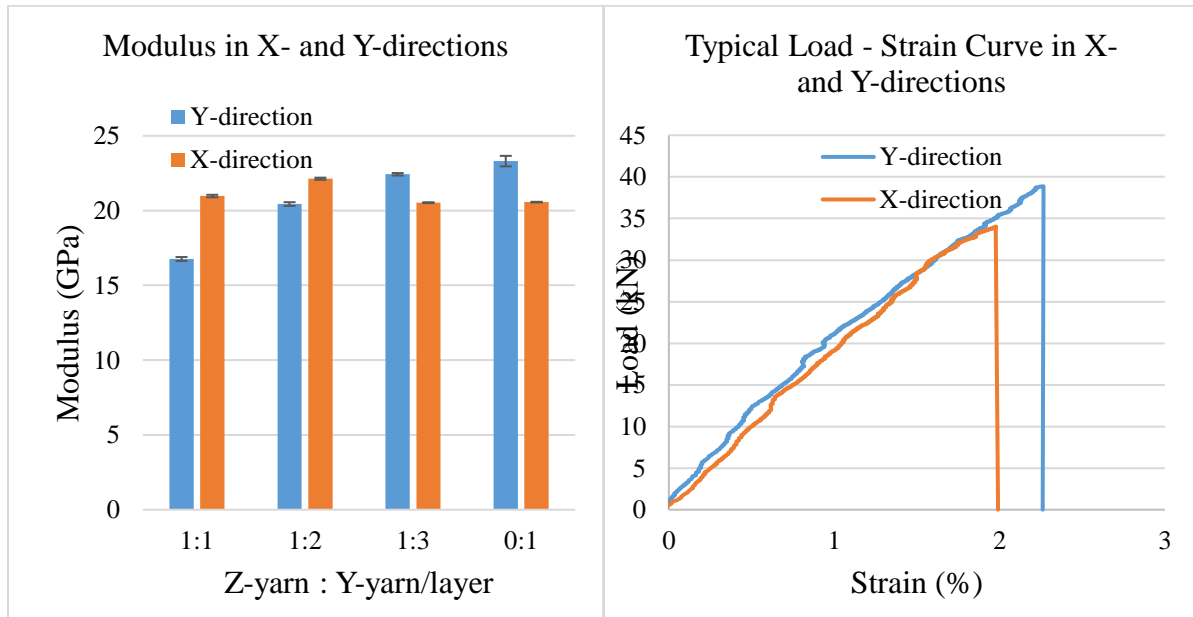
When the peak load was normalized by the composite thickness in Figure 128 (a) the trend didn't change much from the non-normalized case in either direction, the effect of changing the Z: Y ratio was still not statistically significant. Similarly, when the peak load was normalized by the composite areal density, there was no significant difference between the responses of the four samples as illustrated in Figure 128 (b). Further, when the peak load was normalized by the preform areal density and total fiber Tex in both X- and Y-directions, it indicated no significant effect, however by looking at the plots in Figure 128 (c) and 128 (d) respectively, one can see a slight increasing trend in the normalized load by reducing the amount of the Z-yarns in the structure.

From the analysis of the tensile responses of the composite samples due to reducing the amount of Z-yarn in the structure, it can be concluded that changing the Z: Y ratio didn't have any significant effect on the tensile peak load in either direction. Because, the Z-yarn linear density used in this experiment was very small compared to that of the X- and Y-yarns, which didn't have any negative effect on the in-plane tensile properties. On the other hand, reducing the amount of Z-yarn in the structure slightly decreased the failure strain in the Y-direction only, and this can be due to the higher chance of misalignment of the Y-yarns, which would result in local defects that increase the chance of premature failure, and this is seen in the high level of variability in the 0:1 samples, represented by the error bars. Additionally, reducing the Z: Y ratio slightly increased the tensile modulus. Finally, reducing the amount of Z-yarns in the structure didn't have any significant effect on the normalized peak load in either direction, and this indicated that there weren't any significant changes in thickness, areal density, or total fiber Tex.



(a)

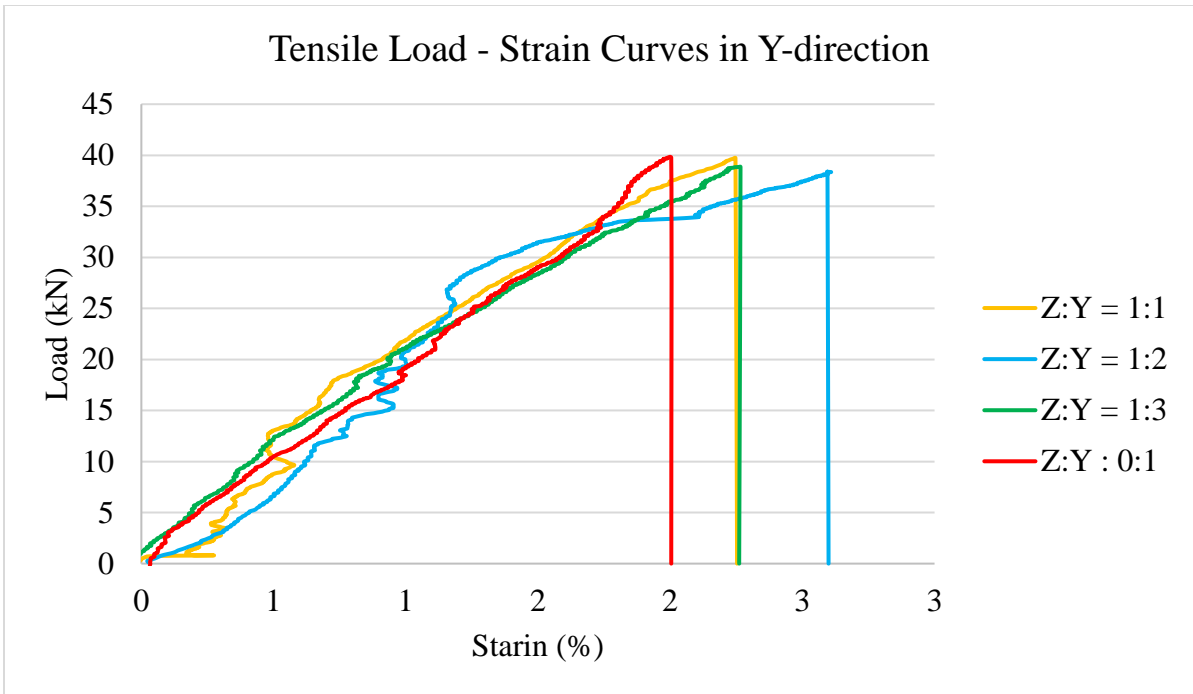
(b)



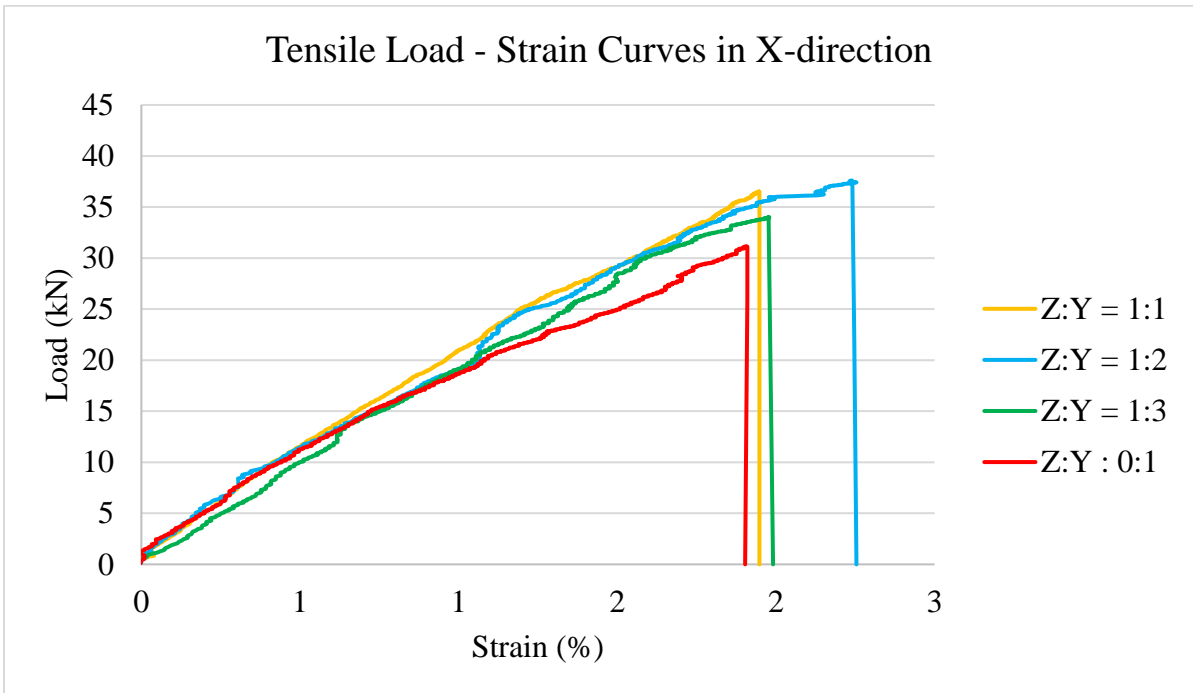
(c)

(d)

Figure 126 Tensile properties in X- and Y-directions, (a) peak load, (b) failure strain, (c) Modulus, and (d) typical load-strain curve

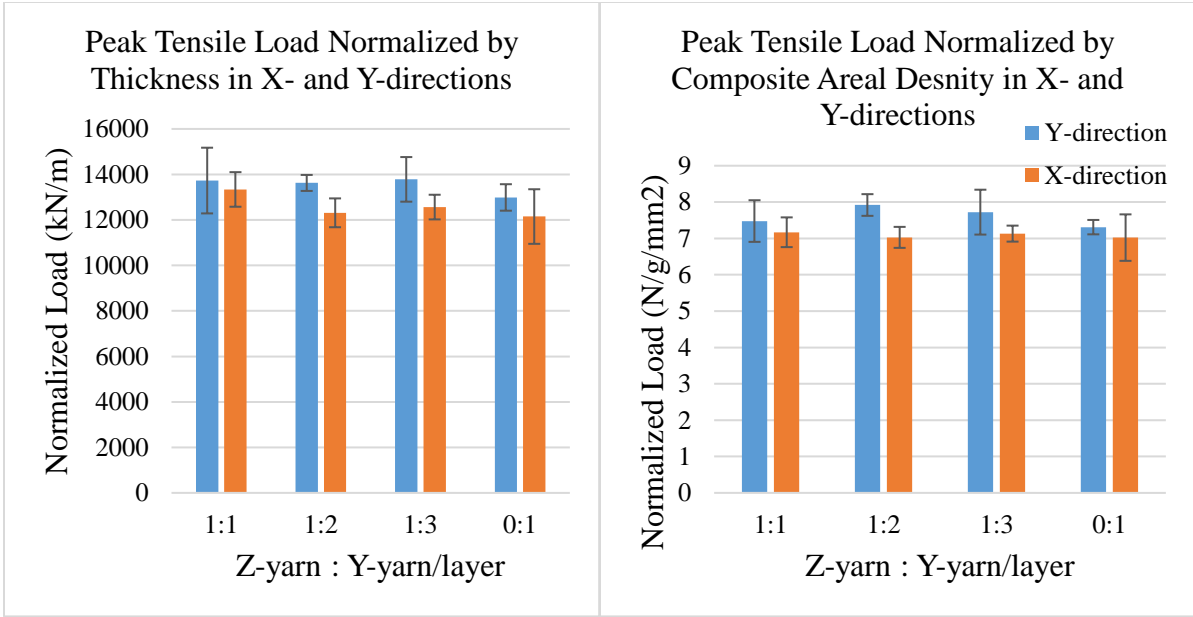


(a)



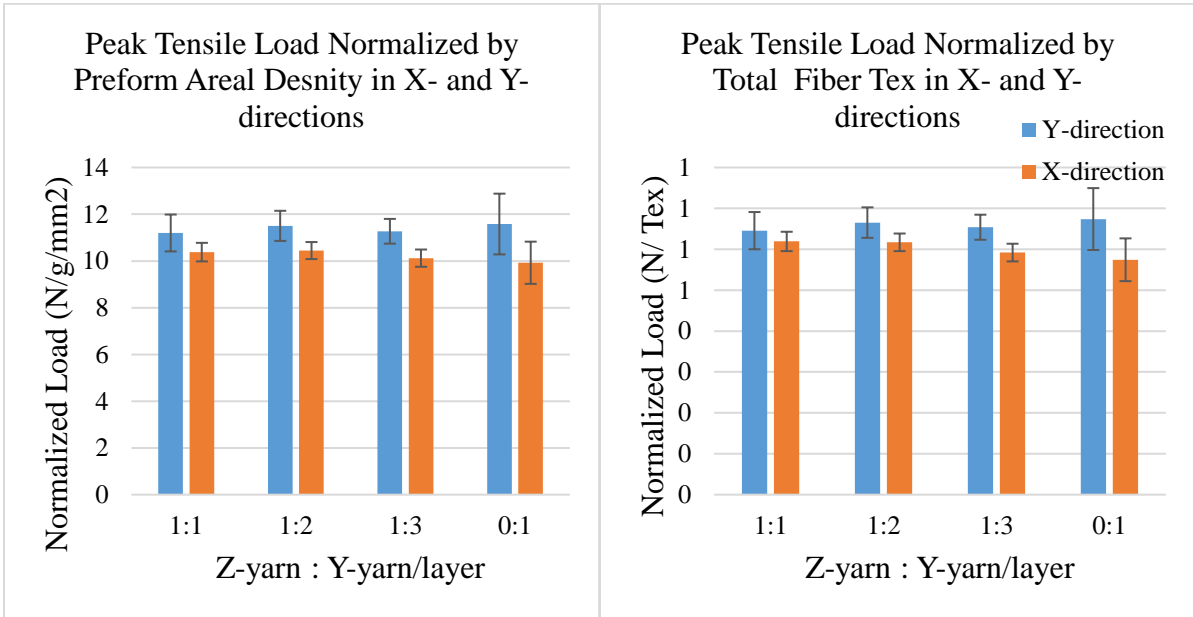
(b)

Figure 127 Typical tensile load – strain curves, (a) Y-direction, and (b) X-direction



(a)

(b)



(c)

(d)

Figure 128 Normalized tensile load in X- and Y-directions, (a) by composite thickness, (b) by composite areal density, (c) by preform areal density, and (d) total fiber Tex

Izod impact

In case of Izod impact testing, the analyzed responses included, total impact energy, and normalized impact energy in both X- and Y-directions. The results of the Izod impact tests in the Y- and X-directions are listed in Table 24 and 25 respectively. The results were analyzed using one-way ANOVA test to reveal the effect of the Z: Y-yarn/ layer ratio on the Izod impact properties of the composites. The results of the one-way ANOVA test were confirmed using a follow up post hoc Duncan test. The statistical analysis results are listed in Appendix M.

Table 24 Izod impact results in Y-axis direction

ID	Thickness (mm)	Comp. Areal Density (g/m ²)	Total Energy (J)	CV (%)	Energy/ Thickness (J/m)	Energy/ Composite Areal Density (kJ/g/mm ²)	Energy/ preform Areal Density (kJ/g/mm ²)	Energy/ Total Tex (J/kTex)
13	2.7	4856	8.16	11.5	3022	1.68	2.37	0.136
28	2.7	5217	8.79	20.1	3255	1.68	2.57	0.149
29	2.55	4863	8.74	26.2	3426	1.80	2.58	0.150
30	2.7	4910	8.12	53.9	3007	1.65	2.43	0.141

Table 25 Izod impact results in X-axis direction

ID	Thickness (mm)	Comp. Areal Density (g/m ²)	Total Energy (J)	CV (%)	Energy/ Thickness (J/m)	Energy/ Composite Areal Density (kJ/g/mm ²)	Energy/ preform Areal Density (kJ/g/mm ²)	Energy/ Total Tex (J/kTex)
13	2.7	4823	9.5	24.6	3528	1.98	2.76	0.165
28	2.8	4966	10.1	26.8	3623	2.04	2.97	0.175
29	2.6	4698	9.0	12.3	3479	1.93	2.67	0.156
30	2.4	4583	9.5	34.0	3953	2.07	2.83	0.164

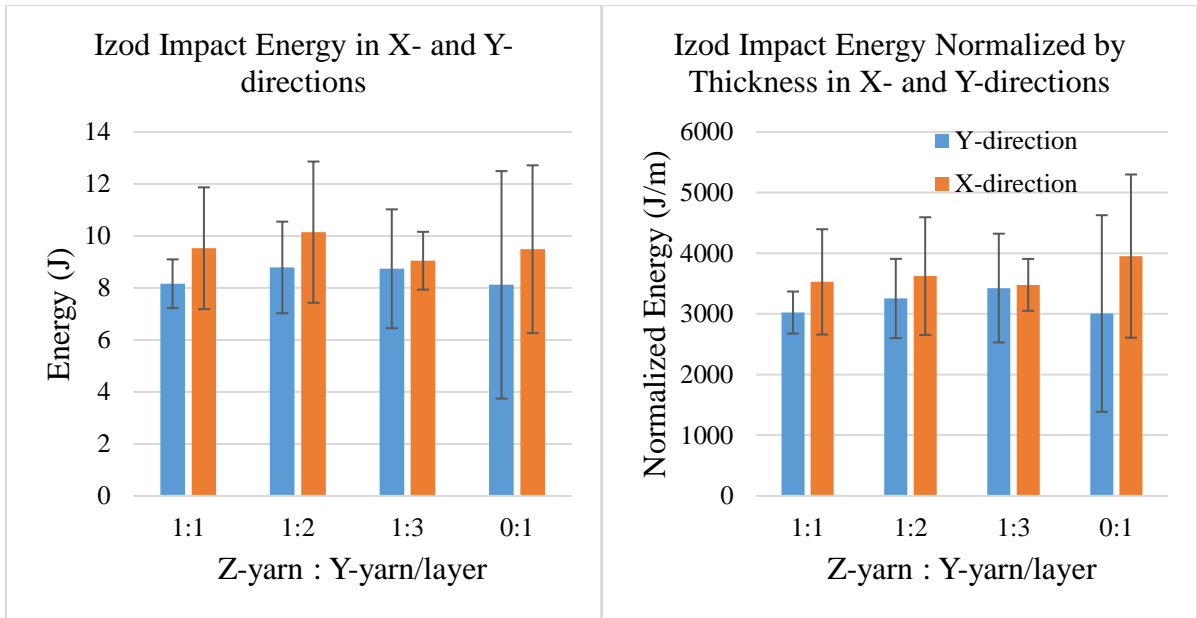
Figure 129 (a) shows the effect of the Z: Y ratio on the Izod impact energy in the X- and Y-directions, the graph indicated that there was no significant difference between the samples, and this was also confirmed by the ANOVA test in Y- and X-directions in Table M.1 and M.16 respectively.

Further, the Izod impact energy was normalized by several normalization approaches, in order to segregate the effect of some dependent parameters from the analysis and to have a fair comparison between the samples. Hence, it was normalized by the composite thickness, composite areal density, preform areal density, and total fiber Tex.

When the Izod impact energy was normalized by the composite thickness in Figure 129 (b) the trend didn't change much from the non-normalized case in either direction, the effect of changing the Z: Y ratio was still not statistically significant. Similarly, when the Izod energy was normalized by the composite areal density, there was no significant difference between the responses of the four samples as illustrated in Figure 129 (c). Additionally, when the Izod energy was normalized by the preform areal density in Figure 129 (d) and total fiber Tex in Figure 129 (e), both X- and Y-directions indicated no significant effect.

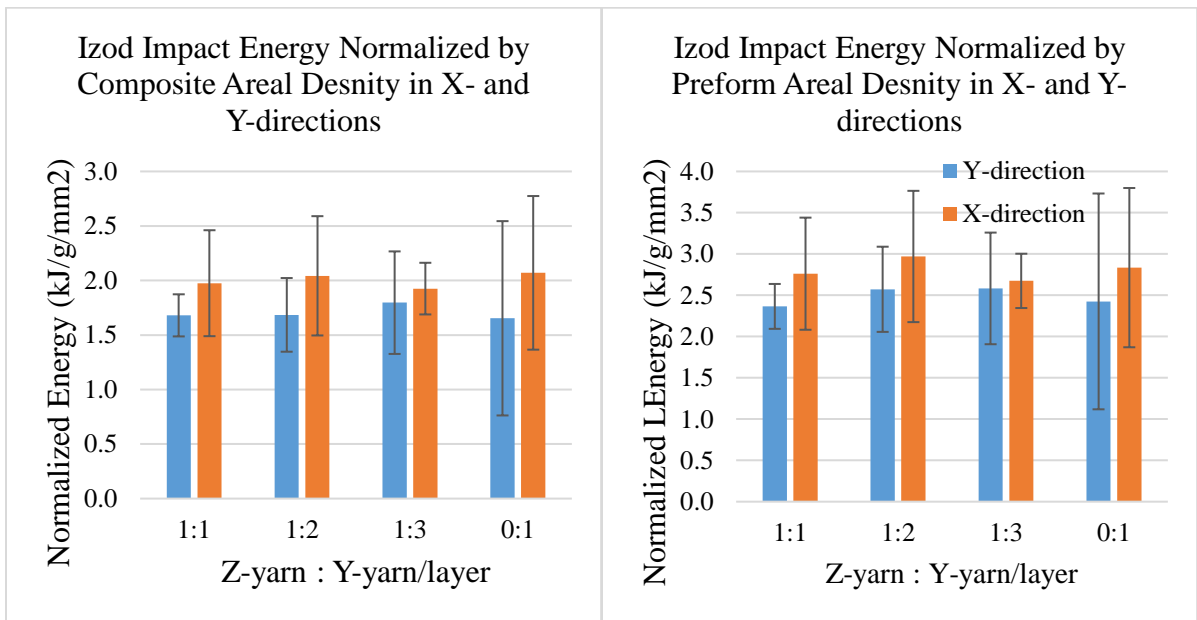
From the analysis of the Izod impact responses of the composite samples due to reducing the amount of the Z-yarns in the structure, it can be concluded that changing the Z: Y ratio didn't have any significant effect on the Izod impact energy in either direction. Because, the Z-yarn linear density used in this experiment was very small compared to that of the X- and Y-yarns, which didn't result in any knock down in the in-plane properties. Similarly, reducing the amount of Z-yarns in the structure didn't have any significant effect on the normalized Izod impact energies in either direction, and this indicated that there weren't any significant changes in thickness, areal density, or total fiber Tex. Finally, from the error bars, one can tell that the variability in the responses of each sample increases as the amount of Z-yarn in the structure is reduced, because the Z-yarn is the only yarn component that interlocks the structure and maintain the alignment, orientation, and spacing of the Y- and X-yarns in the structure.

Figure 129 Izod impact energy in X- and Y-directions, (a) non-normalized, (b) normalized by composite thickness, (c) by composite areal density, (d) by preform areal density, and (e) by total fiber Tex



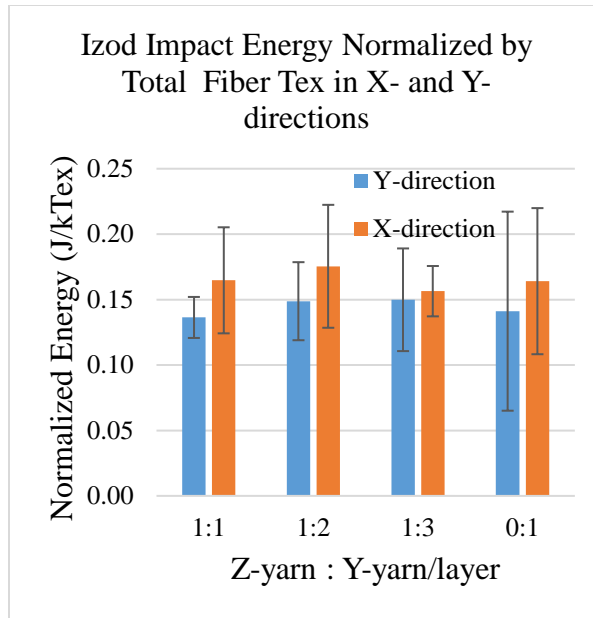
(a)

(b)



(c)

(d)



(e)

Charpy Impact

In case of Charpy impact testing, the analyzed responses included, total impact energy, as well as normalized impact energy in both Y- and X-directions. The results of the Izod impact tests in the Y- and X-directions are listed in Table 26 and 27 respectively. The results were analyzed using one-way ANOVA test to reveal the effect of the Z: Y-yarn/ layer ratio on the Izod impact properties of the composites. The results of the one-way ANOVA test were confirmed using a follow up post hoc Duncan test. The statistical analysis results are listed in Appendix N.

Table 26 Charpy impact results in Y-axis direction

ID	Thickness (mm)	Comp. Areal Density (g/m ²)	Total Energy (J)	CV (%)	Energy/ Thickness (J/m)	Energy/ Comp. Areal Density (kJ/g/mm ²)	Energy/ Preform Areal Density (kJ/g/mm ²)	Energy/ Total Tex (J/kTex)
13	4809	2.70	6.0	12.9	2228	1.25	1.74	0.101
28	5096	2.70	6.4	14.8	2371	1.26	1.87	0.108
29	4793	2.55	5.8	21.4	2289	1.22	1.73	0.100
30	5188	2.70	7.3	22.2	2700	1.41	2.18	0.118

Table 27 Charpy impact results in X-axis direction

ID	Thickness (mm)	Comp. Areal Density (g/m ²)	Total Energy (J)	CV (%)	Energy/ Thickness (J/m)	Energy/ Comp. Areal Density (kJ/g/mm ²)	Energy/ Preform Areal Density (kJ/g/mm ²)	Energy/ Total Tex (J/kTex)
13	4815	2.70	6.8	27.6	2500	1.40	1.96	0.117
28	5069	2.80	7.4	15.3	2643	1.46	2.17	0.128
29	4729	2.60	6.4	16.1	2461	1.35	1.89	0.111
30	4790	2.40	4.5	20.2	1856	0.93	1.33	0.077

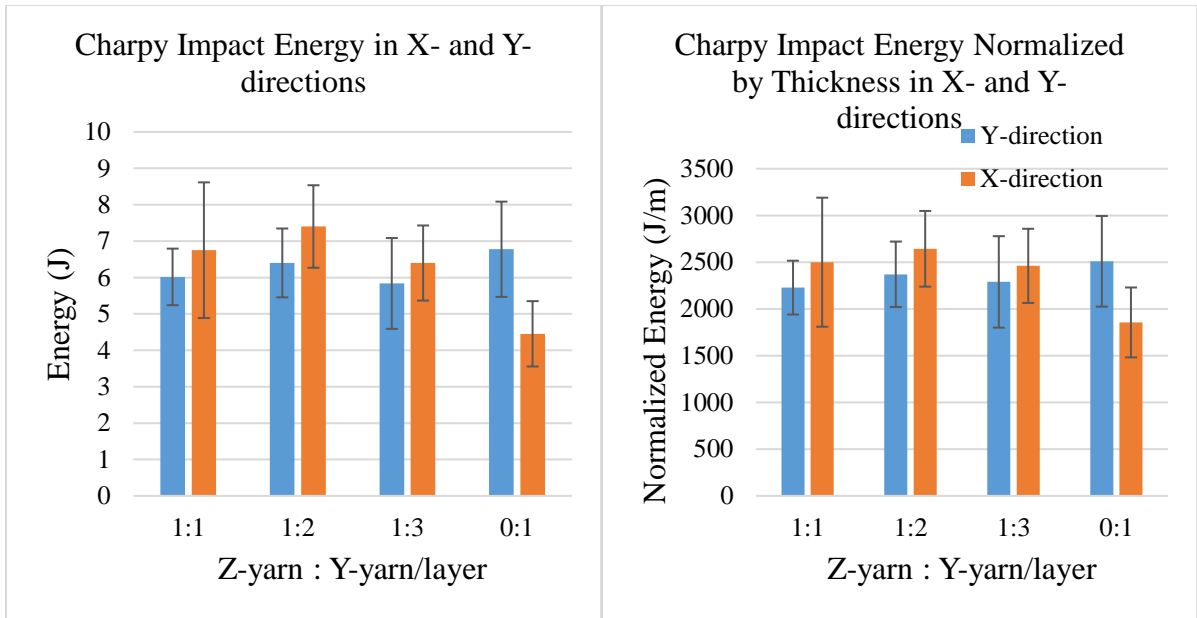
Figure 130 (a) shows the effect of the Z: Y ratio on the Izod impact energy in the X- and Y-directions, the graph indicated that there was no significant difference between the samples in the Y-direction. However, in the X-direction the results were significantly different as shown in Table N.16, and by performing a post hoc test, it indicated that the sample with Z: Y ratio 0:1 is significantly different from the 3 other samples, and that it belongs to a different subset, and it was always lower as shown in Table N.18.

Further, the Charpy impact energy was normalized by several normalization approaches, in order to segregate the effect of some dependent parameters from the analysis and to have a fair comparison between the samples. So, it was normalized by the composite thickness, composite areal density, preform areal density, and total fiber Tex.

When the Charpy impact energy was normalized by the composite thickness in Figure 130 (b) the trend didn't change much from the non-normalized case in either direction, the effect of changing the Z: Y ratio was still not statistically significant in the Y-direction, while it was statistically significant in the X-direction. Similarly, when the Izod energy was normalized by the composite areal density, there was no significant difference between the responses of the four samples in the Y-direction as illustrated in Figure 130 (c), while being significantly different in the X-direction, with a slight decreasing trend. Additionally, when the Izod energy was normalized by the preform areal density in Figure 130 (d) and total fiber Tex in Figure 130 (e), they also showed no significant effect in the Y-direction, and a slight significance in the X-direction, with a decreasing trend.

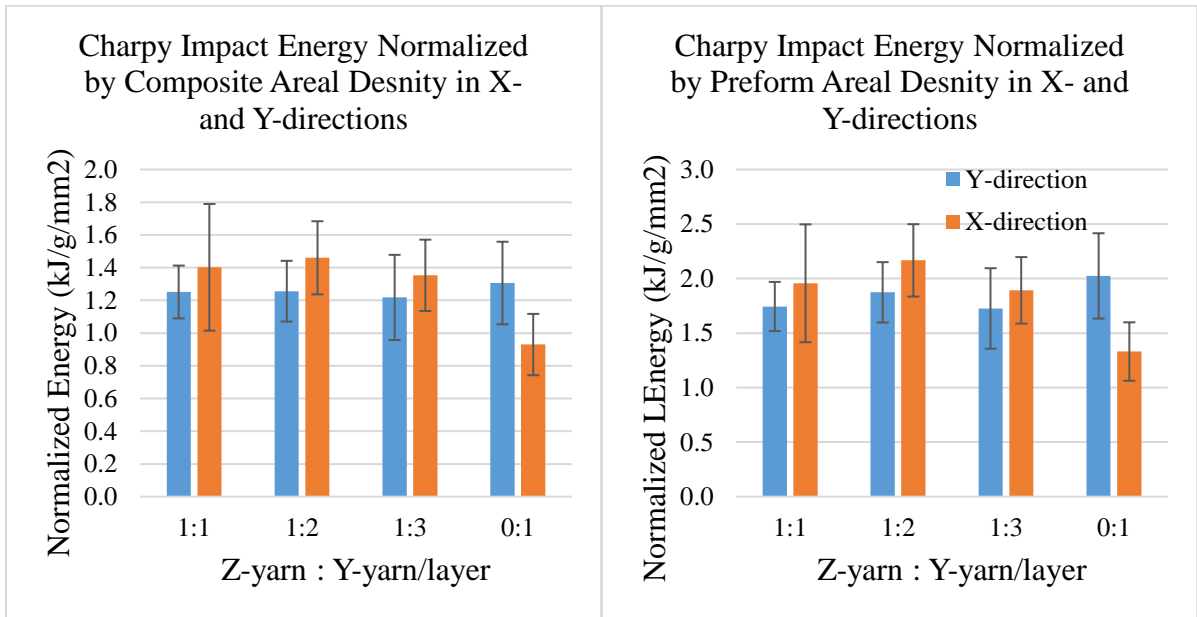
From the analysis of the Charpy impact responses of the composite samples, it can be concluded that changing the Z: Y ratio didn't have any significant effect on the Charpy impact energy in the Y-direction, while there was a significant effect in the X-direction, with the sample having Z: Y ratio 0:1 having the lowest energy. This response was similar to the Tup impact response, and this is because there is an intermediate correlation between the responses of the Tup impact and the Charpy in the X-direction for balanced samples as previously mentioned in section 6.2.1. Similarly, reducing the amount of Z-yarns in the structure didn't have any significant effect on the normalized Charpy impact energies in the Y-direction, while it was significant in the X-direction, and this indicated that there weren't any significant changes in thickness, areal density, or total fiber Tex.

Figure 130 Charpy impact energy in X- and Y-directions, (a) non-normalized, (b) normalized by composite thickness, (c) by composite areal density, (d) by preform areal density, and (e) by total fiber Tex



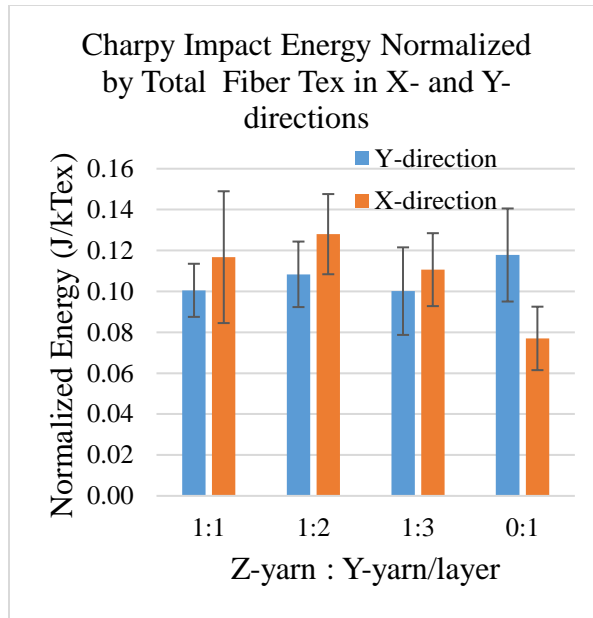
(a)

(b)



(c)

(d)



(e)

6.2.2. Failure analysis

In this section a visual failure analysis was performed on the test specimens for the Tup impact, Tensile, Izod impact and Charpy impact. Typical specimens were selected for the analysis to represent the samples with the Z: Y-yarn/ layer ratio of 1:1, 1:2, 1:3, and 0:1. Each picture was identified by these ratios to indicate the amount of Z-yarns in the structure.

Tup impact

From the previous analysis on the effect of Z: Y-yarn/ layer ratio on mechanical properties, it indicated that the Z: Y ratio had a significant effect on the total Tup penetration energy. Further, it indicated that total energy was systematically reduced by reducing the amount of Z-yarn in the structure, yet the most significant drop in the total energy was observed in the specimen with the Z: Y ratio 0:1. However, only by looking at the failure mechanism of each sample, one can see the full picture.

In Figure 124 (b) the typical load-deflection curves of the four samples were plotted, the chart shows that the sample with Z: Y ratio 1:1 had 2 peaks, which indicated that this sample experienced minor delamination, and that the fiber failure was dominant. The number of peaks kept increasing by systematically reducing the amount of Z-yarns in the structure, which indicated that the delamination was becoming more dominant. Until it reached a point in the sample with Z: Y ratio 0:1 where the top of the curve became flattened with a series of successive small peaks, which indicated that this particular structure had undergone progressive delamination which dominated the failure of the sample, with minor fiber breakage. Appendix O includes the load-deflection curves of all individual specimens, the curves are shown in Figure O.1 and Figure O.2.

Further, by looking at the three views of the test specimens after being subjected to a Tup impact in Figure 131, the failure behavior indicated by the load – deflection curves were confirmed. One can see in the sample with Z: Y ratio 1:1, negligible delamination, while the fiber breakage dominated the failure. Whereas, in the sample with Z: Y ratio 1:2 more delamination occurred, but still the fiber breakage is dominant. As for the sample with Z: Y ratio 1:3 the failure had an equal share of delamination and fiber breakage. On the other hand,

when all the Z-yarns were removed in the sample with Z: Y ratio 0:1, the failure was dominated by a series of successive delamination, with minor fiber breakage.

Moreover, a simple image analysis was performed to quantify the effect of the Z: Y-yarn/ layer ratio on the Tup impact delamination area. The delamination area of all specimens from all samples were traced and measured using ImageJ software for image analysis and processing. Figure 132 shows the difference in the average delamination area for all samples, which also indicated that, as the amount of Z-yarn in the structure was systematically reduced, the delamination energy significantly increased. The individual specimens' images used for the analysis are shown in Appendix P.

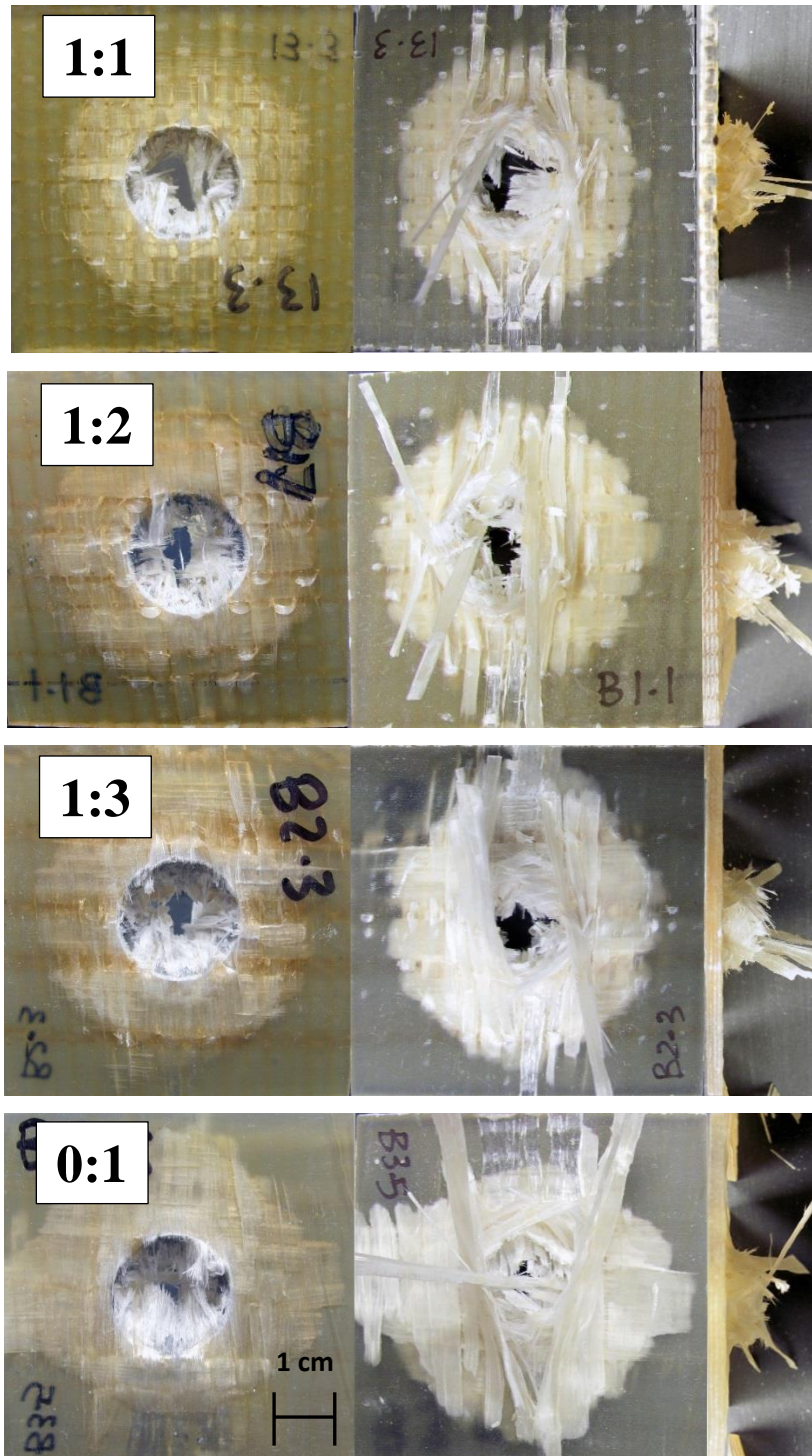


Figure 131 Failure analysis of typical Tup impact specimens, showing 3 different views

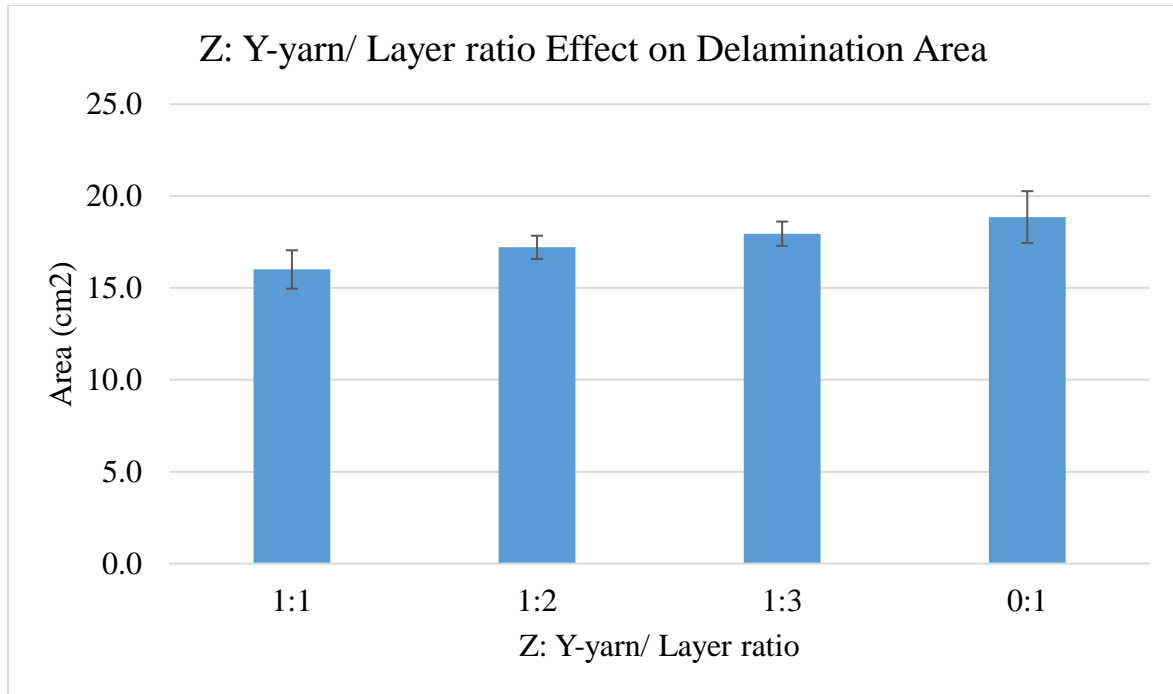


Figure 132 Effect of Z: Y-yarn/ layer ration on delamination area

From the previous analysis, it can be concluded that the Z-yarn not only had a significant effect on the out-of-plane properties represented by the Tup impact energy, but also it significantly affected the failure mechanism, from a fully interlaced sample with a fiber breakage dominant failure, to the non-interlaced sample with delamination dominant failure.

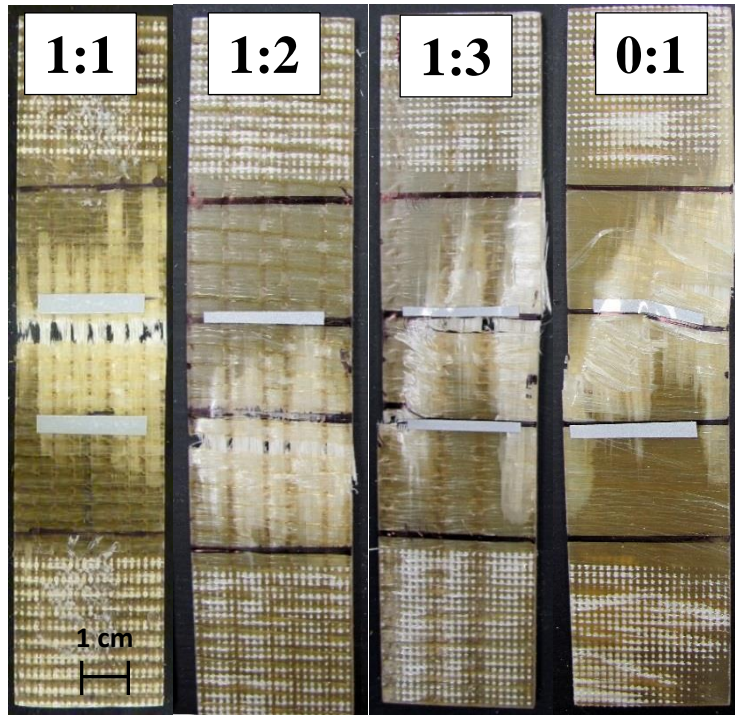
Tensile

The previous analysis on the effect of Z: Y-yarn/ layer ratio on the mechanical properties, indicated that the Z: Y ratio had no significant effect on the tensile peak load in both X- and Y-directions. While it had a slight significant effect on the tensile modulus, and failure strain, the most significant difference in the tensile modulus, and failure strain was observed in the specimen with the Z: Y ratio 0:1. However, only by looking at the failure mechanism of each sample, one can see the full picture.

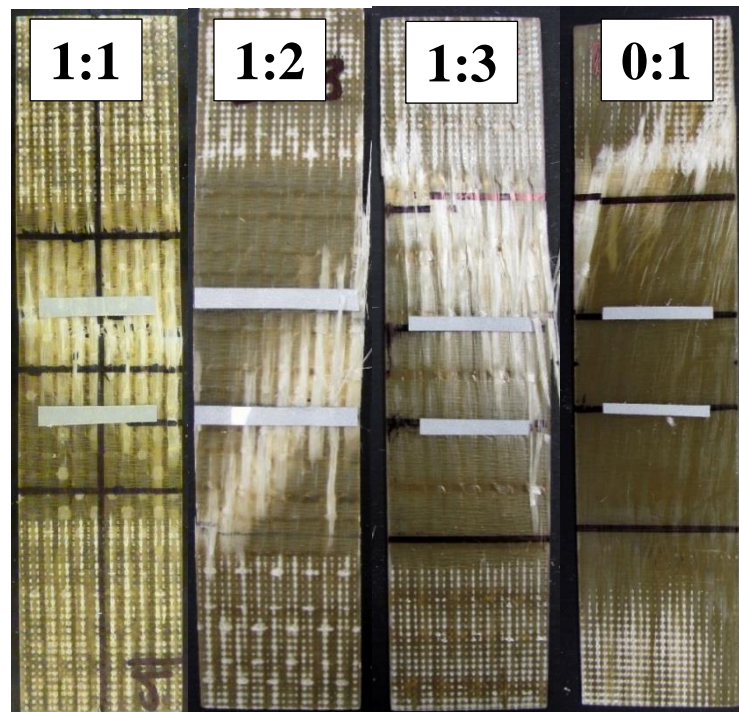
Thus, by looking at the test specimens after being subjected to a tensile loading in the Y-direction in Figure 133 (a), one can see in the sample with Z: Y ratio 1:1, no delamination, and the fiber breakage dominated the failure. Moreover, there was no fiber pull-out observed,

which indicated that the interfacial adhesion between the fiber and the matrix was good. Whereas, in the sample with Z: Y ratio 1:2 minor delamination occurred, but still the fiber breakage is dominant. As for the sample with Z: Y ratio 1:3 the failure had an equal share of delamination and fiber breakage. On the other hand, when all the Z-yarns were removed in the sample with Z: Y ratio 0:1, the failure was dominated by a series of successive delamination, with minor fiber breakage. This explains why in this particular sample the failure strain was lower.

On the other hand, by looking at the tensile test specimens in the X-direction after failure in Figure 133 (b), one can see in the sample with Z: Y ratio 1:1, no delamination occurred, and the fiber breakage dominated the failure. Whereas, in the sample with Z: Y ratio 1:2 minor delamination occurred, in addition to a diagonal crack propagation across the stress concentration points. As for the sample with Z: Y ratio 1:3 the failure was a combination of a more significant delamination and a diagonal crack propagation. On the other hand, when all the Z-yarns were removed in the sample with Z: Y ratio 0:1, the specimen consistently failed at the grips. This diagonal crack propagation explains, why the sample with the Z: Y ratio 0:1 had a significantly lower failure strain.



(a)



(b)

Figure 133 Failure analysis of typical tensile specimens in, (a) Y-direction, and (b) X-direction

From the previous analysis, it can be concluded that the Z-yarn had a significant effect on the failure mechanism. The fully interlaced structure had a fiber breakage dominated failure, and delamination started to be more dominant as the Z-yarn amount in the structure was reduced in the Y-direction. Whereas, in the X-direction the Z-yarn presence not only minimized the delamination, but also minimized the diagonal crack propagation, that initiated from the misalignment of the X-yarns as the Z-yarn amount in the structure was reduced. Thus, the Z-yarn also had an important role, which was interlocking the other yarn components in place and maintaining their orientation and proper alignment.

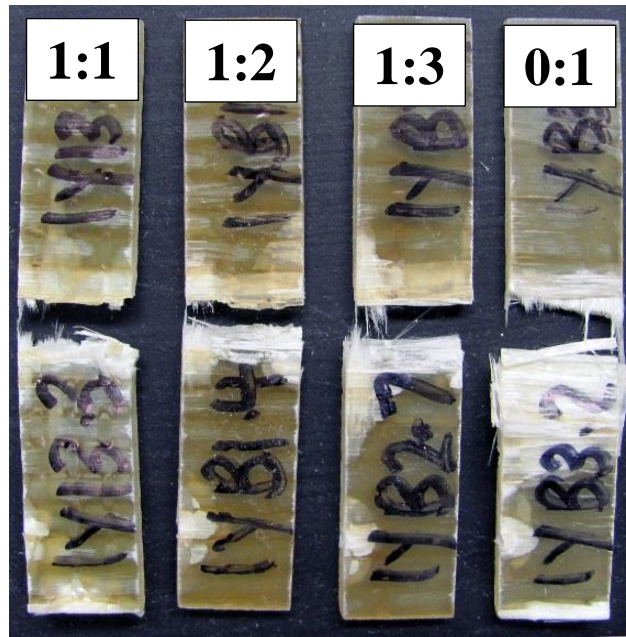
Izod impact

The previous analysis on the effect of Z: Y-yarn/ layer ratio on the Izod impact energy, indicated that the Z: Y ratio had no significant effect on the Izod impact energy in both X- and Y-directions. Yet, a further look at the failure mechanism revealed more details.

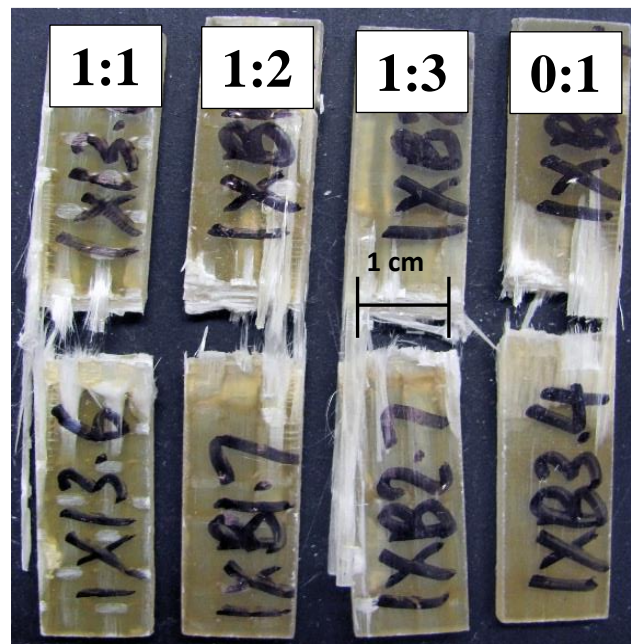
Due to the nature of the Izod impact test, the fibers have to be fully broken, thus the fiber breakage will always dominate the failure. By looking at the test specimens after being subjected to an Izod impact in the Y-direction in Figure 134 (a), one can see in the sample with Z: Y ratio 1:1, no delamination, and the fiber breakage dominated the failure. Whereas, in the sample with Z: Y ratio 1:2 some delamination occurred, and still the fiber breakage is dominant. As for the sample with Z: Y ratio 1:3 the fiber breakage was dominant, in addition to a significant amount of delamination. On the other hand, when all the Z-yarns were removed in the sample with Z: Y ratio 0:1, the amount of delamination further increased.

On the other hand, when looking at the test specimens after being subjected to an Izod impact in the X-direction in Figure 134 (b), a very similar behavior was observed, in addition to some fiber pull-out. The fiber pull-out was observed at the edges of the specimen, which might be due to some defects induced during the waterjet cutting of the specimens.

From the previous analysis, it can be concluded that the Z-yarn had a significant effect on the failure mechanism. The fully interlaced structure had a fiber breakage dominated failure, which continued to be dominant as the Z-yarn amount in the structure was reduced in the X- and Y-directions, yet this was accompanied by an increasing delamination. Moreover, a slight fiber pull-out from the specimens' edge were observed, due to waterjet cutting induced defects.



(a)



(b)

Figure 134 Failure analysis of typical Izod impact specimens in, (a) Y-direction, and (b) X-direction

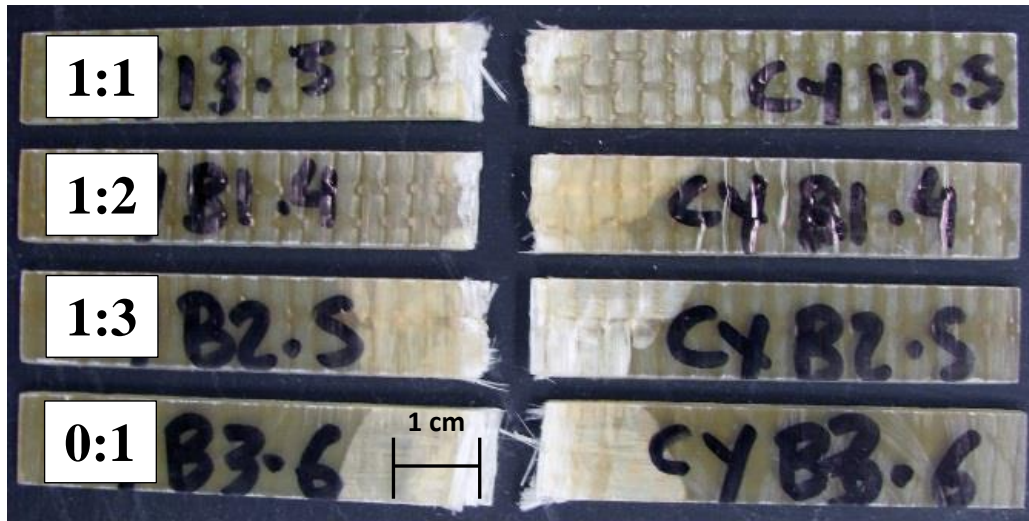
Charpy

The previous analysis on the effect of Z: Y-yarn/ layer ratio on the Charpy impact energy, indicated that it had no significant effect in both X- and Y-directions. Yet, a further look at the failure mechanism of each sample, revealed more details.

Due to the nature of the Charpy impact test, the fibers have to be fully broken, thus the fiber breakage will always dominate the failure. By looking at the test specimens after being subjected to a Charpy impact in the Y-direction in Figure 135 (a), one can see in the sample with Z: Y ratio 1:1, no delamination, and the fiber breakage dominated the failure. Whereas, in the sample with Z: Y ratio 1:2 some delamination occurred, and still the fiber breakage is dominant. As for the sample with Z: Y ratio 1:3 the fiber breakage was dominant, in addition to a significant amount of delamination. On the other hand, when all the Z-yarns were removed in the sample with Z: Y ratio 0:1, the amount of delamination further increased.

On the other hand, when looking at the test specimens after being subjected to an Izod impact in the X-direction in Figure 135 (b), a very similar behavior was observed.

From the previous analysis, it can be concluded that the Z-yarn had a significant effect on the failure mechanism. The fully interlaced structure had a fiber breakage dominated failure, which continued to be dominant as the Z-yarn amount in the structure was reduced in the X- and Y-directions, yet this was accompanied by an increasing delamination.



(a)



(b)

Figure 135 Failure analysis of typical Charpy impact specimens in, (a) Y-direction, and (b) X-direction

6.2.3. Conclusion on Experiment B

From the Tup impact analysis, it was concluded that the Z: Y ratio didn't have any significant effect on the peak impact force. However, it had a significant effect on the total impact energy, specifically the sample with no Z-yarn interlacement, had a significantly lower energy than the

three other samples. After, normalizing the total impact energy by the composite thickness, and composite areal density there was no significant difference between the samples, yet, after normalizing by preform areal density the trend from the non-normalized case was confirmed. This indicated that even a very small amount of Z-yarn in the structure would result in a composite with higher out-of-plane properties. Further, by looking at the failure mechanism of each sample, it was concluded that the amount of Z-yarn significantly affected the failure mechanism, and as the amount of the Z-yarn in the structure was reduced, the failure became more dominated by delamination, rather than fiber breakage.

Moreover, from the analysis of the tensile results, it was concluded that the Z: Y ratio didn't have any significant effect on the peak load, and the normalized load in both the X- and Y-directions. However, it had a slight effect on the failure strain and tensile modulus, since, the sample with Z: Y ratio 0:1 had slightly lower strain, and higher modulus than the three other samples. This indicated that using a Z-yarn with low linear density in the structure wouldn't have any significant effect on the in-plane properties represented by the tensile properties. Yet, the failure mechanism indicated that the amount of Z-yarn significantly affected the failure mechanism, and delamination became more dominant, and damage tolerance was reduced as the amount of Z-yarn in the structure was reduced. Moreover, the Z-yarn played an important role of maintaining the orientation, alignment and spacing of the X- and Y-yarns.

As for the Izod impact results, it indicated that changing the Z: Y ratio in the structure didn't have any significant effect on the impact energy, and the normalized energy, in both X- and Y-directions. It also indicated that there was no significant change in the composite thickness, or areal density by reducing the amount of Z-yarn in the structure. However, the failure analysis of each sample indicated that the amount of Z-yarn significantly affected the failure mechanism, and despite that the fiber breakage dominated the failure of all samples, yet the samples with lower amount of Z-Yarn in the structure, experienced more delamination.

Similarly, the Charpy impact results indicated that changing the Z: Y ratio in the structure didn't have any significant effect on the impact energy, and the normalized energy, in the Y-direction. However, it was significant in the X-direction, with the sample having Z: Y ratio 0:1 having the lowest energy. Moreover, the failure analysis of each sample indicated that the amount of Z-yarn significantly affected the failure mechanism, and despite that the fiber

breakage dominated the failure of all samples, yet the samples with lower amount of Z-Yarn in the structure, experienced more delamination.

7. OVERALL CONCLUSION AND SUGGESTION FOR FUTURE STUDIES

A generalized model to predict the load-extension properties of the 3DOW preforms and composites made of spun or filament yarns, using the finite deformation approach was developed. The model relies on the geometry of the structure, and the tensile properties of the constituent yarn and resin components as input parameters, and the output of the model is the entire load-extension diagram of the composite, including the nonlinear region. The model is generalized to predict the load-extension properties of any non-jammed and jammed 3DOW composite, that have any weave architecture, including hybrid composites.

The model was verified experimentally for a broad range of experimental composites, including hybrid ones. The results show that there is a general good agreement between the experimental and theoretical curves. The theoretical curves generated using the fiber properties had better agreement with the experimental curves, than the ones generated using the yarn properties, due to the weak link effect. One of the significant deviations of the theoretical curves from the experimental ones, was the premature failure, or failure of the composite at a strain level lower than the theoretical. This premature failure was due to the limitations of the strain measurement method, which was discussed in details. Additionally, this theoretical model doesn't account for defects, thus any manufacturing induced defects, such as weaving, VARTM, and material defects, would result in a premature failure of the composite at lower strain.

A full numerical parametric study was performed to reveal the architecture potential of 3DOW preforms, and show how to optimize the in-plane tensile properties of the composite. The study included the effect of changing the Z-yarn linear density, weave factor, pick density and the number of layers on the peak load of the composite, as well as the Z stretch ratios. It was found that increasing the Z-yarn linear density slightly increase the peak load of the composite in the Y-axis direction, whereas increasing the weave factor slightly reduces it. However, the peak load in the X-axis direction wasn't affected by changing neither the Z-yarn linear density nor the weave factor. It was also observed that increasing the Y-yarn number of layers increased the peak load in both X- and Y-axis directions. Whilst, increasing the X-yarn pick density only increased the peak load in the X-axis direction. Finally, increasing the Z-yarn weave factor

increased the strain on the Z-yarn, whilst, increasing the Y-yarn number of layers and X-yarn pick density reduced the strain.

This model is helpful in investigating the potential of using 3DOW preforms in applications other than composites. Since, 3DOW preforms have some attractive features for technical textiles and sports apparel. One of these features are the high drapability and low bending rigidity, due to the very low inter-fiber friction which is an inherent feature of such structure.

A range of 3DOW composites were developed to study their response under different impact modes. In the Tup impact test, it was concluded that increasing the Y-yarn number of layers and X-yarn density significantly increased the impact energy, yet increasing the pick density was generally not as significant as increasing the number of layers, while changing the Z-yarn interlacing pattern had a slight significant effect on the total energy, with the twill being the highest, followed by basket, and then plain. Further, after normalizing the total penetration energy, the effects of the structural parameters became less significant. However, the existence of a residual increasing trend by increasing the number of layers as well as increasing the pick density, and changing the weave pattern, indicated that those three parameters have a significant effect on the composite impact energy irrespective of composite thickness, composite weight, or preform weight.

As for the Izod impact energy, it was concluded that increasing the number of layers increased the total energy in both directions. However, increasing the pick density surprisingly, resulted in a slight decrease in the total energy in the Y-direction, and no effect in the X-direction. Additionally, changing the Z-yarn weave pattern didn't have any effect on the total energy in both directions. Further, after normalization, it was found that increasing the number of layers resulted in a slight increase in the normalized energy in both directions, while increasing the pick density resulted in a more pronounced decrease in the total energy in the Y-direction, and didn't have any effect in the X-direction, and still the weave pattern had no significant effect in either direction. The energy in the X-direction was always higher than the Y- direction, even after normalization.

In the case of Charpy impact energy, it was concluded that increasing the number of layers increased the total energy in both directions, and changing the weave pattern surprisingly had a significant effect as well. Yet, increasing the pick density, was the only significant factor in

the X-direction. Further, after normalization the significance of the number of layers, and weave pattern effects were reduced. Moreover, the results in the X-axis direction were generally higher than that of the Y-axis direction, and they remained significant even after the normalization. However, this effect wasn't as significant as in the case of the Izod impact.

By comparing the main effect of the three impact tests, the Tup results had significantly higher impact energy than both, the Charpy and Izod, and the Charpy impact results were always lower than the Izod results, and this trend remained the same even after normalization.

Additionally, when testing the overall correlation between the three impact energies, it was concluded that, there was a strong correlation between the results of all three impact modes. However, after normalizing by any of the three normalization approaches, the correlations were significantly reduced. The analysis after normalization became more accurate and realistic, it indicated that there was a weak correlation between the Tup and Charpy impact results, very weak correlation between Charpy and Izod results, and no correlation between Izod and Tup results.

Moreover, by looking at the correlation between the normalized results of the plain weave samples, the normalized analysis indicated that there was an intermediate negative correlation between the Tup and Izod impact results in Y-axis direction, weak or no correlation between Charpy and Tup results, and weak correlation between Izod and Tup results. As for the twill samples, there was an intermediate direct correlation between the Tup and Charpy impact results in both Y- and X-axis directions, weak or no correlation between Izod and Tup results, and weak correlation between Izod and Charpy results. While, in case of basket samples there was an intermediate to strong direct correlation between the Tup and Charpy impact results, weak or no correlation between Izod and Tup results, and weak to intermediate correlation between Izod and Charpy results. Finally, in case of balanced samples there was still a direct intermediate correlation between the Charpy and Tup results in the X-axis direction.

Another range of 3DOW samples were developed to study the effect of changing the Z: Y-yarn/ layer ratio in the structure. From the Tup impact analysis, it was concluded that the Z: Y ratio didn't have any significant effect on the peak impact force. However, it had a significant effect on the total impact energy, specifically the sample with no Z-yarn interlacement, had a significantly lower energy than the three other samples. After, normalizing the total impact

energy by the composite thickness, and composite areal density there was no significant difference between the samples, yet, after normalizing by preform areal density the trend from the non-normalized case was confirmed. This indicated that even a very small amount of Z-yarn in the structure would result in a composite with higher out-of-plane properties. Further, by looking at the failure mechanism of each sample, it was concluded that the amount of Z-yarn significantly affected the failure mechanism, and as the amount of the Z-yarn in the structure was reduced, the failure became more dominated by delamination, rather than fiber breakage.

Moreover, from the analysis of the tensile results, it was concluded that the Z: Y ratio didn't have any significant effect on the peak load, and the normalized load in both the X- and Y-directions. However, it had a slight effect on the failure strain and tensile modulus, since, the sample with Z: Y ratio 0:1 had slightly lower strain, and higher modulus than the three other samples. This indicated that using a Z-yarn with low linear density in the structure wouldn't have any significant effect on the in-plane properties represented by the tensile properties. Yet, the failure mechanism indicated that the amount of Z-yarn significantly affected the failure mechanism, and delamination became more dominant, and damage tolerance was reduced as the amount of Z-yarn in the structure was reduced. Moreover, the Z-yarn played an important role of maintaining the orientation, alignment and spacing of the X- and Y-yarns.

As for the Izod impact results, it indicated that changing the Z: Y ratio in the structure didn't have any significant effect on the impact energy, and the normalized energy, in both X- and Y-directions. It also indicated that there was no significant change in the composite thickness, or areal density by reducing the amount of Z-yarn in the structure. However, the failure analysis of each sample indicated that the amount of Z-yarn significantly affected the failure mechanism, and despite that the fiber breakage dominated the failure of all samples, yet the samples with lower amount of Z-Yarn in the structure, experienced more delamination.

Similarly, the Charpy impact results indicated that changing the Z: Y ratio in the structure didn't have any significant effect on the impact energy, and the normalized energy, in the Y-direction. However, it was significant in the X-direction, with the sample having Z: Y ratio 0:1 having the lowest energy. Moreover, the failure analysis of each sample indicated that the amount of Z-yarn significantly affected the failure mechanism, and despite that the fiber

breakage dominated the failure of all samples, yet the samples with lower amount of Z-Yarn in the structure, experienced more delamination.

For future studies, the developed generalized model will be experimentally verified for spun yarns with circular cross sections, using Hemp and Flax. 3DOW Hemp composites are currently under development, and the Flax composites will be developed in the near future at the composite core facility, College of Textiles, NC State University. This will be a simple and helpful model for researchers working with green composites.

Moreover, for the purpose of studying the effect of the amount of Z-yarn on the in- and out-of-plane properties of 3DOW composites, it would be a good addition to expand on the existing work, and include samples with different Z-yarn linear density, and number of Y-yarn layers. This will help in understanding the effect of the Z: Y ratio in the light of the Z-yarn size, and number of layers.

REFERENCES

- [1] Callister W. D., "Material Science and Engineering an Introduction," New York: John Wiley & Sons, Inc., 2007.
- [2] Campbell F. C., "Manufacturing Processes for Advanced Composites," Oxford, UK: Elsevier, 2004.
- [3] Strong A. B., "Fundamentals of Composites Manufacturing, Dearborn," Michigan: SME, 2008.
- [4] Wambua P.M. and Anandjiwala R., "A Review of Preforms for the Composites Industry," *Journal of Industrial Textiles*, vol. 40, no. 4, pp. 310-333, 2011.
- [5] Dow M.B. and Dexter H. B., "Development of Stitched, Braided and Woven Composite Structures in the ACT Program and at Langley Research Center (1985 to 1997)," NASA, Hampton, Virginia, 1997.
- [6] Cox B.N. and Flanagan G., "Handbook of Analytical Methods for Textile Composites," NASA, Hampton, Virginia, 1997.
- [7] Hearle J.S. and Du G.W., "Forming Rigid Fibre Assemblies: The Interaction of Textile Technology and Composites Engineering," *Journal of Textile Institute*, vol. 81, no. 4, pp. 360-383, 1990.
- [8] Hearle J.S., Thwaites J.J. and Amirbayat J., "Mechanics of Flexible Fiber Assemblies," (NATO Advanced Study Institute Series: E, Applied Sciences No. 38), Alpen aan den Rijn, The Netherlands, Sijthoff and Noordhoff, 1980.
- [9] Grosberg P. and Kedia S., "The Mechanical Properties of Woven Fabrics Part I: The Initial Load-Extension Modulus of Woven Fabrics," *Textile Research Journal*, 38, 1966.
- [10] Hu J. L. and Newton A., "Modelling of tensile stress-strain curves of woven fabrics," *Journal of China Textile University*, 10(4), 1993.
- [11] Schwartz P., "Structure and Mechanics of Textile Fibre Assemblies", Woodhead publishing Ltd., 2008.

- [12] Campbell F. C., "Manufacturing Processes for Advanced Composites," Oxford, UK: Elsevier, 2004.
- [13] Khokar N., "3D Fabric-Forming Processes: Distinguishing Between 2D-Weaving, 3Dweaving and an Unspecified Non-Interlacing Process," Journal of The Textile Institute, Vol. 87, No. 1, Pp. 97-106, 1996.
- [14] Khokar N., "3D-Weaving: Theory and Practice," Journal of The Textile Institute, Vol. 92, No. 2, Pp. 193-207, 2001.
- [15] Khokar N., "Noobing: A Nonwoven 3D Fabric-Forming Process Explained," Journal of The Textile Institute, Vol. 93, No. 1, Pp. 52-74, 2002.
- [16] Stig F., "An Introduction to The Mechanics of 3D-Woven Fibre Reinforced Composites," Stockholm, Sweden: KTH School of Engineering Sciences, 2009.
- [17] Mohamed M. H. And Zhang Z.H., "Method of Forming Variable Cross-Sectional Shaped Three-Dimensional Fabrics". US Patent 5085252, 4th February 1992.
- [18] Newton A. And Hu J., "The Geometry of Cloth Structure," Proc Inaugural Conference of the Chinese Students and Scholars Textile Association in UK, Manchester 23, 1992.
- [19] Peirce F.T., "5—The Geometry of Cloth Structure," Journal of The Textile Institute Transactions; 28(3): T45-96, March 1937.
- [20] Seyam A.M., El-Shiekh A., "Mechanics of Woven Fabrics: Part III: Critical Review of Weavability Limit Studies," Textile Research Journal; 63(7):371-8, July 1993.
- [21] Kemp A., "An Extension of Peirce's Cloth Geometry to The Treatment of Nonlinear Threads," Journal of Textile Institute, 49, 1958.
- [22] Hearle J. W. S. And Shanahan J. W., "An Energy Method for Calculations in Fabric Mechanics, Part I: Principles of The Method, Journal of Textile Institute, 69, 1978.
- [23] Seyam A. M., "Structural Design of Woven Fabric: Theory and Practice," Journal of Textile Institute, Vol. 31. Manchester, UK, 2002.

- [24] Kawabata S., Niwa M., Kawai H., “3—The Finite-Deformation Theory of Plain-Weave Fabrics Part I: The Biaxial-Deformation Theory,” *The Journal of the Textile Institute*;64(1):21-46, January 1973.
- [25] Kawabata S., Niwa M., “Kawai H. 4—The Finite-Deformation Theory of Plain-Weave Fabrics. Part II: The Uniaxial-Deformation Theory,” *The Journal of the Textile Institute*; 64(2):47-61, February 1973.
- [26] Kawabata S, Niwa M., “38—A Finite-Deformation Theory Of The 2/2-Twill Weave Under Biaxial Extension,” *The Journal Of The Textile Institute*; 70(10):417-26, October 1979.
- [27] Kawabata, S. And Niwa M., *The Textile Machinery Society of Japan*, Osaka, 1984.
- [28] Sun F., Seyam A. M., And Gupta B. S., “A Generalized Model for Predicting Load-Extension Properties of Woven Fabrics,” *Textile Research Journal*; 67: 866-874, December 1997.
- [29] Daniel I., Ishai O., “*Engineering Mechanics of Composite Materials*,” 2nd Ed., Oxford University Press, 2005.
- [30] Nagai K., Yokoyama A., Maekawa Z.I., Hamada H., “The Stress Analysis Method for Three-Dimensional Composite Materials,” *Journal of Applied Composite Materials*; 1:197–216, 1994.
- [31] Kregers A.F., Melbardis Y.G., “Determination of The Elastoplastic Properties of Spatially Reinforced Composites by The Averaging Method,” *Journal of Polymer Mechanics*; 1:25–31, 1978.
- [32] Kregers A.F., Teters G.A., “Determination of The Elasto-Plastic Properties of Spatially Reinforced Composites by The Averaging Method,” *Journal of Mechanics of Composite Materials*; 17:25–31, 1981.
- [33] Cox B.N., Dadkhah M.S., “The Macroscopic Elasticity of 3D Woven Composites,” *Journal of Composite Materials*; 29(6):785–819, 1995.
- [34] Kuo W.S., Pon B.J., “Elastic Moduli and Damage Evolution of Three-Axis Woven Fabric Composites” *Journal of Material Science*; 32:5445–55, 1997.

- [35] Tan P., Tong L., Steven G.P., “A 3D Modeling Technique for Predicting the Linear Elastic Properties Open-Packing Woven Fabric Unit Cell,” In: 9th International Conference On Composite Structure, Paisley, Scotland; 1–3 September 1997.
- [36] Tan P., Tong L., Steven G.P., “Modeling Approaches for 3D Orthogonal Woven Composites,” *Journal of Reinforced Plastic Composites*; 17(6):545–77, 1998.
- [37] Yushanov S. P., Bogdanovich A. E., And Mohamed M. H., “Manufacturing and Property Analysis of a Novel Class of 3-D Woven Composites,” *Journal of Thermoplastic Composite Materials*, 12: 70-82, January 1999.
- [38] Abolinsh D.S., “Compliance Tensor for an Elastic Material Reinforced in Two Directions.” *Journal of Polymer Mechanics*; 2(3):372–9, 1996.
- [39] Naik N.K., Azad S.N.M., Prasad P.D., Thuruthimattan B.J., “Stress and Failure Analysis of 3D Orthogonal Interlock Woven Composites,” *Journal of Reinforced Plastic Composites*; 20(17):1485–523, 2001.
- [40] Wu Z.J., Brown D., Davies J.M., “An Analytical Modelling Technique for Predicting the Stiffness of 3-D Orthotropic Laminated Fabric Composites,” *Composite Structures*, Volume 56, Issue 4, Pages 407-412, June 2002.
- [41] Buchanan S., Grigorash A., Archer E., Mcilhagger A., Quinn J., Stewart G., “Analytical Elastic Stiffness Model for 3D Woven Orthogonal Interlock Composites,” *Composites Science and Technology*, Volume 70, Issue 11, Pages 1597-1604, 15 October 2010.
- [42] Buchanan S., Grigorash A., Quinn J.P., Mcilhagger A.T., Young C., “Modelling The Geometry of the Repeat Unit Cell of Three-Dimensional Weave Architectures,” *The Journal of the Textile Institute*; 101(7):679-85, June 2010.
- [43] Zuorong C., Shouwen Y., Xiqiao F., Lu M., Ye L., “Evaluation of Thermo-Elastic Properties of Three-Dimensional Orthogonal Woven Composites,” *Composites Part B: Engineering*, Volume 33, Issue 3, Pages 241-251, April 2002.
- [44] Huang D., Abdi F., “Analytical Characterization and Damage Propagation of Three Dimensional Composites,” 47th AIAA/ASME/ASCE/AHS/ASC Structures, Structural Dynamics, And Materials Conference; Newport, RI; USA, Pages 1-11, May 2006.

- [45] Pankow M., Waas A. M., Yen C., Ghiorse S., "A New Lamination Theory for Layered Textile Composites That Account for Manufacturing Induced Effects," *Composites Part A: Applied Science and Manufacturing*, Volume 40, Issue 12, Pages 1991-2003, December 2009.
- [46] Leong K.H., Lee B., Herszberg I., Bannister M.K., "The Effect of Binder Path On the Tensile Properties and Failure of Multilayer Woven CFRP Composites," *Composites Science and Technology*, Volume 60, Issue 1, Pages 149-156, 1 January 2000.
- [47] Rao M.P., Sankar B.V., Subhash G., "Effect of Z-Yarns On the Stiffness and Strength of Three-Dimensional Woven Composites," *Composites Part B: Engineering*, Volume 40, Issue 6, Pages 540-551, September 2009.
- [48] Mouritz A.P., Cox B.N., "A Mechanistic Interpretation of the Comparative In-Plane Mechanical Properties of 3D Woven, Stitched and Pinned Composites," *Composites Part A: Applied Science and Manufacturing*, Volume 41, Issue 6, Pages 709-728, June 2010.
- [49] Peerzada M. H., Abbasi S.A., Khatri A., "Effect of Weave Structure On Tensile Strength and Yarn Crimp of Three-Dimensional Fibre Woven Fabric," *Science International*. 24(1):47-50, 2012.
- [50] Bilisik K., Sahbaz Karaduman N, Bilisik NE, Bilisik HE., "Three-Dimensional Fully Interlaced Woven Preforms for Composites," *Textile Research Journal* 2013 May 21.
- [51] Xu H., Zhang L., Cheng L., "Effects of Yarn Size and Z-Yarn Density On the Interlaminar Shear Properties of Two Z-Reinforced 3D C/Sic Composites," *Materials & Design*, Volume 64, Pages 434-440, December 2014.
- [52] Dhiman S., Potluri P., Silva C., "Influence of Binder Configuration On 3D Woven Composites, Composite Structures," Volume 134, Pages 862-868, 15 December 2015.
- [53] Dai S., Cunningham P.R., Marshall S., Silva C., "Influence of Fibre Architecture On the Tensile, Compressive and Flexural Behaviour of 3D Woven Composites," *Composites Part A: Applied Science and Manufacturing*, Volume 69, Pages 195-207, February 2015.
- [54] Jackson W.C. And Poe C.C., "The Use of Impact Force as A Scale Parameter for The Impact Response of Composite Laminates", *Journal of Composites Technology and Research*, Winter 1993.

- [55] Kakarala S.N. And Roche J.L., "Experimental Comparison of Several Impact Test Methods", Instrumented Impact Testing of Plastics and Composite Materials, ASTM STP 936, Eds S L Kessler, G C Adams, S B Driscoll and D R Ireland, American Society for Testing and Materials, 1987.
- [56] Seyam A. M., Taylor D., Mohamed M., Powell N. And Meng J. "3D Woven Composites for Automotive Applications: Structure Parameters/Impact Energy Relationships," World Journal of Engineering, Vol. 7, No. 1, Pp. 23-29, 2010.
- [57] Buchanan S., Grigorash A., Quinn J. P., Mcilhagger A. T. And Young C., "Modelling The Geometry of the Repeat Unit Cell of Three-Dimensional Weave Architectures," The Journal of The Textile Institute, Vol. 101, No. 7, Pp. 679-685, July 2010.
- [58] Bogdanovich A.E. And Mohamed M.H., "Three-Dimensional Reinforcements for Composites," SAMPE Journal, Vol. 45, No. 6, Pp. 8-28, 2009.
- [59] Ince, M., "Performance of Composites from 3D Orthogonal Woven Preforms in Terms of Architecture and Sample Location During Resin Infusion," Dissertation. North Carolina State University, 2013. Electronic Thesis and Dissertation.
- [60] Seyam A. M. and Ince M. E., "Generalized geometric modeling of three-dimensional orthogonal woven preforms from spun yarns," The Journal of the Textile Institute 104(9):914-28, 2013.
- [61] Ince M. E. and Seyam A. M., "Generalized geometric modeling of 3D orthogonal woven preforms from flat filament yarns: the influence of weave and number of layers on preforms physical properties," Proceedings of the 6th World Conference on 3D Fabrics and their Applications, NC State University College of Textiles, Raleigh, NC, USA, May 26-28, 2015.
- [62] Hamburger W.J., "The Industrial Application of the Stress-Strain Relationship," Journal of the Textile Institute, 1949; 40:7, P700-P720
- [63] Xie, H., "The Role of Fiber Type in Performance of their Composites from 3D Orthogonal Woven Preforms," Thesis. North Carolina State University, 2016. Electronic Thesis and Dissertation.

- [64] Peirce, F. T., "Tensile Tests for Cotton Yams, the Weakest Link," *Journal of Textile Institute* 17, T355-T368, 1926.
- [65] Hussain, G. F. S., Nachane, R. P., Krishna Iyer, K. R., & Srinathan, B., "Weak-link effect on tensile properties of cotton yarns," *Textile Research Journal*, 60(2), 69-77, 1990.
- [66] Pan, N., Hua, T., & Qiu, Y., "Relationship between fiber and yarn strength," *Textile Research Journal*, 71(11), 960-964, 2001.
- [67] Pinnell, M. and Hill, S., "Assessment of Techniques Used to Measure Strain During Tensile Testing of Polymeric Materials," SAE Technical Paper 2008-01-1338, 2008.
- [68] Lo W. M. and Tsang Y. Y., "Anisotropy of tensile strain of balance twill woven fabrics, 2nd International Textile and Apparel Conference," SENA 1/CETIQT Rio de Janeiro, Brazil, July, 1999.
- [69] Wu, G. M., & Shyng, Y. T., "Effects of Basic Chemical Surface Treatment on PBO and PBO Fiber Reinforced Epoxy Composites," *Journal of Polymer Research*, 12(2), 93–102, 2005.
- [70] "Hybon Direct Roving Fiber Glass 2022 Product Bulletin" PPG Fiber Glass, 2016.
- [71] "DERAKANE® 8084 Epoxy Vinylester Resin Data Sheet," Ashland Inc., 2006.
- [72] "NOROX® MEKP-925H Data Sheet," NORAC, INC., Azusa, 2010.

APPENDICES

APPENDIX A: Statistical analysis of Tup impact energy for Experiment A

Table A.1. Between subject-effects on Tup impact energy

Tests of Between-Subjects Effects

Dependent Variable: Tup Energy

Source	Type III Sum of Squares	df	Mean Square	F	Sig.
Corrected Model	23073.175 ^a	26	887.430	68.103	.000
Intercept	259125.159	1	259125.159	19885.884	.000
F1	19827.241	2	9913.620	760.795	.000
F2	1087.301	2	543.650	41.721	.000
F3	118.700	2	59.350	4.555	.012
F1 * F2	511.150	4	127.787	9.807	.000
F1 * F3	784.282	4	196.071	15.047	.000
F2 * F3	81.237	4	20.309	1.559	.188
F1 * F2 * F3	204.122	8	25.515	1.958	.055
Error	2150.050	165	13.031		
Total	306302.275	192			
Corrected Total	25223.226	191			

Table A.2. Estimates of number of layers' effect on Tup impact energy

Estimates

Dependent Variable: Tup Energy

No. Layers	Mean	Std. Error	95% Confidence Interval	
			Lower Bound	Upper Bound
2	27.473	.398	26.688	28.259
3	41.783	.453	40.887	42.678
4	55.871	.651	54.586	57.156

Table A.3. ANOVA of number of layers' effect on Tup impact energy

Univariate Tests

Dependent Variable: Tup Energy

	Sum of Squares	df	Mean Square	F	Sig.
Contrast	19827.241	2	9913.620	760.795	.000
Error	2150.050	165	13.031		

Table A.4. Duncan post hoc test of number of layers' effect on Tup impact energy

Tup Energy

Duncan^{a,b,c}

No. Layers	N	Subset		
		1	2	3
2	84	27.6321		
3	67		41.7480	
4	41			54.3420
Sig.		1.000	1.000	1.000

Table A.5. Estimates of pick density effect on Tup impact energy

Estimates

Dependent Variable: Tup Energy

Pick Desnity	Mean	Std. Error	95% Confidence Interval	
			Lower Bound	Upper Bound
4.87	38.141	.475	37.202	39.080
5.48	42.135	.459	41.229	43.042
5.85	44.851	.592	43.682	46.020

Table A.6. ANOVA of pick density effect on Tup impact energy

Univariate Tests

Dependent Variable: Tup Energy

	Sum of Squares	df	Mean Square	F	Sig.
Contrast	1087.301	2	543.650	41.721	.000
Error	2150.050	165	13.031		

Table A.7. Duncan post hoc test of pick density effect on Tup impact energy

Tup Energy

Duncan^{a,b,c}

Pick Desnity	N	Subset	
		1	2
4.87	62	36.8172	
5.48	70		38.7222
5.85	60		39.2170
Sig.		1.000	.440

Table A.8. Estimates of weave pattern effect on Tup impact energy

Estimates

Dependent Variable: Tup Energy

Weave	Mean	Std. Error	95% Confidence Interval	
			Lower Bound	Upper Bound
Plain	40.620	.444	39.742	41.497
Twill	42.828	.591	41.661	43.995
Basket	41.679	.491	40.711	42.648

Table A.9. ANOVA of weave pattern effect on Tup impact energy

Univariate Tests

Dependent Variable: Tup Energy

	Sum of Squares	df	Mean Square	F	Sig.
Contrast	118.700	2	59.350	4.555	.012
Error	2150.050	165	13.031		

Table A.10. Duncan post hoc test of weave pattern effect on Tup impact energy

Tup Energy

Duncan^{a,b,c}

Weave	N	Subset
		1
Twill	61	37.9831
Plain	72	38.3325
Basket	59	38.4631
Sig.		.485

Table A.11. Between subject-effects on Tup impact energy/ thickness**Tests of Between-Subjects Effects**

Dependent Variable: Tup Energy/ Thickness

Source	Type III Sum of Squares	df	Mean Square	F	Sig.
Corrected Model	324302864.300 ^a	26	12473187.090	4.880	.000
Intercept	36321385470.000	1	36321385470.000	14211.679	.000
F1	122205161.700	2	61102580.830	23.908	.000
F2	41054146.780	2	20527073.390	8.032	.000
F3	31489443.190	2	15744721.590	6.161	.003
F1 * F2	29503301.960	4	7375825.489	2.886	.024
F1 * F3	118374216.300	4	29593554.070	11.579	.000
F2 * F3	3630499.640	4	907624.910	.355	.840
F1 * F2 * F3	21188754.190	8	2648594.274	1.036	.411
Error	421697432.200	165	2555742.014		
Total	45795234920.000	192			
Corrected Total	746000296.500	191			

Table A.12. Estimates of number of layers' effect on Tup impact energy/ thickness

Estimates

Dependent Variable: Tup Energy/ Thickness

No. Layers	Mean	Std. Error	95% Confidence Interval	
			Lower Bound	Upper Bound
2	14471.658	176.114	14123.930	14819.386
3	15808.925	200.794	15412.469	16205.381
4	16565.965	288.250	15996.831	17135.098

Table A.13. ANOVA of number of layers' effect on Tup impact energy/ thickness

Univariate Tests

Dependent Variable: Tup Energy/ Thickness

	Sum of Squares	df	Mean Square	F	Sig.
Contrast	122205161.700	2	61102580.830	23.908	.000
Error	421697432.200	165	2555742.014		

Table A.14. Duncan post hoc test of number of layers' effect on Tup impact energy/ thickness

Tup Energy/ Thickness

Duncan^{a,b,c}

No. Layers	N	Subset	
		1	2
2	84	14484.7402	
3	67		15808.2248
4	41		16222.5857
Sig.		1.000	.163

Table A.15. Estimates of pick density effect on Tup impact energy/ thickness

Estimates				
Dependent Variable: Tup Energy/ Thickness				
Pick Desnity	Mean	Std. Error	95% Confidence Interval	
			Lower Bound	Upper Bound
4.87	15005.530	210.561	14589.788	15421.272
5.48	15489.038	203.368	15087.500	15890.577
5.85	16351.979	262.160	15834.359	16869.599

Table A.16. ANOVA of pick density effect on Tup impact energy/ thickness

Univariate Tests					
Dependent Variable: Tup Energy/ Thickness					
	Sum of Squares	df	Mean Square	F	Sig.
Contrast	41054146.780	2	20527073.390	8.032	.000
Error	421697432.200	165	2555742.014		

Table A.17. Duncan post hoc test of pick density effect on Tup impact energy/ thickness

Tup Energy/ Thickness			
Duncan ^{a,b,c}			
Pick Desnity	N	Subset	
		1	2
4.87	62	14935.5524	
5.48	70	15277.4601	15277.4601
5.85	60		15759.4798
Sig.		.229	.091

Table A.18. Estimates of weave pattern effect on Tup impact energy/ thickness

Estimates

Dependent Variable: Tup Energy/ Thickness

Weave	Mean	Std. Error	95% Confidence Interval	
			Lower Bound	Upper Bound
Plain	15011.785	196.797	14623.220	15400.350
Twill	16063.964	261.730	15547.193	16580.734
Basket	15770.799	217.234	15341.881	16199.716

Table A.19. ANOVA of weave pattern effect on Tup impact energy/ thickness

Univariate Tests

Dependent Variable: Tup Energy/ Thickness

	Sum of Squares	df	Mean Square	F	Sig.
Contrast	31489443.190	2	15744721.590	6.161	.003
Error	421697432.200	165	2555742.014		

Table A.20. Duncan post hoc test of weave pattern effect on Tup impact energy/ thickness

Tup Energy/ Thickness

Duncan^{a,b,c}

Weave	N	Subset
		1
Plain	72	15049.1302
Basket	59	15375.9257
Twill	61	15578.3321
Sig.		.079

Table A.21. Between subject-effects on Tup impact energy/ composite areal density

Tests of Between-Subjects Effects

Dependent Variable: Tup Energy/ Composite Areal Density

Source	Type III Sum of Squares	df	Mean Square	F	Sig.
Corrected Model	75.304 ^a	26	2.896	5.132	.000
Intercept	10721.591	1	10721.591	18997.118	.000
F1	35.645	2	17.823	31.579	.000
F2	7.875	2	3.938	6.977	.001
F3	4.748	2	2.374	4.206	.017
F1 * F2	9.102	4	2.275	4.032	.004
F1 * F3	19.939	4	4.985	8.832	.000
F2 * F3	1.772	4	.443	.785	.537
F1 * F2 * F3	7.517	8	.940	1.665	.111
Error	93.123	165	.564		
Total	13481.466	192			
Corrected Total	168.426	191			

Table A.22. Estimates of number of layers' effect on Tup impact energy/ composite areal density

Estimates				
Dependent Variable: Tup Energy/ Composite Areal Density				
No. Layers	Mean	Std. Error	95% Confidence Interval	
			Lower Bound	Upper Bound
2	7.865	.083	7.702	8.028
3	8.615	.094	8.428	8.801
4	8.972	.135	8.705	9.240

Table A.23. ANOVA of number of layers' effect on Tup impact energy/ composite areal density

Univariate Tests					
Dependent Variable: Tup Energy/ Composite Areal Density					
	Sum of Squares	df	Mean Square	F	Sig.
Contrast	35.645	2	17.823	31.579	.000
Error	93.123	165	.564		

Table A.24. Duncan post hoc test of number of layers' effect on Tup impact energy/ composite areal density

Tup Energy/ Composite Areal Density			
Duncan ^{a,b,c}			
No. Layers	N	Subset	
		1	2
2	84	7.8679	
3	67		8.6118
4	41		8.8021
Sig.		1.000	.172

Table A.25. Estimates of pick density effect on Tup impact energy/ composite areal density

Estimates

Dependent Variable: Tup Energy/ Composite Areal Density

Pick Desnity	Mean	Std. Error	95% Confidence Interval	
			Lower Bound	Upper Bound
4.87	8.198	.099	8.003	8.393
5.48	8.468	.096	8.280	8.657
5.85	8.786	.123	8.543	9.029

Table A.26. ANOVA of pick density effect on Tup impact energy/ composite areal density

Univariate Tests

Dependent Variable: Tup Energy/ Composite Areal Density

	Sum of Squares	df	Mean Square	F	Sig.
Contrast	7.875	2	3.938	6.977	.001
Error	93.123	165	.564		

Table A.27. Duncan post hoc test of pick density effect on Tup impact energy/ composite areal density

Tup Energy/ Composite Areal Density

Duncan^{a,b,c}

Pick Desnity	N	Subset	
		1	2
4.87	62	8.1722	
5.48	70	8.3359	8.3359
5.85	60		8.4766
Sig.		.220	.292

Table A.28. Estimates of weave pattern effect on Tup impact energy/ composite areal density

Estimates

Dependent Variable: Tup Energy/ Composite Areal Density

Weave	Mean	Std. Error	95% Confidence Interval	
			Lower Bound	Upper Bound
Plain	8.248	.092	8.065	8.430
Twill	8.633	.123	8.390	8.876
Basket	8.572	.102	8.370	8.773

Table A.29. ANOVA of weave pattern effect on Tup impact energy/ composite areal density

Univariate Tests

Dependent Variable: Tup Energy/ Composite Areal Density

	Sum of Squares	df	Mean Square	F	Sig.
Contrast	4.748	2	2.374	4.206	.017
Error	93.123	165	.564		

Table A.30. Duncan post hoc test of weave pattern effect on Tup impact energy/ composite areal density

Tup Energy/ Composite Areal Density

Duncan^{a,b,c}

Weave	N	Subset
		1
Plain	72	8.2394
Twill	61	8.3682
Basket	59	8.3912
Sig.		.287

Table A.31. Between subject-effects on Tup impact energy/ preform areal density

Tests of Between-Subjects Effects

Dependent Variable: Tup ENergy/ Preform Areal Denisty

Source	Type III Sum of Squares	df	Mean Square	F	Sig.
Corrected Model	140.960 ^a	26	5.422	4.945	.000
Intercept	21847.832	1	21847.832	19927.842	.000
F1	56.195	2	28.097	25.628	.000
F2	8.128	2	4.064	3.707	.027
F3	2.691	2	1.345	1.227	.296
F1 * F2	25.236	4	6.309	5.755	.000
F1 * F3	57.017	4	14.254	13.002	.000
F2 * F3	4.399	4	1.100	1.003	.408
F1 * F2 * F3	10.661	8	1.333	1.216	.293
Error	180.897	165	1.096		
Total	27526.253	192			
Corrected Total	321.857	191			

Table A.32. Estimates of number of layers' effect on Tup impact energy/ preform areal density

Estimates				
Dependent Variable: Tup EEnergy/ Preform Areal Denisty				
No. Layers	Mean	Std. Error	95% Confidence Interval	
			Lower Bound	Upper Bound
2	11.335	.115	11.107	11.563
3	12.247	.132	11.987	12.506
4	12.751	.189	12.378	13.124

Table A.33. ANOVA of number of layers' effect on Tup impact energy/ preform areal density

Univariate Tests					
Dependent Variable: Tup EEnergy/ Preform Areal Denisty					
	Sum of Squares	df	Mean Square	F	Sig.
Contrast	56.195	2	28.097	25.628	.000
Error	180.897	165	1.096		

Table A.34. Duncan post hoc test of number of layers' effect on Tup impact energy/ preform areal density

Tup EEnergy/ Preform Areal Denisty			
Duncan ^{a,b,c}			
No. Layers	N	Subset	
		1	2
2	84	11.3503	
3	67		12.2425
4	41		12.4822
Sig.		1.000	.217

Table A.35. Estimates of pick density effect on Tup impact energy/ preform areal density

Estimates

Dependent Variable: Tup Energy/ Preform Areal Density

Pick Desnity	Mean	Std. Error	95% Confidence Interval	
			Lower Bound	Upper Bound
4.87	11.814	.138	11.542	12.086
5.48	12.111	.133	11.848	12.374
5.85	12.408	.172	12.069	12.747

Table A.36. ANOVA of pick density effect on Tup impact energy/ preform areal density

Univariate Tests

Dependent Variable: Tup Energy/ Preform Areal Density

	Sum of Squares	df	Mean Square	F	Sig.
Contrast	8.128	2	4.064	3.707	.027
Error	180.897	165	1.096		

Table A.37. Duncan post hoc test of pick density effect on Tup impact energy/ preform areal density

Tup Energy/ Preform Areal Density

Duncan^{a,b,c}

Pick Desnity	N	Subset
		1
4.87	62	11.8393
5.48	70	11.8989
5.85	60	11.9748
Sig.		.496

Table A.38. Estimates of weave pattern effect on Tup impact energy/ preform areal density

Estimates

Dependent Variable: Tup ENergy/ Preform Areal Denisty

Weave	Mean	Std. Error	95% Confidence Interval	
			Lower Bound	Upper Bound
Plain	11.950	.129	11.695	12.204
Twill	12.284	.171	11.945	12.622
Basket	12.100	.142	11.819	12.381

Table A.39. ANOVA of weave pattern effect on Tup impact energy/ preform areal density

Univariate Tests

Dependent Variable: Tup ENergy/ Preform Areal Denisty

	Sum of Squares	df	Mean Square	F	Sig.
Contrast	2.691	2	1.345	1.227	.296
Error	180.897	165	1.096		

Table A.40. Duncan post hoc test of weave pattern effect on Tup impact energy/ preform areal density

Tup ENergy/ Preform Areal Denisty

Duncan^{a,b,c}

Weave	N	Subset
		1
Twill	61	11.8341
Basket	59	11.8541
Plain	72	12.0023
Sig.		.398

**APPENDIX B: Statistical analysis of Izod impact energy in Y-axis direction for
Experiment A**

Table B.1. Between-subject effects on Izod Y impact energy

Tests of Between-Subjects Effects

Dependent Variable: Izod Y Energy

Source	Type III Sum of Squares	df	Mean Square	F	Sig.
Corrected Model	1428.077 ^a	26	54.926	17.784	.000
Intercept	12608.898	1	12608.898	4082.546	.000
F1	1054.345	2	527.173	170.689	.000
F2	23.932	2	11.966	3.874	.023
F3	5.795	2	2.897	.938	.394
F1 * F2	76.560	4	19.140	6.197	.000
F1 * F3	20.503	4	5.126	1.660	.164
F2 * F3	18.124	4	4.531	1.467	.216
F1 * F2 * F3	89.611	8	11.201	3.627	.001
Error	376.796	122	3.088		
Total	16563.532	149			
Corrected Total	1804.873	148			

Table B.2. Estimates of number of layers' effect on Izod Y impact energy

Estimates				
Dependent Variable: Izod Y Energy				
No. Layers	Mean	Std. Error	95% Confidence Interval	
			Lower Bound	Upper Bound
2	6.525	.295	5.941	7.109
3	9.029	.237	8.560	9.498
4	13.401	.249	12.907	13.895

Table B.3. ANOVA of number of layers' effect on Izod Y impact energy

Univariate Tests					
Dependent Variable: Izod Y Energy					
	Sum of Squares	df	Mean Square	F	Sig.
Contrast	1054.345	2	527.173	170.689	.000
Error	376.796	122	3.088		

Table B.4. Duncan post hoc test of number of layers' effect on Izod Y impact energy

Izod Y Energy				
Duncan ^{a,b,c}				
No. Layers	N	Subset		
		1	2	3
2	39	6.3775		
3	56		9.0854	
4	54			13.4336
Sig.		1.000	1.000	1.000

Table B.5. Estimates of pick density effect on Izod Y impact energy

Estimates

Dependent Variable: Izod Y Energy

Pick Desnity	Mean	Std. Error	95% Confidence Interval	
			Lower Bound	Upper Bound
4.87	10.159	.286	9.594	10.725
5.48	9.692	.242	9.214	10.171
5.85	9.103	.255	8.597	9.609

Table B.6. ANOVA of pick density effect on Izod Y impact energy

Univariate Tests

Dependent Variable: Izod Y Energy

	Sum of Squares	df	Mean Square	F	Sig.
Contrast	23.932	2	11.966	3.874	.023
Error	376.796	122	3.088		

Table B.7. Duncan post hoc test of pick density effect on Izod Y impact energy

Izod Y Energy

Duncan^{a,b,c}

Pick Desnity	N	Subset	
		1	2
5.85	50	9.3660	
5.48	55		10.1155
4.87	44		10.4150
Sig.		1.000	.399

Table B.8. Estimates of weave pattern effect on Izod Y impact energy

Estimates

Dependent Variable: Izod Y Energy

Weave	Mean	Std. Error	95% Confidence Interval	
			Lower Bound	Upper Bound
Plain	9.934	.243	9.453	10.414
Twill	9.522	.262	9.004	10.040
Basket	9.499	.279	8.946	10.051

Table B.9. ANOVA of weave pattern effect on Izod Y impact energy

Univariate Tests

Dependent Variable: Izod Y Energy

	Sum of Squares	df	Mean Square	F	Sig.
Contrast	5.795	2	2.897	.938	.394
Error	376.796	122	3.088		

Table B.10. Duncan post hoc test of weave pattern effect on Izod Y impact energy

Izod Y Energy

Duncan^{a,b,c}

Weave	N	Subset
		1
Basket	47	9.6179
Twill	48	10.0667
Plain	54	10.1420
Sig.		.165

Table B.11. Between-subject effects on Izod Y impact energy/ thickness

Tests of Between-Subjects Effects

Dependent Variable: Izod Y Energy/ Thickness

Source	Type III Sum of Squares	df	Mean Square	F	Sig.
Corrected Model	58158748.080 ^a	26	2236874.926	5.186	.000
Intercept	1868661126.000	1	1868661126.000	4332.341	.000
F1	12676545.010	2	6338272.505	14.695	.000
F2	9312549.988	2	4656274.994	10.795	.000
F3	816708.170	2	408354.085	.947	.391
F1 * F2	14543916.700	4	3635979.175	8.430	.000
F1 * F3	5219915.332	4	1304978.833	3.025	.020
F2 * F3	5221151.364	4	1305287.841	3.026	.020
F1 * F2 * F3	13861216.250	8	1732652.031	4.017	.000
Error	52622046.710	122	431328.252		
Total	2161477772.000	149			
Corrected Total	110780794.800	148			

Table B.12. Estimates of number of layers' effect on Izod Y impact energy/ thickness

Estimates

Dependent Variable: Izod Y Energy/ Thickness

No. Layers	Mean	Std. Error	95% Confidence Interval	
			Lower Bound	Upper Bound
2	3516.121	110.267	3297.836	3734.406
3	3497.318	88.518	3322.088	3672.548
4	4133.212	93.193	3948.728	4317.696

Table B.13. ANOVA of number of layers' effect on Izod Y impact energy/ thickness

Univariate Tests

Dependent Variable: Izod Y Energy/ Thickness

	Sum of Squares	df	Mean Square	F	Sig.
Contrast	12676545.010	2	6338272.505	14.695	.000
Error	52622046.710	122	431328.252		

Table B.14. Duncan post hoc test of number of layers' effect on Izod Y impact energy/ thickness

Izod Y Energy/ Thickness

Duncan^{a,b,c}

No. Layers	N	Subset	
		1	2
2	39	3406.1412	
3	56	3510.3909	
4	54		4136.0715
Sig.		.437	1.000

Table B.15. Estimates of pick density effect on Izod Y impact energy/ thickness

Estimates

Dependent Variable: Izod Y Energy/ Thickness

Pick Desnity	Mean	Std. Error	95% Confidence Interval	
			Lower Bound	Upper Bound
4.87	4074.598	106.821	3863.135	4286.062
5.48	3660.803	90.291	3482.064	3839.542
5.85	3411.250	95.478	3222.243	3600.257

Table B.16. ANOVA of pick density effect on Izod Y impact energy/ thickness

Univariate Tests

Dependent Variable: Izod Y Energy/ Thickness

	Sum of Squares	df	Mean Square	F	Sig.
Contrast	9312549.988	2	4656274.994	10.795	.000
Error	52622046.710	122	431328.252		

Table B.17. Duncan post hoc test of pick density effect on Izod Y impact energy/ thickness

Izod Y Energy/ Thickness

Duncan^{a,b,c}

Pick Desnity	N	Subset	
		1	2
5.85	50	3474.2851	
5.48	55	3706.2752	
4.87	44		3982.0424
Sig.		.082	1.000

Table B.18. Estimates of weave pattern effect on Izod Y impact energy/ thickness

Estimates

Dependent Variable: Izod Y Energy/ Thickness

Weave	Mean	Std. Error	95% Confidence Interval	
			Lower Bound	Upper Bound
Plain	3669.262	90.711	3489.691	3848.834
Twill	3648.529	97.774	3454.976	3842.082
Basket	3828.860	104.360	3622.270	4035.451

Table B.19. ANOVA of weave pattern effect on Izod Y impact energy/ thickness

Univariate Tests

Dependent Variable: Izod Y Energy/ Thickness

	Sum of Squares	df	Mean Square	F	Sig.
Contrast	816708.170	2	408354.085	.947	.391
Error	52622046.710	122	431328.252		

Table B.20. Duncan post hoc test of weave pattern effect on Izod Y impact energy/ thickness

Izod Y Energy/ Thickness

Duncan^{a,b,c}

Weave	N	Subset
		1
Plain	54	3674.1273
Twill	48	3723.8198
Basket	47	3736.6603
Sig.		.659

Table B.21. Between-subject effects on Izod Y impact energy/ composite areal density

Tests of Between-Subjects Effects

Dependent Variable: Izod Y Energy/ Composite Areal Density

Source	Type III Sum of Squares	df	Mean Square	F	Sig.
Corrected Model	15.140 ^a	26	.582	4.710	.000
Intercept	541.692	1	541.692	4381.657	.000
F1	2.670	2	1.335	10.798	.000
F2	3.091	2	1.545	12.500	.000
F3	.090	2	.045	.366	.694
F1 * F2	3.583	4	.896	7.245	.000
F1 * F3	.862	4	.216	1.744	.145
F2 * F3	1.097	4	.274	2.218	.071
F1 * F2 * F3	4.275	8	.534	4.322	.000
Error	15.083	122	.124		
Total	623.847	149			
Corrected Total	30.222	148			

Table B.22. Estimates of number of layers' effect on Izod Y impact energy/ composite areal density

Estimates

Dependent Variable: Izod Y Energy/ Composite Areal Density

No. Layers	Mean	Std. Error	95% Confidence Interval	
			Lower Bound	Upper Bound
2	1.924	.059	1.807	2.040
3	1.888	.047	1.795	1.982
4	2.189	.050	2.091	2.288

Table B.23. ANOVA of number of layers' effect on Izod Y impact energy/ composite areal density

Univariate Tests

Dependent Variable: Izod Y Energy/ Composite Areal Density

	Sum of Squares	df	Mean Square	F	Sig.
Contrast	2.670	2	1.335	10.798	.000
Error	15.083	122	.124		

Table B.24. Duncan post hoc test of number of layers' effect on Izod Y impact energy/ composite areal density

Izod Y Energy/ Composite Areal Density

Duncan^{a,b,c}

No. Layers	N	Subset	
		1	2
2	39	1.8660	
3	56	1.8973	
4	54		2.1923
Sig.		.662	1.000

Table B.25. Estimates of pick density effect on Izod Y impact energy/ composite areal density

Estimates				
Dependent Variable: Izod Y Energy/ Composite Areal Density				
Pick Density	Mean	Std. Error	95% Confidence Interval	
			Lower Bound	Upper Bound
4.87	2.202	.057	2.089	2.315
5.48	1.981	.048	1.885	2.076
5.85	1.819	.051	1.718	1.920

Table B.26. ANOVA of pick density effect on Izod Y impact energy/ composite areal density

Univariate Tests					
Dependent Variable: Izod Y Energy/ Composite Areal Density					
	Sum of Squares	df	Mean Square	F	Sig.
Contrast	3.091	2	1.545	12.500	.000
Error	15.083	122	.124		

Table B.27. Duncan post hoc test of pick density effect on Izod Y impact energy/ composite areal density

Izod Y Energy/ Composite Areal Density				
Duncan ^{a,b,c}				
Pick Density	N	Subset		
		1	2	3
5.85	50	1.8423		
5.48	55		2.0053	
4.87	44			2.1591
Sig.		1.000	1.000	1.000

Table B.28. Estimates of weave pattern effect on Izod Y impact energy/ composite areal density

Estimates

Dependent Variable: Izod Y Energy/ Composite Areal Density

Weave	Mean	Std. Error	95% Confidence Interval	
			Lower Bound	Upper Bound
Plain	2.023	.049	1.927	2.119
Twill	1.965	.052	1.861	2.069
Basket	2.013	.056	1.903	2.124

Table B.29. ANOVA of weave pattern effect on Izod Y impact energy/ composite areal density

Univariate Tests

Dependent Variable: Izod Y Energy/ Composite Areal Density

	Sum of Squares	df	Mean Square	F	Sig.
Contrast	.090	2	.045	.366	.694
Error	15.083	122	.124		

Table B.30. Duncan post hoc test of weave pattern effect on Izod Y impact energy/ composite areal density

Izod Y Energy/ Composite Areal Density

Duncan^{a,b,c}

Weave	N	Subset
		1
Basket	47	1.9557
Twill	48	2.0106
Plain	54	2.0181
Sig.		.410

Table B.31. Between-subject effects on Izod Y impact energy/ preform areal density

Tests of Between-Subjects Effects

Dependent Variable: Izod Y ENergy/ Preform Areal Denisty

Source	Type III Sum of Squares	df	Mean Square	F	Sig.
Corrected Model	29.477 ^a	26	1.134	4.659	.000
Intercept	1069.182	1	1069.182	4393.351	.000
F1	5.294	2	2.647	10.877	.000
F2	7.514	2	3.757	15.438	.000
F3	.259	2	.130	.532	.589
F1 * F2	5.855	4	1.464	6.014	.000
F1 * F3	1.323	4	.331	1.360	.252
F2 * F3	2.054	4	.514	2.110	.084
F1 * F2 * F3	8.469	8	1.059	4.350	.000
Error	29.690	122	.243		
Total	1229.791	149			
Corrected Total	59.167	148			

Table B.32. Estimates of number of layers' effect on Izod Y impact energy/ preform areal density

Estimates				
Dependent Variable: Izod Y ENergy/ Preform Areal Denisty				
No. Layers	Mean	Std. Error	95% Confidence Interval	
			Lower Bound	Upper Bound
2	2.708	.083	2.544	2.872
3	2.648	.066	2.517	2.780
4	3.075	.070	2.937	3.214

Table B.33. ANOVA of number of layers' effect on Izod Y impact energy/ preform areal density

Univariate Tests					
Dependent Variable: Izod Y ENergy/ Preform Areal Denisty					
	Sum of Squares	df	Mean Square	F	Sig.
Contrast	5.294	2	2.647	10.877	.000
Error	29.690	122	.243		

Table B.34. Duncan post hoc test of number of layers' effect on Izod Y impact energy/ preform areal density

Izod Y ENergy/ Preform Areal Denisty			
Duncan ^{a,b,c}			
No. Layers	N	Subset	
		1	2
2	39	2.6250	
3	56	2.6614	
4	54		3.0782
Sig.		.717	1.000

Table B.35. Estimates of pick density effect on Izod Y impact energy/ preform areal density

Estimates

Dependent Variable: Izod Y ENergy/ Preform Areal Denisty

Pick Desnity	Mean	Std. Error	95% Confidence Interval	
			Lower Bound	Upper Bound
4.87	3.129	.080	2.970	3.288
5.48	2.770	.068	2.636	2.904
5.85	2.532	.072	2.390	2.674

Table B.36. ANOVA of pick density effect on Izod Y impact energy/ preform areal density

Univariate Tests

Dependent Variable: Izod Y ENergy/ Preform Areal Denisty

	Sum of Squares	df	Mean Square	F	Sig.
Contrast	7.514	2	3.757	15.438	.000
Error	29.690	122	.243		

Table B.37. Duncan post hoc test of pick density effect on Izod Y impact energy/ preform areal density

Izod Y ENergy/ Preform Areal Denisty

Duncan^{a,b,c}

Pick Desnity	N	Subset		
		1	2	3
5.85	50	2.5688		
5.48	55		2.8025	
4.87	44			3.0695
Sig.		1.000	1.000	1.000

Table B.38. Estimates of weave pattern effect on Izod Y impact energy/ preform areal density

Estimates

Dependent Variable: Izod Y ENergy/ Preform Areal Denisty

Weave	Mean	Std. Error	95% Confidence Interval	
			Lower Bound	Upper Bound
Plain	2.866	.068	2.731	3.001
Twill	2.764	.073	2.619	2.909
Basket	2.802	.078	2.646	2.957

Table B.39. ANOVA of weave pattern effect on Izod Y impact energy/ preform areal density

Univariate Tests

Dependent Variable: Izod Y ENergy/ Preform Areal Denisty

	Sum of Squares	df	Mean Square	F	Sig.
Contrast	.259	2	.130	.532	.589
Error	29.690	122	.243		

Table B.40. Duncan post hoc test of weave pattern effect on Izod Y impact energy/ preform areal density

**Izod Y ENergy/ Preform
Areal Denisty**

Duncan^{a,b,c}

Weave	N	Subset 1
Basket	47	2.7150
Twill	48	2.8265
Plain	54	2.8585
Sig.		.176

**APPENDIX C: Statistical analysis of Izod impact energy in X- axis direction for
Experiment A**

Table C.1. Between-subject effects on Izod X impact energy

Tests of Between-Subjects Effects

Dependent Variable: Izod X Energy

Source	Type III Sum of Squares	df	Mean Square	F	Sig.
Corrected Model	1597.097 ^a	26	61.427	22.178	.000
Intercept	17458.833	1	17458.833	6303.486	.000
F1	1234.751	2	617.375	222.902	.000
F2	8.959	2	4.479	1.617	.203
F3	1.884	2	.942	.340	.712
F1 * F2	62.435	4	15.609	5.635	.000
F1 * F3	43.131	4	10.783	3.893	.005
F2 * F3	42.909	4	10.727	3.873	.005
F1 * F2 * F3	66.996	8	8.374	3.024	.004
Error	321.286	116	2.770		
Total	21682.794	143			
Corrected Total	1918.384	142			

Table C.2. Estimates of number of layers' effect on Izod X impact energy

Estimates

Dependent Variable: Izod X Energy

No. Layers	Mean	Std. Error	95% Confidence Interval	
			Lower Bound	Upper Bound
2	7.919	.278	7.367	8.470
3	11.211	.237	10.743	11.680
4	15.553	.239	15.079	16.027

Table C.3. ANOVA of number of layers' effect on Izod X impact energy

Univariate Tests

Dependent Variable: Izod X Energy

	Sum of Squares	df	Mean Square	F	Sig.
Contrast	1234.751	2	617.375	222.902	.000
Error	321.286	116	2.770		

Table C.4. Duncan post hoc test of number of layers' effect on Izod X impact energy

Izod X Energy

Duncan^{a,b,c}

No. Layers	N	Subset		
		1	2	3
2	40	7.7760		
3	53		11.2491	
4	50			15.4784
Sig.		1.000	1.000	1.000

Table C.5. Estimates of pick density effect on Izod X impact energy

Izod X Energy

Duncan^{a,b,c}

Pick Desnity	N	Subset 1
4.87	47	11.5745
5.48	48	11.7049
5.85	48	11.9860
Sig.		.259

Table C.6. ANOVA of pick density effect on Izod X impact energy

Univariate Tests

Dependent Variable: Izod X Energy

	Sum of Squares	df	Mean Square	F	Sig.
Contrast	8.959	2	4.479	1.617	.203
Error	321.286	116	2.770		

Table C.7. Duncan post hoc test of pick density effect on Izod X impact energy

Izod X Energy

Duncan^{a,b,c}

Pick Desnity	N	Subset 1
4.87	47	11.5745
5.48	48	11.7049
5.85	48	11.9860
Sig.		.259

Table C.8. Estimates of weave pattern effect on Izod X impact energy

Estimates

Dependent Variable: Izod X Energy

Weave	Mean	Std. Error	95% Confidence Interval	
			Lower Bound	Upper Bound
Plain	11.426	.268	10.897	11.956
Twill	11.535	.240	11.060	12.011
Basket	11.721	.248	11.230	12.213

Table C.9. ANOVA of weave pattern effect on Izod X impact energy

Univariate Tests

Dependent Variable: Izod X Energy

	Sum of Squares	df	Mean Square	F	Sig.
Contrast	1.884	2	.942	.340	.712
Error	321.286	116	2.770		

Table C.10. Duncan post hoc test of weave pattern effect on Izod X impact energy

Izod X Energy

Duncan^{a,b,c}

Weave	N	Subset
		1
Twill	50	11.5573
Plain	45	11.5743
Basket	48	12.1346
Sig.		.113

Table C.11. Between-subject effects on Izod X impact energy/ thickness**Tests of Between-Subjects Effects**

Dependent Variable: Izod X Energy/ Thickness

Source	Type III Sum of Squares	df	Mean Square	F	Sig.
Corrected Model	42579545.560 ^a	26	1637674.829	4.209	.000
Intercept	2443723618.000	1	2443723618.000	6279.989	.000
F1	6454015.116	2	3227007.558	8.293	.000
F2	433640.649	2	216820.324	.557	.574
F3	1505777.156	2	752888.578	1.935	.149
F1 * F2	11688086.450	4	2922021.613	7.509	.000
F1 * F3	8920637.009	4	2230159.252	5.731	.000
F2 * F3	2260185.444	4	565046.361	1.452	.221
F1 * F2 * F3	7520140.013	8	940017.502	2.416	.019
Error	45138923.190	116	389128.648		
Total	2751668637.000	143			
Corrected Total	87718468.740	142			

Table C.12. Estimates of number of layers' effect on Izod X impact energy/ thickness

Estimates

Dependent Variable: Izod X Energy/ Thickness

No. Layers	Mean	Std. Error	95% Confidence Interval	
			Lower Bound	Upper Bound
2	4146.824	104.351	3940.143	4353.504
3	4197.310	88.710	4021.609	4373.012
4	4631.772	89.736	4454.039	4809.505

Table C.13. ANOVA of number of layers' effect on Izod X impact energy/ thickness

Univariate Tests

Dependent Variable: Izod X Energy/ Thickness

	Sum of Squares	df	Mean Square	F	Sig.
Contrast	6454015.116	2	3227007.558	8.293	.000
Error	45138923.190	116	389128.648		

Table C.14. Duncan post hoc test of number of layers' effect on Izod X impact energy/ thickness

Izod X Energy/ Thickness

Duncan^{a,b,c}

No. Layers	N	Subset	
		1	2
2	40	4061.5055	
3	53	4225.4944	
4	50		4615.9179
Sig.		.205	1.000

Table C.15. Estimates of pick density effect on Izod X impact energy/ thickness

Estimates

Dependent Variable: Izod X Energy/ Thickness

Pick Desnity	Mean	Std. Error	95% Confidence Interval	
			Lower Bound	Upper Bound
4.87	4406.378	98.487	4211.312	4601.443
5.48	4269.348	92.374	4086.390	4452.306
5.85	4300.180	92.621	4116.732	4483.628

Table C.16. ANOVA of pick density effect on Izod X impact energy/ thickness

Univariate Tests

Dependent Variable: Izod X Energy/ Thickness

	Sum of Squares	df	Mean Square	F	Sig.
Contrast	433640.649	2	216820.324	.557	.574
Error	45138923.190	116	389128.648		

Table C.17. Duncan post hoc test of pick density effect on Izod X impact energy/ thickness

Izod X Energy/ Thickness

Duncan^{a,b,c}

Pick Desnity	N	Subset
		1
5.48	48	4285.6252
5.85	48	4315.9539
4.87	47	4347.4792
Sig.		.652

Table C.18. Estimates of weave pattern effect on Izod X impact energy/ thickness

Estimates

Dependent Variable: Izod X Energy/ Thickness

Weave	Mean	Std. Error	95% Confidence Interval	
			Lower Bound	Upper Bound
Plain	4189.524	100.271	3990.925	4388.123
Twill	4454.507	89.990	4276.270	4632.744
Basket	4331.875	93.052	4147.573	4516.177

Table C.19. ANOVA of weave pattern effect on Izod X impact energy/ thickness

Univariate Tests

Dependent Variable: Izod X Energy/ Thickness

	Sum of Squares	df	Mean Square	F	Sig.
Contrast	1505777.156	2	752888.578	1.935	.149
Error	45138923.190	116	389128.648		

Table C.20. Duncan post hoc test of weave pattern effect on Izod X impact energy/ thickness

Izod X Energy/ Thickness

Duncan^{a,b,c}

Weave	N	Subset	
		1	2
Plain	45	4154.9162	
Basket	48	4348.4142	4348.4142
Twill	50		4430.2441
Sig.		.133	.524

Table C.21. Between-subject effects on Izod X impact energy/ composite areal density

Tests of Between-Subjects Effects

Dependent Variable: Izod X Energy/ Composite Areal Density

Source	Type III Sum of Squares	df	Mean Square	F	Sig.
Corrected Model	11.237 ^a	26	.432	3.644	.000
Intercept	748.979	1	748.979	6315.856	.000
F1	1.349	2	.675	5.690	.004
F2	.403	2	.202	1.701	.187
F3	.113	2	.057	.477	.622
F1 * F2	3.416	4	.854	7.201	.000
F1 * F3	2.133	4	.533	4.496	.002
F2 * F3	1.118	4	.279	2.356	.058
F1 * F2 * F3	2.357	8	.295	2.485	.016
Error	13.756	116	.119		
Total	836.054	143			
Corrected Total	24.993	142			

Table C.22. Estimates of number of layers' effect on Izod X impact energy/ composite areal density

Estimates				
Dependent Variable: Izod X Energy/ Composite Areal Density				
No. Layers	Mean	Std. Error	95% Confidence Interval	
			Lower Bound	Upper Bound
2	2.343	.058	2.229	2.457
3	2.310	.049	2.213	2.407
4	2.531	.050	2.433	2.629

Table C.23. ANOVA of number of layers' effect on Izod X impact energy/ composite areal density

Univariate Tests					
Dependent Variable: Izod X Energy/ Composite Areal Density					
	Sum of Squares	df	Mean Square	F	Sig.
Contrast	1.349	2	.675	5.690	.004
Error	13.756	116	.119		

Table C.24. Duncan post hoc test of number of layers' effect on Izod X impact energy/ composite areal density

Izod X Energy/ Composite Areal Density			
Duncan ^{a,b,c}			
No. Layers	N	Subset	
		1	2
2	40	2.2815	
3	53	2.3192	
4	50		2.5276
Sig.		.597	1.000

Table C.25. Estimates of pick density effect on Izod X impact energy/ composite areal density

Estimates				
Dependent Variable: Izod X Energy/ Composite Areal Density				
Pick Density	Mean	Std. Error	95% Confidence Interval	
			Lower Bound	Upper Bound
4.87	2.464	.054	2.356	2.572
5.48	2.393	.051	2.292	2.494
5.85	2.326	.051	2.225	2.428

Table C.26. ANOVA of pick density effect on Izod X impact energy/ composite areal density

Univariate Tests					
Dependent Variable: Izod X Energy/ Composite Areal Density					
	Sum of Squares	df	Mean Square	F	Sig.
Contrast	.403	2	.202	1.701	.187
Error	13.756	116	.119		

Table C.27. Duncan post hoc test of pick density effect on Izod X impact energy/ composite areal density

Izod X Energy/ Composite Areal Density

Duncan^{a,b,c}

Pick Density	N	Subset
		1
5.85	48	2.3373
5.48	48	2.4010
4.87	47	2.4069
Sig.		.357

Table C.28. Estimates of weave pattern effect on Izod X impact energy/ composite areal density

Estimates

Dependent Variable: Izod X Energy/ Composite Areal Density

Weave	Mean	Std. Error	95% Confidence Interval	
			Lower Bound	Upper Bound
Plain	2.352	.055	2.242	2.461
Twill	2.415	.050	2.317	2.514
Basket	2.417	.051	2.315	2.518

Table C.29. ANOVA of weave pattern effect on Izod X impact energy/ composite areal density

Univariate Tests

Dependent Variable: Izod X Energy/ Composite Areal Density

	Sum of Squares	df	Mean Square	F	Sig.
Contrast	.113	2	.057	.477	.622
Error	13.756	116	.119		

Table C.30. Duncan post hoc test of weave pattern effect on Izod X impact energy/ composite areal density

Izod X Energy/ Composite Areal Density

Duncan^{a,b,c}

Weave	N	Subset
		1
Plain	45	2.3188
Twill	50	2.4054
Basket	48	2.4156
Sig.		.200

Table C.31. Between-subject effects on Izod X impact energy/ preform areal density

Tests of Between-Subjects Effects

Dependent Variable: Izod X ENergy/ Preform Areal Denisty

Source	Type III Sum of Squares	df	Mean Square	F	Sig.
Corrected Model	25.223 ^a	26	.970	4.138	.000
Intercept	1487.482	1	1487.482	6344.649	.000
F1	2.251	2	1.125	4.800	.010
F2	1.443	2	.722	3.078	.050
F3	.212	2	.106	.453	.637
F1 * F2	7.298	4	1.825	7.782	.000
F1 * F3	3.709	4	.927	3.955	.005
F2 * F3	3.393	4	.848	3.618	.008
F1 * F2 * F3	5.917	8	.740	3.155	.003
Error	27.196	116	.234		
Total	1665.369	143			
Corrected Total	52.419	142			

Table C.32. Estimates of number of layers' effect on Izod X impact energy/ preform areal density

Estimates				
Dependent Variable: Izod X ENergy/ Preform Areal Denisty				
No. Layers	Mean	Std. Error	95% Confidence Interval	
			Lower Bound	Upper Bound
2	3.285	.081	3.125	3.446
3	3.284	.069	3.147	3.420
4	3.555	.070	3.417	3.693

Table C.33. ANOVA of number of layers' effect on Izod X impact energy/ preform areal density

Univariate Tests					
Dependent Variable: Izod X ENergy/ Preform Areal Denisty					
	Sum of Squares	df	Mean Square	F	Sig.
Contrast	2.251	2	1.125	4.800	.010
Error	27.196	116	.234		

Table C.34. Duncan post hoc test of number of layers' effect on Izod X impact energy/ preform areal density

Izod X ENergy/ Preform Areal Denisty			
Duncan ^{a,b,c}			
No. Layers	N	Subset	
		1	2
2	40	3.2031	
3	53	3.2960	
4	50		3.5489
Sig.		.354	1.000

Table C.35. Estimates of pick density effect on Izod X impact energy/ preform areal density

Estimates

Dependent Variable: Izod X ENergy/ Preform Areal Denisty

Pick Desnity	Mean	Std. Error	95% Confidence Interval	
			Lower Bound	Upper Bound
4.87	3.516	.076	3.364	3.667
5.48	3.351	.072	3.209	3.493
5.85	3.257	.072	3.115	3.400

Table C.36. ANOVA of pick density effect on Izod X impact energy/ preform areal density

Univariate Tests

Dependent Variable: Izod X ENergy/ Preform Areal Denisty

	Sum of Squares	df	Mean Square	F	Sig.
Contrast	1.443	2	.722	3.078	.050
Error	27.196	116	.234		

Table C.37. Duncan post hoc test of pick density effect on Izod X impact energy/ preform areal density

Izod X ENergy/ Preform Areal Denisty

Duncan^{a,b,c}

Pick Desnity	N	Subset 1
5.85	48	3.2797
5.48	48	3.3593
4.87	47	3.4381
Sig.		.135

Table C.38. Estimates of weave pattern effect on Izod X impact energy/ preform areal density

Estimates

Dependent Variable: Izod X ENergy/ Preform Areal Denisty

Weave	Mean	Std. Error	95% Confidence Interval	
			Lower Bound	Upper Bound
Plain	3.316	.078	3.162	3.470
Twill	3.403	.070	3.265	3.542
Basket	3.405	.072	3.261	3.548

Table C.39. ANOVA of weave pattern effect on Izod X impact energy/ preform areal density

Univariate Tests

Dependent Variable: Izod X ENergy/ Preform Areal Denisty

	Sum of Squares	df	Mean Square	F	Sig.
Contrast	.212	2	.106	.453	.637
Error	27.196	116	.234		

Table C.40. Duncan post hoc test of weave pattern effect on Izod X impact energy/ preform areal density

**Izod X ENergy/ Preform
Areal Denisty**

Duncan^{a,b,c}

Weave	N	Subset 1
Plain	45	3.2812
Twill	50	3.3875
Basket	48	3.4008
Sig.		.260

**APPENDIX D: Statistical analysis of Charpy impact energy in Y- axis direction for
Experiment A**

Table D.1. Between-subject effects on Charpy Y impact energy

Tests of Between-Subjects Effects

Dependent Variable: Charpy Y Energy

Source	Type III Sum of Squares	df	Mean Square	F	Sig.
Corrected Model	1118.961 ^a	26	43.037	27.238	.000
Intercept	5547.902	1	5547.902	3511.192	.000
F1	915.960	2	457.980	289.849	.000
F2	3.751	2	1.875	1.187	.308
F3	25.650	2	12.825	8.117	.000
F1 * F2	19.378	4	4.845	3.066	.019
F1 * F3	10.767	4	2.692	1.704	.153
F2 * F3	5.425	4	1.356	.858	.491
F1 * F2 * F3	32.593	8	4.074	2.578	.012
Error	206.988	131	1.580		
Total	7635.588	158			
Corrected Total	1325.949	157			

Table D.2. Estimates of number of layers' effect on Charpy Y impact energy

Estimates

Dependent Variable: Charpy Y Energy

No. Layers	Mean	Std. Error	95% Confidence Interval	
			Lower Bound	Upper Bound
2	3.154	.197	2.764	3.544
3	5.809	.161	5.490	6.128
4	9.477	.179	9.123	9.830

Table D.3. ANOVA of number of layers' effect on Charpy Y impact energy

Univariate Tests

Dependent Variable: Charpy Y Energy

	Sum of Squares	df	Mean Square	F	Sig.
Contrast	915.960	2	457.980	289.849	.000
Error	206.988	131	1.580		

Table D.4. Duncan post hoc test of number of layers' effect on Charpy Y impact energy

Charpy Y Energy

Duncan^{a,b,c}

No. Layers	N	Subset		
		1	2	3
2	44	3.1443		
3	61		5.7992	
4	53			9.5539
Sig.		1.000	1.000	1.000

Table D.5. Estimates of pick density effect on Charpy Y impact energy

Estimates

Dependent Variable: Charpy Y Energy

Pick Density	Mean	Std. Error	95% Confidence Interval	
			Lower Bound	Upper Bound
4.87	5.960	.176	5.611	6.308
5.48	6.354	.186	5.986	6.721
5.85	6.126	.177	5.777	6.476

Table D.6. ANOVA of pick density effect on Charpy Y impact energy

Univariate Tests

Dependent Variable: Charpy Y Energy

	Sum of Squares	df	Mean Square	F	Sig.
Contrast	3.751	2	1.875	1.187	.308
Error	206.988	131	1.580		

Table D.7. Duncan post hoc test of pick density effect on Charpy Y impact energy

Charpy Y Energy

Duncan^{a,b,c}

Pick Density	N	Subset
		1
4.87	55	6.2228
5.85	52	6.2903
5.48	51	6.4531
Sig.		.380

Table D.8. Estimates of weave pattern effect on Charpy Y impact energy

Estimates

Dependent Variable: Charpy Y Energy

Weave	Mean	Std. Error	95% Confidence Interval	
			Lower Bound	Upper Bound
Plain	6.639	.179	6.286	6.993
Twill	6.177	.182	5.817	6.536
Basket	5.623	.178	5.271	5.976

Table D.9. ANOVA of weave pattern effect on Charpy Y impact energy

Univariate Tests

Dependent Variable: Charpy Y Energy

	Sum of Squares	df	Mean Square	F	Sig.
Contrast	25.650	2	12.825	8.117	.000
Error	206.988	131	1.580		

Table D.10. Duncan post hoc test of weave pattern effect on Charpy Y impact energy

Charpy Y Energy

Duncan^{a,b,c}

Weave	N	Subset	
		1	2
Basket	53	5.9264	
Twill	51	6.1157	
Plain	54		6.8974
Sig.		.441	1.000

Table D.11. Between-subject effects on Charpy Y impact energy/ thickness

Tests of Between-Subjects Effects

Dependent Variable: Charpy Y Energy/ Thickness

Source	Type III Sum of Squares	df	Mean Square	F	Sig.
Corrected Model	56021215.300 ^a	26	2154662.127	10.112	.000
Intercept	764220735.400	1	764220735.400	3586.488	.000
F1	35928246.210	2	17964123.110	84.306	.000
F2	330251.502	2	165125.751	.775	.463
F3	2112353.764	2	1056176.882	4.957	.008
F1 * F2	4264763.465	4	1066190.866	5.004	.001
F1 * F3	2848537.024	4	712134.256	3.342	.012
F2 * F3	927184.046	4	231796.012	1.088	.365
F1 * F2 * F3	4319884.460	8	539985.558	2.534	.013
Error	27913915.100	131	213083.321		
Total	934926470.000	158			
Corrected Total	83935130.400	157			

Table D.12. Estimates of number of layers' effect on Charpy Y impact energy/ thickness

Estimates

Dependent Variable: Charpy Y Energy/ Thickness

No. Layers	Mean	Std. Error	95% Confidence Interval	
			Lower Bound	Upper Bound
2	1673.066	72.405	1529.831	1816.301
3	2238.678	59.225	2121.518	2355.839
4	2932.024	65.645	2802.163	3061.886

Table D.13. ANOVA of number of layers' effect on Charpy Y impact energy/ thickness

Univariate Tests

Dependent Variable: Charpy Y Energy/ Thickness

	Sum of Squares	df	Mean Square	F	Sig.
Contrast	35928246.210	2	17964123.110	84.306	.000
Error	27913915.100	131	213083.321		

Table D.14. Duncan post hoc test of number of layers' effect on Charpy Y impact energy/ thickness

Charpy Y Energy/ Thickness

Duncan^{a,b,c}

No. Layers	N	Subset		
		1	2	3
2	44	1674.0367		
3	61		2230.2238	
4	53			2961.9249
Sig.		1.000	1.000	1.000

Table D.15. Estimates of pick density effect on Charpy Y impact energy/ thickness

Estimates

Dependent Variable: Charpy Y Energy/ Thickness

Pick Density	Mean	Std. Error	95% Confidence Interval	
			Lower Bound	Upper Bound
4.87	2244.844	64.684	2116.884	2372.804
5.48	2349.431	68.264	2214.388	2484.474
5.85	2249.493	64.925	2121.055	2377.931

Table D.16. ANOVA of pick density effect on Charpy Y impact energy/ thickness

Univariate Tests

Dependent Variable: Charpy Y Energy/ Thickness

	Sum of Squares	df	Mean Square	F	Sig.
Contrast	330251.502	2	165125.751	.775	.463
Error	27913915.100	131	213083.321		

Table D.17. Duncan post hoc test of pick density effect on Charpy Y impact energy/ thickness

Charpy Y Energy/ Thickness

Duncan^{a,b,c}

Pick Density	N	Subset
		1
5.85	52	2279.6380
4.87	55	2320.6853
5.48	51	2362.8317
Sig.		.388

Table D.18. Estimates of weave pattern effect on Charpy Y impact energy/ thickness for Experiment A

Estimates

Dependent Variable: Charpy Y Energy/ Thickness

Weave	Mean	Std. Error	95% Confidence Interval	
			Lower Bound	Upper Bound
Plain	2402.982	65.693	2273.026	2532.937
Twill	2321.433	66.780	2189.326	2453.540
Basket	2119.354	65.454	1989.870	2248.837

Table D.19. ANOVA of weave pattern effect on Charpy Y impact energy/ thickness

Univariate Tests

Dependent Variable: Charpy Y Energy/ Thickness

	Sum of Squares	df	Mean Square	F	Sig.
Contrast	2112353.764	2	1056176.882	4.957	.008
Error	27913915.100	131	213083.321		

Table D.20. Duncan post hoc test of weave pattern effect on Charpy Y impact energy/ thickness

Charpy Y Energy/ Thickness

Duncan^{a,b,c}

Weave	N	Subset	
		1	2
Basket	53	2203.2367	
Twill	51	2310.4713	2310.4713
Plain	54		2445.8834
Sig.		.236	.135

Table D.21. Between-subject effects on Charpy Y impact energy/ composite areal density

Tests of Between-Subjects Effects

Dependent Variable: Charpy Y Energy/ Composite Areal Density

Source	Type III Sum of Squares	df	Mean Square	F	Sig.
Corrected Model	14.307 ^a	26	.550	8.890	.000
Intercept	219.610	1	219.610	3548.227	.000
F1	8.573	2	4.286	69.254	.000
F2	.167	2	.084	1.350	.263
F3	1.127	2	.563	9.104	.000
F1 * F2	.908	4	.227	3.670	.007
F1 * F3	.654	4	.163	2.640	.037
F2 * F3	.259	4	.065	1.047	.386
F1 * F2 * F3	1.268	8	.158	2.560	.013
Error	8.108	131	.062		
Total	266.009	158			
Corrected Total	22.415	157			

Table D.22. Estimates of number of layers' effect on Charpy Y impact energy/ composite areal density

Estimates				
Dependent Variable: Charpy Y Energy/ Composite Areal Density				
No. Layers	Mean	Std. Error	95% Confidence Interval	
			Lower Bound	Upper Bound
2	.926	.039	.849	1.003
3	1.202	.032	1.138	1.265
4	1.541	.035	1.471	1.611

Table D.23. ANOVA of number of layers' effect on Charpy Y impact energy/ composite areal density

Univariate Tests					
Dependent Variable: Charpy Y Energy/ Composite Areal Density					
	Sum of Squares	df	Mean Square	F	Sig.
Contrast	8.573	2	4.286	69.254	.000
Error	8.108	131	.062		

Table D.24. Duncan post hoc test of number of layers' effect on Charpy Y impact energy/ composite areal density

Charpy Y Energy/ Composite Areal Density				
Duncan ^{a,b,c}				
No. Layers	N	Subset		
		1	2	3
2	44	.9239		
3	61		1.1995	
4	53			1.5540
Sig.		1.000	1.000	1.000

Table D.25. Estimates of pick density effect on Charpy Y impact energy/ composite areal density

Estimates				
Dependent Variable: Charpy Y Energy/ Composite Areal Density				
Pick Density	Mean	Std. Error	95% Confidence Interval	
			Lower Bound	Upper Bound
4.87	1.213	.035	1.144	1.282
5.48	1.269	.037	1.196	1.342
5.85	1.187	.035	1.118	1.256

Table D.26. ANOVA of pick density effect on Charpy Y impact energy/ composite areal density

Univariate Tests					
Dependent Variable: Charpy Y Energy/ Composite Areal Density					
	Sum of Squares	df	Mean Square	F	Sig.
Contrast	.167	2	.084	1.350	.263
Error	8.108	131	.062		

Table D.27. Duncan post hoc test of pick density effect on Charpy Y impact energy/ composite areal density

Charpy Y Energy/ Composite Areal Density		
Duncan ^{a,b,c}		
Pick Density	N	Subset
5.85	52	1.2011
4.87	55	1.2500
5.48	51	1.2741
Sig.		.158

Table D.28. Estimates of weave pattern effect on Charpy Y impact energy/ composite areal density

Estimates

Dependent Variable: Charpy Y Energy/ Composite Areal Density

Weave	Mean	Std. Error	95% Confidence Interval	
			Lower Bound	Upper Bound
Plain	1.316	.035	1.246	1.386
Twill	1.246	.036	1.175	1.317
Basket	1.107	.035	1.037	1.176

Table D.29. ANOVA of weave pattern effect on Charpy Y impact energy/ composite areal density

Univariate Tests

Dependent Variable: Charpy Y Energy/ Composite Areal Density

	Sum of Squares	df	Mean Square	F	Sig.
Contrast	1.127	2	.563	9.104	.000
Error	8.108	131	.062		

Table D.30. Duncan post hoc test of weave pattern effect on Charpy Y impact energy/ composite areal density

Charpy Y Energy/ Composite Areal Density

Duncan^{a,b,c}

Weave	N	Subset		
		1	2	3
Basket	53	1.1448		
Twill	51		1.2410	
Plain	54			1.3374
Sig.		1.000	1.000	1.000

Table D.31. Between-subject effects on Charpy Y impact energy/ preform areal density

Tests of Between-Subjects Effects

Dependent Variable: Charpy Y ENergy/ Preform Areal Denisty

Source	Type III Sum of Squares	df	Mean Square	F	Sig.
Corrected Model	28.647 ^a	26	1.102	8.871	.000
Intercept	436.570	1	436.570	3514.864	.000
F1	17.217	2	8.609	69.310	.000
F2	.357	2	.179	1.438	.241
F3	2.511	2	1.255	10.107	.000
F1 * F2	1.612	4	.403	3.245	.014
F1 * F3	1.317	4	.329	2.650	.036
F2 * F3	.276	4	.069	.555	.695
F1 * F2 * F3	2.567	8	.321	2.583	.012
Error	16.271	131	.124		
Total	530.692	158			
Corrected Total	44.918	157			

Table D.32. Estimates of number of layers' effect on Charpy Y impact energy/ preform areal density

Estimates				
Dependent Variable: Charpy Y ENergy/ Preform Areal Density				
No. Layers	Mean	Std. Error	95% Confidence Interval	
			Lower Bound	Upper Bound
2	1.299	.055	1.190	1.408
3	1.701	.045	1.612	1.791
4	2.172	.050	2.073	2.271

Table D.33. ANOVA of number of layers' effect on Charpy Y impact energy/ preform areal density

Univariate Tests					
Dependent Variable: Charpy Y ENergy/ Preform Areal Density					
	Sum of Squares	df	Mean Square	F	Sig.
Contrast	17.217	2	8.609	69.310	.000
Error	16.271	131	.124		

Table D.34. Duncan post hoc test of number of layers' effect on Charpy Y impact energy/ preform areal density

Charpy Y Energy/ Preform Areal Density				
Duncan ^{a,b,c}				
No. Layers	N	Subset		
		1	2	3
2	44	1.2963		
3	61		1.7009	
4	53			2.1934
Sig.		1.000	1.000	1.000

Table D.35. Estimates of pick density effect on Charpy Y impact energy/ preform areal density

Estimates				
Dependent Variable: Charpy Y ENergy/ Preform Areal Density				
Pick Density	Mean	Std. Error	95% Confidence Interval	
			Lower Bound	Upper Bound
4.87	1.741	.049	1.643	1.838
5.48	1.775	.052	1.672	1.878
5.85	1.657	.050	1.559	1.755

Table D.36. ANOVA of pick density effect on Charpy Y impact energy/ preform areal density

Univariate Tests					
Dependent Variable: Charpy Y ENergy/ Preform Areal Denisty					
	Sum of Squares	df	Mean Square	F	Sig.
Contrast	.357	2	.179	1.438	.241
Error	16.271	131	.124		

Table D.37. Duncan post hoc test of pick density effect on Charpy Y impact energy/ preform areal density

Charpy Y Energy/ Preform Areal Density		
Duncan ^{a,b,c}		
Pick Density	N	Subset
		1
5.85	52	1.6802
5.48	51	1.7829
4.87	55	1.7953
Sig.		.116

Table D.38. Estimates of weave pattern effect on Charpy Y impact energy/ preform areal density

Estimates

Dependent Variable: Charpy Y Energy/ Preform Areal Density

Weave	Mean	Std. Error	95% Confidence Interval	
			Lower Bound	Upper Bound
Plain	1.869	.050	1.770	1.968
Twill	1.750	.051	1.649	1.851
Basket	1.554	.050	1.455	1.653

Table D.39. ANOVA of weave pattern effect on Charpy Y impact energy/ preform areal density

Univariate Tests

Dependent Variable: Charpy Y Energy/ Preform Areal Density

	Sum of Squares	df	Mean Square	F	Sig.
Contrast	2.511	2	1.255	10.107	.000
Error	16.271	131	.124		

Table D.40. Duncan post hoc test of weave pattern effect on Charpy Y impact energy/ preform areal density

Charpy Y Energy/ Preform Areal Density

Duncan^{a,b,c}

Weave	N	Subset		
		1	2	3
Basket	53	1.6079		
Twill	51		1.7448	
Plain	54			1.9043
Sig.		1.000	1.000	1.000

**APPENDIX E: Statistical analysis of Charpy impact energy in X- axis direction for
Experiment A**

Table E.1. Between-subject effect on Charpy X impact energy

Tests of Between-Subjects Effects

Dependent Variable: Charpy X Energy

Source	Type III Sum of Squares	df	Mean Square	F	Sig.
Corrected Model	1213.944 ^a	26	46.690	28.830	.000
Intercept	6070.795	1	6070.795	3748.514	.000
F1	949.120	2	474.560	293.025	.000
F2	106.708	2	53.354	32.944	.000
F3	14.415	2	7.207	4.450	.014
F1 * F2	10.991	4	2.748	1.697	.158
F1 * F3	13.690	4	3.423	2.113	.086
F2 * F3	47.583	4	11.896	7.345	.000
F1 * F2 * F3	30.366	8	3.796	2.344	.025
Error	145.757	90	1.620		
Total	7937.613	117			
Corrected Total	1359.700	116			

Table E.2. Estimates of number of layers' effect on Charpy X impact energy

Estimates				
Dependent Variable: Charpy X Energy				
No. Layers	Mean	Std. Error	95% Confidence Interval	
			Lower Bound	Upper Bound
2	3.808	.213	3.385	4.231
3	7.294	.205	6.887	7.701
4	10.998	.207	10.586	11.410

Table E.3. ANOVA of number of layers' effect on Charpy X impact energy

Univariate Tests					
Dependent Variable: Charpy X Energy					
	Sum of Squares	df	Mean Square	F	Sig.
Contrast	949.120	2	474.560	293.025	.000
Error	145.757	90	1.620		

Table E.4. Duncan post hoc test of number of layers' effect on Charpy X impact energy

Charpy X Energy				
Duncan ^{a,b,c}				
No. Layers	N	Subset		
		1	2	3
2	38	3.8681		
3	40		7.5132	
4	39			11.0196
Sig.		1.000	1.000	1.000

Table E.5. Estimates of pick density effect on Charpy X impact energy

Estimates

Dependent Variable: Charpy X Energy

Pick Density	Mean	Std. Error	95% Confidence Interval	
			Lower Bound	Upper Bound
4.87	6.122	.210	5.705	6.538
5.48	7.521	.217	7.090	7.951
5.85	8.457	.198	8.063	8.851

Table E.6. ANOVA of pick density effect on Charpy X impact energy

Univariate Tests

Dependent Variable: Charpy X Energy

	Sum of Squares	df	Mean Square	F	Sig.
Contrast	106.708	2	53.354	32.944	.000
Error	145.757	90	1.620		

Table E.7. Duncan post hoc test of pick density effect on Charpy X impact energy

Charpy X Energy

Duncan^{a,b,c}

Pick Density	N	Subset		
		1	2	3
4.87	39	6.4119		
5.48	36		7.5964	
5.85	42			8.4225
Sig.		1.000	1.000	1.000

Table E.8. Estimates of weave pattern effect on Charpy X impact energy

Estimates

Dependent Variable: Charpy X Energy

Weave	Mean	Std. Error	95% Confidence Interval	
			Lower Bound	Upper Bound
Plain	7.852	.192	7.470	8.234
Twill	7.073	.215	6.645	7.500
Basket	7.176	.217	6.745	7.606

Table E.9. ANOVA of weave pattern effect on Charpy X impact energy

Univariate Tests

Dependent Variable: Charpy X Energy

	Sum of Squares	df	Mean Square	F	Sig.
Contrast	14.415	2	7.207	4.450	.014
Error	145.757	90	1.620		

Table E.10. Duncan post hoc test of weave pattern effect on Charpy X impact energy

Charpy X Energy

Duncan^{a,b,c}

Weave	N	Subset	
		1	2
Twill	36	7.0350	
Basket	36	7.5388	7.5388
Plain	45		7.8360
Sig.		.086	.308

Table E.11. Between-subject effect on Charpy X impact energy/ thickness

Tests of Between-Subjects Effects

Dependent Variable: Charpy X Energy/ Thickness

Source	Type III Sum of Squares	df	Mean Square	F	Sig.
Corrected Model	53689049.650 ^a	26	2064963.448	9.757	.000
Intercept	780556240.000	1	780556240.000	3688.213	.000
F1	29959372.770	2	14979686.380	70.781	.000
F2	10027816.100	2	5013908.052	23.691	.000
F3	1361440.913	2	680720.457	3.216	.045
F1 * F2	773125.372	4	193281.343	.913	.460
F1 * F3	2014279.506	4	503569.877	2.379	.058
F2 * F3	5156682.441	4	1289170.610	6.091	.000
F1 * F2 * F3	2358943.583	8	294867.948	1.393	.210
Error	19047182.200	90	211635.358		
Total	911160496.000	117			
Corrected Total	72736231.850	116			

Table E.12. Estimates of number of layers' effect on Charpy X impact energy/ thickness

Estimates

Dependent Variable: Charpy X Energy/ Thickness

No. Layers	Mean	Std. Error	95% Confidence Interval	
			Lower Bound	Upper Bound
2	1978.148	76.957	1825.261	2131.036
3	2691.962	74.073	2544.802	2839.121
4	3254.399	74.950	3105.498	3403.300

Table E.13. ANOVA of number of layers' effect on Charpy X impact energy/ thickness

Univariate Tests

Dependent Variable: Charpy X Energy/ Thickness

	Sum of Squares	df	Mean Square	F	Sig.
Contrast	29959372.770	2	14979686.380	70.781	.000
Error	19047182.200	90	211635.358		

Table E.14. Duncan post hoc test of number of layers' effect on Charpy X impact energy/ thickness

Charpy X Energy/ Thickness

Duncan^{a,b,c}

No. Layers	N	Subset		
		1	2	3
2	38	1991.3508		
3	40		2751.1209	
4	39			3268.8735
Sig.		1.000	1.000	1.000

Table E.15. Estimates of pick density effect on Charpy X impact energy/ thickness

Estimates

Dependent Variable: Charpy X Energy/ Thickness

Pick Density	Mean	Std. Error	95% Confidence Interval	
			Lower Bound	Upper Bound
4.87	2245.339	75.816	2094.716	2395.961
5.48	2725.263	78.358	2569.590	2880.935
5.85	2953.907	71.683	2811.496	3096.318

Table E.16. ANOVA of pick density effect on Charpy X impact energy/ thickness

Univariate Tests

Dependent Variable: Charpy X Energy/ Thickness

	Sum of Squares	df	Mean Square	F	Sig.
Contrast	10027816.100	2	5013908.052	23.691	.000
Error	19047182.200	90	211635.358		

Table E.17. Duncan post hoc test of pick density effect on Charpy X impact energy/ thickness

Charpy X Energy/ Thickness

Duncan^{a,b,c}

Pick Density	N	Subset		
		1	2	3
4.87	39	2315.1237		
5.48	36		2736.6216	
5.85	42			2961.7627
Sig.		1.000	1.000	1.000

Table E.18. Estimates of weave pattern effect on Charpy X impact energy/ thickness

Estimates

Dependent Variable: Charpy X Energy/ Thickness

Weave	Mean	Std. Error	95% Confidence Interval	
			Lower Bound	Upper Bound
Plain	2788.321	69.524	2650.198	2926.443
Twill	2597.899	77.801	2443.334	2752.463
Basket	2538.289	78.358	2382.617	2693.962

Table E.19. ANOVA of weave pattern effect on Charpy X impact energy/ thickness

Univariate Tests

Dependent Variable: Charpy X Energy/ Thickness

	Sum of Squares	df	Mean Square	F	Sig.
Contrast	1361440.913	2	680720.457	3.216	.045
Error	19047182.200	90	211635.358		

Table E.20. Duncan post hoc test of weave pattern effect on Charpy X impact energy/ thickness

Charpy X Energy/ Thickness

Duncan^{a,b,c}

Weave	N	Subset
		1
Twill	36	2598.1403
Basket	36	2613.7867
Plain	45	2790.5081
Sig.		.085

Table E.21. Between-subject effect on Charpy X impact energy/ composite areal density

Tests of Between-Subjects Effects

Dependent Variable: Charpy X Energy/ Composite Areal Density

Source	Type III Sum of Squares	df	Mean Square	F	Sig.
Corrected Model	15.014 ^a	26	.577	8.722	.000
Intercept	240.348	1	240.348	3630.300	.000
F1	8.406	2	4.203	63.480	.000
F2	2.740	2	1.370	20.696	.000
F3	.481	2	.240	3.632	.030
F1 * F2	.178	4	.044	.671	.614
F1 * F3	.671	4	.168	2.534	.046
F2 * F3	1.416	4	.354	5.347	.001
F1 * F2 * F3	.802	8	.100	1.514	.164
Error	5.959	90	.066		
Total	280.131	117			
Corrected Total	20.972	116			

Table E.22. Estimates of number of layers' effect on Charpy X impact energy/ composite areal density

Estimates

Dependent Variable: Charpy X Energy/ Composite Areal Density

No. Layers	Mean	Std. Error	95% Confidence Interval	
			Lower Bound	Upper Bound
2	1.111	.043	1.026	1.197
3	1.500	.041	1.417	1.582
4	1.786	.042	1.703	1.870

Table E.23. ANOVA of number of layers' effect on Charpy X impact energy/ composite areal density

Univariate Tests

Dependent Variable: Charpy X Energy/ Composite Areal Density

	Sum of Squares	df	Mean Square	F	Sig.
Contrast	8.406	2	4.203	63.480	.000
Error	5.959	90	.066		

Table E.24. Duncan post hoc test of number of layers' effect on Charpy X impact energy/ composite areal density

Charpy X Energy/ Composite Areal Density

Duncan^{a,b,c}

No. Layers	N	Subset		
		1	2	3
2	38	1.1263		
3	40		1.5341	
4	39			1.7941
Sig.		1.000	1.000	1.000

Table E.25. Estimates of pick density effect on Charpy X impact energy/ composite areal density

Estimates				
Dependent Variable: Charpy X Energy/ Composite Areal Density				
Pick Density	Mean	Std. Error	95% Confidence Interval	
			Lower Bound	Upper Bound
4.87	1.259	.042	1.175	1.343
5.48	1.508	.044	1.421	1.596
5.85	1.630	.040	1.550	1.709

Table E.26. ANOVA of pick density effect on Charpy X impact energy/ composite areal density

Univariate Tests					
Dependent Variable: Charpy X Energy/ Composite Areal Density					
	Sum of Squares	df	Mean Square	F	Sig.
Contrast	2.740	2	1.370	20.696	.000
Error	5.959	90	.066		

Table E.27. Duncan post hoc test of pick density effect on Charpy X impact energy/ composite areal density

Charpy X Energy/ Composite Areal Density			
Duncan ^{a,b,c}			
Pick Density	N	Subset	
		1	2
4.87	39	1.2991	
5.48	36		1.5221
5.85	42		1.6350
Sig.		1.000	.056

Table E.28. Estimates of weave pattern effect on Charpy X impact energy/ composite areal density

Estimates

Dependent Variable: Charpy X Energy/ Composite Areal Density

Weave	Mean	Std. Error	95% Confidence Interval	
			Lower Bound	Upper Bound
Plain	1.555	.039	1.478	1.632
Twill	1.419	.044	1.333	1.506
Basket	1.423	.044	1.336	1.510

Table E.29. ANOVA of weave pattern effect on Charpy X impact energy/ composite areal density

Univariate Tests

Dependent Variable: Charpy X Energy/ Composite Areal Density

	Sum of Squares	df	Mean Square	F	Sig.
Contrast	.481	2	.240	3.632	.030
Error	5.959	90	.066		

Table E.30. Duncan post hoc test of weave pattern effect on Charpy X impact energy/ composite areal density

Charpy X Energy/ Composite Areal Density

Duncan^{a,b,c}

Weave	N	Subset	
		1	2
Twill	36	1.4208	
Basket	36	1.4727	1.4727
Plain	45		1.5548
Sig.		.379	.164

Table E.31. Between-subject effect on Charpy X impact energy/ preform areal density

Tests of Between-Subjects Effects

Dependent Variable: Charpy X ENergy/ Preform Areal Denisty

Source	Type III Sum of Squares	df	Mean Square	F	Sig.
Corrected Model	31.233 ^a	26	1.201	9.217	.000
Intercept	477.466	1	477.466	3663.367	.000
F1	16.683	2	8.342	64.002	.000
F2	4.906	2	2.453	18.823	.000
F3	1.148	2	.574	4.402	.015
F1 * F2	.495	4	.124	.949	.440
F1 * F3	1.441	4	.360	2.763	.032
F2 * F3	3.683	4	.921	7.065	.000
F1 * F2 * F3	2.035	8	.254	1.952	.062
Error	11.730	90	.130		
Total	558.776	117			
Corrected Total	42.963	116			

Table E.32. Estimates of number of layers' effect on Charpy X impact energy/ preform areal density

Estimates				
Dependent Variable: Charpy X Energy/ Preform Areal Density				
No. Layers	Mean	Std. Error	95% Confidence Interval	
			Lower Bound	Upper Bound
2	1.559	.060	1.439	1.679
3	2.132	.058	2.016	2.247
4	2.507	.059	2.390	2.624

Table E.33. ANOVA of number of layers' effect on Charpy X impact energy/ preform areal density

Univariate Tests					
Dependent Variable: Charpy X Energy/ Preform Areal Density					
	Sum of Squares	df	Mean Square	F	Sig.
Contrast	16.683	2	8.342	64.002	.000
Error	11.730	90	.130		

Table E.34. Duncan post hoc test of number of layers' effect on Charpy X impact energy/ preform areal density

Charpy X Energy/ Preform Areal Density				
Duncan ^{a,b,c}				
No. Layers	N	Subset		
		1	2	3
2	38	1.5811		
3	40		2.1847	
4	39			2.5178
Sig.		1.000	1.000	1.000

Table E.35. Estimates of pick density effect on Charpy X impact energy/ preform areal density

Estimates				
Dependent Variable: Charpy X Energy/ Preform Areal Density				
Pick Density	Mean	Std. Error	95% Confidence Interval	
			Lower Bound	Upper Bound
4.87	1.791	.059	1.673	1.909
5.48	2.119	.061	1.997	2.241
5.85	2.288	.056	2.176	2.400

Table E.36. ANOVA of pick density effect on Charpy X impact energy/ preform areal density

Univariate Tests					
Dependent Variable: Charpy X ENergy/ Preform Areal Denisty					
	Sum of Squares	df	Mean Square	F	Sig.
Contrast	4.906	2	2.453	18.823	.000
Error	11.730	90	.130		

Table E.37. Duncan post hoc test of pick density effect on Charpy X impact energy/ preform areal density

Charpy X Energy/ Preform Areal Density			
Duncan ^{a,b,c}			
Pick Density	N	Subset	
		1	2
4.87	39	1.8465	
5.48	36		2.1427
5.85	42		2.2979
Sig.		1.000	.061

Table E.38. Estimates of weave pattern effect on Charpy X impact energy/ preform areal density

Estimates

Dependent Variable: Charpy X Energy/ Preform Areal Density

Weave	Mean	Std. Error	95% Confidence Interval	
			Lower Bound	Upper Bound
Plain	2.204	.055	2.095	2.312
Twill	2.000	.061	1.879	2.121
Basket	1.994	.061	1.872	2.116

Table E.39. ANOVA of weave pattern effect on Charpy X impact energy/ preform areal density

Univariate Tests

Dependent Variable: Charpy X Energy/ Preform Areal Density

	Sum of Squares	df	Mean Square	F	Sig.
Contrast	1.148	2	.574	4.402	.015
Error	11.730	90	.130		

Table E.40. Duncan post hoc test of weave pattern effect on Charpy X impact energy/ preform areal density

Charpy X energy/ Preform Areal Density

Duncan^{a,b,c}

Weave	N	Subset	
		1	2
Twill	36	2.0036	
Basket	36	2.0637	2.0637
Plain	45		2.2053
Sig.		.466	.089

APPENDIX F: Statistical correlation between impact energies of Tup, Izod, and Charpy impact tests of all samples for Experiment A

Table F.1. Pearson correlation matrix between Tup, Izod, and Charpy impact energies in Y-axis direction

		Correlations		
		Tup Energy	Izod Energy Y	Charpy Energy Y
Tup Energy	Pearson Correlation	1	.776**	.866**
	Sig. (2-tailed)		.000	.000
	N	27	27	27
Izod Energy Y	Pearson Correlation	.776**	1	.910**
	Sig. (2-tailed)	.000		.000
	N	27	27	27
Charpy Energy Y	Pearson Correlation	.866**	.910**	1
	Sig. (2-tailed)	.000	.000	
	N	27	27	27

Table F.2. Pearson correlation matrix between Tup, Izod, and Charpy impact energies in X-axis direction

		Correlations		
		Tup Energy	Izod Energy X	Charpy Energy X
Tup Energy	Pearson Correlation	1	.882**	.912**
	Sig. (2-tailed)		.000	.000
	N	27	27	27
Izod Energy X	Pearson Correlation	.882**	1	.909**
	Sig. (2-tailed)	.000		.000
	N	27	27	27
Charpy Energy X	Pearson Correlation	.912**	.909**	1
	Sig. (2-tailed)	.000	.000	
	N	27	27	27

Table F.3. Pearson correlation matrix between Tup, Izod, and Charpy impact energies/
thickness in Y-axis direction

		Correlations		
		Tup Energy/ Thickness	Izod Energy/ Thickness Y	Charpy Energy/ Thickness Y
Tup Energy/ Thickness	Pearson Correlation	1	-.147	.338
	Sig. (2-tailed)		.465	.085
	N	27	27	27
Izod Energy/ Thickness Y	Pearson Correlation	-.147	1	.438*
	Sig. (2-tailed)	.465		.022
	N	27	27	27
Charpy Energy/ Thickness Y	Pearson Correlation	.338	.438*	1
	Sig. (2-tailed)	.085	.022	
	N	27	27	27

Table F.4. Pearson correlation matrix between Tup, Izod, and Charpy impact energies/
thickness in X-axis direction

		Correlations		
		Tup Energy/ Thickness	Izod Energy/ Thickness X	Charpy Energy/ Thickness X
Tup Energy/ Thickness	Pearson Correlation	1	.252	.575**
	Sig. (2-tailed)		.204	.002
	N	27	27	27
Izod Energy/ Thickness X	Pearson Correlation	.252	1	.307
	Sig. (2-tailed)	.204		.119
	N	27	27	27
Charpy Energy/ Thickness X	Pearson Correlation	.575**	.307	1
	Sig. (2-tailed)	.002	.119	
	N	27	27	27

Table F.5. Pearson correlation matrix between Tup, Izod, and Charpy impact energies/
composite areal density in Y-axis direction

		Correlations		
		Tup Energy/ Composite Areal Density	Izod Energy/ Composite Areal Density y	Charpy Energy/ Composite Areal Density Y
Tup Energy/ Composite Areal Density	Pearson Correlation	1	-.091	.368
	Sig. (2-tailed)		.651	.059
	N	27	27	27
Izod Energy/ Composite Areal Density y	Pearson Correlation	-.091	1	.406*
	Sig. (2-tailed)	.651		.035
	N	27	27	27
Charpy Energy/ Composite Areal Density Y	Pearson Correlation	.368	.406*	1
	Sig. (2-tailed)	.059	.035	
	N	27	27	27

Table F.6. Pearson correlation matrix between Tup, Izod, and Charpy impact energies/
composite areal density in X-axis direction

		Correlations		
		Tup Energy/ Composite Areal Density	Izod Energy/ Composite Areal Density X	Charpy Energy/ Composite Areal Density X
Tup Energy/ Composite Areal Density	Pearson Correlation	1	.195	.591**
	Sig. (2-tailed)		.331	.001
	N	27	27	27
Izod Energy/ Composite Areal Density X	Pearson Correlation	.195	1	.230
	Sig. (2-tailed)	.331		.248
	N	27	27	27
Charpy Energy/ Composite Areal Density X	Pearson Correlation	.591**	.230	1
	Sig. (2-tailed)	.001	.248	
	N	27	27	27

Table F.7. Pearson correlation matrix between Tup, Izod, and Charpy impact energies/
preform areal density in Y-axis direction

		Correlations		
		Tup Energy/ Preform Areal Density	Izod Energy/ Preform Areal Density Y	Charpy Energy/ Preform Areal Density Y
Tup Energy/ Preform Areal Density	Pearson Correlation	1	-.026	.345
	Sig. (2-tailed)		.899	.078
	N	27	27	27
Izod Energy/ Preform Areal Density Y	Pearson Correlation	-.026	1	.409*
	Sig. (2-tailed)	.899		.034
	N	27	27	27
Charpy Energy/ Preform Areal Density Y	Pearson Correlation	.345	.409*	1
	Sig. (2-tailed)	.078	.034	
	N	27	27	27

Table F.8. Pearson correlation matrix between Tup, Izod, and Charpy impact energies/
preform areal density in X-axis direction

		Correlations		
		Tup Energy/ Preform Areal Density	Izod Energy/ Preform Areal Density X	Charpy Energy/ Preform Areal Density X
Tup Energy/ Preform Areal Density	Pearson Correlation	1	.162	.500**
	Sig. (2-tailed)		.421	.008
	N	27	27	27
Izod Energy/ Preform Areal Density X	Pearson Correlation	.162	1	.244
	Sig. (2-tailed)	.421		.221
	N	27	27	27
Charpy Energy/ Preform Areal Density X	Pearson Correlation	.500**	.244	1
	Sig. (2-tailed)	.008	.221	
	N	27	27	27

APPENDIX G: Statistical correlation between impact energies of Tup, Izod, and Charpy impact tests of plain samples for Experiment A

Table G.1. Pearson correlation matrix between Tup, Izod, and Charpy impact energies of plain samples in Y-axis direction

		Correlations		
		Tup Energy	Izod Energy Y	Charpy Energy Y
Tup Energy	Pearson Correlation	1	.829**	.946**
	Sig. (2-tailed)		.006	.000
	N	9	9	9
Izod Energy Y	Pearson Correlation	.829**	1	.918**
	Sig. (2-tailed)	.006		.000
	N	9	9	9
Charpy Energy Y	Pearson Correlation	.946**	.918**	1
	Sig. (2-tailed)	.000	.000	
	N	9	9	9

Table G.2. Pearson correlation matrix between Tup, Izod, and Charpy impact energies of plain samples in X-axis direction

		Correlations		
		Tup Energy	Izod Energy X	Charpy Energy X
Tup Energy	Pearson Correlation	1	.900**	.934**
	Sig. (2-tailed)		.001	.000
	N	9	9	9
Izod Energy X	Pearson Correlation	.900**	1	.910**
	Sig. (2-tailed)	.001		.001
	N	9	9	9
Charpy Energy X	Pearson Correlation	.934**	.910**	1
	Sig. (2-tailed)	.000	.001	
	N	9	9	9

Table G.3. Pearson correlation matrix between Tup, Izod, and Charpy impact energies/
thickness of plain samples in Y-axis direction

		Correlations		
		Tup Energy/ Thickness	Izod Energy/ Thickness Y	Charpy Energy/ Thickness Y
Tup Energy/ Thickness	Pearson Correlation	1	-.718*	-.340
	Sig. (2-tailed)		.030	.370
	N	9	9	9
Izod Energy/ Thickness Y	Pearson Correlation	-.718*	1	.670*
	Sig. (2-tailed)	.030		.048
	N	9	9	9
Charpy Energy/ Thickness Y	Pearson Correlation	-.340	.670*	1
	Sig. (2-tailed)	.370	.048	
	N	9	9	9

Table G.4. Pearson correlation matrix between Tup, Izod, and Charpy impact energies/
thickness of plain samples in X-axis direction

		Correlations		
		Tup Energy/ Thickness	Izod Energy/ Thickness X	Charpy Energy/ Thickness X
Tup Energy/ Thickness	Pearson Correlation	1	-.200	-.014
	Sig. (2-tailed)		.606	.972
	N	9	9	9
Izod Energy/ Thickness X	Pearson Correlation	-.200	1	.385
	Sig. (2-tailed)	.606		.307
	N	9	9	9
Charpy Energy/ Thickness X	Pearson Correlation	-.014	.385	1
	Sig. (2-tailed)	.972	.307	
	N	9	9	9

Table G.5. Pearson correlation matrix between Tup, Izod, and Charpy impact energies/
composite areal density of plain samples in Y-axis direction

		Correlations		
		Tup Energy/ Composite Areal Density	Izod Energy/ Composite Areal Density y	Charpy Energy/ Composite Areal Density Y
Tup Energy/ Composite Areal Density	Pearson Correlation	1	-.660	-.003
	Sig. (2-tailed)		.053	.994
	N	9	9	9
Izod Energy/ Composite Areal Density y	Pearson Correlation	-.660	1	.499
	Sig. (2-tailed)	.053		.172
	N	9	9	9
Charpy Energy/ Composite Areal Density Y	Pearson Correlation	-.003	.499	1
	Sig. (2-tailed)	.994	.172	
	N	9	9	9

Table G.6. Pearson correlation matrix between Tup, Izod, and Charpy impact energies/
composite areal density of plain samples in X-axis direction

		Correlations		
		Tup Energy/ Composite Areal Density	Izod Energy/ Composite Areal Density X	Charpy Energy/ Composite Areal Density X
Tup Energy/ Composite Areal Density	Pearson Correlation	1	-.243	.144
	Sig. (2-tailed)		.528	.711
	N	9	9	9
Izod Energy/ Composite Areal Density X	Pearson Correlation	-.243	1	.128
	Sig. (2-tailed)	.528		.742
	N	9	9	9
Charpy Energy/ Composite Areal Density X	Pearson Correlation	.144	.128	1
	Sig. (2-tailed)	.711	.742	
	N	9	9	9

Table G.7. Pearson correlation matrix between Tup, Izod, and Charpy impact energies/
preform areal density of plain samples in Y-axis direction

		Correlations		
		Tup Energy/ Preform Areal Density	Izod Energy/ Preform Areal Density Y	Charpy Energy/ Preform Areal Density Y
Tup Energy/ Preform Areal Density	Pearson Correlation	1	-.821**	-.395
	Sig. (2-tailed)		.007	.293
	N	9	9	9
Izod Energy/ Preform Areal Density Y	Pearson Correlation	-.821**	1	.496
	Sig. (2-tailed)	.007		.175
	N	9	9	9
Charpy Energy/ Preform Areal Density Y	Pearson Correlation	-.395	.496	1
	Sig. (2-tailed)	.293	.175	
	N	9	9	9

Table G.8. Pearson correlation matrix between Tup, Izod, and Charpy impact energies/
preform areal density of plain samples in X-axis direction

		Correlations		
		Tup Energy/ Preform Areal Density	Izod Energy/ Preform Areal Density X	Charpy Energy/ Preform Areal Density X
Tup Energy/ Preform Areal Density	Pearson Correlation	1	-.174	-.388
	Sig. (2-tailed)		.654	.303
	N	9	9	9
Izod Energy/ Preform Areal Density X	Pearson Correlation	-.174	1	.157
	Sig. (2-tailed)	.654		.686
	N	9	9	9
Charpy Energy/ Preform Areal Density X	Pearson Correlation	-.388	.157	1
	Sig. (2-tailed)	.303	.686	
	N	9	9	9

APPENDIX H: Statistical correlation between impact energies of Tup, Izod, and Charpy impact tests of twill samples for Experiment A

Table H.1. Pearson correlation matrix between Tup, Izod, and Charpy impact energies of twill samples in Y-axis direction

		Correlations		
		Tup Energy	Izod Energy Y	Charpy Energy Y
Tup Energy	Pearson Correlation	1	.843**	.933**
	Sig. (2-tailed)		.004	.000
	N	9	9	9
Izod Energy Y	Pearson Correlation	.843**	1	.917**
	Sig. (2-tailed)	.004		.000
	N	9	9	9
Charpy Energy Y	Pearson Correlation	.933**	.917**	1
	Sig. (2-tailed)	.000	.000	
	N	9	9	9

Table H.2. Pearson correlation matrix between Tup, Izod, and Charpy impact energies of twill samples in X-axis direction

		Correlations		
		Tup Energy	Izod Energy X	Charpy Energy X
Tup Energy	Pearson Correlation	1	.962**	.959**
	Sig. (2-tailed)		.000	.000
	N	9	9	9
Izod Energy X	Pearson Correlation	.962**	1	.912**
	Sig. (2-tailed)	.000		.001
	N	9	9	9
Charpy Energy X	Pearson Correlation	.959**	.912**	1
	Sig. (2-tailed)	.000	.001	
	N	9	9	9

Table H.3. Pearson correlation matrix between Tup, Izod, and Charpy impact energies/
thickness of twill samples in Y-axis direction

		Correlations		
		Tup Energy/ Thickness	Izod Energy/ Thickness Y	Charpy Energy/ Thickness Y
Tup Energy/ Thickness	Pearson Correlation	1	.103	.545
	Sig. (2-tailed)		.792	.129
	N	9	9	9
Izod Energy/ Thickness Y	Pearson Correlation	.103	1	.334
	Sig. (2-tailed)	.792		.380
	N	9	9	9
Charpy Energy/ Thickness Y	Pearson Correlation	.545	.334	1
	Sig. (2-tailed)	.129	.380	
	N	9	9	9

Table H.4. Pearson correlation matrix between Tup, Izod, and Charpy impact energies/
thickness of twill samples in X-axis direction

		Correlations		
		Tup Energy/ Thickness	Izod Energy/ Thickness X	Charpy Energy/ Thickness X
Tup Energy/ Thickness	Pearson Correlation	1	-.012	.741*
	Sig. (2-tailed)		.975	.022
	N	9	9	9
Izod Energy/ Thickness X	Pearson Correlation	-.012	1	-.306
	Sig. (2-tailed)	.975		.424
	N	9	9	9
Charpy Energy/ Thickness X	Pearson Correlation	.741*	-.306	1
	Sig. (2-tailed)	.022	.424	
	N	9	9	9

Table H.5. Pearson correlation matrix between Tup, Izod, and Charpy impact energies/
composite areal density of twill samples in Y-axis direction

		Correlations		
		Tup Energy/ Composite Areal Density	Izod Energy/ Composite Areal Density y	Charpy Energy/ Composite Areal Density Y
Tup Energy/ Composite Areal Density	Pearson Correlation	1	.122	.563
	Sig. (2-tailed)		.754	.114
	N	9	9	9
Izod Energy/ Composite Areal Density y	Pearson Correlation	.122	1	.326
	Sig. (2-tailed)	.754		.392
	N	9	9	9
Charpy Energy/ Composite Areal Density Y	Pearson Correlation	.563	.326	1
	Sig. (2-tailed)	.114	.392	
	N	9	9	9

Table H.6. Pearson correlation matrix between Tup, Izod, and Charpy impact energies/
composite areal density of twill samples in X-axis direction

		Correlations		
		Tup Energy/ Composite Areal Density	Izod Energy/ Composite Areal Density X	Charpy Energy/ Composite Areal Density X
Tup Energy/ Composite Areal Density	Pearson Correlation	1	-.063	.679*
	Sig. (2-tailed)		.872	.044
	N	9	9	9
Izod Energy/ Composite Areal Density X	Pearson Correlation	-.063	1	-.394
	Sig. (2-tailed)	.872		.294
	N	9	9	9
Charpy Energy/ Composite Areal Density X	Pearson Correlation	.679*	-.394	1
	Sig. (2-tailed)	.044	.294	
	N	9	9	9

Table H.7. Pearson correlation matrix between Tup, Izod, and Charpy impact energies/ preform areal density of twill samples in Y-axis direction

		Correlations		
		Tup Energy/ Preform Areal Density	Izod Energy/ Preform Areal Density Y	Charpy Energy/ Preform Areal Density Y
Tup Energy/ Preform Areal Density	Pearson Correlation	1	.202	.603
	Sig. (2-tailed)		.602	.085
	N	9	9	9
Izod Energy/ Preform Areal Density Y	Pearson Correlation	.202	1	.328
	Sig. (2-tailed)	.602		.388
	N	9	9	9
Charpy Energy/ Preform Areal Density Y	Pearson Correlation	.603	.328	1
	Sig. (2-tailed)	.085	.388	
	N	9	9	9

Table H.8. Pearson correlation matrix between Tup, Izod, and Charpy impact energies/ preform areal density of twill samples in X-axis direction

		Correlations		
		Tup Energy/ Preform Areal Density	Izod Energy/ Preform Areal Density X	Charpy Energy/ Preform Areal Density X
Tup Energy/ Preform Areal Density	Pearson Correlation	1	-.025	.673*
	Sig. (2-tailed)		.948	.047
	N	9	9	9
Izod Energy/ Preform Areal Density X	Pearson Correlation	-.025	1	-.411
	Sig. (2-tailed)	.948		.272
	N	9	9	9
Charpy Energy/ Preform Areal Density X	Pearson Correlation	.673*	-.411	1
	Sig. (2-tailed)	.047	.272	
	N	9	9	9

APPENDIX I: Statistical correlation between impact energies of Tup, Izod, and Charpy impact tests of basket samples for Experiment A

Table I.1. Pearson correlation matrix between Tup, Izod, and Charpy impact energies of basket samples in Y-axis direction

		Correlations		
		Tup Energy	Izod Energy Y	Charpy Energy Y
Tup Energy	Pearson Correlation	1	.761*	.878**
	Sig. (2-tailed)		.017	.002
	N	9	9	9
Izod Energy Y	Pearson Correlation	.761*	1	.913**
	Sig. (2-tailed)	.017		.001
	N	9	9	9
Charpy Energy Y	Pearson Correlation	.878**	.913**	1
	Sig. (2-tailed)	.002	.001	
	N	9	9	9

Table I.2. Pearson correlation matrix between Tup, Izod, and Charpy impact energies of basket samples in X-axis direction

		Correlations		
		Tup Energy	Izod Energy X	Charpy Energy X
Tup Energy	Pearson Correlation	1	.910**	.968**
	Sig. (2-tailed)		.001	.000
	N	9	9	9
Izod Energy X	Pearson Correlation	.910**	1	.928**
	Sig. (2-tailed)	.001		.000
	N	9	9	9
Charpy Energy X	Pearson Correlation	.968**	.928**	1
	Sig. (2-tailed)	.000	.000	
	N	9	9	9

Table I.3. Pearson correlation matrix between Tup, Izod, and Charpy impact energies/
thickness of basket samples in Y-axis direction

		Correlations		
		Tup Energy/ Thickness	Izod Energy/ Thickness Y	Charpy Energy/ Thickness Y
Tup Energy/ Thickness	Pearson Correlation	1	-.112	.619
	Sig. (2-tailed)		.774	.076
	N	9	9	9
Izod Energy/ Thickness Y	Pearson Correlation	-.112	1	.376
	Sig. (2-tailed)	.774		.319
	N	9	9	9
Charpy Energy/ Thickness Y	Pearson Correlation	.619	.376	1
	Sig. (2-tailed)	.076	.319	
	N	9	9	9

Table I.4. Pearson correlation matrix between Tup, Izod, and Charpy impact energies/
thickness of basket samples in X-axis direction

		Correlations		
		Tup Energy/ Thickness	Izod Energy/ Thickness X	Charpy Energy/ Thickness X
Tup Energy/ Thickness	Pearson Correlation	1	.630	.918**
	Sig. (2-tailed)		.069	.000
	N	9	9	9
Izod Energy/ Thickness X	Pearson Correlation	.630	1	.699*
	Sig. (2-tailed)	.069		.036
	N	9	9	9
Charpy Energy/ Thickness X	Pearson Correlation	.918**	.699*	1
	Sig. (2-tailed)	.000	.036	
	N	9	9	9

Table I.5. Pearson correlation matrix between Tup, Izod, and Charpy impact energies/
composite areal density of basket samples in Y-axis direction

		Correlations		
		Tup Energy/ Composite Areal Density	Izod Energy/ Composite Areal Density y	Charpy Energy/ Composite Areal Density Y
Tup Energy/ Composite Areal Density	Pearson Correlation	1	-.012	.577
	Sig. (2-tailed)		.975	.104
	N	9	9	9
Izod Energy/ Composite Areal Density y	Pearson Correlation	-.012	1	.421
	Sig. (2-tailed)	.975		.259
	N	9	9	9
Charpy Energy/ Composite Areal Density Y	Pearson Correlation	.577	.421	1
	Sig. (2-tailed)	.104	.259	
	N	9	9	9

Table I.6. Pearson correlation matrix between Tup, Izod, and Charpy impact energies/
composite areal density of basket samples in X-axis direction

		Correlations		
		Tup Energy/ Composite Areal Density	Izod Energy/ Composite Areal Density X	Charpy Energy/ Composite Areal Density X
Tup Energy/ Composite Areal Density	Pearson Correlation	1	.587	.901**
	Sig. (2-tailed)		.096	.001
	N	9	9	9
Izod Energy/ Composite Areal Density X	Pearson Correlation	.587	1	.645
	Sig. (2-tailed)	.096		.060
	N	9	9	9
Charpy Energy/ Composite Areal Density X	Pearson Correlation	.901**	.645	1
	Sig. (2-tailed)	.001	.060	
	N	9	9	9

Table I.7. Pearson correlation matrix between Tup, Izod, and Charpy impact energies/
preform areal density of basket samples in Y-axis direction

		Correlations		
		Tup Energy/ Preform Areal Density	Izod Energy/ Preform Areal Density Y	Charpy Energy/ Preform Areal Density Y
Tup Energy/ Preform Areal Density	Pearson Correlation	1	.082	.572
	Sig. (2-tailed)		.833	.108
	N	9	9	9
Izod Energy/ Preform Areal Density Y	Pearson Correlation	.082	1	.410
	Sig. (2-tailed)	.833		.273
	N	9	9	9
Charpy Energy/ Preform Areal Density Y	Pearson Correlation	.572	.410	1
	Sig. (2-tailed)	.108	.273	
	N	9	9	9

Table I.8. Pearson correlation matrix between Tup, Izod, and Charpy impact energies/
preform areal density of basket samples in X-axis direction

		Correlations		
		Tup Energy/ Preform Areal Density	Izod Energy/ Preform Areal Density X	Charpy Energy/ Preform Areal Density X
Tup Energy/ Preform Areal Density	Pearson Correlation	1	.435	.853**
	Sig. (2-tailed)		.242	.003
	N	9	9	9
Izod Energy/ Preform Areal Density X	Pearson Correlation	.435	1	.604
	Sig. (2-tailed)	.242		.085
	N	9	9	9
Charpy Energy/ Preform Areal Density X	Pearson Correlation	.853**	.604	1
	Sig. (2-tailed)	.003	.085	
	N	9	9	9

APPENDIX J: Statistical correlation between impact energies of Tup, Izod, and Charpy impact tests of balanced samples for Experiment A

Table J.1. Pearson correlation matrix between Tup, Izod, and Charpy impact energies of balanced samples in Y-axis direction

		Correlations		
		Tup Energy	Izod Energy Y	Charpy Energy Y
Tup Energy	Pearson Correlation	1	.671*	.928**
	Sig. (2-tailed)		.048	.000
	N	9	9	9
Izod Energy Y	Pearson Correlation	.671*	1	.856**
	Sig. (2-tailed)	.048		.003
	N	9	9	9
Charpy Energy Y	Pearson Correlation	.928**	.856**	1
	Sig. (2-tailed)	.000	.003	
	N	9	9	9

Table J.2. Pearson correlation matrix between Tup, Izod, and Charpy impact energies of balanced samples in X-axis direction

		Correlations		
		Tup Energy	Izod Energy X	Charpy Energy X
Tup Energy	Pearson Correlation	1	.896**	.939**
	Sig. (2-tailed)		.001	.000
	N	9	9	9
Izod Energy X	Pearson Correlation	.896**	1	.955**
	Sig. (2-tailed)	.001		.000
	N	9	9	9
Charpy Energy X	Pearson Correlation	.939**	.955**	1
	Sig. (2-tailed)	.000	.000	
	N	9	9	9

Table J.3. Pearson correlation matrix between Tup, Izod, and Charpy impact energies/
thickness of balanced samples in Y-axis direction

		Correlations		
		Tup Energy/ Thickness	Izod Energy/ Thickness Y	Charpy Energy/ Thickness Y
Tup Energy/ Thickness	Pearson Correlation	1	-.617	.624
	Sig. (2-tailed)		.077	.073
	N	9	9	9
Izod Energy/ Thickness Y	Pearson Correlation	-.617	1	-.339
	Sig. (2-tailed)	.077		.373
	N	9	9	9
Charpy Energy/ Thickness Y	Pearson Correlation	.624	-.339	1
	Sig. (2-tailed)	.073	.373	
	N	9	9	9

Table J.4. Pearson correlation matrix between Tup, Izod, and Charpy impact energies/
thickness of balanced samples in X-axis direction

		Correlations		
		Tup Energy/ Thickness	Izod Energy/ Thickness X	Charpy Energy/ Thickness X
Tup Energy/ Thickness	Pearson Correlation	1	.137	.703*
	Sig. (2-tailed)		.726	.035
	N	9	9	9
Izod Energy/ Thickness X	Pearson Correlation	.137	1	.012
	Sig. (2-tailed)	.726		.975
	N	9	9	9
Charpy Energy/ Thickness X	Pearson Correlation	.703*	.012	1
	Sig. (2-tailed)	.035	.975	
	N	9	9	9

Table J.5. Pearson correlation matrix between Tup, Izod, and Charpy impact energies/ composite areal density of balanced samples in Y-axis direction

		Correlations		
		Tup Energy/ Composite Areal Density	Izod Energy/ Composite Areal Density y	Charpy Energy/ Composite Areal Density Y
Tup Energy/ Composite Areal Density	Pearson Correlation	1	-.677*	.566
	Sig. (2-tailed)		.045	.112
	N	9	9	9
Izod Energy/ Composite Areal Density y	Pearson Correlation	-.677*	1	-.454
	Sig. (2-tailed)	.045		.220
	N	9	9	9
Charpy Energy/ Composite Areal Density Y	Pearson Correlation	.566	-.454	1
	Sig. (2-tailed)	.112	.220	
	N	9	9	9

Table J.6. Pearson correlation matrix between Tup, Izod, and Charpy impact energies/ composite areal density of balanced samples in X-axis direction

		Correlations		
		Tup Energy/ Composite Areal Density	Izod Energy/ Composite Areal Density X	Charpy Energy/ Composite Areal Density X
Tup Energy/ Composite Areal Density	Pearson Correlation	1	-.102	.675*
	Sig. (2-tailed)		.793	.046
	N	9	9	9
Izod Energy/ Composite Areal Density X	Pearson Correlation	-.102	1	-.137
	Sig. (2-tailed)	.793		.725
	N	9	9	9
Charpy Energy/ Composite Areal Density X	Pearson Correlation	.675*	-.137	1
	Sig. (2-tailed)	.046	.725	
	N	9	9	9

Table J.7. Pearson correlation matrix between Tup, Izod, and Charpy impact energies/
preform areal density of balanced samples in Y-axis direction

		Correlations		
		Tup Energy/ Preform Areal Density	Izod Energy/ Preform Areal Density Y	Charpy Energy/ Preform Areal Density Y
Tup Energy/ Preform Areal Density	Pearson Correlation	1	-.654	.463
	Sig. (2-tailed)		.056	.210
	N	9	9	9
Izod Energy/ Preform Areal Density Y	Pearson Correlation	-.654	1	-.487
	Sig. (2-tailed)	.056		.184
	N	9	9	9
Charpy Energy/ Preform Areal Density Y	Pearson Correlation	.463	-.487	1
	Sig. (2-tailed)	.210	.184	
	N	9	9	9

Table J.8. Pearson correlation matrix between Tup, Izod, and Charpy impact energies/
preform areal density of balanced samples in X-axis direction

		Correlations		
		Tup Energy/ Preform Areal Density	Izod Energy/ Preform Areal Density X	Charpy Energy/ Preform Areal Density X
Tup Energy/ Preform Areal Density	Pearson Correlation	1	-.025	.544
	Sig. (2-tailed)		.949	.130
	N	9	9	9
Izod Energy/ Preform Areal Density X	Pearson Correlation	-.025	1	-.098
	Sig. (2-tailed)	.949		.802
	N	9	9	9
Charpy Energy/ Preform Areal Density X	Pearson Correlation	.544	-.098	1
	Sig. (2-tailed)	.130	.802	
	N	9	9	9

APPENDIX K: Statistical analysis of tensile results from Experiment B

Table K.1. ANOVA of Z: Y-yarns/ layer effect on tensile modulus in Y-direction

Tests of Between-Subjects Effects

Dependent Variable: Modulus

Source	Type III Sum of Squares	df	Mean Square	F	Sig.
Corrected Model	103.919 ^a	3	34.640	2.440	.115
Intercept	6654.680	1	6654.680	468.810	.000
ZtoY	103.919	3	34.640	2.440	.115
Error	170.338	12	14.195		
Total	7233.521	16			
Corrected Total	274.256	15			

Table K.2. Estimates of Z: Y-yarns/ layer effect on tensile modulus in Y-direction

1. Z:Y

Dependent Variable: Modulus

Z:Y	Mean	Std. Error	95% Confidence Interval	
			Lower Bound	Upper Bound
1:1	16.761	1.884	12.656	20.865
1:2	20.435	2.175	15.695	25.174
1:3	22.425	1.685	18.754	26.096
0:1	23.305	1.884	19.201	27.409

Table K.3. Duncan post hoc test of Z: Y-yarns/ layer effect on tensile modulus in Y-direction

Modulus

Duncan^{a,b,c}

Z:Y	N	Subset	
		1	2
1:1	4	16.7605	
1:2	3	20.4346	20.4346
1:3	5	22.4247	22.4247
0:1	4		23.3050
Sig.		.069	.333

Table K.4. ANOVA of Z: Y-yarns/ layer effect on tensile failure strain in Y-direction

Tests of Between-Subjects Effects

Dependent Variable: Failure Strain

Source	Type III Sum of Squares	df	Mean Square	F	Sig.
Corrected Model	.617 ^a	3	.206	5.478	.013
Intercept	74.527	1	74.527	1984.611	.000
ZtoY	.617	3	.206	5.478	.013
Error	.451	12	.038		
Total	76.693	16			
Corrected Total	1.068	15			

Table K.5. Estimates of Z: Y-yarns/ layer effect on tensile failure strain in Y-direction

1. Z:Y

Dependent Variable: Failure Strain

Z:Y	Mean	Std. Error	95% Confidence Interval	
			Lower Bound	Upper Bound
1:1	2.200	.097	1.989	2.411
1:2	2.497	.112	2.253	2.740
1:3	2.179	.087	1.991	2.368
0:1	1.899	.097	1.688	2.110

Table K.6. Duncan post hoc test of Z: Y-yarns/ layer effect on tensile failure strain in Y-direction

Failure Strain

Duncan^{a,b,c}

Z:Y	N	Subset	
		1	2
0:1	4	1.8993	
1:3	5	2.1794	2.1794
1:1	4	2.2003	2.2003
1:2	3		2.4967
Sig.		.061	.050

Table K.7. ANOVA of Z: Y-yarns/ layer effect on tensile peak load in Y-direction

Tests of Between-Subjects Effects

Dependent Variable: Peak Load

Source	Type III Sum of Squares	df	Mean Square	F	Sig.
Corrected Model	2692335.897 ^a	3	897445.299	.106	.955
Intercept	23191814740.000	1	23191814740.000	2740.556	.000
ZtoY	2692335.897	3	897445.299	.106	.955
Error	101549392.100	12	8462449.338		
Total	23978297110.000	16			
Corrected Total	104241728.000	15			

Table K.8. Estimates of Z: Y-yarns/ layer effect on tensile peak load in Y-direction

1. Z:Y

Dependent Variable: Peak Load

Z:Y	Mean	Std. Error	95% Confidence Interval	
			Lower Bound	Upper Bound
1:1	38632.430	1454.514	35463.315	41801.544
1:2	39294.210	1679.529	35634.831	42953.589
1:3	38119.758	1300.957	35285.216	40954.300
0:1	38759.530	1454.514	35590.415	41928.645

Table K.9. Duncan post hoc test of Z: Y-yarns/ layer effect on tensile peak load in Y-direction

Peak Load

Duncan^{a,b,c}

Z:Y	N	Subset
1:3	5	38119.7580
1:1	4	38632.4297
0:1	4	38759.5300
1:2	3	39294.2100
Sig.		.612

Table K.10. ANOVA of Z: Y-yarns/ layer effect on tensile load/ thickness in Y-direction

Tests of Between-Subjects Effects

Dependent Variable: Load/ Thickness

Source	Type III Sum of Squares	df	Mean Square	F	Sig.
Corrected Model	1680617.352 ^a	3	560205.784	.592	.632
Intercept	2835171692.000	1	2835171692.000	2993.570	.000
ZtoY	1680617.352	3	560205.784	.592	.632
Error	11365046.050	12	947087.171		
Total	2946965539.000	16			
Corrected Total	13045663.400	15			

Table K.11. Estimates of Z: Y-yarns/ layer effect on tensile load/ thickness in Y-direction

1. Z:Y

Dependent Variable: Load/ Thickness

Z:Y	Mean	Std. Error	95% Confidence Interval	
			Lower Bound	Upper Bound
1:1	13730.357	486.592	12670.164	14790.550
1:2	13625.802	561.868	12401.597	14850.008
1:3	13782.507	435.221	12834.241	14730.772
0:1	12987.829	486.592	11927.636	14048.022

Table K.12. Duncan post hoc test of Z: Y-yarns/ layer effect on tensile load/ thickness in Y-direction

Load/ Thickness

Duncan^{a,b,c}

Z:Y	N	Subset
		1
0:1	4	12987.8286
1:2	3	13625.8025
1:1	4	13730.3567
1:3	5	13782.5067
Sig.		.313

Table K.13. ANOVA of Z: Y-yarns/ layer effect on tensile load/ composite areal density in Y-direction

Tests of Between-Subjects Effects

Dependent Variable: Load/ Composite Areal Density

Source	Type III Sum of Squares	df	Mean Square	F	Sig.
Corrected Model	.777 ^a	3	.259	1.109	.384
Intercept	896.213	1	896.213	3837.363	.000
ZtoY	.777	3	.259	1.109	.384
Error	2.803	12	.234		
Total	926.673	16			
Corrected Total	3.579	15			

Table K.14. Estimates of Z: Y-yarns/ layer effect on tensile load/ composite areal density in Y-direction

1. Z:Y

Dependent Variable: Load/ Composite Areal Density

Z:Y	Mean	Std. Error	95% Confidence Interval	
			Lower Bound	Upper Bound
1:1	7.478	.242	6.952	8.005
1:2	7.920	.279	7.312	8.528
1:3	7.723	.216	7.252	8.194
0:1	7.311	.242	6.784	7.837

Table K.15. Duncan post hoc test of Z: Y-yarns/ layer effect on tensile load/ composite areal density in Y-direction

Load/ Composite Areal Density

Duncan^{a,b,c}

Z:Y	N	Subset 1
0:1	4	7.3106
1:1	4	7.4782
1:3	5	7.7230
1:2	3	7.9199
Sig.		.129

Table K.16. ANOVA of Z: Y-yarns/ layer effect on tensile load/ preform areal density in Y-direction

Tests of Between-Subjects Effects

Dependent Variable: Load/ Preform Areal Density

Source	Type III Sum of Squares	df	Mean Square	F	Sig.
Corrected Model	.397 ^a	3	.132	.179	.909
Intercept	2008.097	1	2008.097	2710.539	.000
ZtoY	.397	3	.132	.179	.909
Error	8.890	12	.741		
Total	2079.049	16			
Corrected Total	9.287	15			

Table K.17. Estimates of Z: Y-yarns/ layer effect on tensile load/ preform areal density in Y-direction

1. Z:Y

Dependent Variable: Load/ Preform Areal Density

Z:Y	Mean	Std. Error	95% Confidence Interval	
			Lower Bound	Upper Bound
1:1	11.198	.430	10.260	12.135
1:2	11.503	.497	10.420	12.586
1:3	11.271	.385	10.433	12.110
0:1	11.580	.430	10.643	12.518

Table K.18. Duncan post hoc test of Z: Y-yarns/ layer effect on tensile load/ preform areal density in Y-direction

Load/ Preform Areal Density

Duncan^{a,b,c}

Z:Y	N	Subset
		1
1:1	4	11.1978
1:3	5	11.2714
1:2	3	11.5030
0:1	4	11.5804
Sig.		.577

Table K.19. ANOVA of Z: Y-yarns/ layer effect on tensile load/ total fiber tex in Y-direction

Tests of Between-Subjects Effects

Dependent Variable: Load/ Total Tex

Source	Type III Sum of Squares	df	Mean Square	F	Sig.
Corrected Model	.002 ^a	3	.001	.248	.861
Intercept	6.738	1	6.738	2701.347	.000
ZtoY	.002	3	.001	.248	.861
Error	.030	12	.002		
Total	6.979	16			
Corrected Total	.032	15			

Table K.20. Estimates of Z: Y-yarns/ layer effect on tensile load/ total fiber tex in Y-direction

1. Z:Y

Dependent Variable: Load/ Total Tex

Z:Y	Mean	Std. Error	95% Confidence Interval	
			Lower Bound	Upper Bound
1:1	.646	.025	.591	.700
1:2	.665	.029	.602	.728
1:3	.654	.022	.605	.703
0:1	.674	.025	.619	.728

Table K.21. Duncan post hoc test of Z: Y-yarns/ layer effect on tensile load/ total fiber tex in Y-direction

Load/ Total Tex

Duncan^{a,b,c}

Z:Y	N	Subset
		1
1:1	4	.6456
1:3	5	.6540
1:2	3	.6652
0:1	4	.6739
Sig.		.478

Table K.22. ANOVA of Z: Y-yarns/ layer effect on tensile modulus in X-direction

Tests of Between-Subjects Effects

Dependent Variable: Modulus

Source	Type III Sum of Squares	df	Mean Square	F	Sig.
Corrected Model	6.164 ^a	3	2.055	.202	.892
Intercept	5315.628	1	5315.628	522.845	.000
ZtoY	6.164	3	2.055	.202	.892
Error	91.501	9	10.167		
Total	5900.362	13			
Corrected Total	97.664	12			

Table K.23. Estimates of Z: Y-yarns/ layer effect on tensile modulus in X-direction

1. Z:Y

Dependent Variable: Modulus

Z:Y	Mean	Std. Error	95% Confidence Interval	
			Lower Bound	Upper Bound
1:1	20.969	1.841	16.805	25.133
1:2	22.128	1.594	18.522	25.735
1:3	20.527	1.594	16.920	24.133
0:1	20.563	2.255	15.463	25.663

Table K.24. Duncan post hoc test of Z: Y-yarns/ layer effect on tensile modulus in X-direction

Modulus

Duncan^{a,b,c}

Z:Y	N	Subset
		1
1:3	4	20.5269
0:1	2	20.5629
1:1	3	20.9690
1:2	4	22.1285
Sig.		.578

Table K.25. ANOVA of Z: Y-yarns/ layer effect on tensile failure strain in X-direction

Tests of Between-Subjects Effects

Dependent Variable: Failure Strain

Source	Type III Sum of Squares	df	Mean Square	F	Sig.
Corrected Model	.093 ^a	3	.031	.713	.568
Intercept	47.910	1	47.910	1103.441	.000
ZtoY	.093	3	.031	.713	.568
Error	.391	9	.043		
Total	53.340	13			
Corrected Total	.484	12			

Table K.26. Estimates of Z: Y-yarns/ layer effect on tensile failure strain in X-direction

1. Z:Y

Dependent Variable: Failure Strain

Z:Y	Mean	Std. Error	95% Confidence Interval	
			Lower Bound	Upper Bound
1:1	1.951	.120	1.679	2.223
1:2	2.133	.104	1.897	2.368
1:3	2.006	.104	1.770	2.242
0:1	1.903	.147	1.570	2.236

Table K.27. Duncan post hoc test of Z: Y-yarns/ layer effect on tensile failure strain in X-direction

Failure Strain

Duncan^{a,b,c}

Z:Y	N	Subset
		1
0:1	2	1.9030
1:1	3	1.9510
1:3	4	2.0060
1:2	4	2.1325
Sig.		.238

Table K.28. ANOVA of Z: Y-yarns/ layer effect on tensile peak load in X-direction

Tests of Between-Subjects Effects

Dependent Variable: Peak Load

Source	Type III Sum of Squares	df	Mean Square	F	Sig.
Corrected Model	12360573.840 ^a	3	4120191.280	1.668	.242
Intercept	14475912610.000	1	14475912610.000	5861.712	.000
ZtoY	12360573.840	3	4120191.280	1.668	.242
Error	22226135.880	9	2469570.654		
Total	15853422870.000	13			
Corrected Total	34586709.720	12			

Table K.29. Estimates of Z: Y-yarns/ layer effect on tensile peak load in X-direction

1. Z:Y

Dependent Variable: Peak Load

Z:Y	Mean	Std. Error	95% Confidence Interval	
			Lower Bound	Upper Bound
1:1	35805.019	907.298	33752.568	37857.471
1:2	35679.362	785.743	33901.887	37456.838
1:3	34229.727	785.743	32452.252	36007.203
0:1	33214.710	1111.209	30700.981	35728.439

Table K.30. Duncan post hoc test of Z: Y-yarns/ layer effect on tensile peak load in X-direction

Peak Load

Duncan^{a,b,c}

Z:Y	N	Subset 1
0:1	2	33214.7100
1:3	4	34229.7275
1:2	4	35679.3625
1:1	3	35805.0192
Sig.		.092

Table K.31. ANOVA of Z: Y-yarns/ layer effect on tensile load/ thickness in X-direction

Tests of Between-Subjects Effects

Dependent Variable: Load/ Thickness

Source	Type III Sum of Squares	df	Mean Square	F	Sig.
Corrected Model	2382183.439 ^a	3	794061.146	1.527	.273
Intercept	1902482313.000	1	1902482313.000	3657.662	.000
ZtoY	2382183.439	3	794061.146	1.527	.273
Error	4681226.113	9	520136.235		
Total	2071527179.000	13			
Corrected Total	7063409.553	12			

Table K.32. Estimates of Z: Y-yarns/ layer effect on tensile load/ thickness in X-direction

1. Z:Y

Dependent Variable: Load/ Thickness

Z:Y	Mean	Std. Error	95% Confidence Interval	
			Lower Bound	Upper Bound
1:1	13339.285	416.388	12397.351	14281.220
1:2	12312.484	360.602	11496.745	13128.223
1:3	12564.358	360.602	11748.618	13380.097
0:1	12148.971	509.969	10995.342	13302.601

Table K.33. Duncan post hoc test of Z: Y-yarns/ layer effect on tensile load/ thickness in X-direction

Load/ Thickness

Duncan^{a,b,c}

Z:Y	N	Subset
		1
0:1	2	12148.9713
1:2	4	12312.4838
1:3	4	12564.3577
1:1	3	13339.2851
Sig.		.091

Table K.34. ANOVA of Z: Y-yarns/ layer effect on tensile load/ composite areal density in X-direction

Tests of Between-Subjects Effects					
Dependent Variable: Load/ Composite Areal Density					
Source	Type III Sum of Squares	df	Mean Square	F	Sig.
Corrected Model	.050 ^a	3	.017	.132	.938
Intercept	602.959	1	602.959	4766.794	.000
ZtoY	.050	3	.017	.132	.938
Error	1.138	9	.126		
Total	655.111	13			
Corrected Total	1.189	12			

Table K.35. Estimates of Z: Y-yarns/ layer effect on tensile load/ composite areal density in X-direction

1. Z:Y				
Dependent Variable: Load/ Composite Areal Density				
Z:Y	Mean	Std. Error	95% Confidence Interval	
			Lower Bound	Upper Bound
1:1	7.170	.205	6.706	7.635
1:2	7.029	.178	6.627	7.432
1:3	7.132	.178	6.730	7.534
0:1	7.022	.251	6.453	7.591

Table K.36. Duncan post hoc test of Z: Y-yarns/ layer effect on tensile load/ composite areal density in X-direction

Load/ Composite Areal Density		
Duncan ^{a,b,c}		
Z:Y	N	Subset 1
0:1	2	7.0223
1:2	4	7.0293
1:3	4	7.1321
1:1	3	7.1703
Sig.		.644

Table K.37. ANOVA of Z: Y-yarns/ layer effect on tensile load/ preform areal density in X-direction

Tests of Between-Subjects Effects					
Dependent Variable: Load/ Preform Areal Density					
Source	Type III Sum of Squares	df	Mean Square	F	Sig.
Corrected Model	.480 ^a	3	.160	.743	.553
Intercept	1252.640	1	1252.640	5813.793	.000
ZtoY	.480	3	.160	.743	.553
Error	1.939	9	.215		
Total	1368.149	13			
Corrected Total	2.420	12			

Table K.38. Estimates of Z: Y-yarns/ layer effect on tensile load/ preform areal density in X-direction

1. Z:Y				
Dependent Variable: Load/ Preform Areal Density				
Z:Y	Mean	Std. Error	95% Confidence Interval	
			Lower Bound	Upper Bound
1:1	10.378	.268	9.772	10.985
1:2	10.445	.232	9.920	10.970
1:3	10.121	.232	9.596	10.646
0:1	9.924	.328	9.181	10.666

Table K.39. Duncan post hoc test of Z: Y-yarns/ layer effect on tensile load/ preform areal density in X-direction

Load/ Preform Areal Density		
Duncan ^{a,b,c}		
Z:Y	N	Subset 1
0:1	2	9.9237
1:3	4	10.1211
1:1	3	10.3783
1:2	4	10.4448
Sig.		.230

Table K.40. ANOVA of Z: Y-yarns/ layer effect on tensile load/ total fiber tex in X-direction

Tests of Between-Subjects Effects

Dependent Variable: Load/ Total Tex

Source	Type III Sum of Squares	df	Mean Square	F	Sig.
Corrected Model	.004 ^a	3	.001	1.668	.242
Intercept	4.329	1	4.329	5861.712	.000
ZtoY	.004	3	.001	1.668	.242
Error	.007	9	.001		
Total	4.741	13			
Corrected Total	.010	12			

Table K.41. Estimates of Z: Y-yarns/ layer effect on tensile load/ total fiber tex in X-direction

1. Z:Y

Dependent Variable: Load/ Total Tex

Z:Y	Mean	Std. Error	95% Confidence Interval	
			Lower Bound	Upper Bound
1:1	.619	.016	.584	.655
1:2	.617	.014	.586	.648
1:3	.592	.014	.561	.623
0:1	.574	.019	.531	.618

Table K.42. Duncan post hoc test of Z: Y-yarns/ layer effect on tensile load/ total fiber tex in X-direction

Load/ Total Tex

Duncan^{a,b,c}

Z:Y	N	Subset
		1
0:1	2	.5744
1:3	4	.5920
1:2	4	.6170
1:1	3	.6192
Sig.		.092

APPENDIX L: Statistical analysis of Tup impact results from Experiment B

Table L.1. ANOVA of Z: Y-yarns/ layer effect on Tup impact peak load

Tests of Between-Subjects Effects

Dependent Variable: Peak Load

Source	Type III Sum of Squares	df	Mean Square	F	Sig.
Corrected Model	1865501.788 ^a	3	621833.929	1.566	.242
Intercept	955334227.400	1	955334227.400	2405.168	.000
ZtoY	1865501.788	3	621833.929	1.566	.242
Error	5560809.010	14	397200.644		
Total	1047679749.000	18			
Corrected Total	7426310.797	17			

Table L.2. Estimates of Z: Y-yarns/ layer effect on Tup impact peak load

1. Z:Y

Dependent Variable: Peak Load

Z:Y	Mean	Std. Error	95% Confidence Interval	
			Lower Bound	Upper Bound
1:1	7762.726	315.119	7086.863	8438.590
1:2	7744.295	281.851	7139.784	8348.806
1:3	7736.274	257.294	7184.433	8288.114
0:1	6882.566	363.868	6102.146	7662.986

Table L.3. Duncan post hoc test of Z: Y-yarns/ layer effect on Tup impact peak load

Peak Load

Duncan^{a,b,c}

Z:Y	N	Subset 1
0:1	3	6882.5663
1:3	6	7736.2737
1:2	5	7744.2950
1:1	4	7762.7263
Sig.		.081

Table L.4. ANOVA of Z: Y-yarns/ layer effect on Tup impact total energy

Tests of Between-Subjects Effects

Dependent Variable: Total Energy

Source	Type III Sum of Squares	df	Mean Square	F	Sig.
Corrected Model	164.581 ^a	3	54.860	4.503	.021
Intercept	43804.505	1	43804.505	3595.633	.000
ZtoY	164.581	3	54.860	4.503	.021
Error	170.558	14	12.183		
Total	48072.136	18			
Corrected Total	335.138	17			

Table L.5. Estimates of Z: Y-yarns/ layer effect on Tup impact total energy

1. Z:Y

Dependent Variable: Total Energy

Z:Y	Mean	Std. Error	95% Confidence Interval	
			Lower Bound	Upper Bound
1:1	54.042	1.745	50.299	57.785
1:2	53.417	1.561	50.069	56.765
1:3	51.367	1.425	48.311	54.424
0:1	45.169	2.015	40.847	49.491

Table L.6. Duncan post hoc test of Z: Y-yarns/ layer effect on Tup impact total energy

Total Energy

Duncan^{a,b,c}

Z:Y	N	Subset	
		1	2
0:1	3	45.1690	
1:3	6		51.3673
1:2	5		53.4172
1:1	4		54.0423
Sig.		1.000	.309

Table L.7. ANOVA of Z: Y-yarns/ layer effect on Tup impact energy/ composite thickness

Tests of Between-Subjects Effects

Dependent Variable: Energy/ Thickness

Source	Type III Sum of Squares	df	Mean Square	F	Sig.
Corrected Model	4484655.522 ^a	3	1494885.174	.576	.640
Intercept	5776481704.000	1	5776481704.000	2226.621	.000
ZtoY	4484655.522	3	1494885.174	.576	.640
Error	36319933.370	14	2594280.955		
Total	6287284798.000	18			
Corrected Total	40804588.900	17			

Table L.8. Estimates of Z: Y-yarns/ layer effect on Tup impact energy/ composite thickness

1. Z:Y

Dependent Variable: Energy/ Thickness

Z:Y	Mean	Std. Error	95% Confidence Interval	
			Lower Bound	Upper Bound
1:1	18876.212	805.339	17148.932	20603.491
1:2	18487.596	720.317	16942.671	20032.522
1:3	19076.052	657.556	17665.734	20486.370
0:1	17638.866	929.925	15644.375	19633.356

Table L.9. Duncan post hoc test of Z: Y-yarns/ layer effect on Tup impact energy/ composite thickness

Energy/ Thickness

Duncan^{a,b,c}

Z:Y	N	Subset 1
0:1	3	17638.8659
1:2	5	18487.5965
1:1	4	18876.2117
1:3	6	19076.0518
Sig.		.252

Table L.10. ANOVA of Z: Y-yarns/ layer effect on Tup impact energy/ composite areal density

Tests of Between-Subjects Effects

Dependent Variable: Energy/ Composite Areal Density

Source	Type III Sum of Squares	df	Mean Square	F	Sig.
Corrected Model	1.666 ^a	3	.555	1.114	.377
Intercept	1879.845	1	1879.845	3771.520	.000
ZtoY	1.666	3	.555	1.114	.377
Error	6.978	14	.498		
Total	2035.405	18			
Corrected Total	8.644	17			

Table L.11. Estimates of Z: Y-yarns/ layer effect on Tup impact energy/ composite areal density

1. Z:Y

Dependent Variable: Energy/ Composite Areal Density

Z:Y	Mean	Std. Error	95% Confidence Interval	
			Lower Bound	Upper Bound
1:1	10.962	.353	10.204	11.719
1:2	10.659	.316	9.982	11.337
1:3	10.648	.288	10.030	11.266
0:1	9.991	.408	9.116	10.865

Table L.12. Duncan post hoc test of Z: Y-yarns/ layer effect on Tup impact energy/ composite areal density

Energy/ Composite Areal Density

Duncan^{a,b,c}

Z:Y	N	Subset 1
0:1	3	9.9906
1:3	6	10.6478
1:2	5	10.6595
1:1	4	10.9615
Sig.		.086

Table L.13. ANOVA of Z: Y-yarns/ layer effect on Tup impact energy/ preform areal density

Tests of Between-Subjects Effects					
Dependent Variable: Energy/ Preform Areal Density					
Source	Type III Sum of Squares	df	Mean Square	F	Sig.
Corrected Model	10.465 ^a	3	3.488	3.284	.053
Intercept	3787.654	1	3787.654	3565.357	.000
ZtoY	10.465	3	3.488	3.284	.053
Error	14.873	14	1.062		
Total	4149.512	18			
Corrected Total	25.338	17			

Table L.14. Estimates of Z: Y-yarns/ layer effect on Tup impact energy/ preform areal density

1. Z:Y				
Dependent Variable: Energy/ Preform Areal Density				
Z:Y	Mean	Std. Error	95% Confidence Interval	
			Lower Bound	Upper Bound
1:1	15.664	.515	14.559	16.770
1:2	15.637	.461	14.649	16.626
1:3	15.188	.421	14.286	16.091
0:1	13.495	.595	12.219	14.772

Table L.15. Duncan post hoc test of Z: Y-yarns/ layer effect on Tup impact energy/ preform areal density

Energy/ Preform Areal Density			
Duncan ^{a,b,c}			
Z:Y	N	Subset	
		1	2
0:1	3	13.4954	
1:3	6		15.1884
1:2	5		15.6374
1:1	4		15.6644
Sig.		1.000	.536

APPENDIX M: Statistical analysis of Izod impact results from Experiment B

Table M.1. ANOVA of Z: Y-yarns/ layer effect on Izod impact energy in Y-direction

Tests of Between-Subjects Effects

Dependent Variable: Total Energy

Source	Type III Sum of Squares	df	Mean Square	F	Sig.
Corrected Model	2.729 ^a	3	.910	.128	.942
Intercept	1999.478	1	1999.478	282.145	.000
ZtoY	2.729	3	.910	.128	.942
Error	170.081	24	7.087		
Total	2172.288	28			
Corrected Total	172.810	27			

Table M.2. Estimates of Z: Y-yarns/ layer effect on Izod impact energy in Y-direction

1. Z:Y

Dependent Variable: Total Energy

Z:Y	Mean	Std. Error	95% Confidence Interval	
			Lower Bound	Upper Bound
1:1	8.160	1.006	6.083	10.237
1:2	8.788	1.006	6.711	10.864
1:3	8.736	1.006	6.659	10.812
0:1	8.118	1.006	6.042	10.195

Table M.3. Duncan post hoc test of Z: Y-yarns/ layer effect on Izod impact energy in Y-direction

Total Energy

Duncan^{a,b}

Z:Y	N	Subset 1
0:1	7	8.1183
1:1	7	8.1599
1:3	7	8.7358
1:2	7	8.7877
Sig.		.672

Table M.4. ANOVA of Z: Y-yarns/ layer effect on Izod impact energy/ thickness in Y-direction

Tests of Between-Subjects Effects					
Dependent Variable: Energy/ Thickness					
Source	Type III Sum of Squares	df	Mean Square	F	Sig.
Corrected Model	846121.011 ^a	3	282040.337	.284	.837
Intercept	282679566.000	1	282679566.000	284.438	.000
ZtoY	846121.011	3	282040.337	.284	.837
Error	23851628.950	24	993817.873		
Total	307377316.000	28			
Corrected Total	24697749.960	27			

Table M.5. Estimates of Z: Y-yarns/ layer effect on Izod impact energy/ thickness in Y-direction

1. Z:Y				
Dependent Variable: Energy/ Thickness				
Z:Y	Mean	Std. Error	95% Confidence Interval	
			Lower Bound	Upper Bound
1:1	3022.196	376.794	2244.530	3799.861
1:2	3254.698	376.794	2477.033	4032.364
1:3	3425.804	376.794	2648.139	4203.469
0:1	3006.794	376.794	2229.128	3784.459

Table M.6. Duncan post hoc test of Z: Y-yarns/ layer effect on Izod impact energy/ thickness in Y-direction

Energy/ Thickness		
Duncan ^{a,b}		
Z:Y	N	Subset 1
0:1	7	3006.7937
1:1	7	3022.1958
1:2	7	3254.6984
1:3	7	3425.8039
Sig.		.481

Table M.7. ANOVA of Z: Y-yarns/ layer effect on Izod impact energy/ composite areal density in Y-direction

Tests of Between-Subjects Effects					
Dependent Variable: Energy/ Composite Areal Density					
Source	Type III Sum of Squares	df	Mean Square	F	Sig.
Corrected Model	.085 ^a	3	.028	.097	.961
Intercept	81.268	1	81.268	278.779	.000
ZtoY	.085	3	.028	.097	.961
Error	6.996	24	.292		
Total	88.349	28			
Corrected Total	7.081	27			

Table M.8. Estimates of Z: Y-yarns/ layer effect on Izod impact energy/ composite areal density in Y-direction

1. Z:Y				
Dependent Variable: Energy/ Composite Areal Density				
Z:Y	Mean	Std. Error	95% Confidence Interval	
			Lower Bound	Upper Bound
1:1	1.680	.204	1.259	2.101
1:2	1.685	.204	1.263	2.106
1:3	1.797	.204	1.375	2.218
0:1	1.653	.204	1.232	2.074

Table M.9. Duncan post hoc test of Z: Y-yarns/ layer effect on Izod impact energy/ composite areal density in Y-direction

Energy/ Composite Areal Density		
Duncan ^{a,b}		
Z:Y	N	Subset 1
0:1	7	1.6533
1:1	7	1.6802
1:2	7	1.6845
1:3	7	1.7965
Sig.		.656

Table M.10. ANOVA of Z: Y-yarns/ layer effect on Izod impact energy/ preform areal density in Y-direction

Tests of Between-Subjects Effects					
Dependent Variable: Energy/ Preform Areal Density					
Source	Type III Sum of Squares	df	Mean Square	F	Sig.
Corrected Model	.246 ^a	3	.082	.131	.941
Intercept	173.125	1	173.125	276.435	.000
ZtoY	.246	3	.082	.131	.941
Error	15.031	24	.626		
Total	188.402	28			
Corrected Total	15.277	27			

Table M.11. Estimates of Z: Y-yarns/ layer effect on Izod impact energy/ preform areal density in Y-direction

1. Z:Y				
Dependent Variable: Energy/ Preform Areal Density				
Z:Y	Mean	Std. Error	95% Confidence Interval	
			Lower Bound	Upper Bound
1:1	2.365	.299	1.748	2.983
1:2	2.573	.299	1.955	3.190
1:3	2.583	.299	1.966	3.200
0:1	2.426	.299	1.808	3.043

Table M.12. Duncan post hoc test of Z: Y-yarns/ layer effect on Izod impact energy/ preform areal density in Y-direction

Energy/ Preform Areal Density		
Duncan ^{a,b}		
Z:Y	N	Subset
1:1	7	2.3652
0:1	7	2.4256
1:2	7	2.5725
1:3	7	2.5830
Sig.		.644

Table M.13. ANOVA of Z: Y-yarns/ layer effect on Izod impact energy/ total fiber tex in Y-direction

Tests of Between-Subjects Effects

Dependent Variable: Energy/ Total Tex

Source	Type III Sum of Squares	df	Mean Square	F	Sig.
Corrected Model	.001 ^a	3	.000	.137	.937
Intercept	.581	1	.581	274.709	.000
ZtoY	.001	3	.000	.137	.937
Error	.051	24	.002		
Total	.633	28			
Corrected Total	.052	27			

Table M.14. Estimates of Z: Y-yarns/ layer effect on Izod impact energy/ total fiber tex in Y-direction

1. Z:Y

Dependent Variable: Energy/ Total Tex

Z:Y	Mean	Std. Error	95% Confidence Interval	
			Lower Bound	Upper Bound
1:1	.136	.017	.100	.172
1:2	.149	.017	.113	.185
1:3	.150	.017	.114	.186
0:1	.141	.017	.105	.177

Table M.15. Duncan post hoc test of Z: Y-yarns/ layer effect on Izod impact energy/ total fiber tex in Y-direction

Energy/ Total Tex

Duncan^{a,b}

Z:Y	N	Subset
		1
1:1	7	.1364
0:1	7	.1412
1:2	7	.1488
1:3	7	.1499
Sig.		.621

Table M.16. ANOVA of Z: Y-yarns/ layer effect on Izod impact energy in X-direction

Tests of Between-Subjects Effects

Dependent Variable: Total Energy

Source	Type III Sum of Squares	df	Mean Square	F	Sig.
Corrected Model	3.929 ^a	3	1.310	.211	.887
Intercept	1857.463	1	1857.463	299.553	.000
ZtoY	3.929	3	1.310	.211	.887
Error	117.815	19	6.201		
Total	2210.253	23			
Corrected Total	121.744	22			

Table M.17. Estimates of Z: Y-yarns/ layer effect on Izod impact energy in X-direction

1. Z:Y

Dependent Variable: Total Energy

Z:Y	Mean	Std. Error	95% Confidence Interval	
			Lower Bound	Upper Bound
1:1	9.526	1.438	6.517	12.535
1:2	10.145	1.017	8.017	12.273
1:3	9.045	.941	7.075	11.015
0:1	9.487	.941	7.518	11.457

Table M.18. Duncan post hoc test of Z: Y-yarns/ layer effect on Izod impact energy in X-direction

Total Energy

Duncan^{a,b,c}

Z:Y	N	Subset
		1
1:3	7	9.0447
0:1	7	9.4874
1:1	3	9.5257
1:2	6	10.1448
Sig.		.527

Table M.19. ANOVA of Z: Y-yarns/ layer effect on Izod impact energy/ thickness in X-direction

Tests of Between-Subjects Effects

Dependent Variable: Energy/ Thickness

Source	Type III Sum of Squares	df	Mean Square	F	Sig.
Corrected Model	890547.602 ^a	3	296849.201	.311	.818
Intercept	270662433.300	1	270662433.300	283.112	.000
ZtoY	890547.602	3	296849.201	.311	.818
Error	18164495.330	19	956026.070		
Total	328367554.300	23			
Corrected Total	19055042.930	22			

Table M.20. Estimates of Z: Y-yarns/ layer effect on Izod impact energy/ thickness in X-direction

1. Z:Y

Dependent Variable: Energy/ Thickness

Z:Y	Mean	Std. Error	95% Confidence Interval	
			Lower Bound	Upper Bound
1:1	3528.025	564.513	2346.485	4709.565
1:2	3623.125	399.171	2787.650	4458.600
1:3	3478.736	369.561	2705.237	4252.236
0:1	3953.095	369.561	3179.596	4726.595

Table M.21. Duncan post hoc test of Z: Y-yarns/ layer effect on Izod impact energy/ thickness in X-direction

Energy/ Thickness

Duncan^{a,b,c}

Z:Y	N	Subset 1
1:3	7	3478.7363
1:1	3	3528.0247
1:2	6	3623.1250
0:1	7	3953.0952
Sig.		.487

Table M.22. ANOVA of Z: Y-yarns/ layer effect on Izod impact energy/ composite areal density in X-direction

Tests of Between-Subjects Effects

Dependent Variable: Energy/ Composite Areal Density

Source	Type III Sum of Squares	df	Mean Square	F	Sig.
Corrected Model	.085 ^a	3	.028	.102	.958
Intercept	81.723	1	81.723	294.050	.000
ZtoY	.085	3	.028	.102	.958
Error	5.280	19	.278		
Total	97.964	23			
Corrected Total	5.366	22			

Table M.23. Estimates of Z: Y-yarns/ layer effect on Izod impact energy/ composite areal density in X-direction

1. Z:Y

Dependent Variable: Energy/ Composite Areal Density

Z:Y	Mean	Std. Error	95% Confidence Interval	
			Lower Bound	Upper Bound
1:1	1.975	.304	1.338	2.612
1:2	2.043	.215	1.592	2.493
1:3	1.925	.199	1.508	2.342
0:1	2.070	.199	1.653	2.487

Table M.24. Duncan post hoc test of Z: Y-yarns/ layer effect on Izod impact energy/ composite areal density in X-direction

Energy/ Composite Areal Density

Duncan^{a,b,c}

Z:Y	N	Subset
		1
1:3	7	1.9254
1:1	3	1.9750
1:2	6	2.0428
0:1	7	2.0700
Sig.		.693

Table M.25. ANOVA of Z: Y-yarns/ layer effect on Izod impact energy/ preform areal density in X-direction

Tests of Between-Subjects Effects					
Dependent Variable: Energy/ Preform Areal Density					
Source	Type III Sum of Squares	df	Mean Square	F	Sig.
Corrected Model	.293 ^a	3	.098	.180	.909
Intercept	160.788	1	160.788	296.197	.000
ZtoY	.293	3	.098	.180	.909
Error	10.314	19	.543		
Total	192.412	23			
Corrected Total	10.607	22			

Table M.26. Estimates of Z: Y-yarns/ layer effect on Izod impact energy/ preform areal density in X-direction

1. Z:Y				
Dependent Variable: Energy/ Preform Areal Density				
Z:Y	Mean	Std. Error	95% Confidence Interval	
			Lower Bound	Upper Bound
1:1	2.761	.425	1.871	3.651
1:2	2.970	.301	2.340	3.599
1:3	2.674	.278	2.092	3.257
0:1	2.835	.278	2.252	3.417

Table M.27. Duncan post hoc test of Z: Y-yarns/ layer effect on Izod impact energy/ preform areal density in X-direction

Energy/ Preform Areal Density		
Duncan ^{a,b,c}		
Z:Y	N	Subset 1
1:3	7	2.6744
1:1	3	2.7611
0:1	7	2.8346
1:2	6	2.9698
Sig.		.565

Table M.28. ANOVA of Z: Y-yarns/ layer effect on Izod impact energy/ total fiber tex in X-direction

Tests of Between-Subjects Effects					
Dependent Variable: Energy/ Total Tex					
Source	Type III Sum of Squares	df	Mean Square	F	Sig.
Corrected Model	.001 ^a	3	.000	.211	.887
Intercept	.556	1	.556	299.553	.000
ZtoY	.001	3	.000	.211	.887
Error	.035	19	.002		
Total	.661	23			
Corrected Total	.036	22			

Table M.29. Estimates of Z: Y-yarns/ layer effect on Izod impact energy/ total fiber tex in X-direction

1. Z:Y				
Dependent Variable: Energy/ Total Tex				
Z:Y	Mean	Std. Error	95% Confidence Interval	
			Lower Bound	Upper Bound
1:1	.165	.025	.113	.217
1:2	.175	.018	.139	.212
1:3	.156	.016	.122	.190
0:1	.164	.016	.130	.198

Table M.30. Duncan post hoc test of Z: Y-yarns/ layer effect on Izod impact energy/ total fiber tex in X-direction

Energy/ Total Tex		
Duncan ^{a,b,c}		
Z:Y	N	Subset
1:3	7	.1564
0:1	7	.1641
1:1	3	.1647
1:2	6	.1754
Sig.		.527

APPENDIX N: Statistical analysis of Charpy impact results from Experiment B

Table N.1. ANOVA of Z: Y-yarns/ layer effect on Charpy impact energy in Y-direction

Tests of Between-Subjects Effects

Dependent Variable: Total Energy

Source	Type III Sum of Squares	df	Mean Square	F	Sig.
Corrected Model	2.329 ^a	3	.776	.743	.540
Intercept	797.353	1	797.353	763.100	.000
ZtoY	2.329	3	.776	.743	.540
Error	18.808	18	1.045		
Total	878.887	22			
Corrected Total	21.137	21			

Table N.2. Estimates of Z: Y-yarns/ layer effect on Charpy impact energy in Y-direction

1. Z:Y

Dependent Variable: Total Energy

Z:Y	Mean	Std. Error	95% Confidence Interval	
			Lower Bound	Upper Bound
1:1	6.016	.386	5.205	6.828
1:2	6.401	.386	5.589	7.212
1:3	5.837	.511	4.763	6.911
0:1	6.776	.511	5.702	7.850

Table N.3. Duncan post hoc test of Z: Y-yarns/ layer effect on Charpy impact energy in Y-direction

Total Energy

Duncan^{a,b,c}

Z:Y	N	Subset
		1
1:3	4	5.8370
1:1	7	6.0162
1:2	7	6.4007
0:1	4	6.7759
Sig.		.195

Table N.4. ANOVA of Z: Y-yarns/ layer effect on Charpy impact energy/ thickness in Y-direction

Tests of Between-Subjects Effects					
Dependent Variable: Energy/ Thickness					
Source	Type III Sum of Squares	df	Mean Square	F	Sig.
Corrected Model	219060.790 ^a	3	73020.263	.495	.691
Intercept	112397606.600	1	112397606.600	761.275	.000
ZtoY	219060.790	3	73020.263	.495	.691
Error	2657588.622	18	147643.812		
Total	122902254.600	22			
Corrected Total	2876649.412	21			

Table N.5. Estimates of Z: Y-yarns/ layer effect on Charpy impact energy/ thickness in Y-direction

1. Z:Y				
Dependent Variable: Energy/ Thickness				
Z:Y	Mean	Std. Error	95% Confidence Interval	
			Lower Bound	Upper Bound
1:1	2228.233	145.231	1923.114	2533.351
1:2	2370.614	145.231	2065.495	2675.732
1:3	2289.020	192.122	1885.386	2692.653
0:1	2509.602	192.122	2105.968	2913.236

Table N.6. Duncan post hoc test of Z: Y-yarns/ layer effect on Charpy impact energy/ thickness in Y-direction

Energy/ Thickness		
Duncan ^{a,b,c}		
Z:Y	N	Subset 1
1:1	7	2228.2328
1:3	4	2289.0196
1:2	7	2370.6138
0:1	4	2509.6019
Sig.		.298

Table N.7. ANOVA of Z: Y-yarns/ layer effect on Charpy impact energy/ composite areal density in Y-direction

Tests of Between-Subjects Effects

Dependent Variable: Energy/ Composite Areal Density

Source	Type III Sum of Squares	df	Mean Square	F	Sig.
Corrected Model	.016 ^a	3	.005	.127	.943
Intercept	32.214	1	32.214	765.054	.000
ZtoY	.016	3	.005	.127	.943
Error	.758	18	.042		
Total	35.513	22			
Corrected Total	.774	21			

Table N.8. Estimates of Z: Y-yarns/ layer effect on Charpy impact energy/ composite areal density in Y-direction

1. Z:Y

Dependent Variable: Energy/ Composite Areal Density

Z:Y	Mean	Std. Error	95% Confidence Interval	
			Lower Bound	Upper Bound
1:1	1.251	.078	1.088	1.414
1:2	1.256	.078	1.093	1.419
1:3	1.218	.103	1.002	1.433
0:1	1.306	.103	1.091	1.522

Table N.9. Duncan post hoc test of Z: Y-yarns/ layer effect on Charpy impact energy/ composite areal density in Y-direction

Energy/ Composite Areal Density

Duncan^{a,b,c}

Z:Y	N	Subset 1
1:3	4	1.2179
1:1	7	1.2511
1:2	7	1.2560
0:1	4	1.3061
Sig.		.538

Table N.10. ANOVA of Z: Y-yarns/ layer effect on Charpy impact energy/ preform areal density in Y-direction

Tests of Between-Subjects Effects					
Dependent Variable: Energy/ Preform Areal Density					
Source	Type III Sum of Squares	df	Mean Square	F	Sig.
Corrected Model	.260 ^a	3	.087	.955	.435
Intercept	69.092	1	69.092	761.983	.000
ZtoY	.260	3	.087	.955	.435
Error	1.632	18	.091		
Total	75.804	22			
Corrected Total	1.892	21			

Table N.11. Estimates of Z: Y-yarns/ layer effect on Charpy impact energy/ preform areal density in Y-direction

1. Z:Y				
Dependent Variable: Energy/ Preform Areal Density				
Z:Y	Mean	Std. Error	95% Confidence Interval	
			Lower Bound	Upper Bound
1:1	1.744	.114	1.505	1.983
1:2	1.874	.114	1.635	2.113
1:3	1.726	.151	1.410	2.042
0:1	2.024	.151	1.708	2.341

Table N.12. Duncan post hoc test of Z: Y-yarns/ layer effect on Charpy impact energy/ preform areal density in Y-direction

Energy/ Preform Areal Density		
Duncan ^{a,b,c}		
Z:Y	N	Subset 1
1:3	4	1.7259
1:1	7	1.7438
1:2	7	1.8737
0:1	4	2.0245
Sig.		.163

Table N.13. ANOVA of Z: Y-yarns/ layer effect on Charpy impact energy/ total fiber tex in Y-direction

Tests of Between-Subjects Effects					
Dependent Variable: Energy/ Total Tex					
Source	Type III Sum of Squares	df	Mean Square	F	Sig.
Corrected Model	.001 ^a	3	.000	1.033	.402
Intercept	.232	1	.232	761.703	.000
ZtoY	.001	3	.000	1.033	.402
Error	.005	18	.000		
Total	.254	22			
Corrected Total	.006	21			

Table N.14. Estimates of Z: Y-yarns/ layer effect on Charpy impact energy/ total fiber tex in Y-direction

1. Z:Y				
Dependent Variable: Energy/ Total Tex				
Z:Y	Mean	Std. Error	95% Confidence Interval	
			Lower Bound	Upper Bound
1:1	.101	.007	.087	.114
1:2	.108	.007	.095	.122
1:3	.100	.009	.082	.118
0:1	.118	.009	.099	.136

Table N.15. Duncan post hoc test of Z: Y-yarns/ layer effect on Charpy impact energy/ total fiber tex in Y-direction

Energy/ Total Tex		
Duncan ^{a,b,c}		
Z:Y	N	Subset
1:3	4	.1001
1:1	7	.1005
1:2	7	.1084
0:1	4	.1178
Sig.		.154

Table N.16. ANOVA of Z: Y-yarns/ layer effect on Charpy impact energy in X-direction

Tests of Between-Subjects Effects

Dependent Variable: Total Energy

Source	Type III Sum of Squares	df	Mean Square	F	Sig.
Corrected Model	20.563 ^a	3	6.854	4.413	.021
Intercept	721.372	1	721.372	464.437	.000
ZtoY	20.563	3	6.854	4.413	.021
Error	23.298	15	1.553		
Total	804.449	19			
Corrected Total	43.862	18			

Table N.17. Estimates of Z: Y-yarns/ layer effect on Charpy impact energy in X-direction

1. Z:Y

Dependent Variable: Total Energy

Z:Y	Mean	Std. Error	95% Confidence Interval	
			Lower Bound	Upper Bound
1:1	6.751	.623	5.422	8.079
1:2	7.402	.557	6.214	8.590
1:3	6.398	.509	5.314	7.483
0:1	4.453	.623	3.125	5.782

Table N.18. Duncan post hoc test of Z: Y-yarns/ layer effect on Charpy impact energy in X-direction

Total Energy

Duncan^{a,b,c}

Z:Y	N	Subset	
		1	2
0:1	4	4.4534	
1:3	6		6.3982
1:1	4		6.7507
1:2	5		7.4016
Sig.		1.000	.264

Table N.19. ANOVA of Z: Y-yarns/ layer effect on Charpy impact energy/ thickness in X-direction

Tests of Between-Subjects Effects					
Dependent Variable: Energy/ Thickness					
Source	Type III Sum of Squares	df	Mean Square	F	Sig.
Corrected Model	1542226.471 ^a	3	514075.490	2.343	.114
Intercept	103261119.700	1	103261119.700	470.547	.000
ZtoY	1542226.471	3	514075.490	2.343	.114
Error	3291734.448	15	219448.963		
Total	113341706.800	19			
Corrected Total	4833960.919	18			

Table N.20. Estimates of Z: Y-yarns/ layer effect on Charpy impact energy/ thickness in X-direction

1. Z:Y				
Dependent Variable: Energy/ Thickness				
Z:Y	Mean	Std. Error	95% Confidence Interval	
			Lower Bound	Upper Bound
1:1	2500.241	234.227	2000.998	2999.484
1:2	2643.421	209.499	2196.885	3089.958
1:3	2460.827	191.245	2053.197	2868.457
0:1	1855.583	234.227	1356.341	2354.826

Table N.21. Duncan post hoc test of Z: Y-yarns/ layer effect on Charpy impact energy/ thickness in X-direction

Energy/ Thickness			
Duncan ^{a,b,c}			
Z:Y	N	Subset	
		1	2
0:1	4	1855.5833	
1:3	6	2460.8269	2460.8269
1:1	4	2500.2407	2500.2407
1:2	5		2643.4214
Sig.		.065	.583

Table N.22. ANOVA of Z: Y-yarns/ layer effect on Charpy impact energy/ composite areal density in X-direction

Tests of Between-Subjects Effects

Dependent Variable: Energy/ Composite Areal Density

Source	Type III Sum of Squares	df	Mean Square	F	Sig.
Corrected Model	.735 ^a	3	.245	3.700	.036
Intercept	30.543	1	30.543	461.476	.000
ZtoY	.735	3	.245	3.700	.036
Error	.993	15	.066		
Total	33.957	19			
Corrected Total	1.727	18			

Table N.23. Estimates of Z: Y-yarns/ layer effect on Charpy impact energy/ composite areal density in X-direction

1. Z:Y

Dependent Variable: Energy/ Composite Areal Density

Z:Y	Mean	Std. Error	95% Confidence Interval	
			Lower Bound	Upper Bound
1:1	1.402	.129	1.128	1.676
1:2	1.460	.115	1.215	1.705
1:3	1.353	.105	1.129	1.577
0:1	.930	.129	.656	1.204

Table N.24. Duncan post hoc test of Z: Y-yarns/ layer effect on Charpy impact energy/ composite areal density in X-direction

Energy/ Composite Areal Density

Duncan^{a,b,c}

Z:Y	N	Subset	
		1	2
0:1	4	.9298	
1:3	6		1.3530
1:1	4		1.4020
1:2	5		1.4601
Sig.		1.000	.558

Table N.25. ANOVA of Z: Y-yarns/ layer effect on Charpy impact energy/ preform areal density in X-direction

Tests of Between-Subjects Effects

Dependent Variable: Energy/ Preform Areal Density

Source	Type III Sum of Squares	df	Mean Square	F	Sig.
Corrected Model	1.635 ^a	3	.545	4.094	.026
Intercept	62.263	1	62.263	467.697	.000
ZtoY	1.635	3	.545	4.094	.026
Error	1.997	15	.133		
Total	69.341	19			
Corrected Total	3.632	18			

Table N.26. Estimates of Z: Y-yarns/ layer effect on Charpy impact energy/ preform areal density in X-direction

1. Z:Y

Dependent Variable: Energy/ Preform Areal Density

Z:Y	Mean	Std. Error	95% Confidence Interval	
			Lower Bound	Upper Bound
1:1	1.957	.182	1.568	2.346
1:2	2.167	.163	1.819	2.515
1:3	1.892	.149	1.574	2.209
0:1	1.331	.182	.942	1.719

Table N.27. Duncan post hoc test of Z: Y-yarns/ layer effect on Charpy impact energy/ preform areal density in X-direction

Energy/ Preform Areal Density

Duncan^{a,b,c}

Z:Y	N	Subset	
		1	2
0:1	4	1.3306	
1:3	6		1.8918
1:1	4		1.9567
1:2	5		2.1667
Sig.		1.000	.295

Table N.28. ANOVA of Z: Y-yarns/ layer effect on Charpy impact energy/ total fiber tex in X-direction

Tests of Between-Subjects Effects					
Dependent Variable: Energy/ Total Tex					
Source	Type III Sum of Squares	df	Mean Square	F	Sig.
Corrected Model	.006 ^a	3	.002	4.413	.021
Intercept	.216	1	.216	464.476	.000
ZtoY	.006	3	.002	4.413	.021
Error	.007	15	.000		
Total	.241	19			
Corrected Total	.013	18			

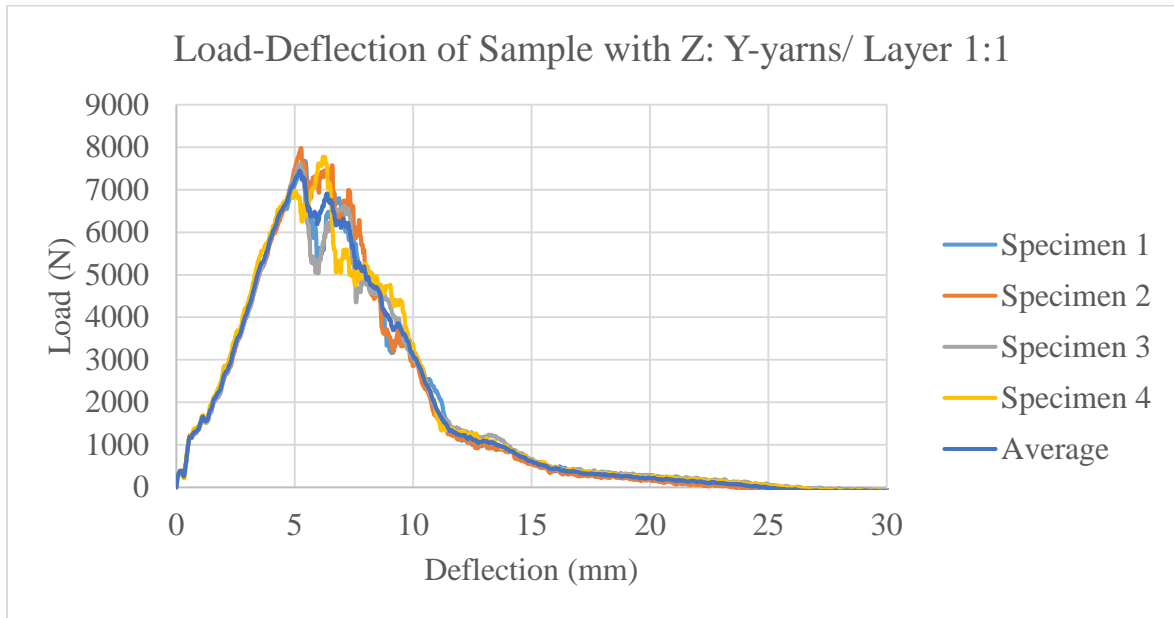
Table N.29. Estimates of Z: Y-yarns/ layer effect on Charpy impact energy/ total fiber tex in X-direction

1. Z:Y				
Dependent Variable: Energy/ Total Tex				
Z:Y	Mean	Std. Error	95% Confidence Interval	
			Lower Bound	Upper Bound
1:1	.117	.011	.094	.140
1:2	.128	.010	.107	.149
1:3	.111	.009	.092	.129
0:1	.077	.011	.054	.100

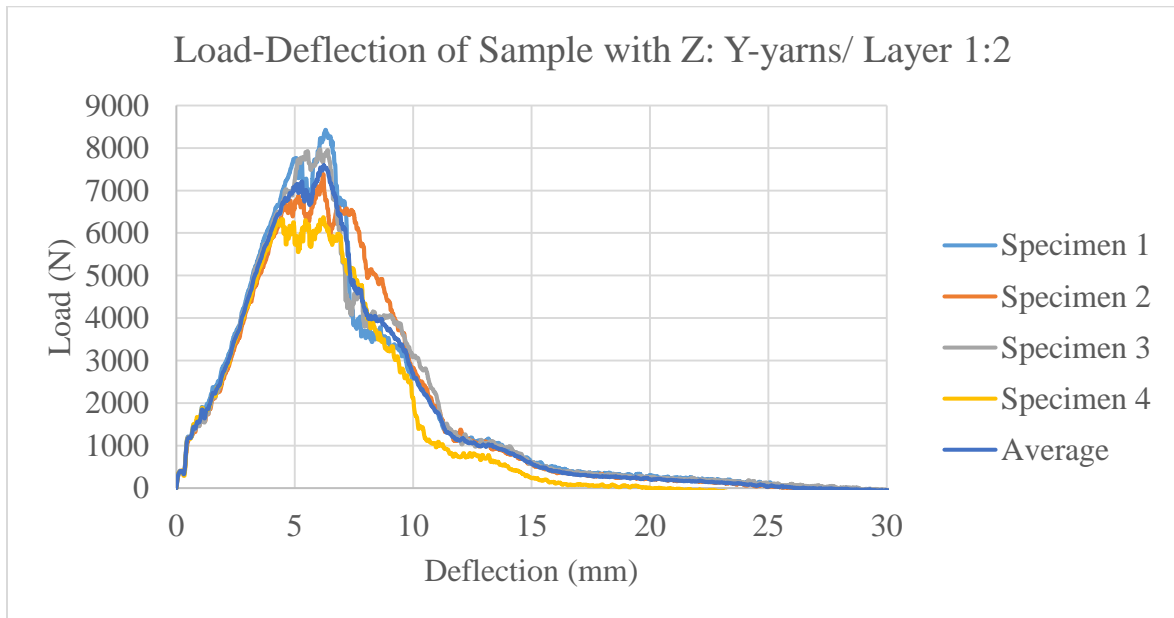
Table N.30. Duncan post hoc test of Z: Y-yarns/ layer effect on Charpy impact energy/ total fiber tex in X-direction

Energy/ Total Tex			
Duncan ^{a,b,c}			
Z:Y	N	Subset	
		1	2
0:1	4	.0770	
1:3	6		.1106
1:1	4		.1167
1:2	5		.1280
Sig.		1.000	.264

APPENDIX O: Top Impact Load-Deflection Curves for all Specimens in Experiment B

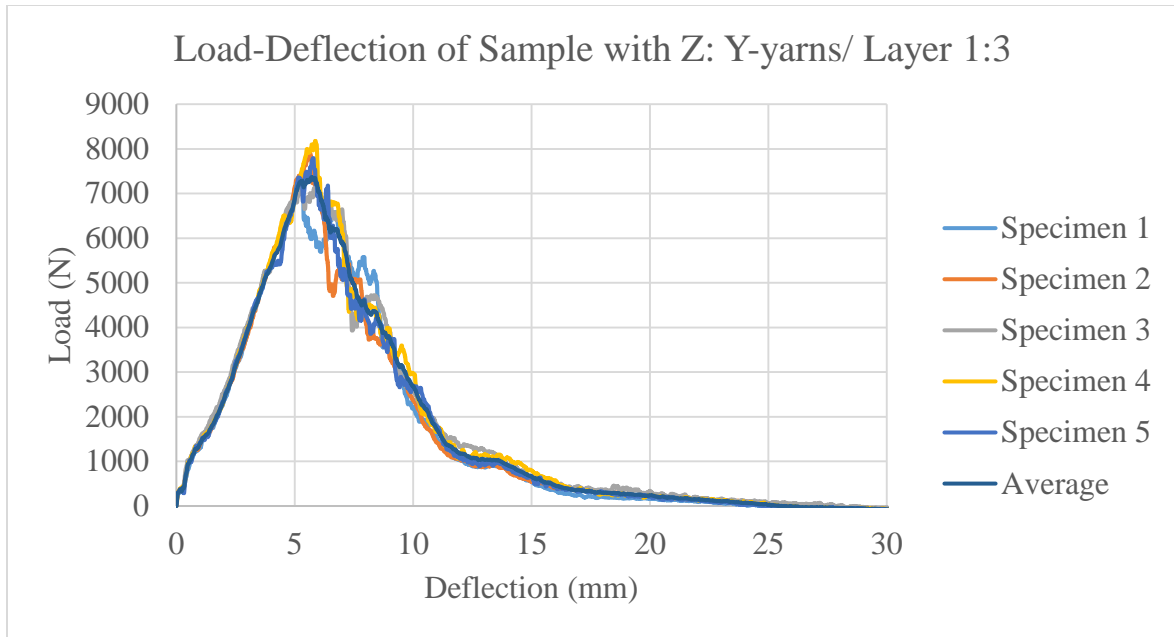


(a)

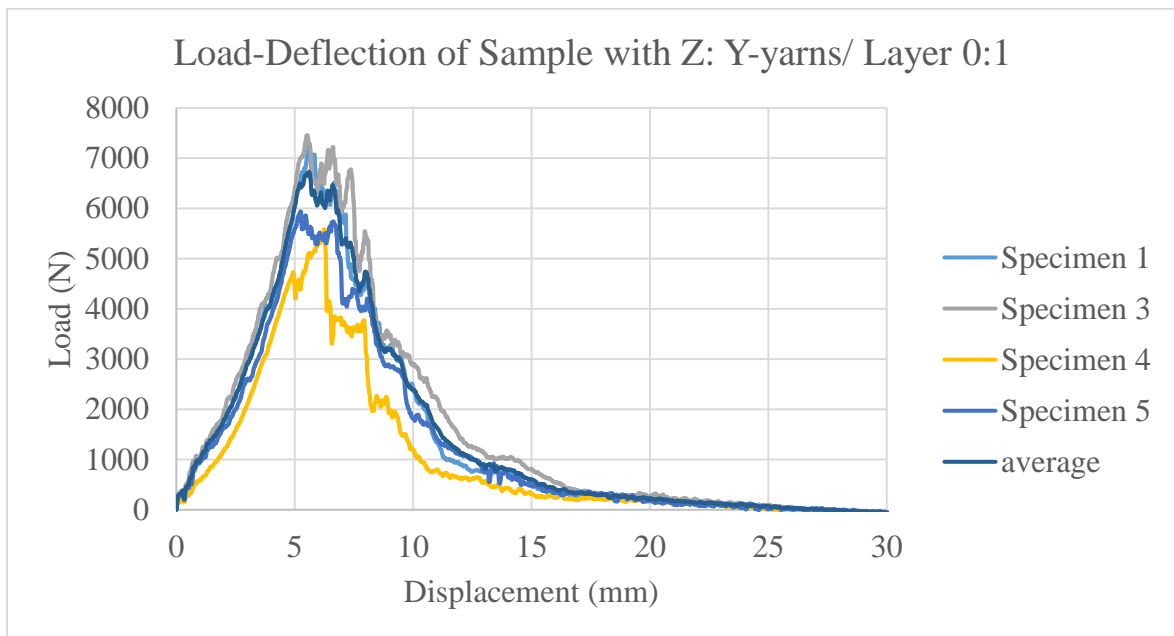


(b)

Figure O.1. Top impact load-deflection curves for individual specimens in Experiment B for samples with different Z: Y-yarns/ layer, (a) 1:1, (b) 1:2



(a)



(b)

Figure O.2. Top impact load-deflection curves for individual specimens in Experiment B for samples with different Z: Y-yarns/ layer, (a) 1:3, and (b) 1:0

APPENDIX P: Top Impact Delamination Area Image Analysis for Experiment B

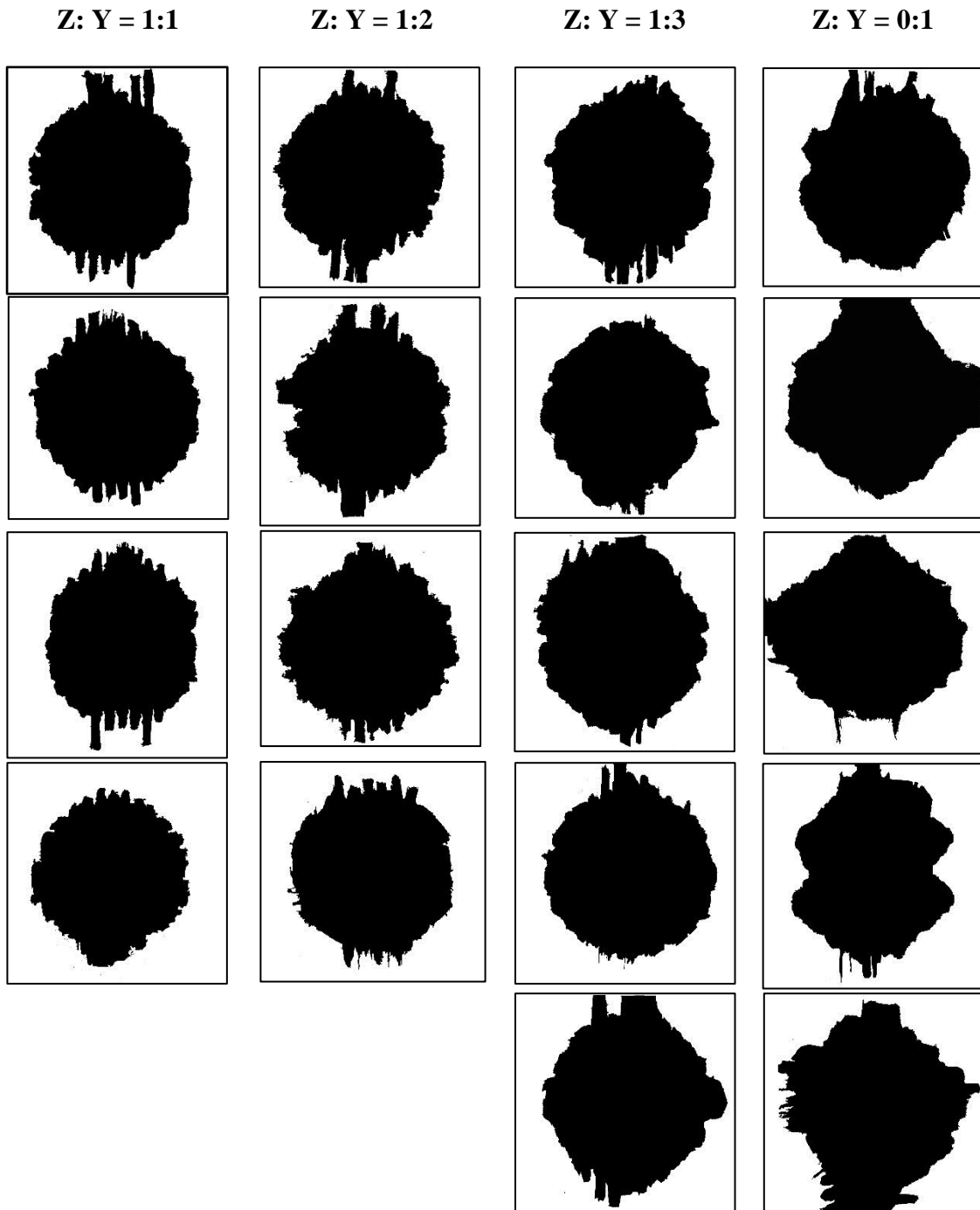


Figure P.1. Top impact delamination area image analysis for Experiment B